MATHEMATICAL ANALYSIS, SCALING AND SIMULATION OF FLOW AND TRANSPORT DURING IMMISCIBLE TWO-PHASE FLOW

KAREN SOPHIE SCHMID

Submitted for the degree of Doctor of Philosophy

Institute of Petroleum Engineering
Heriot-Watt University

2nd of March 2012

Karen Sophie Schmid: *Mathematical Analysis, Scaling and Simulation of Flow and Transport during immiscible Two-Phase Flow,* Submitted for the degree of Doctor of Philosophy.

SUPERVISORS:
Prof. Sebastian Geiger
Prof. Ken Sorbie
Dr. Rachel Wood

LOCATION:
Edinburgh

2nd of March 2012

ABSTRACT

Fluid flow and transport in fractured geological formations is of fundamental socio-economic importance, with applications ranging from oil recovery from the largest remaining hydrocarbon reserves to bioremediation techniques. Two mechanisms are particularly relevant for flow and transport, namely spontaneous imbibition (SI) and hydrodynamic dispersion. This thesis investigates the influence of SI and dispersion on flow and transport during immiscible two-phase flow.
We make four main contributions. Firstly, we derive general, exact analytic solutions for SI that are valid for arbitrary petrophysical properties. This should finalize the decades-long search for analytical solutions for SI. Secondly, we derive the first non-dimensional time for SI that incorporates the influence of all parameters present in the two-phase Darcy formulation - a problem that was open for more than 90 years. Thirdly, we show how the growth of the dispersive zone depends on the flow regime and on adsorption. To that end we derive the first known set of analytical solutions for transport that fully accounts for the effects of capillarity, viscous forces and dispersion. Finally, we provide numerical tools to investigate the influence of heterogeneity by extending the higher order finite-element finite-volume method on unstructured grids to the case of transport and two-phase flow.

Dedicated to my wonderful family:
To my parents Ingrid and Joe,
and to my sisters Hannah and Maximiliane.[1]

1 ...und natürlich dem ganzen Rest der Bande!

ACADEMIC REGISTRY
Research Thesis Submission

Name*:*	Karen S Schmid		
School/PGI:	IPE		
Version: *(i.e. First, Resubmission, Final)*	FINAL	Degree Sought (Award **and** Subject area)	PhD in Petroleum Engineering

Declaration

In accordance with the appropriate regulations I hereby submit my thesis and I declare that:

1) the thesis embodies the results of my own work and has been composed by myself
2) where appropriate, I have made acknowledgement of the work of others and have made reference to work carried out in collaboration with other persons
3) the thesis is the correct version of the thesis for submission and is the same version as any electronic versions submitted*.
4) my thesis for the award referred to, deposited in the Heriot-Watt University Library, should be made available for loan or photocopying and be available via the Institutional Repository, subject to such conditions as the Librarian may require
5) I understand that as a student of the University I am required to abide by the Regulations of the University and to conform to its discipline.

* *Please note that it is the responsibility of the candidate to ensure that the correct version of the thesis is submitted.*

Signature of Candidate*:*		Date:	27/03/2012

Submission

Submitted By *(name in capitals):*	Karen S Schmid
Signature of Individual Submitting:	
Date Submitted:	

For Completion in the Student Service Centre (SSC)

Received in the SSC by *(name in capitals):*			
Method of Submission *(Handed in to SSC; posted through internal/external mail):*			
*E-thesis Submitted (**mandatory for final theses)***			
Signature:		Date:	

Please note this form should bound into the submitted thesis.

Updated February 2008, November 2008, February 2009, January 2011

I can no other answer make but thanks,
And thanks.

- William Shakespeare, *Twelfth Night*

ACKNOWLEDGMENTS

During my PhD, many people have made my life a lot easier (and also more interesting!), and I am honoured that I finally can say thank you to them. Given that fluid flow in fractured media is such an unusually interdisciplinary topic, this list has grown unusually long.

First of all: A big thank you goes to my supervisor Sebastian Geiger! Sebastian, thank your for your absolutely outstanding commitment during the whole time of my PhD, for creating such a wonderful working atmosphere, and for your continuing 'no-matter-what' support. And thank you for being so supportive and open minded to new ideas: Chapters 2-4 basically were never planned like this. They 'just happened' because you amazingly managed the delicate balance between giving me the necessary free space to try new ideas while at the same time never giving me the feeling that I was alone with this.

Next, my thanks go to my second supervisor Ken Sorbie for convincing me to do my PhD in Edinburgh, rather than anywhere else. Thanks Ken for many hours of shuffling through concepts and discussions on multiphase flow and core floods. Furthermore, I want to thank Rachel Wood at Edinburgh Uni for supervising me as part of the ECOSSE initiative.

I also want to thank Martin Blunt from Imperial College and Mike Christie from Heriot–Watt for being my examiners. The viva was as vivas should be: Short, inspiring and fun. So thank you Martin and Mike for motivating me to take this research further. And thanks Mike for the past three years of discussions on anything ranging from higher-order methods to the 'dress–code' in Newcastle, and for not living up to your promise (threat?) to correct every single comma and dash in my thesis. — – - Thank, you!

The research for this thesis was carried out and funded as part of the ExxonMobil Research Alliance 'Fundamental Controls of Flow in Carbonates' $(FC)^2$, and it is an honour to thank the leading mind behind $(FC)^2$, Susan Agar. Susan, I still find it truly impressive how you manage to keep such a long-term vision for research while being heavily involved in day-to-day details of so many different projects and with a travel schedule that would make any foreign minister look like someone who doesn't get around much. Thank you! Thanks also to Thomas Willingham and Owen Hehmeyer at EMURC for making the publication and IP process so simple and smooth, and Thomas, Owen and Enrique Rosero for so many highly constructive discussions.

Thanks also to Greg Benson for trying to teach me what a real rock looks like, and Dave Olgaard and Adam Rinehart for making the visit to Corporate Strategic Research (CSR) in New Jersey possible. This part wouldn't be complete without thanking John Kuzan, Scott Clingman, Chick Wattenbarger and Prateek Shah for the possibility to work with them during my stay in Houston. Thanks also to Bhargaw Adibhatla for wonderful discussions, and also for asking the crucial question 'What are analytical solutions good for anyhow?'. For one possible answer, see Chapter 3! My very special thanks go to Camille Schroeder and Slavka Svarc: Thank you for making me feel so welcome in Houston - and thanks for the great Thanksgiving turkey!

During my time in Edinburgh together with other PhD students the idea came up to found one of the worldwide very few student SIAM student chapters that links different departments (engineering, maths and computer science) and different universities. Thanks to my board members Bubacarr Bah and Nneoma Ogbonna, and our faculty advisors Jared Tanner, Sebastian Geiger (again!), Gabriel Lord for your support and commitment. Thanks also Gabriel for discussing numerics for non-linear PDEs with me.

Chapter 5 builds on the C++ library CSMP++, and I want to extend my acknowledgements to the developers at ETH Zurich and Uni Leoben, the groups around Thomas Driesner and Stephan Matthäi. Thomas, thanks again for proof-reading early drafts of Chapter 3, and Gilian Grün and Ingo Steinberger for patiently sending me papers I couldn't access through our subscriptions.

People who started out as office colleagues soon became my friends. Thank you Matteo for Italian coffee, and for hiding under my table just to scare me; thanks Elma for showing me your 'microscopy magic' – hope we can catch up in Berlin! Thanks Yan for your friendship, for tirelessly sharing your IT wisdom with me, and for taking me to my first (and last?) heavy metal concert; thanks Claudia for sharing your passion for CT scans, and organizing many get-togethers; Robert for helping me to see absolutely everything from a different angle; Shanti for all the chocolate, Christine for discussions on dual-porosity models, and both for being so kind; Adnan for taking the time to discuss three phase flow, and thanks to you, Chen and Mohammed for never getting annoyed by my procrastination attacks. Also: Thanks Chen for immediately offering any possible help on that evening when I thought I had lost my wallet! It was such a relief! It was good to have you all around!

My thank you also goes to Rink van Dijke for discussions on pore-scale modelling, Will Thomas for explaining core floods, and Gilian Pickup for playing music with me. A big thank you goes to Heriot-Watt's conductor Steve King for many free tickets for the Scottish Chamber Orchestra and taking the time to set up a string quartett group with me. Thanks to the guys from the Chemical Engineering Department: Noémie for explaining me Rugby rules and for hosting that gigantic Christmas dinner; Panos for giving me good advice, many times; Dalila for being such an optimistic person.

Thanks Jule and Niklas for coming to all our concerts and for many nice dinners, and thanks Emily for discussions about plant seeds which even made it into Chapter 3, and especially for being such a warm–hearted, caring person (yes, you are!). Thanks 'Don' Alejandro for your PhD comics. Thank you, thank you, thank you 'tío y tía' Oscar and Susana: For taking us all to Segovia, for always having a good idea of where to swim/walk/cycle/ski/..., and for always, always having an open door and open ears.

Konstantin: What can I say? With you everything simply makes so much more sense. You make that difference. Danke für Deine Klugheit, und Deine Einsicht.

Finally, I want to thank my family. My love and gratitude for you cannot be expressed in words, and I dedicate this thesis to you.

Edinburgh, March 2012

CONTENTS

LIST OF FIGURES

LIST OF TABLES

PUBLICATIONS

Besides unpublished material this thesis contains excerpts from the following peer-reviewed papers, arranged according to the chapters of this thesis:

- Geiger, S.; Schmid, K. S., Zaretskiy, Y. (invited) *'Mathematical analysis and numerical simulation of multi-phase multi-component flow in heterogeneous porous media'*; Current Opinion in Colloid and Interfacial Sciences; in press, 10.1016/j.cocis.2012.01.003; (Chapter 1)

- Schmid, K. S.; Geiger, S. *'Universal Scaling of Spontaneous Imbibition for Arbitrary Petrophysical Properties: Water-Wet and Mixed-Wet States and Handy's Conjecture'*; submitted (Chapters 2 and 3)

- Schmid, K. S.; Geiger, S. *'Universal Scaling of Spontaneous Imbibition for Water Wet Rocks'*; Water Resources Research, 48, W03507, doi:10.1029/2011WR011566, 2012. Featured article in Water Resources Research; chosen for AGU Spotlight (Chapter 3)

- Schmid, K. S.; Geiger, S., Sorbie, K. S. 'Analytical solutions for co- and countercurrent imbibition of sorbing, dispersive solutes in immiscible two-phase flow'; Computational Geosciences, 16(2), 351-366, 10.1007/s10596-012-9282-6, 2012. (Chapter 4)

- Schmid, K. S.; Geiger, S., Sorbie, K. S. *'Semi analytical solutions for co- and countercurrent imbibition and dispersion of solutes in immiscible two-phase flow'*; Water Resources Research 47: 1-16, 2011; doi: 10.1029/2010WR009686. (Chapter 4)

- Schmid, K. S.; Geiger, S.; Sorbie, K. S.*'Higher Order FE-FV Methods on Unstructured Grids for Transport and Two-Phase Flow with Variable Viscosity in Heterogeneous Porous Media'*; submitted (Chapter 5)

1

INTRODUCTION

1.1 FUNDAMENTAL CONTROL OF FLOW AND TRANSPORT IN FRACTURED RESERVOIRS

The transport of dissolved chemical components (e.g., CO_2, NaCl, CH_4) in different fluid phases (e.g., water, oil, gas) occupying the pore space of geological formations underground (Figure 1.1) is of fundamental importance to a large number of geological and reservoir engineering processes. These include, but are not limited to, enhancing the recovery of oil and gas from hydrocarbon reservoirs through the injection of chemicals [Austad et al., 2008], storing greenhouse gases such as CO_2 in saline aquifers and oil and gas fields [Bickle, 2009], flow in the vicinity of radioactive waste repositories [Tsang et al., 2009], remediation of toxic contaminants in groundwater aquifers [Mulligan et al., 2001], or mineral scale formation in oil reservoirs [Sorbie and Mackay, 2000].
In many of these applications, flow and transport in *fractured* reservoirs are of particular significance. A fractured reservoir consists of a set of fractures that usually are less than 1 cm wide, and different rock layers of varying permeability (Fig. 1.1). In naturally fractured reservoirs these fractures were formed during the geological evolution over time. Carbonate reservoirs, such as the reservoirs of the Middle East, are typically fractured and host about 60% of the world's remaining petroleum reserves. However, they are difficult to produce and recovery factors for traditional waterflooding can be less than 10% [Schlumberger, 2007]. If a reservoir has a low permeability then either to remove hazardous non-aqueous phase liquids (NAPLs) or to produce oil [Frank and Barkley, 1995], fractures are propagated by a technique known as hydraulic fracturing. This method has sparked an extensive debate in the public due to the unclear trade-off between utility on the one hand and risk to the environment on the other hand [Howarth et al., 2011]. Obviously, in either case - to protect the subsurface, and for making hydrocarbon production more efficient - an improved understanding of flow and transport in fractured reservoirs is crucial.

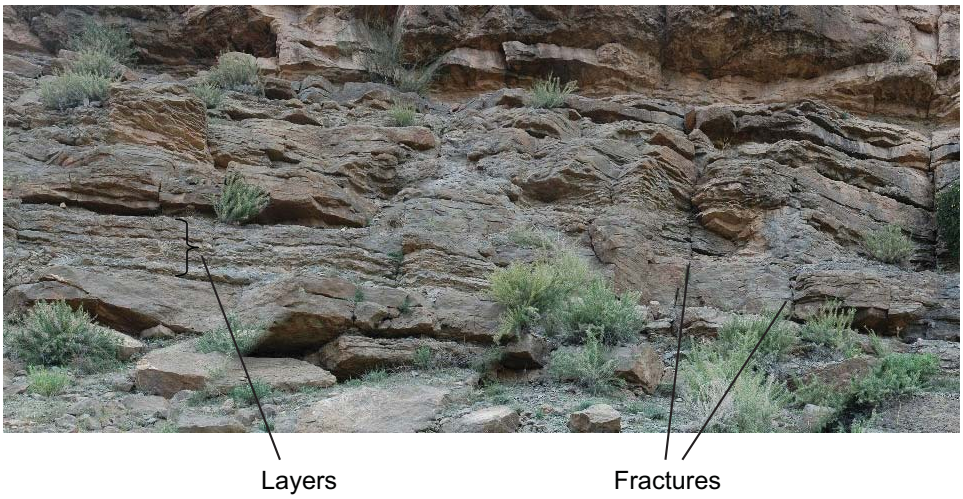

Figure 1.1: Photograph of the fractured carbonate outcrop (dimensions of 30×10 m). Similar rocks like these, but buried underground in approximately 1 to 4 kilometres depth, contain the world's largest oil reservoirs in the Middle East. The outcrop consists of a set of fractures that connect different rock layers of varying permeability. Fractures are usually less than 1 cm wide. Fluid phases (e.g., oil and water) and dissolved chemical components (e.g., CO_2, NaCl, CH_4) mainly flow through the connected fractures that act as fluid conduits which can bypass the low-permeability rock layers. The discretization of this outcrop is used in the numerical Test Case V (Figure 5.16).

Two processes are of particular significance for the control of flow and transport in fractured reservoirs.

The first process is spontaneous imbibition. Spontaneous imbibition (SI) is a key mechanism central to many flow process - ranging from oil recovery from the largest remaining oil reservoirs, to CO_2 storage to water uptake in plant seeds - and also well known from daily life: If a sugar cube is dipped into tea, the fluid 'imbibes' by spontaneous capillary flow. Just as tea imbibes the porous sugar cube, in a fractured reservoir water imbibes from the high-permeability fractures into the oil-rich, low-permeability rock layer. Since water otherwise bypasses the matrix blocks through the high-permeability fractures, spontaneous imbibition often is - besides gravity - the only production mechanism.

The second process is hydrodynamic dispersion. If more than one chemical component is present, both miscible and immiscible displacement occur (Fig. 1.2), and dispersion governs how well the miscible fluids mix [Dentz et al., 2011]. Thus, dispersion limits the amount of reactants available and hence it limits fast chemical reactions [Dentz et al., 2011].

When performing imbibition studies in sandstone, Jadhunandan and

Morrow [1991] noticed that the composition of injection brine can improve recovery and Yildiz and Morrow [1996] amplified these studies to core flood studies with low-salinity injection. This resulted in a large number of core-flood studies [Webb et al., 2005, 2004, Yildiz and Morrow, 1996, Morrow et al., 1998, Tang and Morrow, 1999, Zhang and Morrow, 2007, Agbalaka et al., 2009] at different conditions (ambient and reservoir condition, secondary and tertiary mode) and tests at the field scale [McGuire et al., 2005] that showed an improvement in recovery in the range of $15-40\%$. Fundamental to this improvement was initially oil-wet conditions, crude oil and the presence of clay particles. Motivated by these results for *clastic* rocks, many experiments for imbibition (for a recent overview see [Austad et al., 2008]) and fewer coreflood studies [Yousef et al., 2010] for *carbonate* rocks were performed. As for the case of clastic rocks, many of these studies showed that simply adding or removing ions to the injection water can significantly increase oil recovery. On contrary to the experiments for clastic rocks, however, it was not the salinity level of the brine itself that was important, but rather the combination of different ions - in particular Ca^{2+}, Mg^{2-} and SO_4^{2+} - that had an impact, and which led to the name *controlled salinity effect*. Tweaking the ion composition might thus be a simple and possibly cheap way to improve recovery in a fractured reservoir. Obviously, the efficiency of this so-called salinity effect depends on how fast the dispersive zone $\delta(t)$ grows depending on the interplay between the flow regimes and the subsurface heterogeneity.

1.2 STRUCTURE AND CONTRIBUTIONS OF THIS THESIS

Despite the outstanding importance of capillarity and dispersion during two-phase flow in fractured (carbonate) reservoirs, most published contributions for two-phase, multicomponent flow ignore either capillary effects or dispersion or both. The reasons for this are clear: Dispersive and capillary effects give rise to highly non-linear second order derivatives that make the numerical and analytical treatment of the governing partial differential equations challenging.
This thesis therefore investigates the influence of capillary forces and dispersion on flow and transport during immiscible two-phase flow. The thesis is equally divided into two parts: In the first part we investigate the influence of capillarity on flow without transport. In the second part, we study flow with transport. More specifically, the rest of this thesis is structured as follows:

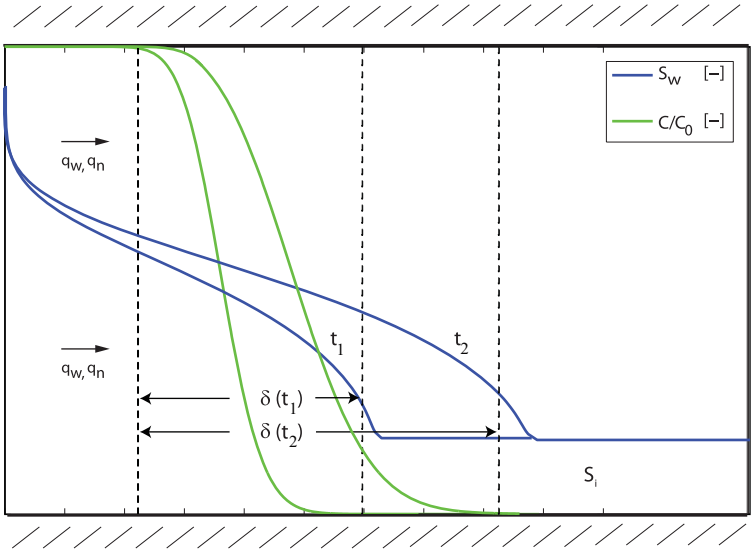

Figure 1.2: Schematic representation of one-dimensional, uni-directional displacement of a non-wetting phase by a wetting phase with saturation S_w with an initial wetting saturation S_i. Behind the wetting front, a mixing zone between the 'old' composition of the wetting phase and the 'new' one of length $\delta(t)$ develops. In most cases, the solute front trails the saturation front (Chapter 4).

1. *Analytical solutions for spontaneous imbibition* In Chapter 2, we repeat known [McWhorter and Sunada, 1990] analytical solutions for two-phase flow with capillarity for arbitrary capillary-hydraulic properties. We show that the boundary conditions are such that these solutions in fact describe the situation of spontaneous co-, and counter-current imbibiton which previously had been overlooked. We demonstrate that the solutions may be interpreted as the long missing capillary analogue to the well-known Buckley-Leverett solutions [Buckley and Leverett, 1942] for viscous dominated flow. This should finalize the decades-long search for analytical solutions for spontaneous imbibition (Table 2.1).

2. *Scaling of spontaneous imbibition for arbitrary petrophysical properties* Based on these analytical solutions, we define a dimensionless time or scaling group that characterizes SI for arbitrary petrophysical properties - a question that was open for more than 90 years. We validate our group against 45 published SI experiments for a wide range of properties. Our results give strong evidence that the standard Darcy model is suitable for describing SI contrary to what recently has been hypothesized. Two key applications of the group are discussed: First, the group can serve as the long sought-after general transfer rate for imbibition used in

dual-porosity models. Second, it is the proportionality constant in imbibition-germination models for plant seeds.

3. *The influence of flow regimes on mixing.* In Chapter 4 we consider flow and transport in a homogeneous, horizontal 1D medium. The growth of the dispersive zone $\delta(t)$ (Fig. 1.2) is influenced by the interplay of three mechanisms: The flow regime, chemical reactions and heterogeneity. In this chapter, we resolve how the flow regime and a simple chemical reaction affects $\delta(t)$. To that end, we derive the first known set of analytical solutions for transport that fully accounts for the effects of capillarity, viscous forces and the effects of hydrodynamic dispersion for the variable two-phase flow field.

4. *Higher order FEFV methods on unstructured grids for transport and two-phase flow* In order to resolve the influence of heterogeneity, flexible numerical methods are imperative. In Chapter 5 we extend higher-order finite-element-finite volume (FEFV) approach to the case of two-phase flow with transport. The higher-order FEFV method that we propose resolves three major challenges in this context, namely the ability to discretize highly fractured reservoirs, the ability to resolve the strong non-linear coupling between fluid and component transport, and finally the ability to give an accurate discretization such that numerical dispersion is small.

Chapters 2-5 contain a literature review for the specific aspect of dispersion and capillarity that is treated in the respective Chapter. We finish this thesis with some conclusions and recommendations for future work in Chapter 6.

Part I

TWO-PHASE FLOW

2

EXACT ANALYTICAL SOLUTIONS HONOURING CAPILLARY PRESSURE: THE BUCKLEY-LEVERETT ANALOGUE

2.1 PROBLEM FORMULATION: TWO-PHASE FLOW AND TRANSPORT

In many of the applications we are interested in - and in particular the controlled-salinity effect [Austad et al., 2010, Yildiz and Morrow, 1996] - the aqueous phase additionally transports components, such as polymers or salts, that change the fluid properties of the aqueous phase. The equations describing the flow of two phases and multiple components through a porous medium can be obtained from combining a continuity equation for both the flow and the components with Darcy's equation for immiscible two-phase flow [Bear, 1972]. The continuity equation for any specific conserved conserved quantity $\mathcal{C}$ is

$$\frac{\partial \mathcal{C}}{\partial t} + \nabla \cdot \mathcal{F} = \mathcal{G}, \tag{2.1}$$

where $\mathcal{F}$ its flux vector, and $\mathcal{G}$ the source/sink term.
We consider immiscible, incompressible, isothermal two-phase flow through a rigid, three dimensional porous medium. For the fluid phase α, flux satisfies $\mathcal{F}_\alpha = \rho_\alpha \mathbf{q}_\alpha$, and thus equation (2.1) becomes

$$\phi \frac{\partial (\rho_\alpha S_\alpha)}{\partial t} = -\nabla \cdot (\rho_\alpha \mathbf{q}_\alpha), \quad S_w + S_n = 1, \tag{2.2}$$

for $\alpha \in \{w, n\}$ where the subscripts w and n denote the aqueous and the non-aqueous phase, respectively. ϕ denotes the porosity, ρ_α the phase density, S_α the phase saturation, and $\mathbf{q}_\alpha$ the phase velocity. We assume that the fluid velocity $\mathbf{q}_\alpha$ is given by the extended Darcy equation [Muskat, 1949]

$$\mathbf{q}_\alpha = -\lambda_\alpha(S_\alpha, C)\mathbf{K}\left(\nabla p_\alpha(S_\alpha, C) - \rho_\alpha \mathbf{g}\right). \tag{2.3}$$

The mobility $\lambda_\alpha = k_{r\alpha}(S_\alpha, C)/\mu_\alpha(C)$ is the ratio between the relative permeability $k_{r\alpha}$ of phase α and its viscosity μ_α, and it describes the

impairment of the flow of one phase by the other. $\mathbf{K}$ is the permeability tensor of the porous medium, p_α is the fluid pressure of phase α, and $\mathbf{g} = [0, 0 - g]^T$ is the gravitational acceleration vector. The fluid pressures are related through the capillary pressure $p_c = p_n - p_w$.
$\mathbf{C}$ is the vector of n components, that represents the varying chemical composition, e.g. water phase salinity, added chemicals such as polymers, or a simple non-partitioning tracer. In the following, we assume that the components

(i) do not alter the porous medium (e.g. through chemical reactions),

(ii) that they do not partition into the other phase, that

(iii) the solute mass flux due to hydrodynamic dispersion within a phase is described by a Fickian model, that

(iv) the volume fraction of the components is small compared to that of the wetting phase, and finally that

(v) the only chemical interaction between the rock and the components can be described by equilibrium adsorption [Pope, 1980].

Then the flux of an individual component C_i, $\quad i = 1, \ldots, n$ contains contributions from advection and dispersion, and the dispersion is modelled by including the effect of the local velocity field [Bear, 1972, Gerritsen and Durlofsky, 2005]:

$$\mathcal{F}_{C_i} = C_i \mathcal{F}_w - \phi S_w \mathbf{D} \nabla C_i, \quad i = 1, \ldots, n. \tag{2.4}$$

where $\mathbf{D}$ is the tensor of hydrodynamic dispersion [Bear, 1972]

$$\mathbf{D} = \alpha_T \left\| \mathbf{q}_w \right\| \delta_{i,j} + (\alpha_L - \alpha_T) \, \mathbf{q}_{w,i} \mathbf{q}_{w,j} / \left\| \mathbf{q}_w \right\|, \qquad 1 \leqslant i, j \leqslant 3. \tag{2.5}$$

Here, $\delta_{i,j}$ is the Kronecker delta, α_L and α_T are the longitudinal and transversal dispersivity constant, respectively, that are determined experimentally. The modelling of $\mathbf{D}$ accounts for the effects of the local velocity fields, but ignores the effects of molecular diffusion. Ignoring molecular diffusion is reasonable since – as long as the flow field is non-zero – molecular diffusion normally is orders of magnitude smaller than dispersive effects [Bear, 1972].

Altogether, we obtain n advection-dispersion-reaction (ADR) equations for n components

$$\begin{aligned}\phi\frac{\partial\left(\rho_w C_i S_w\right)}{\partial t}+\underbrace{\frac{\partial\left(\left(1-\phi\right)\rho_r A_{s,i}\rho_w\right)}{\partial t}}_{\text{Reaction}}=\\ \underbrace{-\nabla\cdot\left(C_i\rho_w q_w\right)}_{\text{Advection}}+\underbrace{\nabla\cdot\left(\phi S_w\rho_w\mathbf{D}\nabla C_i\right)}_{\text{Dispersion}},\end{aligned} \tag{2.6}$$

where we denoted the rock density by ρ_r and the adsorption of C_i per unit mass of rock by $A_{s,i}$. Since the components do not influence each other, we will assume $n = 1$, simplify the notation, and write C and A_i instead of $\mathbf{C}$, and $A_{s,i}$, respectively.
If C describes the concentration of a tracer, the fluid properties of water stay constant, i.e. $\rho_w(C) = \rho_w \equiv \text{const}$, $\mu_w(C) = \mu_w \equiv \text{const}$, whereas for other chemical compositions (C=polymers or salts), empirical relations that can be expressed as analytical expressions or lookup tables may be used (e.g. Herbert et al. [1988]). We further set

$$\Gamma := \frac{(1-\phi)}{\phi}\rho_r A_s. \tag{2.7}$$

For thermodynamic equilibrium, the isotherm is a function of C only, i.e. $\Gamma = \Gamma(C)$ [Bedrikovetsky, 1993], and is described through a linear or non-linear isotherm depending on the components considered.
We assume that the Oberbeck-Boussinesq approximation holds, i.e. that variations in density due to a change in component concentration only need to be taken into account for the gravity term [Nield and Bejan, 2006]. Combining equation (2.3) with the definition of capillary pressure, we obtain a parabolic partial differential equation (PDE) to model the water pressure p_w [Peaceman, 1977]

$$\begin{aligned}\phi c_t\frac{\partial p_w}{\partial t}=\nabla\cdot\Big(&\mathbf{K}\lambda_t(S_w,C)\nabla p_w-\mathbf{K}\lambda_n(S_w,C)\nabla p_c\\ &-\left(\rho_w\lambda_w(S_w,C)+\rho_n\lambda_n(S_w,C)\right)\mathbf{g}\Big),\end{aligned} \tag{2.8}$$

where c_t is the total compressibility of the fluid-rock system, and we set $\lambda_\alpha := k_{r\alpha}/\mu_\alpha$, $\alpha \in \{w, o\}$ and $\lambda_t = \lambda_w + \lambda_n$. Oil and water are assumed to be incompressible which on the reservoir scale leads to $c_t\Delta p_w \ll 1$, such that the left hand side of equation (2.8) can be approximated as zero [Durlofsky, 1993].
We introduce the fractional flow function

$$f(S_w,C)=\left(1+\frac{k_{rn}(S_w)\mu_n}{k_{rw}(S_w,C)\mu_w(C)}\right)^{-1}, \tag{2.9}$$

and the total velocity $\mathbf{q}_t = \mathbf{q}_w + \mathbf{q}_n$. The equation for q_w and S_w can be further simplified to

$$\mathbf{q}_w = f\mathbf{q}_t - \mathbf{K}\frac{fk_{ro}}{\mu_n}\nabla p_c + \frac{\lambda_w\lambda_n}{\lambda_t}(\rho_w - \rho_n)\mathbf{g}, \tag{2.10}$$

and

$$\begin{aligned}\phi\frac{\partial S_w}{\partial t} = &-\nabla\cdot\left(f\mathbf{q}_t\right) + \nabla\cdot\left(\mathbf{K}\frac{fk_{ro}}{\mu_n}\nabla p_c\right)\\ &-\nabla\cdot\left(\frac{\lambda_w\lambda_n}{\lambda_t}(\rho_w-\rho_n)\mathbf{g}\right) + \frac{q_w}{\rho_w}.\end{aligned} \tag{2.11}$$

Equation (2.6) for the components becomes

$$\begin{aligned}&\phi\frac{\partial\left(CS_w\right)}{\partial t} + \frac{\partial\Gamma}{\partial t} = -\nabla\cdot\Big(Cf(S_w,C)\mathbf{q}_t - C\mathbf{K}\frac{fk_{ro}}{\mu_n}(S_w,C)\nabla p_c\\ &+ C\frac{\lambda_w\lambda_n}{\lambda_t}(S_w,C)\mathbf{K}\left(\rho_w(C)-\rho_n\right)\mathbf{g}\Big)\\ &+\nabla\cdot\left(\phi S_w\mathbf{D}\nabla C\right).\end{aligned} \tag{2.12}$$

Before we proceed, three remarks on the assumptions made above are in order. First, equations (2.1) and (2.2) are *laws*, i.e. they can be derived rigorously from first principles [Muskat, 1949]. In contrast, equation (2.3) is an *assumption* that cannot be derived from first principles. This recently has led to intensive research on if equation (2.3) is suitable to describe two-phase flow, and to the question whether and how the parametrizations in Darcy's equation should be supplemented with additional parameters (e.g. [Barenblatt et al., 2003]). We further discuss this in chapter 3, and give strong evidence that for capillary dominated flow no further parameters are necessary, contrary to what recently has been hypothesized.

Secondly, while there is an extensive debate concerning the modelling of dispersion in *single* phase flow (for a recent overview see e.g. [Dentz et al., 2011, Berkowitz, 2002]), the effect of two phases on transport and dispersion is unclear. It has been established that for solute transport in *single* phase flow, the parametrization used for $\mathbf{D}$ in general is no good representation of dispersion on the continuum scale, and that in general no representative values for α_l and α_t can be found. There, the interplay between spatial heterogeneity, temporal fluctuations and local dispersion leads to a macroscopic dispersion effect and to arrival distributions that do not conform to Gaussian solutions which is known as 'anomalous transport'. For transport and *two* phase flow, however, the situation is less clear. For two phase flow without transport and under the condition that capillary effects can be ignored, it has been shown

[Bolster et al., 2009] that the macroscopic dispersion effect becomes negligible. Thus, the effect of spatial heterogeneity and dispersion on a tracer carried by a two phase flow field can be fundamentally different from the single phase case, and its not clear if and under which conditions D can be parametrized according to equation (2.5). We therefore assume that equation (2.5) is reasonable, and develop analytical and numerical methods that may help in evaluating the reliability of a classical dispersion description for transport and two phase flow.
Finally, for most practical applications, like different ion-compositions, assumption (iv) is an excellent approximation [Pope, 1980].
In Part I of this thesis we consider flow only, i.e. the situation where $C = 0$, and the equations (2.11) and (2.8). In Part II, we consider flow with components, i.e. $C > 0$.

2.2 THE BUCKLEY-LEVERETT SOLUTION FOR THE VISCOUS LIMIT

In this section, we repeat some of the main results of the Buckley-Leverett theory that will prove to be useful for our understanding of section 2.2. A full account of the Buckley-Leverett theory can be found in any standard textbook on multiphase flow through porous media (e.g. [Helmig, 1997, Lake, 1989]) and therefore is omitted.
The Buckley-Leverett theory and the corresponding Buckley-Leverett solutions [Buckley and Leverett, 1942] are analytical solutions for equation (2.11) obtained under additional simplifying assumptions, most importantly for the assumption that capillary effects can be ignored. They have proved to be imperative for the understanding of many two-phase flow phenomena, such as enhanced oil recovery techniques or core flood studies [Lake, 1989].
The additional assumptions are:

(1) There are no dissolved components, i.e. $C = 0$,

(2) the porous medium is homogeneous;

(3) the porous medium is one-dimensional and horizontal, such that in particular gravity can be ignored;

(4) there are no sources or sink terms.

This reduces equation (2.11) to

$$\phi \frac{\partial S_w}{\partial t} = -q_t \frac{df}{dS_w} \frac{\partial}{\partial x} S_w + \frac{\partial}{\partial x} \left(D(S_w) \frac{dp_c}{dS_w} \frac{\partial S_w}{\partial t} \right), \tag{2.13}$$

where

$$D(S_w) = -f\lambda_n \frac{dp_c}{dS_w} \tag{2.14}$$

and $D(S_w)$ can be thought of as a 'capillary dispersion coefficient' of the fluid phases. Note that the common extension

$$\frac{\partial p_c}{\partial x} = \frac{dp_c}{dS_w}\frac{\partial S_w}{\partial x}$$

requires that the saturation field is smooth and thus that the medium is homogeneous. This point is further discussed in Chapter 5.
Additionally to (1)-(4) stated above, we make the assumption:

(5) Viscous effects dominate, i.e. capillary pressure effects are negligible.

Then the second term in the right hand side of equation (2.13) becomes zero, and the conservation equation changes its character from a second order parabolic PDE into a first order hyperbolic one

$$\phi\frac{\partial S_w}{\partial t} = -q_t\frac{df}{dS_w}\frac{\partial S_w}{\partial x}. \tag{2.15}$$

For the case where capillary effects can be ignored, we have $p_n = p_w$ and both can be denoted by p. For this case, the name 'fractional flow function' becomes clear, since

$$\begin{aligned} f(S_w) &= \left(1 + \frac{k_{ro}\mu_w}{k_{rw}\mu_n}\right)^{-1} \\ &= \frac{K\lambda_w\frac{\partial p}{\partial x}}{K\lambda_w\frac{\partial p}{\partial x} + K\lambda_n\frac{\partial p}{\partial x}} = \frac{q_w}{q_t}. \end{aligned} \tag{2.16}$$

The PDE (2.15) is supplemented with the following initial and boundary conditions for S_w:

$$\begin{aligned} &S_w(x = 0, t) = S_0 \\ &S_w(x, t = 0) = S_w(\infty, t) = S_{wi}, \end{aligned} \tag{2.17}$$

and for the velocity

$$q_w(x = 0, t) = q_t(t). \tag{2.18}$$

The velocity q_w then satisfies [Buckley and Leverett, 1942]

$$q_w = q_t f'(S_w), \tag{2.19}$$

and consequently the $x(S_w, t)$ profile is (Fig. 2.1b)

$$\begin{aligned} x(S_w, t) &= \int_0^t q_w(S_w)d\tau = \int_0^t q_t(\tau)f'(S_w)d\tau \\ &= \frac{V_w(t)}{\phi}f'(S_w), \end{aligned} \tag{2.20}$$

where $V_w(t)$ is the cumulative volume of the injected wetting phase at time t. Since the velocity depends on the derivative f', it can be non-monotonic if f'' shows non-monotonic behaviour like an s-shape that is typical for many parametrizations of k_{rw} and k_{ro} (Fig. 2.1a). The saturation level S_{wf} at which the shock front occurs can be determined graphically by the Welge tangent [Welge, 1952] (Fig. 2.1a).

2.3 ANALYTICAL SOLUTIONS HONOURING CAPILLARY PRESSURE: THE BUCKLEY-LEVERETT ANALOGUE

Introduction

While an analytical solution to equation (2.9) for viscous dominated flow has long been known - the Buckley-Leverett solution [Buckley and Leverett, 1942] (section 2.2) -, the counterpart for capillary-dominated flow has been missing, and the derivation of solutions for capillary dominated two-phase flow stayed to be the matter of ongoing intensive research over the last decades (Table 2.1).

The reasons for this strong interest are clear: Just like the Buckley-Leverett solutions they are imperative for understanding which parameters control a flow process, and thus are the starting point for understanding enhanced oil recovery (EOR) techniques. They form the basis for scaling groups (chapters 3 and 4), are used to derive transfer functions essential for predicting one of the most important production mechanism in fractured reservoirs, and are important for benchmarking numerical code (chapter 5.) The obtained solutions fall into two categories: In the first category, additional assumptions on equation (2.21) are made, like specific functional forms of $D(S_w)$, that flow occurs under steady-state, and so forth (Table 2.1). In the second category [McWhorter and Sunada, 1990], no additional assumptions on the physics or $D(S_w)$ are made. Instead, an additional boundary condition on the inflow rate is imposed that at the first sight makes the obtained solutions look like another specific case.

In the following, we first introduce the situation of co,- and countercurrent imbibition. Assuming that $(1) - (4)$ holds, we then derive exact

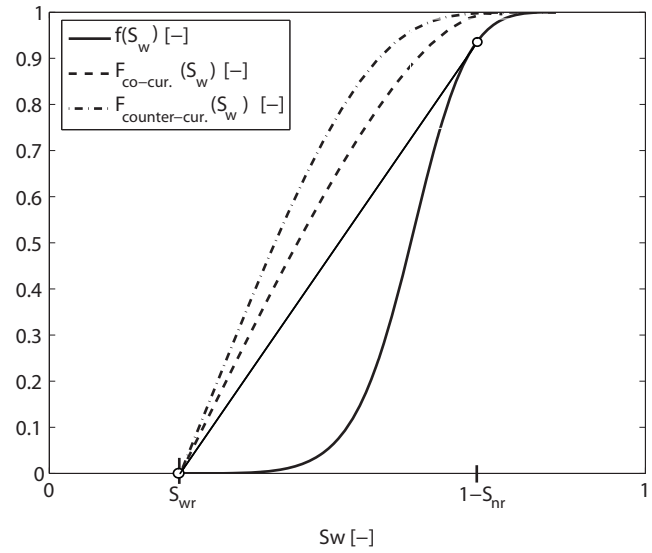

(a)

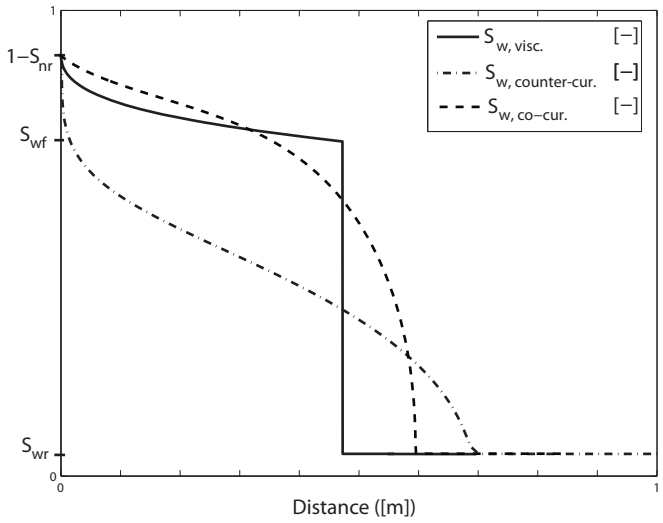

(b)

Figure 2.1: (a) Fractional flow function, and Welge tangent [Welge, 1952] vs. saturation and (b) the resulting saturation profiles vs. distance for counter-current SI and viscous dominated, unidirectional flow. The fractional flow function f for the viscous dominated case is s-shaped which according to equations (2.20) and (2.19) leads to a shock in the saturation profiles at $S_w = S_{wf}$ as determined by the Welge tangent [Welge, 1952]. F can be viewed as the capillary counterpart to f for SI, and is concave. This results in a smooth saturation profile according to equation (2.29).

analytical solutions for equation (2.9) with (2.17) following [McWhorter and Sunada, 1990].

Subsequently, we show that for spontaneous imbibition (SI) the imposed boundary condition is redundant which previously had been overlooked (Table 2.1). Our published results (see Publications, in particular paper [Schmid et al., 2011]) show that the boundary condition is redundant for the case of counter-current imbibition only. However, it

Author and year	Assumption
Fokas and Yortsos [1982], Yortsos and Fokas [1983], Philip [1960], Chen [1988], Ruth and Arthur [2011], Wu and Pan [2003]	Specific Functional Forms for k_{rw}, k_{ro}, p_c
Kashchiev and Firoozabadi [2002]	Steady-State, i.e. $\frac{\partial S_w}{\partial t} = 0$
Li et al. [2003]	Piston-like Displacement, i.e. $F(x,t) = \frac{q_w(x^*,t)}{q_w(0,t)}$
Barenblatt et al. [1990], Zimmerman and Bodvarsson [1989], Tavassoli et al. [2005b], Tavassoli et al. [2005a], Mirzaei-Paiaman et al. [2011]	Approximate Solution for the Weak Form
Handy [1960], Chen et al. [1995], Sanchez Bujanos et al. [1998], Rangel-German and Kovscek [2002]	Existence of an Equivalent Constant Capillary Diffusion Coefficient
Ruth et al. [2007]	Self-Similarity Behaves According to to Specific Functional Form
Cil and Reis [1996], Reis and Cil [1993]	Linear capillary pressure, i.e. $\frac{dp_c}{dx} = \frac{p_c(S_0)}{L}$
Rasmussen and Civan [1998], Civan and Rasmussen [2001]	Asymptotic Approximation of Laplace Transformation for S_w
Zimmerman and Bodvarsson [1991]	Piecewise Linear S_w Profile

Table 2.1: Previously derived analytical solutions for two-phase flow with capillary effects. To resolve the influence of capillarity, all of them need to employ additional, non-essential assumptions that restrict their applicability. On contrary, it can be shown 2.5 that the solution given in [McWhorter and Sunada, 1990] is general. It can be viewed as the 'Buckley-Leverett Analogue' for countercurrent SI (see 2.2). This makes the derivation of further specific solutions unnecessary.

is easy to extend the argument to the case of spontaneous co-current imbibition, which we therefore also state for the sake of completeness. Furthermore, the obtained solutions are the exact early time solutions for spontaneous imbibition, i.e. they are valid until the wetting front reaches the end of the matrix block at some time t^* for which an explicit expression can easily be derived. Finally, we show that the solutions may be viewed as the Buckley-Leverett analogue for two-phase flow with capillarity.

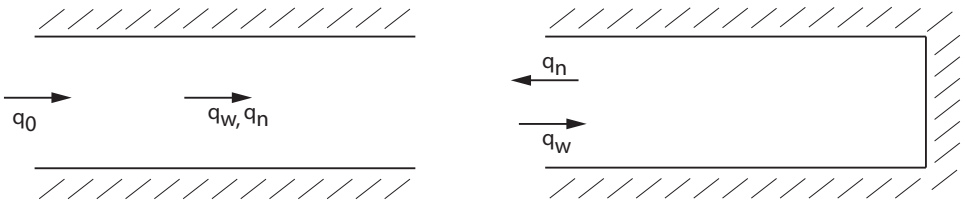

Figure 2.2: Situation of co-current imbibition where the displacement is unidirectional (left), and counter-current imbibition (right).

Co- and countercurrent imbibition

For the case where capillary effects occur, we discern between two different flow scenarios: Co-, and countercurrent imbibition. In the former, the flow occurs in unidirectional manner, i.e. $q_t = q_w + q_n$, and the conservation equation for S_w is given by the PDE (2.13). For the countercurrent case, the tow phases move in opposite directions, i.e. $q_w = -q_n$, and thus $q_t = 0$. This reduces the PDE (2.13) to the nonlinear dispersion equation:

$$\phi \frac{\partial S_w}{\partial t} = \frac{\partial}{\partial x}\Big(D(S_w)\frac{\partial S_w}{\partial x}\Big). \tag{2.21}$$

2.4 EXACT INTEGRAL SOLUTIONS FOR TWO-PHASE FLOW

We derive exact integral solutions for the conservation equation (2.13). The derivation follows [McWhorter and Sunada, 1990], and we only will repeat the main ingredients for obtaining the solutions. Details for all the intermediate steps can be found in [McWhorter and Sunada, 1990]. We consider the initial and boundary conditions (2.17), and additionally assume that the inflow rate for q_w is given by

$$q_0 = q_w(x = 0, t) = At^{-1/2}, \tag{2.22}$$

where A cannot be chosen freely but depends on the fluid and porous media characteristics, and will be determined below. From equation (2.22) we immediately obtain for the net accumulated volume of wetting fluid

$$\begin{aligned} V_w(t) &= \int_0^t (q_0(\tau) - f(S_{wi})q_t)d\tau = \int_0^t q_0(\tau)(1 - f(S_{wi})R)d\tau \\ &= 2A(1 - f(S_{wi})R)t^{+1/2}, \end{aligned} \tag{2.23}$$

where $R = q_t/q_0$. Note that for unidirectional displacement, $q_t = q_0$ and consequently $R = 1$, and for counter-current flow, $q_t = R = 0$. We introduce the similarity variable

$$\lambda = xt^{-1/2}. \tag{2.24}$$

Since the saturation profile $S_w(x,t)$ is a monotone function of (x,t), we have $S_w = S_w(\lambda)$, or $\lambda = \lambda(S_w)$.

Next, we want to introduce a fractional flow function for the case of capillary dominated flow. Obviously, we cannot simply relate q_w to the total flow q_t as we did for $f(S_w)$, since for the counter-current case we have $q_t = 0$. Instead, we can relate $q_w(x,t)$ to the total *inflow* $q_w(x=0,t) = q_0$. Then for the case of co-current imbibition we have $q_t = q_0$, but also can describe counter-current flow. For the case that the initial wetting phase saturation is higher than the residual saturation, the fractional flow function for the viscous case, $f(S_w)$, is bigger than zero. Thus, a part of the wetting phase would flow as described by the *viscous* fractional flow function. Since we are only interested in measuring the flow due to capillary effects, we subtract the contribution of f. Altogether, we define a fractional flow function for spontaneous imbibition as [Philip, 1973, McWhorter, 1971]

$$F(x,t) = \frac{q_w/q_0 - f_i R}{1 - f_i R}, \tag{2.25}$$

where $f_i = f(S_{wi})$, and we have normalized F by $1 - f_i R$ such that $F(x=0,t) = 1$.
Employing the definition of F, equation (2.25), and using that $q_0 = At^{-1/2}$, the conservation equation for S_w, equation (2.13), can be expressed as

$$-\phi \frac{\partial S_w}{\partial t} = At^{-1/2}(1 - f_i R)\frac{\partial F}{\partial x}. \tag{2.26}$$

Then, the similarity variable λ allows equation (2.26) to be written as an ODE [McWhorter and Sunada, 1990]

$$\lambda(S_w) = \frac{2A(1 - f_i R)}{\phi}\frac{dF}{dS_w}. \tag{2.27}$$

Since F is defined in terms of q_w, and q_w depends on S_w, the ODE (2.27) is subject to

$$F = \begin{cases} 1 & \text{for } S_w = S_0 \\ 0 & \text{for } S_w = S_i. \end{cases} \tag{2.28}$$

Employing the definition of λ we can rewrite equation (2.27) to obtain an expression for the $x(S_w, t)$ profile (Fig. 2.1)

$$x(S_w, t) = \frac{2A(1 - f_i R)}{\phi} F'(S_w) t^{1/2}. \tag{2.29}$$

Thus, if A and $F(S_w)$ are known, the an analytical solution for the $x(S_w, t)$ profile can be obtained from equation (2.29).
To eliminate λ from the ODE (2.27), we take the derivative of (2.27) with respect to S_w which after some algebraic manipulations yields a second order ODE for $F(S_w)$

$$\frac{d^2F}{dS_w^2} = -\frac{\phi}{2A^2(1 - f_i R)} \frac{D}{(F - f_n)} \tag{2.30}$$

subject to (2.28). Here, $f_n = (f - f_i)R \cdot (1 - f_i R)^{-1}$ is the normalized fractional flow function. Direct integration of the ODE (2.30) yields the non-linear integral equation [McWhorter and Sunada, 1990]

$$\begin{aligned} F(S_w) = \frac{S_w - S_i}{S_0 - S_i} + \frac{\phi}{2A^2(1 - f_i R)^2} \Bigg\{ \left(1 - \frac{S_w - S_i}{S_0 - S_i}\right) \\ \cdot \int_{S_i}^{S_0} \frac{(\beta - S_i)D}{F - f_n} d\beta - \int_{S_w}^{S_0} \frac{(\beta - S_w)D}{F - f_n} d\beta \Bigg\} \end{aligned} \tag{2.31}$$

In the above equation, A is still unknown. Depending on A, $F'(S_0)$ can show three different behaviours, namely $F'(S_0) < 0$, $F'(S_0) = 0$, and $F'(S_0) > 0$. Equation (2.29) requires that no backflow of the wetting phase occurs which is the case if $F'(S_w) \geqslant 0$ for all $S_{wi} \leqslant S_w \leqslant S_0$. McWhorter and Sunada [1990] demand that $F'(S_w) = 0$. This gives an explicit expression for A,

$$A^2 = \frac{\phi}{2(1 - f_i R)} \int_{S_i}^{S_0} \frac{(S_w - S_0)D(S_w)}{(F - f_n)(S_w)} dS_w. \tag{2.32}$$

Inserting A into equation (2.31) simplifies the expression for F

$$F(S_w) = 1 - \frac{\left(\int_{S_w}^{S_0} \frac{(\beta - S_w)D(\beta)}{(F - f_n)(\beta)} d\beta\right)}{\left(\int_{S_i}^{S_0} \frac{(\beta - S_0)D(\beta)}{(F - f_n)(\beta)} d\beta\right)}. \tag{2.33}$$

This completes the analytical solution. To calculate the $x(S_w, t)$-profile, one first has to calculate F as in (2.33). Equation (2.33) is a non-linear equation, and therefore has to be solved through some iteration (Table 2.2). Then A can be calculated from equation (2.32), and finally $x(S_w, t)$ can be obtained from equation (2.29) (Fig. 2.1). While the physical meaning of F as a fractional flow function is clear from its original definition, (equation (2.25)), the equation for A does not allow for an immediate interpretation of its physical meaning. However, as we will see in the next subsection, A is such that q_0 is the inflow due to spontaneous imbibition, and A therefore quantifies the porous material's ability to spontaneously imbibe.

In order to relate f to fractional flow, p_c had to be negligible (equation (2.16)). For F, no assumptions on p_c, or the relative permeabilities have to be made. Thus, F may be thought of as the capillary counterpart to f in the Buckley-Leverett solutions (Figures 3.3,2.1). The analogue to the Buckley-Leverett theory can be further clarified, if one rewrites the expression for $x(S_w, t)$ in terms of the net accumulated volume of wetting fluid

$$x(S_w, t) = \frac{V_w(t)}{\phi} F'(S_w), \tag{2.34}$$

and consequently

$$q_w = q_0 F'(S_w). \tag{2.35}$$

Thus, equation (2.34) and (2.35) are the analogue to equation (2.20), and (2.19), respectively (Table 2.2). Observe that q_w satisfies equation (2.35), and F is concave since $F'' < 0$ for all S_w. This property of F and F'' is *independent* of the actual parametrization for the capillary-hydraulic properties according to equation (2.30). Thus, the profile $x(S_w, t)$ cannot develop a shock front for any parametrization (Fig. 2.1). This is different from the Buckley-Leverett solutions where a shock front *might* establish depending on the actual parametrization employed and thus on the shape of f (for an example where f is not s-shaped for the parametrization taken from [Bourbiaux and Kalaydjian, 1990] see Figure 3.3). Indeed, if one naively tried to draw a Welge tangent to F

in order to obtain S_{wf} for the case where capillarity is not ignored, the concave shape of F would yield $S_{wf} = S_{wi}$. Mathematically, this is not surprising, as the conservation equation (2.9) is parabolic, and thus all its solutions are smooth.

2.5 EXACT ANALYTICAL SOLUTIONS FOR SPONTANEOUS IMBIBITION

In the previous section, it was assumed that the inflow of the wetting phase adheres to $q_0(t) = At^{-1/2}$, and that A satisfies equation (2.32). Thus, the analytical solution for the x–profile (2.29) derived by McWhorter and Sunada [1990] together with the expression for A and F derived by them, equation (2.33) until very recently was believed to describe the situation of *forced* imbibition with a specific time-dependence of the inflow-rate (Table 2.1). However, as we will show in this section, it is easy to prove that the $t^{-1/2}$ time together with A according to equation (2.32) are exactly such that the analytical solution describes *spontaneous* imbibition, i.e. the situation where an inflow occurs due to the gradient in saturations and the resulting gradients in capillary pressure only. This should finalize the long search for an exact analytical solution for spontaneous imbibition. For the case of counter-current imbibition, this is part of our published results (see Publications, and [Schmid et al., 2011]). However, it is easy to show that the boundary condition also is redundant for the case of co-current imbibition, and for the sake of completeness we will state this part, too.

To see why the boundary condition on the inflow is redundant, we first look at a very simple thought experiment. Consider the situation where we have a rock, saturated with a non-wetting liquid. We now immerse that rock sample in a bath with wetting liquid, but do not apply any pressure, i.e. we do not pump as we would in a core-flood experiment. Let us assume, we want to model what happens to this sample in a Buckley-Leverett system, i.e. gravity and capillary forces are absent. What happens to that immersed sample? The answer is simply: No flow would occur since gravity and capillary pressure are absent. Now, let us consider the same situation, but when capillary pressure is taken into account, and we ask the same question: What happens to the immersed sample? Now the answer is of course: The wetting phase will spontaneously imbibe into the rock. Thus, contrary to the Buckley-Leverett system, for a model with capillary pressure there exists an intrinsic inflow rate through the boundary of the sam-

ple, determined by the capillary-hydraulic properties of the rock-fluid system. In the analytical solution for imbibition presented in the last section, however, we imposed an inflow rate through the boundary condition by specifying q_0 and A. Obviously, this can only be consistent with the intrinsic inflow rate if A and the $\sqrt{t}$–dependence describe the intrinsic inflow rate. Indeed, this can be shown rigorously by exploiting some of the features of the solution.

First, we discuss the $\sqrt{t}$–dependence. Notice that if the inflow occurs spontaneously, then it needs to adhere to Darcy's equation, i.e.

$$\begin{aligned} q_w(x=0,t) &= f(S_0)q_t - D(S_0)\frac{\partial S_w}{\partial x} \\ &= f(S_0)q_w(x=0,t)R - D(S_0)\frac{\partial S_w}{\partial x} \end{aligned} \tag{2.36}$$

which is equivalent with

$$\begin{aligned} q_w(x=0,t) &= -\frac{D(S_0)}{(1-f(S_0)R)}\frac{\partial S_w}{\partial x} \\ &= -\frac{D(S_0)}{(1-f(S_0)R)}\frac{dS_w}{d\lambda}\frac{\partial \lambda}{\partial x} \\ &= -\frac{D(S_0)}{(1-f(S_0)R)}\frac{dS_w}{d\lambda}t^{-1/2}, \end{aligned} \tag{2.37}$$

where the derivatives here denote the right hand side limes $\lim_{x\searrow 0}$ only since the porous medium ends at $x = 0$. Equation (2.37) explains the $t^{-1/2}$-dependency: If Darcy's equation for q_w holds, then the conservation equation with capillarity satisfies (2.13). Non-linear equations of (2.13) allow for self-similar solutions for S_w with similarity variable λ (equation (2.24)), and this in turn allows $q_w(x=0,t)$ to be written as in (2.37).

That $A = -\frac{D(S_0)}{(1-f(S_0)R)}\frac{dS_w}{d\lambda}$ follows from the condition $F'(S_0) = 0$. If an inflow rate according to $q_0 = At^{-1/2}$ is imposed, such that the wetting phase only flows into positive x-direction (Fig. 2.2), this requires $A \geqslant -\frac{D(S_0)}{(1-f(S_0)R)}\frac{dS_w}{d\lambda}$. Otherwise we see from (2.37) that the imposed unidirectional flow of the aqueous phase would be smaller than the spontaneous inflow. Physically, this is only possible, if a fraction of the wetting phase flows back, i.e. $F'(S_0) < 0$ according to equation (2.29). $A = -\frac{D(S_0)}{(1-f(S_0)R)}\frac{dS_w}{d\lambda}$ is therefore the smallest A that does not result in back flow of q_w. Similarly, $F'(S_0) = 0$ is the smallest derivative value that results into $F'(S_w) \geqslant 0$ for all S_w, and thus into q_w only flowing into one direction. On the other hand, $F'(S_0) = 0$ if and only if A is

given by (2.32) such that $A = -\frac{D(S_0)}{(1-f(S_0)R)}\frac{dS_w}{d\lambda}$ and A as in (2.32) must be the same.
Altogether, we arrive at

$$q_0 = q_w(x=0,t) = -\frac{D(S_0)}{(1-f(S_0)R)}\frac{dS_w}{d\lambda}t^{-1/2} = At^{-1/2}, \tag{2.38}$$

and equations (2.29) together with (2.33) and (2.32) are exact analytical solutions for spontaneous imbibition, valid for arbitrary petro-physical properties. A according to (2.32) measures the porous medium's ability to spontaneously imbibe a wetting phase.
Note that for the case that $S_0 \longrightarrow S_{nr}$ we have $f \longrightarrow 0$, but $dpc/dS_w \longrightarrow \infty$, and thus it is not immediately clear that $D(S_{nr})$ in the above is well defined. However, it can be shown analytically [Chen et al., 1992] that $\lim_{S_0 \to S_{nr}} A(S_0) = A_{cr}$ where

$$A_{cr} = \left[\frac{\phi}{2\,(1-f_i)^2}\int_{S_i}^{S_{nr}} \frac{(S_w - S_i)D}{F - f_n}dS_w\right]^{1/2} < \infty. \tag{2.39}$$

Thus, since equation (2.38) holds, it also must be true that $\lim_{S_0 \to S_{nr}} D(S_0) < \infty$.
While the solutions have been derived for an infinite medium according to the initial condition (2.17), the $x-$profile for any time $0 \leqslant t < \infty$ has a finite extend (Fig. 2.1). Thus, the solution is valid in a finite matrix block as long as the water front has not reached the end of the block, which is sometimes referred to as the 'early acting period' of imbibition. The time t^* when the solutions stop to be valid in a finite matrix block of length L can be obtained from setting $x(S_{wi}, t^*) = L$ which yields

$$t^* = \left(\frac{L\phi}{2AF'(S_i)(1-f_iR)}\right)^2. \tag{2.40}$$

For any $t > t^*$, the end of the block influences the saturation profile, and the profiles are no longer given by (2.29).

2.6 SUMMARY

Analytical solutions for spontaneous imbibition are central for many applications. Due to the non-linear parabolic terms many attempts were made to derive analytical solutions or *approximations* valid under *specific* assumptions (Table 2.1).

	Buckley–Leverett for viscous dominated flow	Buckley–Leverett analogue for spontaneous imbibition
x–profiles	$x(S_w, t) = \frac{V_w(t)}{\phi} f'(S_w)$ • V_w: total volume *injected* • f can be s–shaped, shock front might develop	$x(S_w, t) = \frac{V_w(t)}{\phi} F'(S_w)$ • V_w: total volume *imbibed* • F is concave, no shock front
Fractional flow	$f = \frac{q_w}{q_t}$ • viscous dominated flow • co-current flow only • f given by a *linear* equation	$F = \frac{q_w/q_0 - f_i R}{1 - f_i R}$ • capillary dominated flow • co-current flow: $q_w = q_t$ • counter-cur. flow: $q_w = q_0$ • F given by a *nonlinear* equation
Inflow rate	• *chosen* by experimentalist	• *intrinsic* imbibition rate • quantified by A

Table 2.2: Overview and comparison between Buckley–Leverett solution and the Buckley–Leverett analogue for spontaneous imbibition.

- We showed that the solutions derived in [McWhorter and Sunada, 1990] are an *exact* solution for spontaneous co-and counter-current imbibition which previously had been overlooked. They are valid for *general* petrophysical properties. This should finalize the decades-long search for an analytical solution for spontaneous imbibition
- The saturation profiles can be calculated from equation (2.29) with fractional flow function F (equation (2.33)). A given by equation (2.32) measures a porous medium's ability to imbibe.
- The analytical solution may be viewed as the capillary analogue to the Buckley-Leverett equations with fractional flow function F (Table 2.2)f. In contrary to the viscous fractional flow function f, F is concave *independent* of the parametrization used for k_{rw}, k_{rn} and p_c; hence, the saturation profiles cannot develop a shock front, but are smooth (Figure 2.1a, 2.1b).

Based on the analytical solutions for SI, we next derive a non-dimensional time or scaling group for spontaneous imbibition that is valid for arbitrary petrophysical properties.

3

UNIVERSAL SCALING OF SPONTANEOUS IMBIBITION FOR ARBITRARY PETROPHYSICAL PROPERTIES

'I don't know Karen, all these analytical solutions are really nice, but I don't think they can give you anything that experiments or even some smart numerical code can't tell you.'

- A befriended experimentalist during a tea/coffee break

'The value of an idea lies in its usefulness.'

- Thomas A. Edison

If a sugar cube is dipped into tea, the fluid imbibes by spontaneous imbibition, a physical mechanism central to many processes ranging from oil recovery to seed-germination. The observation of the sugar-cube already reveals a characteristic of SI, namely an initially fast in-rush of the fluid that quickly slows down - i.e. a $\sqrt{t}$—scaling in time. While this behaviour has been known for more than 90 years, several dozen scaling groups have been proposed in an attempt to resolve the influence of other key parameters like wetting characteristics or viscosity ratios. To resolve this influence, the complex underlying nonlinear physics and the sheer number of possible parameter combinations, make an approach solely based on experiments or numerical simulations infeasible, and the influence of other key parameters needs to be resolved analytically. Previously, this was not possible since a general analytical solution for SI was missing.

In this chapter, we will rigorously derive the first scaling group for counter-current SI that characterizes the influence of all parameters included in the Darcy formulation, and provide the first closed theory to predict the validity of specialized groups. Furthermore, we will give strong evidence that the standard Darcy formulation is suitable for describing SI, contrary to what has been hypothesized. Scaling groups are central for many applications, and we will present two key

applications: First, the group can serve as the long sought-after general transfer rate for imbibition used in dual-porosity models. Second, it is the so far missing proportionality constant in imbibition-germination models for plant seeds. Note that throughout this chapter, we will focus on spontaneous, counter-current SI only, and will denote it as SI for simplicity.

3.1 INTRODUCTION

Spontaneous imbibition occurs if a wetting fluid (like water or brine) enters a porous medium, and displaces a non-wetting fluid (like oil, gas or CO_2), driven by capillary forces only. It is a process that is of crucial importance for the evaluation of the wettability of a rock [Jadhunandan and Morrow, 1991, Morrow et al., 1994], and also is the key production mechanism in the world's largest remaining oil reservoirs [Morrow and Mason, 2001]. Over 60 % of the world's remaining oil reserves are stored in naturally fractured carbonate rocks [Beydoun, 1998]. There, the oil is locked in the low permeability rock matrix, surrounded by high permeability fractures, and SI of water is often the only way by which the oil is displaced from the rock matrix into the fractures and can be produced. It also is important for the trapping of CO_2 in coal seams and the creation of methane [Chaturvedi et al., 2009], steam migration in geothermal reservoirs [Li and Horne, 2009], the mechanical stability and distribution of gas hydrates [Clennell et al., 1999, Anderson et al., 2009].

Scaling groups are used to characterize the influence of key parameters on SI, and are essential in any context where SI needs to be understood. For example, they are the bottleneck for an appropriate upscaling of laboratory data [Morrow and Mason, 2001], lie at the heart of modelling and simulating flow in fractured and heterogeneous reservoirs [Barenblatt et al., 1960, Warren and Root, 1963], or are needed as the starting point for evaluating the feasibility of water injection into geothermal reservoirs [Li and Horne, 2009].

The enormous practical importance of SI and scaling groups has led to major research activity in that field. In order to resolve how key parameters influence SI and how they should be incorporated into specific scaling groups, a great number of numerical studies on the continuum scale [Pooladi-Darvish and Firoozabadi, 2000, Behbahani et al., 2006, Ruth et al., 2000, Standnes, 2006, Hazlett, 1995, Delijani and Pishvaie, 2010] and the molecular scale [Martic et al., 2002], experiments (see

Tables 3.3,3.4,3.6), and analytical solutions for special cases of SI (Table 2.1) have been proposed (Table 3.1). As mentioned above, however, despite this intense research activity, and although the research on scaling groups and SI spans more than 90 years [Lucas, 1918, Washburn, 1921], not even apparently simple questions - like the influence of viscosity ratios on SI - have been resolved satisfactorily.

In this chapter we derive the first universal scaling group for spontaneous, counter-current imbibition for arbitrary petrophysical properties. We show the validity of our group by applying it to 45 published SI studies for water-oil and water-air experiments for a wide range of viscosity ratios, initial water content, wettability states, different rock types and different boundary conditions (Tables 3.3,3.4,3.6).

Our group is derived rigorously from the general, exact solution of the two-phase Darcy equation for the case of counter-current imbibition, namely the solutions Buckley-Leverett analogue derived in [McWhorter and Sunada, 1990] (section 2.3). No assumptions other than those needed for Darcy's model are made. No fitting parameters are introduced. All the information present in the two-phase Darcy equation is incorporated into our group. Consequently, our group acts as a 'master equation' that contains many of the previously defined scaling groups as special cases (Tables 3.1, and 3.2). Due to the specialized nature of previously defined scaling groups, the question of their range of validity was often left wide open, and we demonstrate how the generality of our approach allows the prediction of the validity range of specialized groups by the derivation of a proportionality constant c (Table 3.2). This is the first predictive theory for evaluating scaling groups.

Furthermore, we show that Handy's conjecture is wrong. In an attempt to link scaling groups to some physical property of the SI process, [Handy, 1960] and subsequent authors [Schembre et al., 1998, Cil et al., 1998, Li et al., 2002, Babadagli and Zeidani, 2004, Li and Horne, 2009] speculated that SI can be characterized by the frontal movement of the wetting phase. We show rigorously that although a scaling based on the frontal movement gives better results than some previously defined methods, SI systems are best characterized by the total volume of the wetting phase imbibed.

Besides resolving these crucial 'practical' questions on how key petrophysical properties affect SI, our scaling group serves as a theoretical tool to assess the validity of Darcy's equation for describing SI. During recent years, the theoretical framework on how to model SI itself has

been debated. Both in the oil-community [Barenblatt et al., 2003], and in related areas such as hydrology, physics and engineering [Mirzaei and Das, 2007, Le Guen and Kovscek, 2006, Hall, 2007], it has been proposed that the extended Darcy model is not suitable for describing SI, and should be replaced by some extended Darcy model ([Mirzaei and Das, 2007, Barenblatt et al., 2003], for a recent overview see [Hall, 2007]). Since our group is based on the validity of Darcy's equation for two-phase flow, the ability of our group to correlate experimental data can be used to measure whether the Darcy formulation is suitable to describe SI, and our results strongly suggest that accounting for these non-Darcy effects is unnecessary.
Finally, we show that an exponential model for mass transfer closely correlates experimental data independent of petrophysical properties. This yields the first general expression for mass transfer due to SI.
The remainder of this chapter is structured as follows: In section 3.2 we review known scaling groups, and related open questions. In section 3.3 we introduce two scaling groups that comprise all the information present in the two-phase Darcy formulation: The first one, $t_{d,front}$ based on an analytical expression for the frontal movement of the wetting phase, and the second one, $t_{d,inflow}$ based on on an analytical expression for the total volume of wetting phase imbibed. We correlate 45 published SI experiments with both groups, and show that while $t_{d,front}$ already strongly improves previously proposed groups, it is $t_{d,inflow}$ that gives the best results, contrary to what has been conjectured by Handy [1960]. Since $t_{d,inflow}$ has a general form, this strongly indicates that the standard Darcy model is suitable for describing SI, in contrast to what has been speculated [Barenblatt et al., 2003, Mirzaei and Das, 2007, Hall, 2007]. In section 3.7 we extend the results to the case of mixed-wet systems. In section 3.8 we show how this can be applied to obtain a mass-transfer function for dual-porosity models that is valid for arbitrary petrophysical properties and therefore overcomes all the major limitations of previously proposed transfer functions for SI. We finish the chapter with some conclusions.

3.2 PREVIOUSLY PROPOSED SCALING GROUPS AND OPEN QUESTIONS

Introduction

Scaling groups for SI were derived mainly by two ways. Either a curve was fitted against a large body of experimental data where only one

parameter, (like the characteristic length) was varied (e.g. [Zhang et al., 1996]), or simplifying theoretical assumptions in the form of scaling laws [Rapoport, 1955, Mattax and Kyte, 1962] or other non-essential assumptions (Table 2.1) were employed. Both approaches yield scaling groups whose applicability is strongly restricted. On the one hand, a general theoretical understanding on which conditions are required that a certain group is applicable, and when it would fail were often left unanswered. On the other hand, the incorporation of three aspects into scaling groups remain open which play a central role in practical applications, namely the influence of viscosity ratios, the influence of the initial water saturation, and the influence of wettability effects.

Viscosity ratios

The viscosities of the phases act as a weighting factor for the relative permeabilities, and it is unclear how this weighting should be formulated depending on the viscosity ratio. It has long been known [Lucas, 1918, Washburn, 1921] that for a negligible non-wetting phase viscosity μ_n, SI is proportional to $1/\sqrt{\mu_w}$. Motivated by this result, a scaling group for two-phase flow was proposed that assumed a scaling proportional to $1/\sqrt{\mu_w \mu_n}$ [Ma et al., 1997]. However, a great number of experimental studies [Behbahani and Blunt, 2005, Fischer and Morrow, 2006, Fischer et al., 2006] and numerical results [Behbahani and Blunt, 2005] showed that for a viscid non-wetting phase, a scaling with the geometric mean does not hold in general. Although subsequently many attempts have been made to generalize predictions for arbitrary viscosity ratios [Ruth et al., 2004, Høgnesen et al., 2004, Fischer and Morrow, 2006, Fischer et al., 2006, Mason et al., 2010, Standnes, 2010b,a, Reis and Cil, 1993], a scaling group for arbitrary viscosity ratios, based on rigorous physical considerations, remains unknown. Similarly, the question on how a single relative permeability value should be chosen in dependence of the viscosity ratio and such that it characterizes the strong non-linear dependence on the wetting saturation over the whole saturation range remains open [Morrow and Mason, 2001, Mason et al., 2010].

Initial water saturation

The influence of initial water saturation S_{wi} is two-fold: On the one side, if a rock is aged at a certain S_{wi}, the ageing time t_a, the rock and the oil properties will influence the capillary-hydraulic properties depending

on S_{wi} [Zhou et al., 2000, Xie and Morrow, 2001, Graue et al., 1999]. This is discussed in the next subsection. On the other hand, if a rock is not aged, S_{wi} does not change the basic petrophysical properties [Narahara et al., 1993], and can be at either residual water saturation S_{wr} or above. If $S_{wi} > S_{wr}$, then competition occurs between the low capillary pressure force and the high phase mobilities.
Also, since the establishment of an $S_{wi} > 0$ can be difficult, many SI experiments are performed for the case where the core is fully saturated with oil or air [Zhang et al., 1996, Zhou et al., 2002], i.e. $S_{wr} = 0$, while one would like to understand SI behavior under actual reservoir conditions where $S_{wi} > 0$.
So far, both the effect of competition and the effect of different S_{wr}'s have only been characterized for cases where the ratio of non-wetting to wetting phase viscosity is close to one, and if the capillary pressure and the wetting behavior can be characterized by a single value [Li and Horne, 2006], which is unlikely in realistic porous media [Valvatne and Blunt, 2004, Jackson et al., 2003]; it also blurs the difference between different rock types, i.e. different capillary-hydraulic properties.

Wettability effects & mixed-wet systems

Capillary pressure curves and the phase mobilities not only depend on the fluids, but also on the geometry of the pore structure [Valvatne and Blunt, 2004, Jackson et al., 2003]. Consequently, even for the water-wet case, they are different for different materials (Fig. 3.3,3.2). Up to now, however, scaling groups try to characterize the influence of capillary pressure and wetting by some single value that is representative of the entire porous medium [Tavassoli et al., 2005a, Li and Horne, 2006, Marmur, 2003, Zhou et al., 2002].
Even for the same rock type, however, this approach is unsatisfactory if different wettabilities need to be compared. If a rock sample is aged at different initial water saturations, S_{wi} controls how many pores are exposed to the non-wetting phase, and thus S_{wi} controls how many pores can change their wettability by the adsorption of the non-wetting phase [Zhou et al., 2000, Xie and Morrow, 2001, Graue et al., 1999]. At the end of the ageing process, the rock contains both water-wet (WW), and oil-wet (OW) pores, known as 'mixed-wet' (MW) behavior [Salathiel, 1973]. MW systems are of enormous practical importance since the majority of the oil reservoirs are not WW, but MW [Anderson, 1987a,b]. SI experiments for MW systems show differences in recov-

ery times that can be several orders of magnitude compared to WW experiments [Zhou et al., 2000, Xie and Morrow, 2001, Graue et al., 1999], specific relative permeabilities and p_c curves (Figures 3.7a, 3.7b), and are also characterized by two different residual oil saturations (Fig. 3.8). Although several attempts have been made to develop scaling groups for a MW scenario, most of them try to lump these different effects - differences in recovery times, different S_{nr}'s, particular relative permeabilities - into a single 'wettability factor' [Cil et al., 1998, Gupta and Civan, 1994, Zhou et al., 2002, Lavi et al., 2008, Xie and Morrow, 2001]. This factor is derived from a mere empirical fit to experiments, lacks any physical meaning, does not allow any theoretical insights and has only limited predictive powers [Anderson, 1987a, Behbahani and Blunt, 2005, Marmur, 2003].

Can Darcy's model describe SI?

In addition to these three practical issues discussed in the previous sections, the theoretical framework for describing SI itself has recently become the centre of a debate in physics and engineering. While the single-phase Darcy model can be derived rigorously from first principles [Hassanizadeh, 1986], this is not the case for the multiphase extension of Darcy's equation [Hassanizadeh and Gray, 1993, Muskat, 1949], and it has been proposed that it should be replaced by some anomalous diffusion model [Barenblatt et al., 2003] (for recent reviews see [Hall, 2007, O'Carroll et al., 2010]). A number of alternative formulations have been proposed [Hall, 2007, O'Carroll et al., 2010] that introduce additional parameters into the classical Darcy formulation. But it is unclear, if and under which conditions which parameters should additionally be taken into account.

The Buckley-Leverett analogue, universal scaling group and the validity of Darcy's equation

In the following, we rigorously derive a scaling group that is valid for arbitrary petrophysical properties. For the first time, all three aforementioned practical aspects - the influence of viscosity ratios, the influence of initial water saturation, and the influence of wetting characteristics - will be accounted for.
Our scaling group is derived rigorously from an exact solution of the extended Darcy equation (Chapter 2). We do not make any assumptions

other than those needed for Darcy's model. We do not introduce any fitting parameters. We show that our group is a 'master equation' for scaling groups, that contains many of the previously defined groups as special cases, and we demonstrate how the generality of our approach allows the prediction of the range of validity of specialized groups (Table 3.2). Furthermore, we will give strong evidence that the classical Darcy description for SI is appropriate.

3.3 DEFINING A UNIVERSAL SCALING GROUP FOR SI: CUMULATIVE INFLOW VS. FRONTAL MOVEMENT

Introduction

The analytical solutions for two-phase flow with capillarity introduced in section 2.3 can be used to introduce a scaling group that incorporates all the information present in the two-phase Darcy equation. There are two possibilities: The scaling group can be based on the frontal movement of the wetting phase, or on the cumulative inflow $Q_w(t)$. Handy [1960] and subsequent authors [Cil et al., 1998, Schembre et al., 1998, Li et al., 2002, Babadagli and Zeidani, 2004] conjectured that it is the frontal movement that characterizes imbibition. Since we can resolve the nonlinear equations exactly, we can rigorously show that although this scaling already gives correlations superior to some of the previously defined scaling groups, SI is characterized best by the cumulative inflow.
To derive a scaling group from equation (2.29), we first normalize x by the characteristic length L_c through x/L_c where [Ma et al., 1997]

$$L_c = \sqrt{\frac{V_b}{\sum_{i=1}^{n} A_i/l_{A_i}}}. \tag{3.1}$$

V_b is the bulk volume of the matrix, A_i the area open to imbibition with respect to the ith direction, and l_{A_i} is the distance that the imbibition front travels from the imbibition face to the no-flow boundary (Fig. 3.1). While the question of how to incorporate the influence of viscosity ratios, wettability information, and so forth into scaling groups is open, the correct incorporation of different boundary conditions (Fig. 3.1) with the help of L_c has been confirmed [Ma et al., 1997, Zhang et al., 1996]. For cases where A_i is not constant in time, but grows because of for example slowly filling fractures, this time-dependency needs to be included in L_c [Rangel-German and Kovscek, 2002, 2006]. However, this

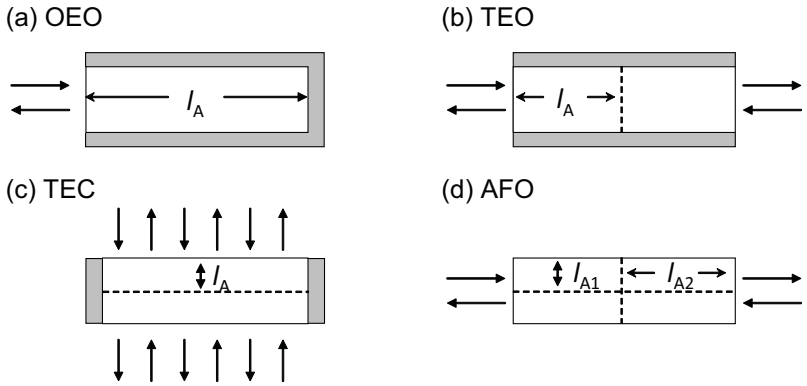

Figure 3.1: Counter-current SI in cores with different boundary conditions. (a) one end open (OEO), (b) two-ends open (TEO), (c) two ends closed (TEC), and (d) all faces open (AFO).

dependency can be treated independently of petrophysical properties, and therefore we will not discuss it here.
In the following, we first will introduce two new scaling groups - one based on the frontal movement of the wetting front, one based on the cumulative inflow of the wetting phase. Subsequently, we compare them to the commonly used group by Ma et al. [1997] for the data set shown in Tables 3.3 and 3.4. Then we will demonstrate how the generality of our approach can be used to predict the range of validity of specialized groups, and how the generality of the scaling group based on Q_w can help to measure the validity of Darcy's equation.

Scaling groups

We first introduce the scaling group $t_{d,front}$ that is based on the frontal movement. The position of the front follows from equation (2.29) with $S_w = S_{wi}$, and motivates the introduction of $t_{d,front}$ as

$$t_{d,front} = \left(\frac{x_{front}(t)}{L_c}\right)^2 = \left(\frac{2A}{\phi L_c} F'(S_{wi})\right)^2 t. \tag{3.2}$$

If in contrast the normalized cumulative inflow $Q_w(t)/(\phi L_c)$ is used, then we obtain

$$\begin{aligned} t_{d,inflow} &= \left(\frac{Q_w(t)}{\phi L_c}\right)^2 = \left(\frac{2A}{\phi L_c}\right)^2 t \\ &= \tau_c t. \end{aligned} \tag{3.3}$$

Two remarks are in order. First, the above scaling groups try to predict the influence on recovery over time if all the parameters are known. This approach is fundamentally different from dimensionless groups that try to predict parameters like S_{nr} from dimensionless groups (e.g.

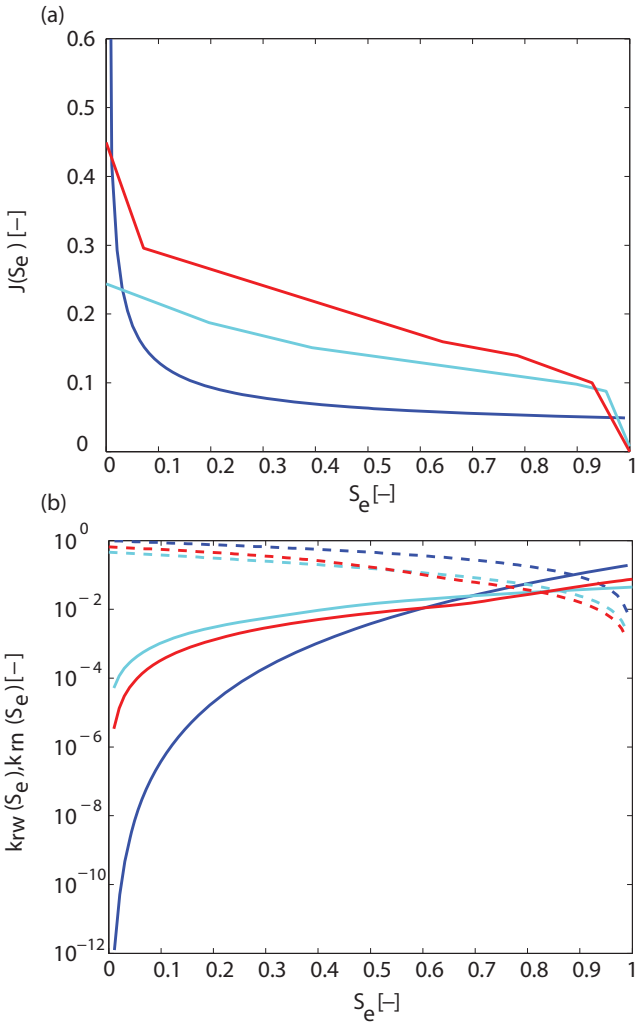

Figure 3.2: Capillary-hydraulic properties vs. effective saturation. Capillary-hydraulic properties of Berea sandstone and a synthetic porous material (-) [Valvatne and Blunt, 2004] from pore-scale predictions , a history match that assumes a Darcy model for sandstone (-) [Bourbiaux and Kalaydjian, 1990], and a non-Darcy-model [Schembre and Kovscek, 2006] for diatomite (-). (a) Dimensionless J-function. (b) Relative permeability for the wetting (—) and non-wetting phase (——).

[Anton and Hilfer, 1999]).

Second, the scaling group based on normalized volume conceptually is the same as the one used EOR for viscous dominated flow (e.g. [Lake, 1989, Chapter 5]). The difference of course lies in the fact that we consider capillary driven flow. This results in a $\sqrt{t}$—dependency of the inflow (Chapter 2.5), and requires that $Q_w(t)$ be squared contrary to the t—dependency for viscous dominated floods where $Q_w(t)$ is not squared.

We next show that $t_{d,inflow}$ is suited best to describe SI by correlating 42 published experiments, and comparing $t_{d,front}$, $t_{d,inflow}$ and the often used group by Ma et al. [1997]. This comparison shows that $t_{d,inflow}$ is

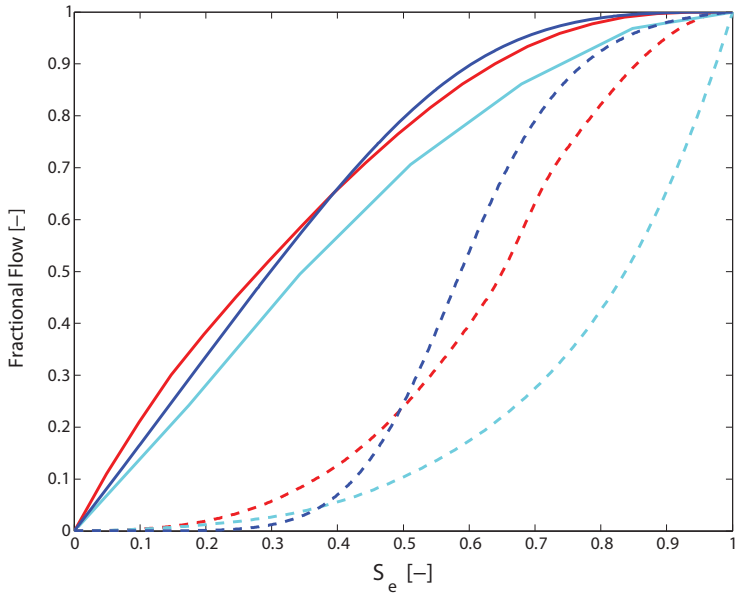

Figure 3.3: Fractional flow functions f (——) without capillarity and its capillary counterpart F (—) vs. effective saturation. The three cases are for pore-scale predicted [Valvatne and Blunt, 2004] capillary pressure and relative permeability functions for Berea sandstone and a synthetic porous material (-) and parameter set AA01, a history match that assumes a Darcy model for sandstone (-) [Bourbiaux and Kalaydjian, 1990] and parameter set GVB-3, and a non-Darcy-model [Schembre and Kovscek, 2006] for diatomite (-) and parameter set Z-2. The parameter sets are listed in Tables 3.3 and 3.4, and the capillary pressure and relative permeability functions are shown in Figure 3.2.

the general scaling group for SI, and forms the so far missing center piece for upscaling, modelling and simulating diverse systems where SI plays a role. τ_c can be thought of as an inverse characteristic time that quantifies both the influence of the capillary-hydraulic properties and the characteristic physical dimensions. Also, $t_{d,inflow}$ can be used as a theoretical tool to assess the validity of Darcy's equation.

3.4 VALIDITY OF THE UNIVERSAL SCALING GROUP FOR THE WATER-WET CASE

To demonstrate the validity of our scaling groups, we correlated them with 42 published imbibition studies for water-wet conditions. (For the correlation of the different degrees of mixed-wet systems, see section 3.7). In the experiments the recovery Rec of the non-wetting phase was measured over time, and we correlated the physical time with $t_{d,frontal}$ and $t_{d,inflow}$, respectively. The experimental data sets were chosen such that the three central open aspects of scaling groups - a wide range of viscosity ratios with the special case of μ_n tending towards zero, the

presence of an initial wetting phase, and different capillary-hydraulic properties - are covered. The experiments were performed on three different porous materials, a synthetic porous medium, Berea sandstone, and diatomite (Fig. 3.2), a wide range of non-wetting phase to wetting phase viscosity ratios ($0.008 \leqslant \mu_{nw}/\mu_w \leqslant 64$), initial water content ($0\% \leqslant S_0 \leqslant 40\%$), characteristic length-scales ($0.54\,cm \leqslant L_c \leqslant 40\,cm$), and water potential ($18\% \leqslant 1 - S_{wi} - S_{nr} \leqslant 70\%$, where S_{nr} is the residual saturation of the non-wetting phase). The wetting phase was water and the non-wetting phase oil or air. Tables 3.3 and 3.4 list all experimental conditions.

Figures 3.4 and 3.5 show the correlation of the data with $t_{d,inflow}$ and $t_{d,front}$. For comparison, we also correlated the data with one of the most commonly used scaling groups $t_{d,Ma}$ (Figures 3.4 and 3.5, and Table 3.1 for the definition of); the improvement is significant and immediately apparent. The correlation achieved by $t_{d,inflow}$ gives the best results and indicates that SI is characterized best by the cumulative inflow and not by the frontal movement that previous authors assumed as a starting point for deriving specialized scaling groups [Handy, 1960, Cil et al., 1998, Schembre et al., 1998, Li et al., 2002, Babadagli and Zeidani, 2004]. In the remaining parts of this thesis we therefore will only discuss $t_{d,inflow}$, and refer to it as t_d for simplicity. t_d reduces the maximal horizontal scatter (i.e. the one for a fixed recovery rate) from a factor of greater than 100 down to approximately 5, and the maximal vertical scatter (i.e. the one for a fixed t_d) from approximately 0.8 to 0.3. This is a remarkably good result given the widely different experimental conditions and thus experimental noise.

To further improve the scaling, one should use the capillary-hydraulic properties for the specific sample when calculating t_d. Most data sets available in the literature only report SI measurements or (k_{rw}, k_{rn}) relationships, or p_c curves. In order to calculate t_d we therefore assumed that the (k_{rw}, k_{rn}, p_c) sets measured for a certain rock type are representative for a given material, see section 3.6.

It is also interesting to note that the data in Figure 3.5 (b) scatters around the curve given by the analytical solution that has been calculated for data where the sample-specific capillary-hydraulic properties are known. It is not clear, whether this is true only for particular data sets, or shows that the analytical solution is a 'master curve' for early times on which all data would collapse if sample-specific predictions for the capillary-hydraulic properties were known. One would have to calculate the analytical prediction for more data sets where the sample

specific properties are known. As we explained, however, complete data sets are rare.

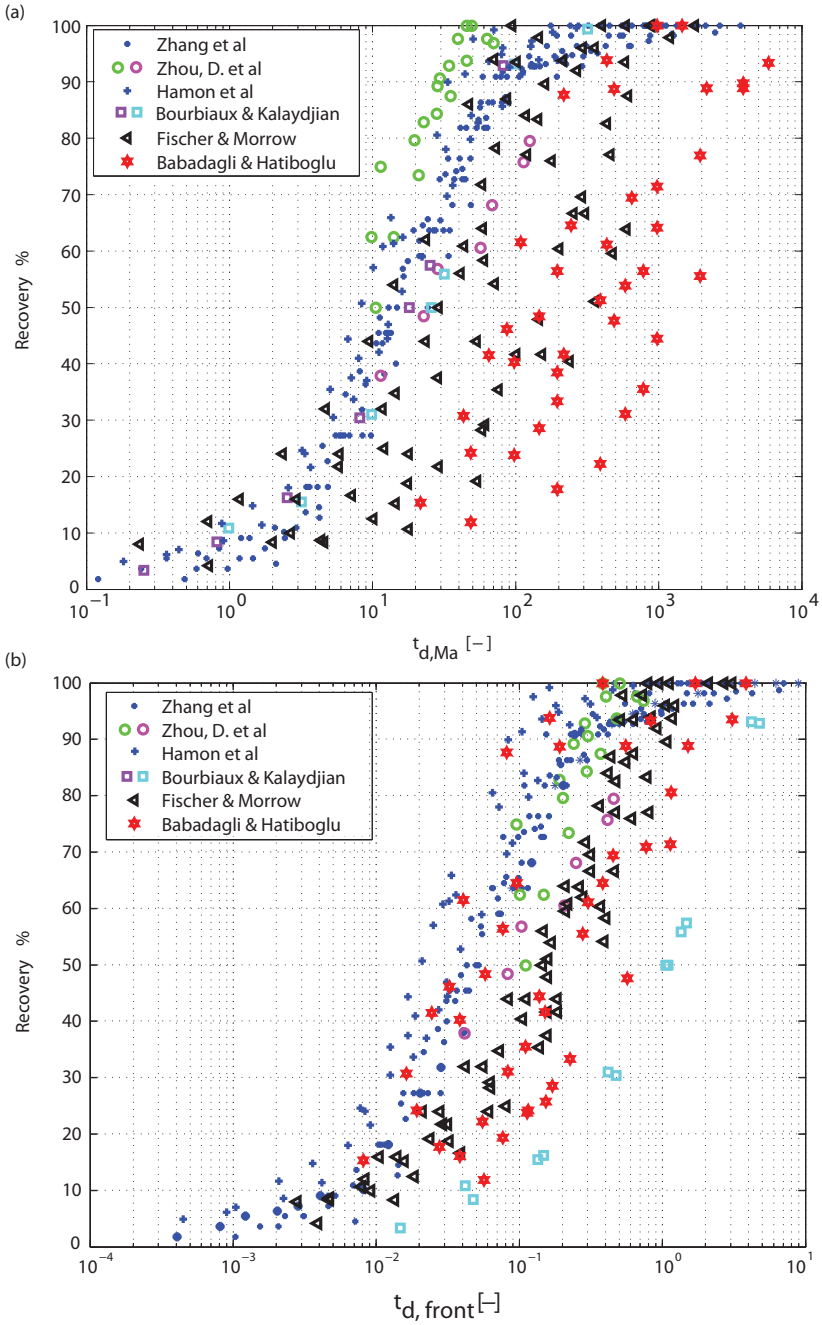

Figure 3.4: Recovery offg the displaced fluid vs. dimensionless time. (a) Time scaled according to Ma et al. [1997]. The scaling does not result in the collapse of the data onto a single curve. The scaling group can only result in a good correlation if the proportionality constant c (Table 3.2) is the same for all the data sets. (b) Time scaled with $t_{d,front}$. This scaling results in an improved scaling compared to the one shown in (a).

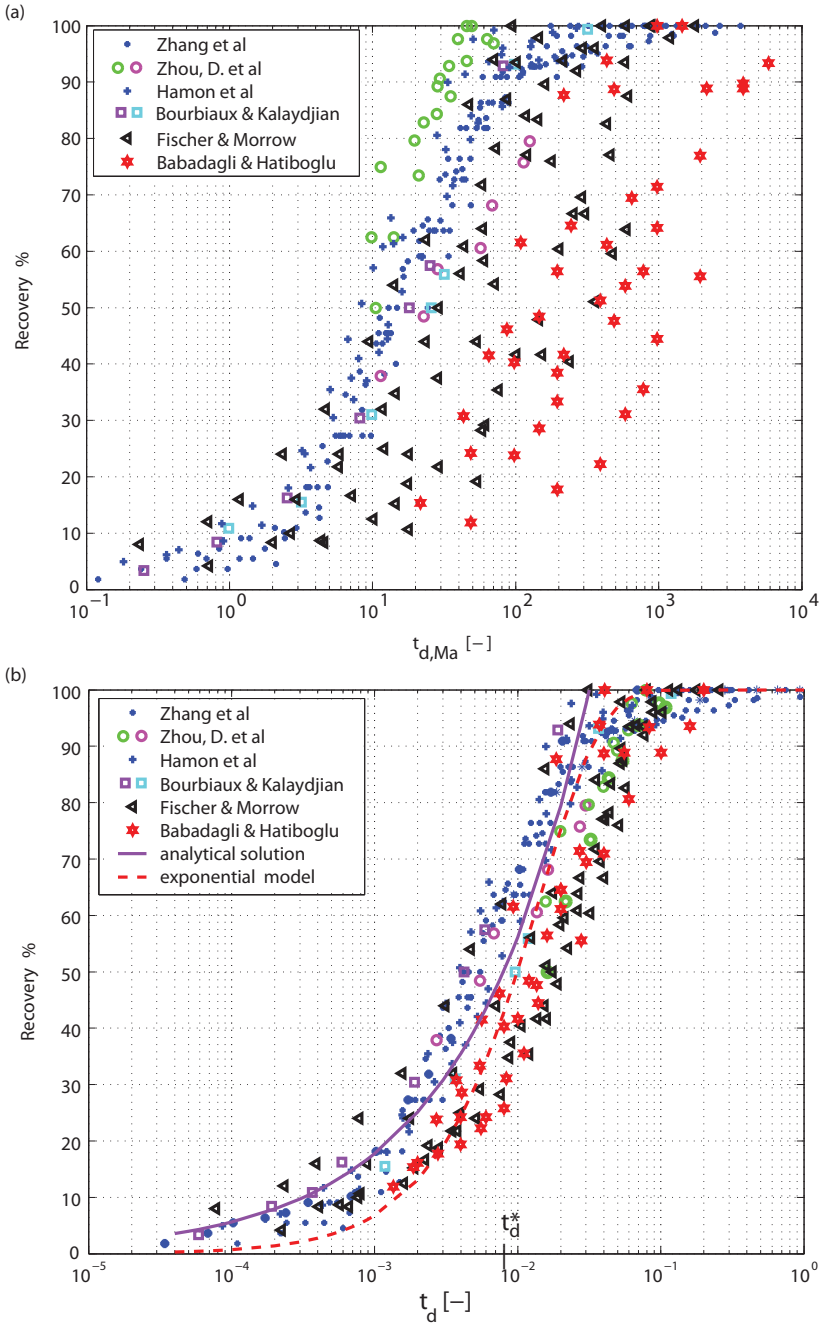

Figure 3.5: Recovery of the displaced fluid vs. dimensionless time. (a) Time scaled according to Ma et al. [1997] (repeated from Fig. 3.4 (a)). The scaling does not result in the collapse of the data onto a single curve. (b) Time scaled with $t_{d,inflow}$. This scaling results into a curve with little scatter of the data that strongly reduces both the horizontal and the vertical scatter compared to $t_{d,Ma}$ and $t_{d,front}$ (Fig. 3.4 (b)). This indicates that SI is best described by the cumulative inflow of the wetting phase rather than the frontal movement. Since $t_{d,inflow}$ comprises all the data present in the Darcy formulation this also indicates that the Darcy model is suitable for modelling SI. The analytical solution is valid as long as $t_d \leqslant t_d^* = \tau_c t^*$. To correlate the behaviour for the whole time range, an exponential model [Aronofsky et al., 1958] is used.

3.5 PREDICTION OF THE VALIDITY OF SPECIALIZED GROUPS

The Lucas-Washburn correlation together with some of the previously defined scaling groups are listed in Table 3.1. Previous scaling groups are related to our scaling group through a proportionality factor c (Table 3.2). Since our group is the general one, explicit expressions for c can be derived. It is now apparent that previous authors (unknowingly) derived successively better approximations to the integral in equation (2.32), making the proportionality constant c increasingly simple. Many of the previously derived t_d can be obtained from simple back-of-the-envelope calculations as special cases of equation (3.3) (see Appendix A).

Equation (3.3) can also be used to derive new scaling groups that are tailored for a specific SI system by using an approximation for A that is appropriate for that specific case. The ability of such a special t_d to correlate a set of experiments depends on the similarity of c for the individual data sets, and thus allows for a rigorous prediction of their validity and a judgment as to which parameters are negligible. This property can be used to derive the validity of some of the phenomenologically derived groups like that of [Ma et al., 1997] (Table 3.2, Figures 3.4 and 3.5). The scaling group in Figure 3.5(a) can only give a good correlation if the proportionality constant c (Table 3.2) is similar for the different data sets. This is the case for some of the SI experiments on sandstone ($*$ in Fig. 3.5(a)) and the synthetic material ($+$ in Fig. 3.5(a)) from which Ma et al. [1997] derived the correlation phenomenologically. Here, the viscosity ratio is approximately one, the initial fluid content is similar, and the capillary hydraulic properties were the same. These conditions result in a similar functional form of F, similar integral boundaries, and the same integrand for c, respectively. Depending on which assumption is violated, five sub-groups different from the ($*$,$+$)-curve emerge: The sub-group for (i) different S_0, different capillary-hydraulic properties (diatomite with (ii) high and (iii) low μ_{nw}/μ_w), (iv) sandstone with strongly varying μ_n/μ_w, and (v) sandstone containing gas, i.e. a non-wetting phase with neglectable μ_n.

3.6 DO WE NEED DYNAMIC EFFECTS IN p_c TO MODEL SI?

While the main part of this chapter is dedicated to derive the first scaling group that rigorously includes all the information given in the standard Darcy formulation, the validity of t_d for such a wide range

Author	Dimensionless time	Assumption
Lucas [1918], Washburn [1921]	$t_d \propto \frac{1}{2}\frac{1}{L_c^2} r \frac{\sigma}{\mu_w} t$	$\mu_n \ll \mu_w$
Rapoport [1955], Mattax and Kyte [1962]	$t_d \propto \frac{1}{L_c^2}\sqrt{\frac{K}{\phi}}\frac{\sigma}{\mu_w} t$	$\mu_n = \mu_w$
Ma et al. [1997]	$t_d \propto \frac{1}{L_c^2}\sqrt{\frac{K}{\phi}}\frac{\sigma}{\sqrt{\mu_w \mu_n}} t$	$\mu_n \approx \mu_w$
Zhou et al. [2002]	$t_d \propto \frac{1}{L_c^2}\sqrt{\frac{K}{\phi}}\sigma(\frac{\lambda_w\lambda_n}{\lambda_t})^* t$	$\left(\frac{\lambda_w\lambda_n}{\lambda_t}\right)(S_w) \approx \left(\frac{\lambda_w\lambda_n}{\lambda_t}\right)^*$
Behbahani and Blunt [2005]	$t_d \propto \frac{1}{L_c^2}\sqrt{\frac{K}{\phi}}\sigma\lambda_w^* t$	MW: $\lambda_w \ll \lambda_n$
Li and Horne [2006]	$t_d \propto \frac{1}{L_c^2}\sqrt{\frac{K}{\phi}}\sigma(\frac{\lambda_w\lambda_n}{\lambda_t})^* J^* \cdot (S_{BC} - S_0) t$	$F(x,t) = \frac{q_w(x^*,t)}{q_w(0,t)}$
This work	$t_d \propto \left(\frac{2A}{\phi L_c}\right)^2 t$	-

Table 3.1: The Lucas-Washburn scaling and some of the recently defined t_d. Characteristic values are denoted by $()^*$, and $\overline{S}(t) = \int_{x_d=0}^{x_d=1} S_{eff} dS_{eff}$. It is now apparent, how previous authors (unknowingly) have derived successively better expressions for t_d by giving approximations to the integral in equation (2.32). A specific t_d will give a good scaling if c (Table 3.2) is the same for the different data sets, and thus c can be used to predict the validity of a special scaling group (Fig. 3.5).

Author	Proportionality constant
Lucas [1918], Washburn [1921]	$c \approx \int_{S_0}^{S_{BC}} \frac{(S_w - S_0) k_{rw} J'(S_w)}{F(S_w)} dS_w$
Rapoport [1955], Mattax and Kyte [1962]	$c = \int_{S_0}^{S_{BC}} \frac{(S_w - S_0)\sqrt{k_{rn} k_{rw}} J'(S_w)}{F(S_w)} dS_w$
Ma et al. [1997]	$c \approx \int_{S_0}^{S_{BC}} \frac{(S_w - S_0)\sqrt{k_{rn} k_{rw}} J'(S_w)}{F(S_w)} dS_w$
Zhou et al. [2002]	$c \approx \int_{S_0}^{S_{BC}} \frac{(S_w - S_0) J'(S_w)}{F(S_w)} dS_w$
Behbahani and Blunt [2005]	$c \approx \int_{S_0}^{S_{BC}} \frac{(S_w - S_0) J'(S_w)}{F(S_w)} dS_w$
Li and Horne [2006]	$c \approx \frac{1}{F(S_w^*)}$
This work	$c = 1$

Table 3.2: The proportionality constant c for the Lucas-Washburn scaling and for some of the recently defined t_d (Tables 3.1 and 3.2). A specific t_d will give a good scaling if c is the same for the different data sets, and thus c can be used to predict the validity of a special scaling group (Fig. 3.5).

of data sets also has theoretical implications: It strongly indicates that a functional relationship for p_c which additionally includes dynamic effects is not necessary for describing SI at the core scale.

In the foregoing analysis, it was assumed that p_c is a unique func-

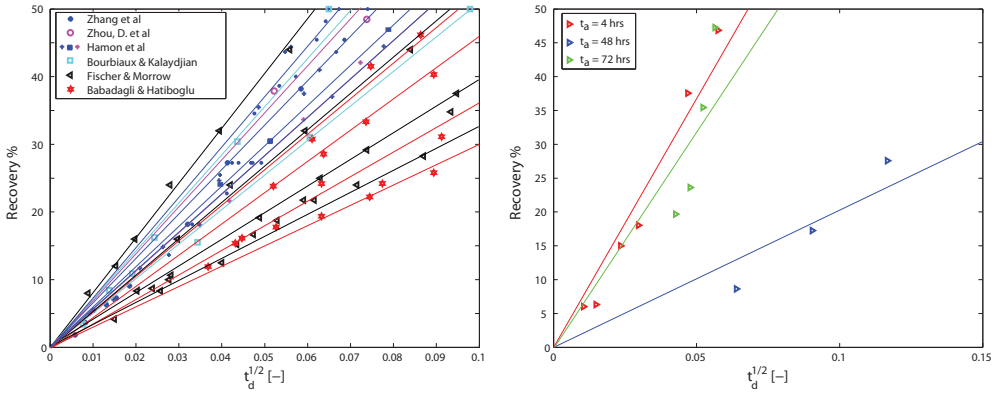

(a) (b)

Figure 3.6: Recovery of the displaced fluid vs. square root of dimensionless time for (a) WW, and (b) MW data. The individual data sets can be correlated by a linear function that emanates from zero. Consequently, dynamic effects in capillary pressure can be neglected. Correlating data for $t_a = 48$ hrs with t_d leads to more scatter caused by weaknesses in the pore-scale predicted capillary-hydraulic properties.

tion of S_w only. Recently, the dependence of p_c on S_w only has been questioned by several authors (for recent overviews see e.g. [Goel and O'Carroll, 2011, Bottero et al., 2011, Manthey et al., 2008]), and it has been proposed that an additional dependence on $\tau \cdot \partial S_w/\partial t$ should be included, where τ is a proportionality factor that possibly depends on material characteristics, the fluid saturations, and the length scale. Some authors ([Barenblatt et al., 2003, Le Guen and Kovscek, 2006], for a recent overview see [Hall, 2007]) argue that non-equlibrium effects are especially important for the case of counter-current SI due to the filling process of the pores by the wetting fluid. Several models have been proposed to incorporate this dynamic effect. For example Hassanizadeh and Gray [1990] and Kalaydjian [1992] consider the linearized form

$$p_n - p_w - p_c = -\tau(S_w) \cdot \frac{\partial S_w}{\partial t}. \tag{3.4}$$

Obviously, τ determines the importance of the dynamic effects, and while it is known that τ can vary over several orders of magnitude [Manthey et al., 2008], the functional dependence of τ, and when/if dynamic effects have to be considered, remains unclear. Thus, recent work has tried to shed light on the exact dependence of τ, to resolve the in part conflicting results for different models, and provide the often missing experimental confirmation for the theoretical considerations [Goel and O'Carroll, 2011]. In this context, the scaling group t_d can be used to measure the validity of the standard formulation for p_c

for describing SI. If dynamic effects are not negligible, this has two consequences for the scaling with t_d.
First, the incorporation of the saturation change makes equation (2.21) pseudoparabolic whose solutions would deviate from the $\sqrt{t}$ dependence [Spayd and Shearer, 2011, Hulshof and King, 1998] the more important dynamic effects become. Consequently, the $\sqrt{t}$ given through t_d as such should fail. Solutions to equations of the non-linear dispersion type like that for SI, equation (2.21), show self-similar behaviour according to $S_w \propto x\sqrt{t}$ ([McWhorter and Sunada, 1990], see previous chapter). There has been a considerable debate in the literature (for recent reviews see e.g. [Alava et al., 2004, Cai and Yu, 2011, Hall, 2007]) as to when the $\sqrt{t}$ scaling first proposed by Lucas [1918] and Washburn [1921] for describing counter-current imbibition holds. However, published experimental data strongly suggests that deviations from this scaling in time only occur for cases where either the porous medium was not rigid (e.g. imbibition into paper, textiles, or rock samples with clay inclusions) [Alava et al., 2004, Cai and Yu, 2011, Hall, 2007], or gravity and evaporation played a role, which leads to pinning of the wetting fronts at late times (e.g. [Alava et al., 2004, Delker et al., 1996, Dubé et al., 2001]). Indeed, plotting recovery against $\sqrt{t_d}$ for the experimental results given in Tables 3.3, 3.4, and 3.6 reveals that for early times recovery depends linearly on $\sqrt{t}$ for data sets obtained under widely varying experimental conditions (Figure 3.6). Thus, assuming a $\sqrt{t}$ scaling and consequently assuming that dynamic effects in capillary pressure are negligible, is strongly supported. What is more important, however, is the fact that the data sets we chose vary all the key parameters. If dynamic effects played any role, one would expect that at least one data set significantly diverges from the $\sqrt{t}$ scaling. We do not observe this.

Second, if τ really depends on material properties as has been suggested, then the wide parameter variation of the data sets we use should also lead to a wider horizontal spread in Figure 3.5. As the scaling with $t_{d,Ma}$ has shown, failing to account for relevant parameters results in the emergence of different subgroups for the different data sets. While the maximal horizontal scatter for t_d (Fig. 3.5(b)) is still around 5, the reported values for τ vary several orders of magnitude [Manthey et al., 2008]. Thus, if dynamic effects matter for SI at the core scale, one should obtain a significantly worse horizontal spread. We also note here, that although we speak of length-scales typical for the core scale, we chose data sets where L_c varies by an order of magnitude (Tables 3.3 and

3.4). Thus, if τ depended on the length-scales as has been suggested [Bottero et al., 2011], this also should result in a wider horizontal spread.

To rigorously test the second part, the method used for calculating the capillary-hydraulic properties in A must not presume the validity of the standard Darcy equation. It is common practice [Gummerson et al., 1979], to obtain k_{rw}, k_{rn}, and p_c from solving an inverse problem that assumes the validity of the standard Darcy equation. Obviously, if all the capillary-hydraulic relationships in the sample dataset were obtained this way, then t_d defined in equation (3.3) would give an excellent correlation, since it is based on an exact solution of Darcy's equation, and the constitutive relations would have been determined to fit the data set, possibly hiding the missing of τ. The question whether the standard Darcy model without dynamic p_c relations model is applicable for capillary flow would thus be bypassed. For the experiments performed on Berea sandstone and the synthetic porous medium, we therefore use pore scale predictions of the relative permeabilities and the capillary pressure [Valvatne and Blunt, 2004] (Fig. 3.2), rather than modelling (k_{rw}, k_{rn}, p_c) through inverse simulation of experimental data.
For the synthetic material, only k_{rw} and k_{rn} have been measured. However, the curves closely resemble that for the sandstone, which indicates that the two materials have a similar pore structure. Therefore the pore scale predictions made for the sandstone sample were used. For the water-air experiments on sandstone, the measured and pore scale predicted k_{rw} and k_{rn} were similar to that of the water-oil system [Valvatne and Blunt, 2004]. Hence, we used the same (k_{rw}, k_{rn}, p_c)-set as for the water-oil system. To account for effects of K and surface tensions σ, we used a Leverett $J-$scaling [Bear, 1972]

$$p_c = \sigma\sqrt{\frac{\phi}{K}}J(S_e), \tag{3.5}$$

where $S_e = (S_w - S_{wr})/(1 - S_{nr} - S_{wr})$ is the effective saturation, and S_{wr} is the residual water phase. We note again, that we used the same (k_{rw}, k_{rn}, J)-set for a certain material, rather than direct measurements for the specific sample. To further reduce the scatter, sample specific relations should be used. For comparison with the pore scale predicted relations, the capillary-hydraulic properties obtained from a standard Darcy and a history match that includes a dynamic p_c were used for some of the sandstone experiments and the diatomite experiments, respectively. For the general scaling t_d, the data sets collapses onto a

Sample	BC	L_c [cm]	K [mD]	ϕ [–]	μ_w [Pa · s]	μ_n [Pa · s]	σ [mN/m]	S_0 [–]
AA01	AFO	0.5364	510.8	0.218	$9.67 \cdot 10^{-4}$	0.03782	50.62	0
AA02	AFO	0.8029	498.5	0.219	$9.67 \cdot 10^{-4}$	0.03782	50.62	0
AA03	AFO	0.9723	519.8	0.222	$9.67 \cdot 10^{-4}$	0.03782	50.62	0
AA04	AFO	1.089	521.7	0.224	$9.67 \cdot 10^{-4}$	0.03782	50.62	0
AA05	AFO	1.1837	505.5	0.215	$9.67 \cdot 10^{-4}$	0.03782	50.62	0
AA06	AFO	1.3059	501.6	0.218	$9.67 \cdot 10^{-4}$	0.03782	50.62	0
BC21	OEO	6.092	481.9	0.213	$9.67 \cdot 10^{-4}$	0.00398	47.38	0
BC13	OEO	4.998	503.6	0.209	$9.67 \cdot 10^{-4}$	0.03782	47.38	0
BC22	OEO	5.687	496.8	0.208	$9.67 \cdot 10^{-4}$	0.1563	51.77	0
BD15	TEC	1.3506	523.8	0.214	$9.67 \cdot 10^{-4}$	0.00398	47.38	0
BD14	TEC	1.3506	518.9	0.218	$9.67 \cdot 10^{-4}$	0.03782	50.62	0
BD18	TEC	1.3506	509.7	0.218	$9.67 \cdot 10^{-4}$	0.1563	51.77	0
BA3	TEO	13.87	907.1	0.214	$9.67 \cdot 10^{-4}$	0.03782	50.62	0
A10	OEO	9.7	4000	0.472	0.001	0.0115	49.0	0.189
A10-20	OEO	19.7	3430	0.453	0.001	0.0115	49.0	0.187
A10-30	OEO	30.0	3830	0.453	0.001	0.0115	49.0	0.151
A10-40	OEO	40.0	3550	0.478	0.001	0.0115	49.0	0.172
A10-85	OEO	84.7	3000	0.478	0.001	0.0115	49.0	0.164
A10-VI-20	TEO	9.8	3200	0.456	0.001	0.0115	49.0	0.164
A10-X-20	AFO	0.85	2300	0.458	0.001	0.0115	49.0	0.132

Table 3.3: Parameter sets and experimental boundary conditions (BC) used in [Zhang et al., 1996, Hamon and Vidal, 1986], respectively. The porous material in [Zhang et al., 1996] was a Berea sandstone, the ones reported in [Hamon and Vidal, 1986] were performed on a synthetic porous material. For all the experiments, the wetting-phase was water, and the non-wetting phase was oil, and for the ones reported in [Babadagli and Hatiboglu, 2007] the non-wetting phase was air. The respective parameters A for these are listed in Table 3.5.

curve with little scatter (Fig. 3.5) showing that the behaviour is well characterized by t_d. Since t_d contains all the information present in the Darcy model, and its validity has not been assumed to calculate the capillary-hydraulic properties in A, this strongly indicates that the Darcy model is suitable for characterizing and modeling SI at the core scale.

However, it is important to point out, that for viscous or gravity dominated flow the rate of change in saturation would be higher, and therefore the influence of non-equilibrium effects might not be negligible any more.

Sample	BC	L_c [cm]	K [mD]	ϕ [–]	μ_w [Pa · s]	μ_n [Pa · s]	σ [mN/m]	S_0 [–]
Z-2	OEO	9.5	6.1	0.72	0.001	$8.4 \cdot 10^{-4}$	51.4	0
Z-3	OEO	9.5	7.9	0.77	0.001	$2.5 \cdot 10^{-2}$	45.7	0
Z-4	OEO	9.5	2.5	0.78	0.001	$8.4 \cdot 10^{-4}$	51.4	0
Z-5	OEO	9.5	6.0	0.68	0.001	$8.4 \cdot 10^{-4}$	51.4	0
GVB-3	OEO	29.0	124.0	0.233	0.0012	0.0015	35.0	0.4
GVB-4	TEO	14.5	118.0	0.233	0.0012	0.0015	35.0	0.411
EV6-22	OEO	7.18	109.2	0.18	0.495	0.0039	28.9	0
EV6-18	OEO	7.62	140.0	0.181	0.001	0.063	51.3	0
EV6-21	OEO	7.7	107.3	0.187	0.0278	0.0039	34.3	0
EV6-13	OEO	7.75	113.2	0.187	0.001	0.0039	50.5	0
EV6-14	OEO	7.66	127.2	0.178	0.0041	0.0039	41.2	0
EV6-20	OEO	7.52	132.9	0.181	0.0041	0.0633	41.7	0
EV6-16	OEO	7.78	136.8	0.181	0.0278	0.0633	34.8	0
EV6-23	OEO	7.36	132.1	0.179	0.0977	0.0039	31.3	0
EV6-15	OEO	7.3	107.0	0.183	0.4946	0.0633	29.8	0
EV6-17	OEO	7.54	128.1	0.19	0.0977	0.0633	32.1	0
F-11	OEO	10.16	500.0	0.21	0.001	$1.8 \cdot 10^{-5}$	72.9	0
F-12	OEO	15.24	500.0	0.21	0.001	$1.8 \cdot 10^{-5}$	72.9	0
F-14	OEO	10.16	500.0	0.21	0.001	$1.8 \cdot 10^{-5}$	72.9	0
F-16	OEO	5.08	500.0	0.21	0.001	$1.8 \cdot 10^{-5}$	72.9	0
F-16	OEO	10.16	500.0	0.21	0.001	$1.8 \cdot 10^{-5}$	72.9	0
F-18	OEO	15.24	500.0	0.21	0.001	$1.8 \cdot 10^{-5}$	72.9	0

Table 3.4: Parameter sets and experimental boundary conditions (BC) used in [Zhou et al., 2002, Bourbiaux and Kalaydjian, 1990, Fischer et al., 2006, Babadagli and Hatiboglu, 2007], respectively. The porous material in [Bourbiaux and Kalaydjian, 1990, Fischer et al., 2006, Babadagli and Hatiboglu, 2007] was a Berea sandstone, and for the ones reported in [Zhou et al., 2002] a diatomite rock was used. For all the experiments, the wetting-phase was water, and for the experiments reported in [Zhou et al., 2002, Bourbiaux and Kalaydjian, 1990, Fischer et al., 2006] the non-wetting phase was oil, and for the ones reported in [Babadagli and Hatiboglu, 2007] the non-wetting phase was air. The respective parameters A for these are listed in Table 3.5.

3.7 SCALING GROUP FOR MIXED-WET SYSTEMS

Introduction: Induction times and two different S_{nr}

The data set used in Figures 3.4, 3.5 were for widely varying conditions, but excluded one scenario: Mixed-Wettability (MW). The majority of reservoirs are not water-wet, but mixed-wet [Anderson, 1987b]. The

Sample	A $[m/\sqrt{s}]$	Sample	A $[m/\sqrt{s}]$	Sample	A $[m/\sqrt{s}]$
AA01	$7.307 \cdot 10^{-6}$	A10-20	$3.1 \cdot 10^{-5}$	EV6-21	$1.86 \cdot 10^{-6}$
AA02	$7.287 \cdot 10^{-6}$	A10-30	$3.18 \cdot 10^{-5}$	EV6-13	$7.48 \cdot 10^{-6}$
AA03	$7.44 \cdot 10^{-6}$	A10-40	$3.33 \cdot 10^{-5}$	EV6-14	$4.45 \cdot 10^{-6}$
AA04	$7.45 \cdot 10^{-6}$	A10-85	$3.13 \cdot 10^{-5}$	EV6-20	$2.45 \cdot 10^{-6}$
AA05	$7.21 \cdot 10^{-6}$	A10-VI-20	$3.17 \cdot 10^{-5}$	EV6-16	$1.36 \cdot 10^{-6}$
AA06	$7.27 \cdot 10^{-6}$	A10-X-20	$2.92 \cdot 10^{-5}$	EV6-23	$9.92 \cdot 10^{-7}$
BC21	$1.25 \cdot 10^{-5}$	Z-2	$3.41 \cdot 10^{-5}$	EV6-15	$3.93 \cdot 10^{-7}$
BC13	$7.05 \cdot 10^{-6}$	Z-3	$1.35 \cdot 10^{-5}$	EV6-17	$8.59 \cdot 10^{-7}$
BC22	$4.46 \cdot 10^{-6}$	Z-4	$2.72 \cdot 10^{-5}$	F-11	$2.75 \cdot 10^{-5}$
BD15	$1.28 \cdot 10^{-5}$	Z-5	$2.86 \cdot 10^{-5}$	F-12	$2.81 \cdot 10^{-5}$
BD14	$7.34 \cdot 10^{-6}$	GVB-3	$9.48 \cdot 10^{-5}$	F-14	$1.95 \cdot 10^{-5}$
BD18	$4.65 \cdot 10^{-6}$	GVB-4	$9.67 \cdot 10^{-5}$	F-16	$2.29 \cdot 10^{-5}$
BA3	$4.65 \cdot 10^{-6}$	EV6-22	$4.29 \cdot 10^{-7}$	F-16	$1.60 \cdot 10^{-5}$
A10	$3.36 \cdot 10^{-5}$	EV6-18	$3.74 \cdot 10^{-6}$	F-18	$2.07 \cdot 10^{-5}$

Table 3.5: A for the data sets listed in Tables 3.3 and 3.4.

term 'mixed-wet' was coined by Salathiel [1973] for rock that contains both water-wet (WW) and oil-wet (OW) pores. On the macro-scale, MW systems are characterized by a p_c-curve that becomes negative for some $S_w > S_w^*$ (Fig. 3.8). If the flow is only driven by capillary forces, then SI stops although $S_w < S_{nr}$, i.e. when the oil is still mobile [Anderson, 1987a,b]. If $S_w > S_w^*$, then $p_c < 0$ would result into oil being imbibed until S_w is such that $p_c = 0$. The difficulty of deriving a scaling group for MW-systems is therefore twofold: First, the behavior of the p_c curve (Figs. 3.7b,3.8), results into two different residual oil saturations: One at which SI stops $S_{nr,SI}$, and one to which S_o could be reduced after a water flood, $S_{nr,WF}$. So far, it is unclear, how a scaling group should account for that. Second, SI experiments for MW systems show that the time until imbibition in a MW system starts can be up to four orders of magnitude different compared to a strongly WW system [Xie and Morrow, 2001, Zhou et al., 2002, Tong et al., 2002]. Previous authors tried to include this retarded behavior, known as 'induction time', by including an expression on the dynamic oil-water contact angle [Cil et al., 1998, Gupta and Civan, 1994, Zhou et al., 2002, Lavi et al., 2008, Xie and Morrow, 2001], as suggested in the original Lucas-Washbburn equation [Lucas, 1918, Washburn, 1921].

However, Behbahani and Blunt [2005] showed that this approach is flawed. They performed pore-scale simulations on MW Berea Sand-

stone from which the obtained relative permeability and p_c curves. The curves were then used in a continuum-scale simulation that could reproduce the MW SI data reported in [Zhou et al., 2002]. The pore-scale predictions for k_{rw}, k_{ro} and p_c (Figs. 3.7b,3.7a) revealed that although p_c declines for increasingly MW systems, this decrease is less than one order of magnitude, and thus negligible compared to the several orders of magnitude decline in induction time. In contrast, they found that the decrease in relative permeabilities was significant (Fig. 3.7a), and concluded that a simple change in contact angle and thus p_c could not explain the induction times, and that any attempt to include the characteristics of MW systems via an effective contact angle would be flawed. Similarly, other pore-scale studies [Van Dijke and Sorbie, 2003, 2002, Valvatne and Blunt, 2004, Jackson et al., 2003] reveal that in the pore-space there is a wide range of advancing contact angles, and not just a single one.

In summary, if one tries to capture the behavior of a MW system via a single, effective contact angle, this angle is merely an empirical fit without any physical meaning [Anderson, 1987a, Behbahani and Blunt, 2005, Marmur, 2003]. Any t_d for MW systems *must* combine the information on phase mobilities and p_c and account for the role of $S_{nr,SI}$ and $S_{nr,WF}$.

In the following subsection, we propose two simple methods for incorporating the information on $S_{nr,SI}$ and $S_{nr,WF}$ such that the complete information on the capillary-hydraulic properties is included. We validate both methods, by correlating some of the MW experiments reported in [Zhou et al., 2002], compare the correlation with the one obtained for the WW experiments, and give recommendations on which method to use. Furthermore, we show how the specific group $t_{d,Beh}$ proposed by Behbahani and Blunt [2005] is another special case (Tables 3.1, 3.2) of our universal scaling group that can be used if the complete information on k_{rw}, k_{ro} and p_c is not known. We derive the respective proportionality constant and discuss its implications for the validity of $t_{d,Beh}$.

Defining an appropriate $D(S_w)$ *for MW systems*

The analytical solution in equation (2.29) was derived assuming boundary conditions of some $S_{BC} > S_0$. The difference in saturation level will be 'smoothed out' as long as $D(S_w) > 0$, resulting in S_w being transported into the porous medium. In a WW system, $p_c > 0$, $dp_c/dS_w < 0$,

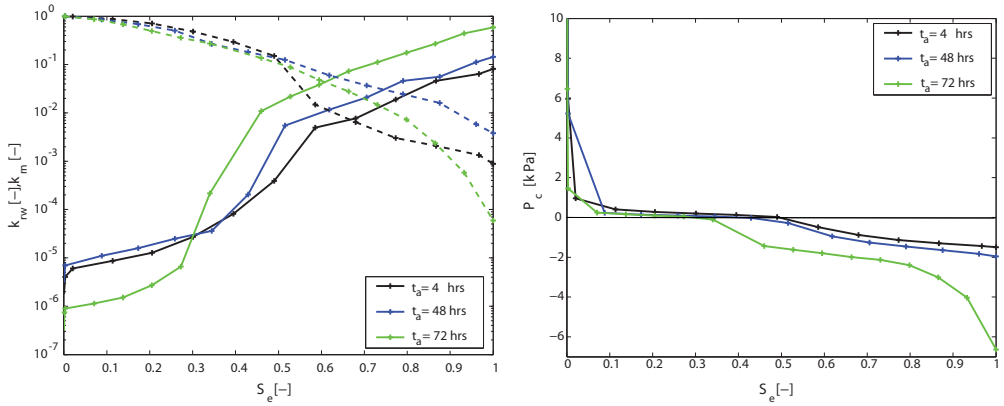

(a) (b)

Figure 3.7: Capillary-hydraulic properties vs. effective saturation for different degrees of mixed wetttability as predicted by pore-scale simulations [Behbahani and Blunt, 2005] for the experiments reported in [Zhou et al., 2000]. (a) Relative permeabilities of the aqueous (—) and non-aqueous phase (– –), and (b) p_c for different ageing times t_a. Initial water saturation was $S_{wi} = 0.15$.

and $D(S_w) > 0$ for $S_{wr} \leqslant S_w \leqslant 1 - S_{nr}$, and $S_{nr} = S_{nr,SI} = S_{nr,WF}$. In an experiment for a MW system, the same $S_0 > S_i$ would only be transported into the porous medium, as long as $p_c > 0$, i.e. as long as $S_w \leqslant 1 - S_{nr,SI}$. However, the mathematical setting given in equation (2.29) together with (2.17) does not use a pressure boundary condition, and therefore for the MW system would wrongly predict that SI occurs even when $S_w > 1 - S_{nr,SI}$, since for that case too $dp_c/dS_w < 0$, and thus $D(S_w) > 0$ over the whole saturation range (Fig. 3.7b). Nevertheless, an analytical solution for (2.21) that somehow employs pressure boundary conditions is unknown, and the setting of equation (2.21) together with (2.17) so far allows for the only analytical solution for a general form of $D(S_w)$ (Table 2.1). We therefore propose a physically motivated way of incorporating the information on p_c and the resulting end of SI at $S_w = S_{nr,SI}$ into $D(S_w)$ that leaves the boundary conditions intact, such that the analytical solution given in equation (2.29) remains valid.

We propose two simple methods. In the first method (termed 'Equivalent p_c'), we define an equivalent capillary pressure curve p_c such that it agrees with the original one up to $S_w = 1 - S_{nr,SI}$, but then is constantly zero (Fig. 3.8a)

$$p_c^{equ.}(S_w) = \begin{cases} p_c(S_w) & \text{if } S_w \leqslant 1 - S_{nr,SI} \\ 0 & \text{otherwise.} \end{cases} \tag{3.6}$$

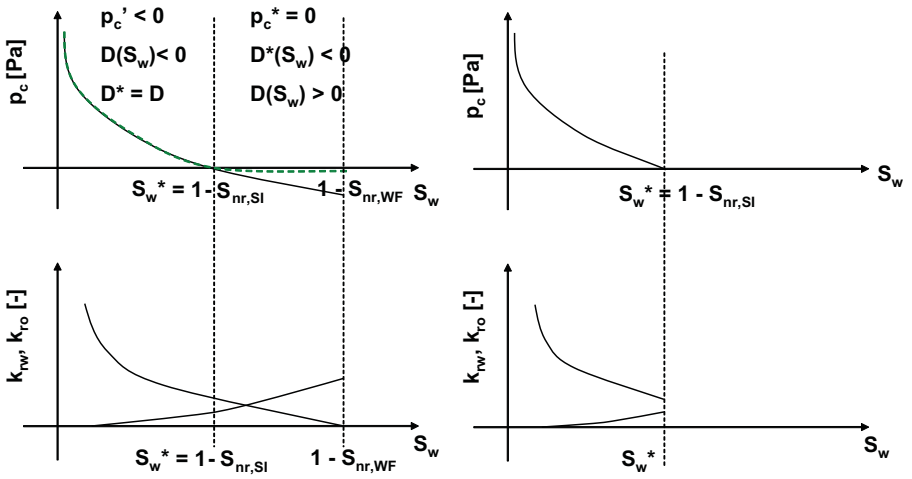

Figure 3.8: Illustration of the two different methods for modifying $D(S_w)$ for MW systems. (a) 'Equivalent p_c' concept: p_c is set to zero for all $S_w > S_w^*$, but the relative permeabilities are left unchanged. (b) Equivalent S_{nr} concept: S_{nr} is set to $S_{nr} = S_{nr,SI}$, and the relative permeabilities are truncated at S_w^*. For MW systems, $p_c < 0$ for some $S_w < 1 - S_{nr,WF}$, such that SI stops at $S_n = S_{ro,SI}$ although the non-aqueous phase is still mobile, and would be reduced to $S_n = S_{nr,WF}$ during a water-flood.

The relative permeabilities are left unchanged, and we also keep the residual saturation at the level, where the oil becomes immobile, i.e. $S_{nr} = S_{nr,WF}$. The resulting non-linear dispersion is identical with the original $D(S_w)$ up to S_w^*, and then becomes zero. Consequently, equation (2.29) correctly predicts that SI stops for $p_c < 0$, $S_w > 1 - S_{nr,SI}$. WW systems are contained as a special case, since then $p_c^{equ.} = p_c$ over the whole saturation range.

In the second method (termed 'Equivalent S_{nr}'), we take $S_{nr} = S_{nr,SI}$. That way, only the information on p_c for $S_w \leqslant 1 - S_{nr,SI}$ is used, and the relative permeabilities and p_c are only evaluated up to $S_w = 1 - S_{nr,SI}$, but otherwise are left unchanged (Fi. 3.8b). Obviously, with this $\left(S_{nr}, D(S_w)\right)$—set, equation (2.29) correctly predicts that SI stops at $S_w = 1 - S_{nr,SI} = 1 - S_{nr}$. As for the first method, WW systems are contained as a special case.

To show the validity of both approaches, we correlated the MW data reported in [Zhou et al., 2002] for the cases where a suitable $\left(k_{rw}, k_{rn}, p_c\right)$-set is known (Table 3.6). We used the $\left(k_{rw}, k_{rn}, p_c\right)$-set derived from a pore-scale model [Behbahani and Blunt, 2005] that gave a reasonable prediction of the measured recoveries of the SI experiments.

Figure 3.9 shows the result for both proposed methods, and the scaling proposed in [Ma et al., 1997] as a comparison. For both methods, the

t_a [hrs]	L_c [cm]	K [mD]	ϕ [–]	μ_w [Pa · s]	μ_n [Pa · s]	S_0 [–]
4	7.62	355.0	0.215	$9.67 \cdot 10^{-4}$	0.0398	0.151
48	7.6	365.0	0.214	$9.67 \cdot 10^{-4}$	0.0398	0.159
72	7.6	400.0	0.2125	$9.67 \cdot 10^{-4}$	0.0398	0.169

Table 3.6: Parameter set used for the MW experiments reported in Zhou et al. [2000]. The rock was a Berea sandstone and the samples were aged for different times t_a yielding different MW states. Brine was used as the aqueous phase, and Soltrol 220 was used as non-aqueous phase, and $\sigma = 24.2$ mN/m.

t_a [hrs]	$A^{\text{Equ. } p_c}$ $[m/\sqrt{s}]$	$A^{\text{Equ. } S_{nr}}$ $[m/\sqrt{s}]$
4	$1.25 \cdot 10^{-6}$	$5.76 \cdot 10^{-7}$
48	$5.64 \cdot 10^{-7}$	$6.48 \cdot 10^{-7}$
72	$3.73 \cdot 10^{-7}$	$1.25 \cdot 10^{-7}$

Table 3.7: Scaling parameters for the MW experiments reported in [Zhou et al., 2000] (Table 3.6). $A^{\text{Method A}}$ and $A^{\text{Method B}}$ are calculated by the two different methods for adjusting $D(S_w)$ (section (3.7)), Fig. 3.8.

data for ageing time $t_a = 4$ hrs falls onto the same master curve as the scaled data for WW conditions, showing that both methods capture the physics of the MW system. The data for $t_a = 48$ hrs and $t_a = 72$ hrs give slightly more scatter but still fall onto the same master curve, i.e. t_d is able to catch the increase in induction time. The increased scatter for $t_a = 48$ hrs and $t_a = 72$ hrs stems from the pore-scale predictions of the $\left(k_{rw}, k_{rn}, p_c\right)$-set. For $t_a = 48$ hrs and $t_a = 72$ hrs, the agreement of the continuum scale simulations in Behbahani and Blunt [2005] degraded compared to the very good agreement achieved for $t_a = 4$ hrs with the experimental data, which leads to the increased scatter.

The constant A is independent of the sample geometry, and therefore is a measure for the behavior of induction times for different MW states. The SI process gets more and more retarded with increasing t_a, and A decreases in a comparable extend (Table 3.7). For the 'Equivalent S_{nr}' method, A between $t_a = 48$ hrs and $t_a = 72$ hrs does not decrease, i.e. A for $t_a = 72$ hrs is slightly too big. As can be seen from Figure 3.8b, the scaling for $t_a = 48$ hrs gives more scatter at early times, and indicates as well, that A is slightly too big stemming again from the weaknesses in the pore-scale predictions for the hydraulic properties.

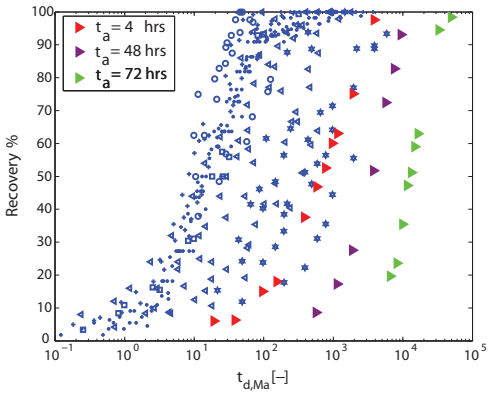

(a)

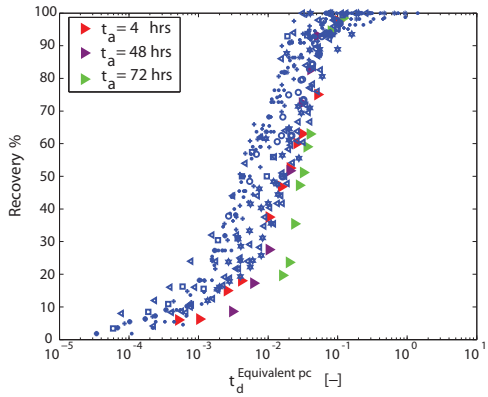

(b)

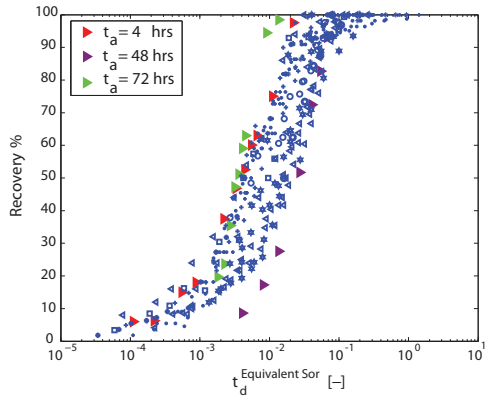

(c)

Figure 3.9: Scaling of experimental data for the MW case. The data in blue is for the WW case and serves as reference. (a) Time scaled according to Ma et al. [1997]. The scaled MW data leads to an even further increase in scatter. (b) Time scaled according to the 'Equivalent p_c' concept, and (c) according to the 'Equivalent S_{nr}' concept. The results for both methods fall onto the same curve as for the WW data but the 'Equivalent S_{nr}' only used information naturally present in an SI system. It therefore should be preferred although for the data set presented here it results in more scatter than the Equivalent p_c concept. For k_{ro}, k_{rw} and p_c pore-scale predictions [Behbahani and Blunt, 2005] were used. The best (k_{rw}, k_{ro}, p_c)–set was obtained for $t_a = 4$ hrs, which therefore gives the best correlation while $t_a = 48$ hrs and $t_a = 72$ hrs leads to more scatter.

A special group for the MW case, and the influence of gravity

The 'Equivalent p_c' method was based on artificially forcing $D(S_w) = 0$ for $S_w > 1 - S_{nr}$ while the 'Equivalent S_{nr}' method was obtained by simply truncating information at a point where an SI process would naturally stop. Therefore, while both give comparable results, we recommend the equivalent S_{nr}' method since it is based on all - but exclusively on - the information present in an SI system, and therefore has a sound physical justification.

For a MW system, the oil mobility exceeds the water mobility by orders of magnitudes (Fig. 3.7a), i.e. $\lambda_w(S_w) \ll \lambda_n(S_w)$ for $S_w < 1 - S_{nr,SI}$. This can be used to derive the scaling group for MW systems given in Behbahani and Blunt [2005] (Appendix A) as another special case of equation (3.3),

$$t_{d,Beh} = \sqrt{\frac{K}{\phi}}\frac{\sigma}{L_c^2}\lambda_w^* t \tag{3.7}$$

which provides the (so far missing) physical justification for that group. From the proportionality constant c for $t_{d,Beh}$ (Table 3.2, Appendix A), the following predictions for the validity of $t_{d,Beh}$ can be made: A good correlation can be achieved independent of viscosity ratios, but for systems with the same initial fluid distribution, and the same capillary hydraulic properties. In particular: The correlation will be satisfactory only if the experiments were obtained under the same degree of mixed wettability.

In the aforementioned analysis, SI due to gravity segregation was ignored. While in WW systems, p_c is strong enough that gravity is negligible, the decrease in p_c for MW systems (Fig. 3.7b) makes gravity more important [Xie and Morrow, 2001] as described by an increase in the dimensionless Bond number

$$Bo = \frac{\text{hydrostatic pressure}}{\text{capillary pressure}} = \frac{\Delta\rho g H\sqrt{K}}{2\sigma\sqrt{\phi}J}, \tag{3.8}$$

where $\Delta\rho$ is the density difference between the oil and the water phase, g is the gravity constant, H is the height. Since the focus of this work is on describing the physics of counter-current SI, we do not discuss gravity segregation any further, but merely remark that it usually is taken into account by defining [Xie and Morrow, 2001]

$$t_{d,complete} = t_{d,SI} + t_{d,grav}, \tag{3.9}$$

and

$$t_{d,grav} = t\frac{K/\phi}{L_H\sqrt{\mu_w\mu_n}}\Delta\rho g, \tag{3.10}$$

where L_H is the characteristic height. It remains open, however, in how far this approach can describe recovery if instabilities, like gravity driven fingers [Cueto-Felgueroso and Juanes, 2008] or gas-gravity drainage [Di Donato et al., 2007] occur, or whether $t_{d,grav}$ gives a good correlation for experiments where the parameters are varied as suggested by section 3.2.

3.8 APPLICATIONS

Scaling groups are essential in any situation where SI needs to be understood, described and modelled which is the case for a wide range of geophysical and petrophysical applications. Examples include the upscaling of laboratory data [Morrow and Mason, 2001], the characterization of a porous rock [Marmur, 2003, Jadhunandan and Morrow, 1991, Morrow et al., 1994], feasibility studies for geothermal reservoirs [Li and Horne, 2009] and even applications not related to petrophysical applications at all [Finch-Savage et al., 2005, Finch-Savage and Leubner-Metzger, 2006].
In the following, we discuss two applications. Our first application are dual-porosity models where scaling groups build the center piece in transfer functions. The second application considers a model not related to petrophysical applications at all, namely the important process of the water uptake and following germination of plant seeds [Finch-Savage et al., 2005, Finch-Savage and Leubner-Metzger, 2006].

Dual-porosity models and the first general transfer rate

A key application are dual-porosity models where scaling groups build the center piece in transfer functions. Dual-porosity models are field-scale representations of fractured reservoirs that separate the subsurface model into stagnant, low permeability regions (the matrix blocks) and high-permeability regions (the fracture network), and the fluid transfer between the two regions is modelled by some transfer function T [Warren and Root, 1963, Kazemi et al., 1976]. Since many expressions of T rest upon an analytical expression for SI and/or a scaling group t_d, the numerous transfer functions for SI that have been proposed to

date [Abushaikha and Gosselin, 2008, Babadagli and Zeidani, 2004, Cil et al., 1998, Kazemi et al., 1992, Unsal et al., 2010] experience similar challenges as the scaling groups themselves: It is unclear how a model can describe the heterogeneity in a reservoir that stems from differences in initial water content, wettability and phase mobility effects, and how SI data obtained for a certain viscosity range translates into the conditions found in the field.

Since our t_d overcomes all these challenges, it is easy to derive an improved transfer rate, as well. In a dual-porosity model, the mass conservation equations for the fracture and the matrix are

$$\begin{aligned} \phi_f \frac{\partial S_{wf}}{\partial t} + q_t \cdot \nabla f_{wf} &= -T \\ \phi_m \frac{\partial S_{wm}}{\partial t} &= T, \end{aligned} \tag{3.11}$$

where the subscripts m and f stand for matrix/stagnant region and fracture/flowing region, respectively. To obtain an expression for T based on t_d, we use that the recovery Rec satisfies

$$\frac{Rec}{R_\infty} = \frac{S_{wm} - S_{wmi}}{1 - S_{nrm} - S_{wim}}, \tag{3.12}$$

where R_∞ is the final recovery.

To predict the shape of R_∞ over the whole time range, the analytical solutions for $x(S_w, t)$ and $Q_w(t)$ presented in section 2.3 cannot be used since they are only valid as long as $t < t^*$. Thus, instead of predicting the s-shape of the correlated data (Fig. 3.5), they instead would predict that Q_w increases indefinitely. Therefore, to fit the data we instead use an exponential model

$$R = R_\infty (1 - e^{-\alpha t_d}). \tag{3.13}$$

Note that while the exponential model does predict recovery over the whole time range, its prediction of early-time recovery is too pessimistic. From fitting the recovery curve in Figure 3.9, we obtain $\alpha \approx 70$. From equations (3.11) and (3.12), we obtain [Di Donato et al., 2007]

$$\begin{aligned} \phi_m \frac{\partial S_{wm}}{\partial t} = T \quad &= \alpha \frac{t_d}{t} (1 - S_{nrm} - S_{wm}) \\ &= \alpha \tau_c (1 - S_{nrm} - S_{wm}). \end{aligned} \tag{3.14}$$

The significance of this result is the following: The value for α is obtained for *arbitrary* experimental conditions, i.e. α is *independent* of wettability states, rock material and so forth. Therefore, the model given

in equation (3.14) is the first one, where α does not have to be 're-fitted' to different experimental conditions as has been the common strategy so far [Di Donato et al., 2007, Abushaikha and Gosselin, 2008, Babadagli and Zeidani, 2004, Cil et al., 1998, Kazemi et al., 1992, Unsal et al., 2010]. It therefore simply can be incorporated into any dual-porosity model without the need for further experiments that would be necessary for obtaining a modified α. Furthermore, equation (3.14) shows that an exponential Aronofsky model for recovery is capable to incorporate the physics of SI if t_d is appropriately chosen, in contrast to what has been claimed before [Chen et al., 1995].
Furthermore, as A contains all the information about the capillary-hydraulic properties and the initial fluid content, but is independent of L_c, it shows the influence of the porous structure and fluid characteristics on SI. For sandstone with water as the wetting phase and oil as the non-wetting phase ($\mu_n/\mu_w = 39, S_{wi} = 0$), we found $A \approx 7 \cdot 10^{-6} m/\sqrt{s}$, while for diatomite (with $\mu_n/\mu_w = 25, S_{wi} = 0$) we found $A \approx 1.5 \cdot 10^{-5} m/\sqrt{s}$, i.e. the fluxes $Q_w(t)$ differ by an order of magnitude. This shows that geological heterogeneity present in the subsurface can give rise to widely different time-scales, independent of different length scales or fluid viscosities. The coefficient A can be used to rigorously capture this behavior through a multi-rate model [Di Donato et al., 2007, Haggerty and Gorelick, 1995].
t_d is based on laboratory results where the core used was surrounded by a constant saturation. In fractured systems, the saturation changes depending on the speed of the fracture flow which leads to different fracture flow regimes [Rangel-German and Kovscek, 2006, 2002, Fernø et al., 2011]. Therefore, accounting for heterogeneities in petrophysical properties alone might not be sufficient, and additionally the characteristic lengths might have to be modified [Rangel-German and Kovscek, 2006, 2002].

Imbibition-germination models for plant seeds

The second application considers imbibition damage during water uptake in porous plant seeds. Since the main focus of this work lies on modelling petrophysical processes, this applications is only shortly discussed.
The transient behaviour of the SI process is crucial for the field emergence of commercial seeds, and determining favorable conditions for SI with the help of coupled imbibition-germination models is of great

practical interest [Finch-Savage et al., 2005]. In imbibition-germination models, the water content in a seed is estimated from an imbibition model. The so-obtained value for the water content is then used to calculate the germination time, i.e. the time until the seed starts growing. For these models, the product $\beta = \alpha\phi\tau_c$ is an explicit expression for the proportionality constant used in coupled imbibition-germination models [Finch-Savage et al., 2005]. Contrary to the phenomenologically derived constant however, β can be used for example to predict how the seed-imbibition depends on L_c and thus on seed size without the need to perform the lengthy and difficult laboratory experiments on plant seeds that up to now have been necessary.

3.9 CONCLUSIONS

While it has been known for over 90 years that SI scales with $\sqrt{t}$ in time, the properties of this scaling were unknown. We derived the first universal scaling group that rigorously accounts for the influence of all parameters on SI that are present in the two-phase Darcy formulation. This allows for the following conclusions:

- *SI is best characterized by the cumulative inflow and not by the frontal movement.* Based on the analytical solution two scaling groups for SI can be derived - one based on the cumulative inflow, one based on the frontal movement of the wetting front. No fitting parameters need to be introduced. The group based on the cumulative wetting phase gives an excellent correlation which is superior to a characterization based on the frontal movement, contrary to what has been speculated previously [Handy, 1960].

- *Our group serves as a 'master equation' that predicts the validity of specialized groups.* Due to its generality, many of the previously defined groups are contained as special cases, and the validity of a special group can rigorously be predicted through the proportionality constant c. Any new specific scaling group with a sound physical foundation necessarily is a special case of our group.

- *Darcy's model can describe SI.* Our group comprises all the information present in the Darcy model, and to calculate necessary parameters (e.g. k_{rw}), the validity of Darcy's model was not presumed. The scatter in the correlated data is small compared to the

reported several-orders-of magnitude range for coefficients for dynamic capillary pressure. This indicates that the Darcy model can characterize SI and no further parameters, like non-equilibrium effects in p_c, are necessary.

- *Applications: A general transfer rate for dual-porosity and imbibition-germination models.* An exponential model for the transfer can be fitted that correlates 45 published water-oil and water-air SI studies for water-wet systems, different degrees of mixed-wettability, a wide range of viscosity ratios, initial water content, different porous media and different boundary conditions. This is the first general transfer rate, and readily can be used in any dual porosity simulator. Also, t_d yields the proportionality constant for imbibition-germination models.

- *Limitations.* The group t_d has been derived making the standard assumptions used for analytical modes (section 3.1). In particular, viscous and gravity forces were ignored. Whether the presence of these forces can be accounted for through e.g. equation (3.9), and whether non-equilibrium effects in p_c would then have to be considered, remains open. Also, t_d is based on laboratory results where the core used was surrounded by a constant saturation. If and how t_d should be changed for e.g. fractured systems, where the saturation changes depending on the speed of the fracture flow, is open. Finally, the analytical solution is only valid as long as $t \leqslant t^*$.

Part II

FLOW AND TRANSPORT DURING TWO-PHASE FLOW

4

THE INFLUENCE OF FLOW REGIMES ON MIXING: SEMIANALYTICAL SOLUTIONS FOR IMBIBITION AND DISPERSION OF SOLUTES IN IMMISCIBILE TWO-PHASE FLOW

Understanding the growth of the dispersive zone $\delta(t)$ (Fig. 1.2) is crucial for many applications where both the flow of immiscible phases and miscible displacement occur. $\delta(t)$ is influenced by the interplay of three mechanisms: The flow regime, chemical reactions and heterogeneity. In this chapter, we resolve how the flow regime and a simple chemical reaction affects $\delta(t)$. To that end, we derive the first known set of analytical solutions that fully account for adsorption, capillary and viscous effects, and hydrodynamic dispersion. Dispersion is parametrized using a Fickian model (equation (2.5)). While there is an extensive debate concerning the modelling of dispersion in *single* phase flow (for a recent overview see e.g. [Dentz et al., 2011, Berkowitz, 2002]), the effect of the added non-linearities due to two phases on transport and dispersion is unclear ([Bolster et al., 2009] and chapter 2). Thus, the analytical solutions developed in this chapter may help in evaluating the reliability of a classical dispersion description for transport and two phase flow.
We show for the first time that for spontaneous imbibition without dispersion the solute front can be located graphically by a modified Welge tangent on the fractional flow function F. For transport with dispersion, we derive approximate analytical solutions by the method of singular perturbation expansion. The solutions reveal that for the viscous dominated regime, the growth of $\delta(t)$ is proportional to $t^{1/2}$. This confirms earlier numerical results [Arya et al., 1985]. Furthermore, the analytical solutions show for the first time that for spontaneous imbibition the spreading has a temporal order proportional to $t^{1/4}$, and that for both viscous and capillary dominated flow adsorption leaves the temporal order unchanged, but decreases the proportionality constant which has been unknown.

4.1 INTRODUCTION: FLOW AND TRANSPORT

The movement of solutes within two phase systems is important in many environmental and engineering applications since in almost all cases each fluid phase consists of different components rather than just one. Consequently, both the unsteady flow of the two phases and at the same time miscible displacement within each phase occur. Displacement processes of this kind take place, for example, if water is pumped into a geological formation or aquifer contaminated with non-aqueous phase liquids (NAPLs) and the ionic composition of the connate water is different from that of the injected water. In that scenario, both for the purpose of bioremediation and cleanup of NAPLs and enhanced oil recovery, surfactants and polymers are dissolved in the injected aqueous phase to mobilize the NAPLs [West and Harwell, 1992, Khan et al., 1996, Sorbie, 1991]. Here, the appropriate design of an efficient chemical flood crucially depends upon the brine composition, since the interfacial activity, phase behavior, and mobility control of the chemical flood depends as much on the concentration of the chemicals as it depends on the composition and mixing behavior of the ionic environment itself [Lake and Helfferich, 1977]. Similarly, for the design of aquifer remediation schemes, a vital step is to identify the location and distribution of the NAPLs. To this end, tracer tests can be performed where a range of both partitioning and non-partitioning solutes are injected into the subsurface and recovered down gradient at the extraction wells [Datta-Gupta et al., 2002]. Another example is carbon sequestration. Recent years have seen a growing awareness of the hazardous consequences of anthropogenic greenhouse gases, and one helpful mitigation method seems to be the sequestration of carbon dioxide in the subsurface, i.e. the reaction of carbon dioxide molecules (CO_2) with mineral grains [Javadpour, 2009, Xu et al., 2006]. In this case, CO_2 is dissolved in the water phase and the mixing with the brine triggers a number of aqueous reactions which lead to the CO_2 being trapped by the minerals. If water is pumped into a hydrocarbon reservoir in order to produce oil, the two aqueous solutions mix while replacing the oil, and the otherwise inert brine components react. In many reservoirs, this leads to the precipitation of minerals, like barium sulphate ($BaSO_4$), and formation of scale [Sorbie and Mackay, 2000, Mackay, 2003]) that can hinder production. In other scenarios, different ionic compositions have been shown to enhance oil recovery, if the injected brine has a salinity different from that of the connate brine [Zhang and Morrow,

2007, Austad and Standnes, 2003, Hiorth et al., 2010] and a good understanding of the transport of the different compositions within the two phases due to the interplay of dispersion, viscous and capillary forces builds the fundament for appropriate upscaling of transport and for determining its field efficiency [Stoll et al., 2008, Stephen et al., 2001].

In all these cases, a proper understanding of miscible displacement and dispersive mixing is fundamental to properly asses the amount of reactive solutes involved in chemical reactions (e.g. [Emmanuel and Berkowitz, 2005, De Simoni et al., 2005, 2007, Cirpka, 2002, Dentz et al., 2011]). Although the effects of dispersion and even spatial heterogeneity on miscible displacement and mixing for single-phase flow are increasingly well understood and a significant body of literature exists (e.g. [Werth et al., 2006, Rahman et al., 2005, Bolster et al., 2011, Paster and Dagan, 2008, Willingham et al., 2008]), investigations for two-phase systems so far only focus on the spreading of the phases themselves ([Neuweiler et al., 2003, Cvetkovic and Dagan, 1996, Langlo and Espedal, 1994, Panfilow and Floriat, 2004]). This is surprising given the practical importance of simultaneous flow and transport in two-phase systems, but can be explained with the complexity of the governing equations where both capillary, viscous and dispersive terms are coupled in a highly non-linear way.
Our solutions provide the framework for the common situation of two-phase core-floods, where both flow rates and breakthrough curves of tracers are available, and where *all* physical mechanisms - viscous and capillary forces and hydrodynamic dispersion - are considered.
The outline of this chapter is as follows: In section 4.3, we solve the advection problem exactly by two different methods: Based on the analytical solutions for two-phase flow with capillarity presented in chapter 2, we first combine a variable transformation with the physical notion that for the dispersion-free limit, the solutes can be written as functions of their carrying fluid only; second, we use the method of characteristics. We show that for spontaneous imbibition, the solution to the transport equation can be represented by a modified Welge tangent [Welge, 1952] to the factional flow function with capillarity F.
In section 4.5, we use a perturbation expansion to derive analytical expressions for hydrodynamic dispersion for the case where the dispersion coefficient is small compared to the characteristic length of the system. Based on these equations, we are able to obtain an analytical expression for the growth rate of the dispersive mixing zone, and show

how the spreading behaviour depends on the flow regime, on how it is influenced by the chemical reaction of the solute. These solutions are the first known analytical expressions for hydrodynamic dispersions in two-phase flow. In section 4.6 we compare the obtained solutions against numerical references solution for the cases of spontaneous co-, and counter-current imbibition and for the capillary-free limit, the Buckley-Leverett problem ([Buckley and Leverett, 1942], see chapter 2) and finish with some conclusions.

4.2 MATHEMATICAL MODEL

In the following, we assume that for the flow (2)-(4) hold (see section 2.2). Also, we assume that (i)-(v) holds for the components (section 2.1), and additionally we demand that

(vi) the components do not change the flow parameters.

Note that since we consider a horizontal, one-dimensional medium, density effects can also be ignored. Then the continuity equations for the components C can be written as [Acs et al., 1985, Gerritsen and Durlofsky, 2005]

$$\begin{aligned}\phi\frac{\partial(S_w C)}{\partial t}+\frac{\partial}{\partial t}\cdot[(1-\phi)\rho_r A_s]=\\ -\frac{\partial}{\partial x}(q_w\cdot C)+\frac{\partial}{\partial x}\cdot\left(\phi S_w D_{H,w}\frac{\partial C}{\partial x}\right).\end{aligned} \tag{4.1}$$

As stated above, the components are assumed to not change the flow field. If chemical flooding with surfactants, polymers, foams, etc., is considered, the constitutive relationships depend on both saturation and component concentration. For this case, analytical solutions can be derived, if both capillarity and hydrodynamic dispersion are ignored. This leads to a system of hyperbolic conservation laws and the method of characteristics or the method of chromatography can be used to derive analytical solutions (e.g. [Pope, 1978, 1980, Johansen and Winther, 1988, Juanes and Blunt, 2006, LaForce and Johns, 2005, Seto and Orr, 2009]). As explained in the introduction, our primary interest is the mixing of the adsorbing but otherwise inert components (Figure 1.2). We hence assume the capillary-hydraulic properties to be functions of saturation only. We denote the one dimensional tensor of hydrodynamic dispersion (equation (2.5)) as $D_{H,\gamma}$

$$D_{H,\gamma}=\alpha_{l,\gamma}\frac{q_\gamma}{\phi},\qquad \gamma\in\{n,w\}. \tag{4.2}$$

In the analysis that follows we mainly will focus on the case where the non-wetting phase has a homogeneous composition and is completely described by the restriction $S_w + S_n = 1$. To simplify notation, we will write D_H instead of $D_{H,w}$. For small concentrations Γ can be approximated by a linear sorption isotherm [Bedrikovetsky, 1993]

$$\Gamma = \Gamma(C) = \left(\frac{d\Gamma}{dC}\right) \cdot C =: \mathcal{D}_s \cdot C., \tag{4.3}$$

where $\mathcal{D}_s$ can be thought of as a 'retardation' term. Both the conservation equation for the fluid phase and the solutes are of parabolic type, and consequently the resulting solutions are smooth. Therefore, we can expand (4.1) to arrive at

$$\phi(S_w + \mathcal{D}_s)\frac{\partial C}{\partial t} = -q_w\frac{\partial C}{\partial x} + \frac{\partial}{\partial x} \cdot \left(\phi S_w D_H \frac{\partial C}{\partial x}\right). \tag{4.4}$$

We derive an analytical solution for the transport equation (4.1) that fully considers linear adsorption, capillary effects and hydrodynamic dispersion. Thus, all the physical mechanisms that account for solute transport and mixing in a homogeneous two-phase system are taken into account. The solution is obtained from two main ideas. First, we note that for cases where S_w and q_w in the conservation equation for C, equation (4.1) are known either from analytical or numerical solutions, the problem of solving the conservation equation for S_w and the coupled conservation equation for C (equation (4.1)) reduces to solving one advection-dispersion-reaction equation (ADRE) for the concentration C, namely equation (4.4). S_w and q_w are fully determined by equations (2.11) and (2.10) and are not affected by the adsorption of the solute.
For describing the flow and saturation field q_w and S_w, we choose the analytical solutions presented in Chapter 2. Thus, our solutions contain three important and common situations, namely: The situation where a sorbing solute is transported during spontaneous, co-and counter-current imbibition, and the situation where a sorbing solute is transported during viscous dominated flow where capillary effects become negligible.
The only time when we make specific use of the special form of these solutions, however, is for the explicit determination of the saturation level at which the solute advective front breaks through and in the examples given in section 4.6. The nonlinear expressions derived for the characteristics and the hydrodynamic dispersion and reaction are valid for any flow and saturation field known either from numerical solutions

like streamline simulations [Blunt et al., 1996, King and Datta-Gupta, 1998, Datta-Gupta and King, 1995] or analytical considerations.
Although this significantly reduces the complexity of the problem, the ADRE (4.4) has still time- and space-dependent coefficients, and no analytical solutions are known. Secondly therefore, to derive a solution for it we separate the two physical transport mechanisms in (4.1), i.e the advective motion due to viscous and capillary forces, and dispersive mixing.
The advective part is solved for exactly by two different approaches: First, we use the physical notion that if dispersion can be ignored, i.e. $D_H = 0$ in (4.1), C is a function of S_w only, and an explicit expression for the location of the solute front can be derived. Secondly, we use the method of characteristics. Both approaches yield the same result. We show that if q_w and S_w describe spontaneous imbibition, then the solution has a particular simple, graphical solution: The location of the solute front can be determined graphically by a modified Welge tangent [Welge, 1952] on the fractional flow function F. This is the first analytical solution that accounts for adsorption and spontaneous imbibition on tracer transport.
Next the effect of hydrodynamic dispersion is superimposed on the advective motion via a singular perturbation expansion around the advective front of the solute. Singular perturbation techniques have been used previously for describing dispersion in unsteady flow fields of a single-phase [Gelhar and Collins, 1971, Dagan, 1971, Eldor and Dagan, 1972, Nachabe et al., 1995, Wilson and Gelhar, 1981, 1974]. We show that if the dispersion is small compared to a characteristic length of the system, very good agreement between our analytical approximation and a numerical reference solution is achieved. While we are mainly concerned with the combined effects of adsorption, capillary, viscous and dispersive processes, and adsorption in this chapter, the equations derived for the characteristics and the hydrodynamic dispersion are valid for any given flow field and for illustration, we also combine them with the solution for the capillary-free limit, the Buckley-Leverett problem ([Buckley and Leverett, 1942], see chapter 2). This is the first analytical solution that fully describes the complex dependence of the effective dispersion on adsorption and the simultaneous and unsteady flow of the two phases.
From these analytical expressions we finally obtain equations for the growth rate of the dispersive zone both for the case of spontaneous imbibition, and for the viscous limit depending on the strength of ad-

sorption. The solutions reveal that for the viscous dominated regime, the growth of $\delta(t)$ is proportional to $t^{1/2}$, while for spontaneous imbibition it is is proportional to $t^{1/4}$. Adsorption leaves the temporal order unchanged, but decreases the proportionality constant.

4.3 SOLUTION OF THE ADVECTIVE PROBLEM

We first consider the dispersion-free limit of equation (4.4), i.e. the case $D_H = 0$. We will show that if an initial wetting phase is present, the solute front travels behind the fluid displacement front, and breaks through at a certain saturation value S_w^*. We will show that the retardation is due to the combination of the initial wetting saturation that acts as a storage for the solute and the adsorption, i.e. that adsorption alone cannot explain the retardation of solutes.
Two possibilities exist for deriving an analytical solution. The first one uses the physical notion that C is carried by the respective fluid phase, and thus we can write $C = C(S_w)$. This together with a variable transformation leads to a simple ODE for C. From this, we obtain an explicit expression for the saturation value S_w^* at which the advective front occurs that can be represented graphically by a modified Welge tangent [Welge, 1952]. We can obtain the same result for the location of the jump, if we employ the method of characteristics for solving equation (4.4). This has two advantages: First, it gives a mathematically rigorous justification for the physical notion that for the dispersion-free limit, C must be a function of S_w. Second, we obtain analytical expressions for the characteristic coordinates. They will prove to be central for the derivation of the dispersion approximation.
For the solute, we consider the boundary and initial conditions

$$\begin{aligned} C(x = 0, t) &= C_0, \\ C(\infty, t) &= C_i, \\ C(x, 0) &= C_i, \end{aligned} \tag{4.5}$$

and for q_w and S_w we use the same initial and boundary conditions as in Chapter 2 (equations (2.17)).

Solution as a Welge tangent

In this section we solve (4.4) together with (4.5) by employing the physical notion that for purely advective transport, a fixed value of C will

be transported at some fixed saturation level, i.e. C can be written as a function $C = C(S_w)$.
To that end, we again use the similarity variable λ (equation (2.24)).Then the conservation equation (4.4) for C can be rewritten as an ODE (Apendix B.1)

$$\frac{dC}{dS_w}\left[-\lambda + \frac{2A\,(F(1-f_iR)+f_iR)}{\phi(S_w+\mathcal{D}_s)}\right] = 0 \tag{4.6}$$

subject to

$$C = \begin{cases} C_0 & \text{for } S_w = S_0, \\ C_i & \text{for } S_w = S_i. \end{cases} \tag{4.7}$$

Equation (4.6) describes the transport of the jump from the initial concentration C_i to the injected concentration C_0 depending on the saturation, and has the simple solution

$$C(S_w) = \begin{cases} C_0 & \text{for } S_w < S_w^* \\ C_i & \text{for } S_w > S_w^*. \end{cases} \tag{4.8}$$

Since the jump C occurs at S_w^*, the value of S_w^* must occur where the expression in the bracket of the ODE (4.6) becomes zero. This yields a non-linear expression for S_w^*

$$\frac{F(S_w^*)}{\mathcal{D}_s + S_w^*} + \frac{f_iR}{(1-f_iR)S_w^*} = \frac{dF}{dS_w}|_{S_w^*}, \tag{4.9}$$

respectively for $S_{wi} = S_{wr}$, and $f_w(S_{wi}) = f_i = 0$:

$$\frac{F(S_w^*)}{\mathcal{D}_s + S_w^*} = \frac{dF}{dS_w}|_{S_w^*}. \tag{4.10}$$

All the functions and parameters in equations (4.9) and (4.10) are known explicitly, and the solution can easily be obtained by prescribing S_0, determining F from equation (2.33) and then solving the non-linear equation (4.9). Any capillary-hydraulic properties can be used. For arbitrary functions, the integrals of the exact solution need to be solved numerically. Determining S_w^* can also be performed graphically by drawing a straight line from $(0, \frac{f_iR}{(1-f_iR)})$ tangent to the fractional flow curve F, see Figure 4.1. Note that if initially a wetting phase is present, which is the case for most realistic geological formations and reservoirs, the component front gets retarded even if $\mathcal{D}_s = 0$ and does not travel

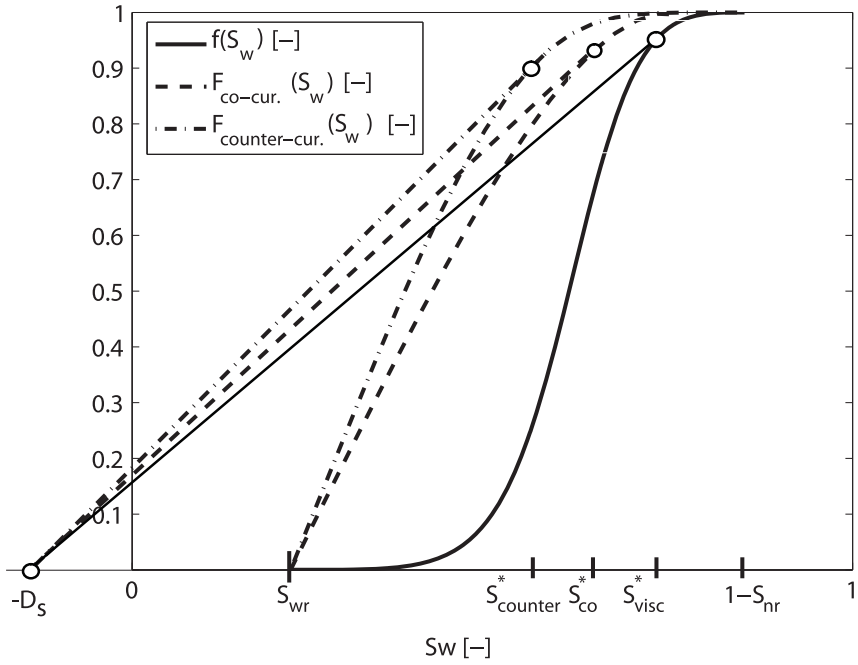

Figure 4.1: Fractional flow functions and corresponding modified Welge tangents [Welge, 1952] for purely viscous, spontaneous co-, and counter-current flow for different inlet saturations S_0. For the viscous and the counter-current case, $S_0 = 1 - S_{nr}$, and for the co-current case $S_0 < 1 - S_{nr}$. The straight lines give the saturation values for the respective cases at which the component, that adsorbs with rate $\mathcal{D}_s$, jumps from its initial value to the injected concentration for the dispersion free limit.

along with the phase front. This is intuitively obvious, since if the connate wetting phase has a composition different from the injected one, the 'new' composition needs to fill the 'old' phase first and thus breaks through behind the wetting front (Figure 1.2).
Whether spontaneous co-, or counter-current imbibiton occurs is determined by the ratio $R = q_t/q_w(x = 0, t)$ (chapter 2). In the foregoing analysis, R was not set to a specific value, and therefore the semi-analytical solution for C directly follows from (4.8) for the appropriate expressions for A and F with

$$\frac{F(S_w^*)}{(S_w^* + \mathcal{D}_s)} = \frac{dF}{dS_w}|(S_w^*). \tag{4.11}$$

4.4 SOLUTIONS FOR SOLUTES DISSOLVED IN THE NON-WETTING PHASE

In the previous sections we focused on solutes in the wetting phase. However, the solutions given above easily can be extended to the case where components χ are dissolved in the non-wetting phase, and satisfy

assumptions (i)-(vi). Their movement is described by the conservation equation

$$\begin{aligned}\phi\frac{\partial(S_n\chi)}{\partial t}+\frac{\partial}{\partial t}\cdot[(1-\phi)\rho_r B_s]=\\ -\frac{\partial}{\partial x}(q_n\cdot\chi)+\frac{\partial}{\partial x}\cdot\left(\phi S_n D_{H,n}\frac{\partial\chi}{\partial x}\right),\end{aligned} \tag{4.12}$$

where B_s denotes the adsorption per unit mass of rock of component. For the case where $S_0 < 1$, the saturation of the non-wetting phase at the left boundary is non-zero and we can prescribe the following initial and boundary conditions for solutes in the non-wetting phase:

$$\begin{aligned}\chi(x=0,t)&=\chi_0,\\ \chi(\infty,t)&=\chi_i,\\ \chi(x,0)&=\chi_i,\end{aligned} \tag{4.13}$$

which immediately gives

$$\chi(S_n)=\begin{cases}\chi_0 & \text{for } S_n < S_n^*\\ \chi_i & \text{for } S_n > S_n^*,\end{cases} \tag{4.14}$$

where S_n^* satisfies

$$S_n^* = 1 - S_w^{**}, \tag{4.15}$$

and

$$\frac{dF}{dS_w}|(S_w^{**})=\frac{F(S_w^{**})}{(1-S_w^{**}+\tilde{\mathcal{D}}_s)}-\frac{R(1-f_i)}{(1-f_iR)(1-S_w^{**}+\tilde{\mathcal{D}_s})}, \tag{4.16}$$

where we use

$$\tilde{\Gamma}:=\left(\frac{1-\phi}{\phi}\right)\rho_r B_s,\quad\text{and}\qquad\tilde{\Gamma}(\chi)=\tilde{\mathcal{D}}_s\cdot\chi. \tag{4.17}$$

Method of characteristics

Next, we derive the location of the jump in C at S_w^* by the method of characteristics, and show that the so derived value for S_w^* agrees with the one given in equation (4.9). The method of characteristics is more technical and lengthy than the intuitive approach taken above, where we simply assumed that C is carried along with the saturation and wrote C as a function of S_w only. However, it has two advantages: First,

it yields a rigorous mathematical justification for the analytical solution given in equations (4.8)-(4.10). Second, it results in the introduction of characteristic coordinates τ and θ that will prove to be useful when we solve for dispersion in section 4.5.
The equation for characteristics for the equation (4.4) is

$$q_w dt - (\phi S_w + \phi \mathcal{D}_s)\, dx = 0. \tag{4.18}$$

Equation (4.18) has an analytical solution in the sense that there exists a function $\eta(x,t)$ such that

$$\begin{aligned} -d\eta &= q_w dt - (\phi S_w + \phi \mathcal{D}_s) dx, \\ \frac{\partial \eta}{\partial t} &= -q_w, \quad \text{and} \quad \frac{\partial \eta}{\partial x} = (\phi S_w + \phi \mathcal{D}_s) \end{aligned} \tag{4.19}$$

if and only if

$$\frac{\partial \left(\phi S_w + \phi \mathcal{D}_s\right)}{\partial t} = \frac{\partial \left(\phi S_w\right)}{\partial t} \stackrel{!}{=} -\frac{\partial q_w}{\partial x}. \tag{4.20}$$

The above is simply the continuity equation for the wetting phase, and thus η as specified above exists. The characteristic can be determined from equation (4.19). From the second equation of (4.19), it follows

$$\eta(x,t) = \int_0^x (\phi S_w(\xi,t) + \phi \mathcal{D}_s)\, d\xi + \tilde{c}(t). \tag{4.21}$$

The function $\tilde{c}(t)$ must be determined from the first equation in (4.19). It follows

$$\begin{aligned} \frac{\partial \eta}{\partial t} =& \frac{\partial}{\partial t} \int_0^x (\phi S_w(\xi,t) + \phi \mathcal{D}_s)\, d\xi + \frac{d\tilde{c}(t)}{dt} \\ =& \int_0^x \frac{\partial}{\partial t} (\phi S_w(\xi,t) + \phi \mathcal{D}_s)\, d\xi + \frac{d\tilde{c}}{dt} = -q_w \\ =& \int_0^x -\frac{\partial q_w}{\partial x}|_\xi d\xi + \frac{d\tilde{c}}{dt}. \end{aligned} \tag{4.22}$$

Altogether, we arrive at

$$\eta(x,t) = \int_0^x (\phi S_w(\xi,t) + \phi \mathcal{D}_s)\, d\xi - \int_0^t q_w(0,\alpha) d\alpha. \tag{4.23}$$

In the following it will be useful to transform the first integral on the right hand side of η onto the (S_w, t) coordinate system, i.e. to use the fact that $x = x(S_w, t)$. By substitution, we thus get

$$\eta(S_w,t) = \int_{S_0}^{S_w} (\phi S_w(\xi,t) + \phi \mathcal{D}_s) \frac{\partial x}{\partial S_w}|_\xi d\xi - \int_0^t q_w(0,\alpha) d\alpha. \tag{4.24}$$

We set

$$\begin{aligned} \theta(S_w, t) &:= \int_{S_0}^{S_w} \left(\phi S_w(\xi, t) + \phi \mathcal{D}_s\right) \frac{\partial x}{\partial S_w}|_\xi \, d\xi, \quad \text{and} \\ \tau(t) &:= \int_0^t q_w(0, \alpha) \, d\alpha. \end{aligned} \tag{4.25}$$

The characteristic coordinates given in equation (4.24) are valid for arbitrary initial and boundary conditions, and any q_w, S_w, and S_n that satisfy equation (2.11). To derive an explicit expression for the value S_w at which the solute front occurs in the case where capillary effects are fully considered, we now capitalize on the features of the solutions for spontaneous imbibition (Chapter 2).
By construction, θ and τ are the coordinates along which equation (4.1) reduces to the simple form

$$\frac{\partial C}{\partial \tau} + \frac{\partial C}{\partial \theta} = 0. \tag{4.26}$$

If C is given by the function $H(x)$ at time $t = 0$, then the above PDE has the simple solution

$$C(\theta, \tau) = H(\theta - \tau) \tag{4.27}$$

and an inital solute front travels along the curve which satisfies $\theta \stackrel{!}{=} \tau$, i.e. S_w^* is such that $\eta \stackrel{!}{=} 0$. If the physically motivated approach of assuming $C = C(S_w)$ is valid, then the saturation S_w^* is again given by equations (4.9) and (4.10), respectively. This is indeed the case, see Appendix B.2. Before we derive the dispersion approximation, we discuss some features of the solution for the advective case.

The extended Buckley-Leverett problem

As discussed in Chapter 2, there is a strong analogy between solutions derived by Buckley and Leverett [1942] for viscous dominated flow and teh solutions derived by McWhorter and Sunada [1990] for capillary dominated flow. The McWhorter & Sunada solutions may be thought of as the capillary analogue to the Buckley-Leverett solutions. It is easy to expand this analogy to the so-called extended Buckley-Leverett problem, i.e. the case where a solute is transported according to equations (4.4), but capillarity and dispersion are ignored.
The extended Buckley-Leverett problem also satisfies (4.8), where for

$S_i = S_{wr}$ the constant S_w^* is given in [Pope, 1978, 1980, Johansen and Winther, 1988]:

$$\frac{f(S_w^*)}{(S_w^* + \mathcal{D}_s)} = \frac{df}{dS_w}|(S_w^*), \tag{4.28}$$

i.e. we again have the same structure of the solution with the only difference that the fractional flow function $f(S_w)$ neglects capillary forces where $F(S_w)$ can be viewed as a 'modified' fractional flow function that incorporates both viscous and capillary effects.

4.5 DISPERSION APPROXIMATION

The analytical solution derived above is valid if hydrodynamic dispersion can be ignored and we will now derive an approximate analytical solution for the case where dispersion is accounted for, i.e. for the ADRE (4.4). The solution is constructed in the same way the solution to the linear ADRE would be constructed, with the only difference that the parameters depend on the solution for the saturation profile. This introduces a strong time and space dependency of the coefficients, for which no exact analytical solutions for dispersion are known, and we will give an approximate analytical solution through an asymptotic expansion. Note again, that although we will focus on the case where the non-wetting phase is homogeneous and consists of one component only, the same analytical procedure can be used for analyzing the effect of hydrodynamic dispersion in the non-wetting phase.
We first normalize the ADRE by introducing $c := C/C_0$, $\bar{x} := x/L_0$, $\bar{t} = t/T_0$ and $\bar{q}_w = q_w/V_0$, where L_0, T_0 and V_0 are a characteristic length, time and velocity, respectively such that $\mathcal{O}(T_0) = \mathcal{O}(L_0) = \mathcal{O}(V_0)$ [Wilson and Gelhar, 1974]:

$$(\phi S_w + \phi \mathcal{D}_s)\frac{\partial c}{\partial \bar{t}} = -\bar{q}_w \nu \frac{\partial c}{\partial \bar{x}} + \varepsilon \nu \frac{\partial}{\partial \bar{x}}\left(S_w \bar{q}_w \frac{\partial c}{\partial \bar{x}}\right), \tag{4.29}$$

with

$$\varepsilon := \frac{\alpha_L}{L_0} \quad \text{and} \quad \nu := \frac{V_0 T_0}{L_0}.$$

For the case where dispersion needs to be taken into account, the only known analytical solutions for the ADE are valid for the single-phase case with a constant flow field where the fact that D_H is constant is heavily exploited to derive a solution [Carslaw and Jaeger, 1959]. We therefore employ a different approach: Singular perturbation expansion. Singular perturbation techniques have been used in many areas of

applied mathematics and fluid mechanics [Kevorkian and Cole, 1981, Van Dyke, 1975] and have been used before for treating the effect of non-uniform flow fields on dispersion of inert and adsorbing tracers in saturated and unsaturated single-phase flow through porous media [Gelhar and Collins, 1971, Dagan, 1971, Eldor and Dagan, 1972, Nachabe et al., 1995, Wilson and Gelhar, 1981, 1974].

While the details are technical (Appendix B.4 and B.3), the fundamental idea is very simple: For small ε, dispersion can be thought of as a perturbation to the advection equation. For $\varepsilon \neq 0$, the mathematical character of equation (4.29) fundamentally changes from a hyperbolic PDE to a parabolic one, and thus the perturbation is of singular nature. The solution (4.8) to the advection problem (4.4) is viewed as an 'outer solution' to the ADRE that is a good approximation away from a boundary layer. The boundary layer is characterized as the zone where dispersive effects are strong and thus will be located around the advective front. By 'magnifying' this zone through appropriate coordinate transformations, and by using the notion that around the front, q_w and S_w can be approximated by their values at the front, the PDE (4.4) reduces to the well-known heat equation. Then inner and outer solution are matched and a uniformly valid, closed form analytical solution is obtained.

Formally, equation (4.1) is the same as for the unsaturated single-phase case, where ϕS_w corresponds to the soil-moisture content and no restriction for a second phase is present. Thus, formally the dispersion approximation for equation (4.1) can be derived in the same manner as the one employed in [Wilson and Gelhar, 1981, 1974], and we will only give a rough outline. However, the characteristic length L_0 for the two-phase case is the distance between the wetting front and the point where the solutes start to break through. This is different from the single-phase case, where L_0 is the total distance traveled by the solute front [Gelhar and Collins, 1971, Dagan, 1971, Eldor and Dagan, 1972, Nachabe et al., 1995, Wilson and Gelhar, 1981, 1974].

Obviously, the idea of finding an approximate solution through a perturbation expansion does not only apply to hydrodynamic dispersion, but to any situation where a sharp front described by a hyperbolic PDE is smeared out by some parabolic terms. Consequently, earlier attempts to account for solute dispersion and capillary effects used a perturbation expansion around the jump in C *and* around the Buckley-Leverett shock in S_w [Bedrikovetsky, 1993, Barenblatt et al., 1990, Zazovskii, 1985].

However, this approach is unsatisfactory for two reasons. First, the per-

turbation expansion for the capillary part is only an approximation and leads to a loss of some of the information on the flow field. Second, to be able to use a perturbation approach, the flow must develop a discontinuity which can serve as the outer solution. While for the co-current situation the outer solution would be the Buckley-Leverett solution, it is not clear what can serve as outer solution for the counter-current case. There, one has $q_t = 0$, and the conservation equation for S_w (2.11) only comprises parabolic terms according to the nonlinear dispersion equation (2.21) for S_w. Indeed, none of the earlier attempts can account for the situation of spontaneous, counter-current imbibition despite its tremendous practical importance for fractured reservoirs (Chapter 3), but rather give an approximate solution for the co-current case only.
To the best of our knowledge, the solutions we present here therefore for the first time describe the situation where all the physical mechanisms - co, and counter-current imbibition, viscous effects, and dispersion - that account for the transport of a sorbing solute and mixing in a homogeneous two-phase system are taken into account.
Dispersive effects are strong around the jump in C which travels along the characteristic coordinates $(\bar{\theta}, \bar{\tau})$, where the overbar denotes normalized variables. Thus, to obtain an inner solution, it makes sense to first transform equation (4.29) onto the $(\bar{\theta}, \bar{\tau})$ coordinate system. Through usage of the Leibnitz rule and the product rule we obtain (Appendix B.3)

$$\frac{\partial c}{\partial \bar{\tau}} + \frac{\partial c}{\partial \bar{\theta}} = \frac{\varepsilon}{\bar{q}_{w0}} \Big[\frac{1}{(S_w + \mathcal{D}_s)(\partial \bar{x}/\partial S_w)} \frac{\partial}{\partial S_w} \Big((S_w + \mathcal{D}_s) S_w \bar{q}_w \Big) \frac{\partial c}{\partial \bar{\theta}} + \Big(\phi (S_w + \mathcal{D}_s) S_w \bar{q}_w \Big) \frac{\partial^2 c}{\partial \bar{\theta}^2} \Big]. \tag{4.30}$$

Note that if $\varepsilon = 0$ in equation (4.30), we indeed obtain the normalized version of the hyperbolic advection equation (4.26).
To magnify the region around the solute front, we introduce the coordinate transformation

$$\xi = \frac{\bar{\theta} - \bar{\tau}}{\varepsilon^m}. \tag{4.31}$$

The exponent m determines the 'thickness' of the boundary layer and can be determined either from physical or mathematical reasoning. Physically, it needs to be such that within the boundary layer dispersive changes are of same order of magnitude as temporal changes. Mathematically, it follows from the principle that it must be possible to match the inner solution 'around' the boundary region with the outer one

close to the boundary region. Formally, this leads to Van Dyke's principle of least degeneracy [Van Dyke, 1975, Kevorkian and Cole, 1981], which yields the same boundary-layer thickness as the one obtained from the physical approach. Transforming equation (4.30) onto the $(\bar{\tau}, \xi)$ coordinate system yields (Appendix B.4)

$$\frac{\partial c}{\partial \bar{\tau}} = \frac{1}{\bar{q}_{w0}\varepsilon^{2m-1}}\left[\frac{\varepsilon^m}{(S_w + \mathcal{D}_s)(\frac{\partial \bar{x}}{\partial S_w})}\frac{\partial}{\partial S_w}\Big((S_w + \mathcal{D}_s)S_w\bar{q}_w\Big)\frac{\partial c}{\partial \xi} + \Big(\phi(S_w + \mathcal{D}_s)S_w\bar{q}_w\Big)\frac{\partial^2 c}{\partial \xi^2}\right]. \tag{4.32}$$

The order of temporal change of the left hand side of (B.21) needs to be the same as the one of the right hand side which leads to $m = 1/2$. This is the same value for m as for the case without adsorption as expected since adsorption does not affect the flow field. The PDE (B.21) was derived through a number of coordinate transformation and thus is equivalent to (4.1).

We now seek an approximate analytical solution for equation (4.29) through an asymptotic expansion

$$C(\bar{\tau}, \xi) \sim C_0(\bar{\tau}, \xi) + \varepsilon^{(1/2)}C_1(\bar{\tau}, \xi) + \mathcal{O}(\varepsilon). \tag{4.33}$$

Inserting this in equation (B.21) with $m = 1/2$ and only retaining terms of zeroth order in ε leads to

$$\frac{\partial c}{\partial \bar{\tau}} = \frac{1}{\bar{q}_{w0}}\Big(\phi S_w(S_w + \mathcal{D}_s)\bar{q}_w\Big)\frac{\partial^2 c}{\partial \xi^2}. \tag{4.34}$$

This is the well-known diffusion equation and for the case where the coefficients on the right hand side are functions of $\bar{\tau}$ only, many analytical solutions are known [Crank, 1979, Carslaw and Jaeger, 1959]. To arrive at that form of the diffusion equation, we use the heuristic notion that S_w and $\bar{q}_w$ will undergo small changes around the solute front, and thus can be approximated by their values at the front. Formally, this corresponds to a Taylor expansion around the solute front that is truncated after the first term and thus gives the same order $\mathcal{O}(\varepsilon^{1/2})$ as the perturbation expansion. Altogether, we arrive at

$$\frac{\partial c}{\partial \bar{\tau}} = \frac{1}{\bar{q}_{w0}}\Big(\phi(S_w^* + \mathcal{D}_s)S_w^*\bar{q}_w^*\Big)\frac{\partial^2 c}{\partial \xi^2}, \tag{4.35}$$

where $()^*$ denotes that the value is taken at the solute front. The consequences and limitations of this approximation are discussed below. To be complete, the diffusion equation (4.35) needs to be supplemented

with initial and boundary conditions. They follow from the inner and outer solution and for the case of the step profile coinciding with (4.5). The diffusion equation (4.35) together with (4.5) written in the $(x,t)-$coordinate system, has the solution [Dagan, 1971, Carslaw and Jaeger, 1959]

$$C(x,t) = \frac{C_0}{2}\operatorname{erfc}\left(\frac{\int_0^x(\phi S_w(\xi,t)+\phi\mathcal{D}_s)d\xi - \int_0^t q_w(0,\delta)d\delta}{2\alpha_l^{1/2}\left[\int_0^{\tau(t)}\phi(S_w^*+\mathcal{D}_s)S_w^*(\frac{q_w(S_w^*)}{q_w(S_0)})dt\right]^{1/2}}\right) \quad (4.36)$$

By construction, the solution given in equation (4.36) is valid for the region around the boundary layer, whereas the solution given through equation (4.8) is valid away from the boundary layer.
For the initial- and boundary conditions as specified in (4.5), the uniformly-valid composite solution for the zeroth-order approximation coincides with equation (4.36). This is obtained as follows: To acquire a zeroth-order approximation that is uniformly valid throughout the whole region, we need to construct the composite solution which is given by [Kevorkian and Cole, 1981, Van Dyke, 1975]

$$c^{comp}(\bar{\theta},\bar{\tau}) = c^{in}(\bar{\theta},\bar{\tau}) + c^{out}(\bar{\theta},\bar{\tau}) - c^{match}(\bar{\theta},\bar{\tau}), \quad (4.37)$$

where the superscripts *comp*, *in*, *out*, and *match* denote the composite, the inner, the outer, and the matched solution, respectively. The inner solution $c^{in}(\bar{\theta},\bar{\tau})$ has been derived above, and is given in equation (4.36) in the (x,t) coordinate system. The outer solution $c^{out}(\bar{\theta},\bar{\tau})$ is the solution to the hyperbolic PDE, and is given by a step profile, equation (4.27). The matched solution $c^{match}(\bar{\theta},\bar{\tau})$ is the function that overlaps with $c^{out}(\bar{\theta},\bar{\tau})$ in the boundary layer, and with $c^{in}(\bar{\theta},\bar{\tau})$ away from it [Kevorkian and Cole, 1981, Van Dyke, 1975]. Given the functional form of $c^{out}(\bar{\theta},\bar{\tau})$ and $c^{in}(\bar{\theta},\bar{\tau})$, we therefore obtain that $c^{match}(\bar{\theta},\bar{\tau})$ must be the step function, i.e. $c^{match}(\bar{\theta},\bar{\tau}) = H(\bar{\theta}-\bar{\tau})$. Alltogether, from equation (4.37) we obtain that $c^{comp}(\bar{\theta},\bar{\tau}) = c^{in}(\bar{\theta},\bar{\tau})$, and thus the solution uniformly valid throughout the whole region $c^{comp}(\bar{\theta},\bar{\tau})$ is given by equation (4.36) in the (x,t) coordinate system.
As in the purely advective case, for the derivation of the first equation in (4.36), no features of the solutions for the flow field q_w or S_w were used. Consequently, this expression is valid for the initial and boundary conditions given in (4.5) and *any* q_w, S_w, and S_n that satisfy equations (2.11). The respective expressions can stem from either analytical solutions or could be combined with numerical calculations from e.g. streamline simulations [Blunt et al., 1996, King and Datta-Gupta, 1998,

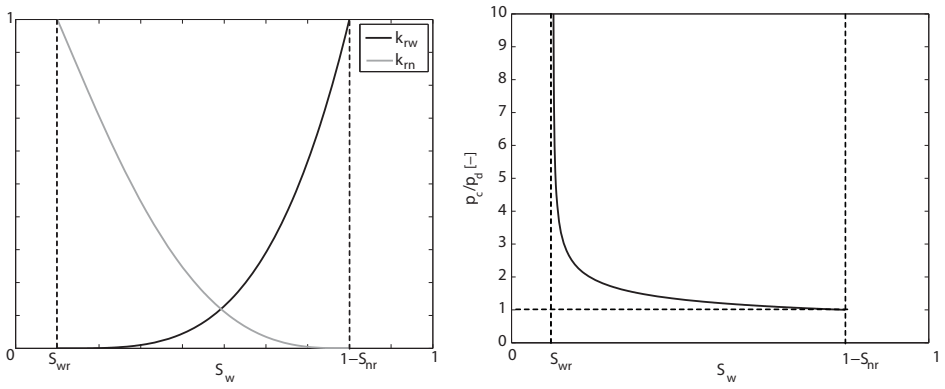

(a) (b)

Figure 4.2: Capillary-hydraulic properties for the Brooks-Corey parametrization for $\lambda_{BC} = 3$ and for residual saturations S_{wr} and S_{nr}. (a) Relative permeability functions k_{rw}, k_{rn}. (b) Capillary pressure function p_c.

Datta-Gupta and King, 1995]. In case boundary and initial conditions other than equation (4.5) are used, the matching function and the composite solution need to be modified accordingly.
From equation (4.36), we can obtain an expression for the growth of the dispersive zone (Figure 1.2), δ. Dispersion only plays a role around the solute front, i.e. where $x = x(S_w^*, t)$, and thus δ can be described by the rate of change around that front. This gives

$$\delta(t) = -\left(\frac{\partial C/C_0}{\partial x}\right)^{-1}_{x=x(S_w^*,t)}. \tag{4.38}$$

4.6 FLOW REGIME DEPENDENT MIXING AND DISCUSSION OF VALIDITY

In this section we combine the definition of $\delta(t)$ with the analytical expressions derived for C for the case of viscous dominated flow and imbibition. Moreover, we compare our analytical expressions to some numerical solutions and discuss under which condition the solutions are valid. For the numerical simulations, we use the algorithm described in Chapter 5.

For the perturbation expansion to be valid, $\varepsilon^{1/2} = (\alpha_L/L_0)^{1/2} << 1$ needs to be satisfied. We show that for the two-phase case L_0 is the distance between the wetting front and the point where the solutes start to break through. This is different from the single-phase case, where L_0 is the total distance travelled by the solute front.

Furthermore, we discuss the difference between the growth rate $\delta(t)$ of the dispersive zone (Figure 1.2) for the cases with and without capillary pressure. We show that for the case of spontaneous imbibition the dispersive zone grows with order $t^{(1/4)}$, while for the viscous limit, i.e. the Buckley-Leverett case, the order is $t^{(1/2)}$. Furthermore, we show that while adsorption does not affect the temporal order, it decreases the constant multiplier in the order, and thus the growth of $\delta(t)$ itself. The parametrizations for $D(S_w)$, $f(S_w)$ and $P_c(S_w)$ are either determined from experimental measurements or described analytically, see Figure 4.2. Several models exist to algebraically describe them. In the foregoing analysis, no assumptions for the functions D, f and P_c were used other than what is known from the underlying physics and thus any description for them can be used in our context. One of the most common models employed in both hydrological applications and the petroleum literature, the Brooks-Corey model [Brooks and Corey, 1964] uses the relations

$$k_{rw}(S_e) = S_e^{(2+3\lambda_{BC})/\lambda_{BC}}, \tag{4.39a}$$

$$k_{rn}(S_e) = (1-S_e)^2(1-S_e^{(2+3\lambda_{BC})/\lambda_{BC}}), \tag{4.39b}$$

$$p_c(S_e)/p_d = S_e^{-1/\lambda_{BC}}, \qquad P_c \geqslant p_d. \tag{4.39c}$$

Here, p_d is the entry pressure for the non-wetting fluid and λ_{BC} is the Brook- Corey parameter, $\lambda_{BC} \in [0.2, 3.0]$, see Figure 4.2. In the following examples, we restrict ourselves to the Brooks-Corey model, but as pointed out several times any choice for k_{rw}, k_{rn} and p_c is applicable.

SPONTANEOUS CO-CURRENT AND COUNTER-CURRENT IMBIBITION

For spontaneous imbibition, equations (4.36) and (4.38) become

$$\begin{aligned} C(x,t) &= \frac{C_0}{2}\operatorname{erfc}\left(\frac{\int_0^x(\phi S_w+\phi\mathcal{D}_s)(\xi,t)d\xi - 2At^{1/2}}{2\alpha_l^{1/2}\left(\phi S_w^*(\mathcal{D}_s+S_w^*)\right)^{1/2}\left(2At^{1/2}(F(S_w^*)(1-f_iR)+f_iR)\right)^{1/2}}\right) \\ \delta(t) &= 2\left[\left(\frac{\pi\alpha_l}{\phi}\right)\cdot\left(\frac{S_w^*}{S_w^*+\mathcal{D}_s}\right)2q_w^*t\right]^{1/2} \\ &= 2\left[\left(\frac{\pi\alpha_l}{\phi}\right)\cdot\left(\frac{S_w^*}{S_w^*+\mathcal{D}_s}\right)2A\sqrt{t}(F(S_w^*)(1-f_iR)+f_iR)\right]^{1/2} \end{aligned} \tag{4.40}$$

Figure 4.3 shows the comparison between numerical solutions and the analytical solution for the cocurrent flow and transport of sorbing and inert solutes for times $t = 0.7$ days, 1.5 days, 2.5 days and the parameter set given in Table 4.2. Figure 4.4 shows the comparison for the case

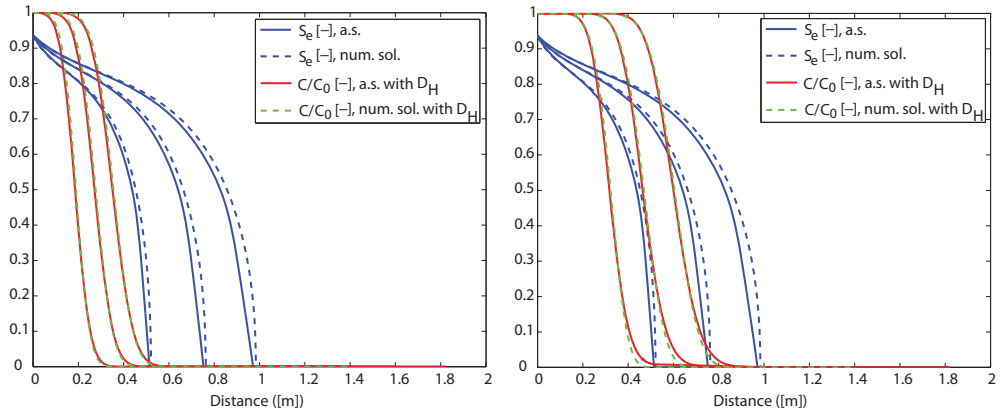

Figure 4.3: Dispersion approximation for cocurrent imbibition and transport for (a) a sorbing solute ($\mathcal{D}_s = 0.5\, m^3_{fluid}/m^3_{pv}$) and (b) an inert solute ($\mathcal{D}_s = 0$) at times $t = 0.7$ days, 1.5 days, 2.5 days. The corresponding ε is (a) $\varepsilon = 0.12, 0.056, 0.03$, and (b) $\varepsilon = 0.4, 0.3, 0.14$.

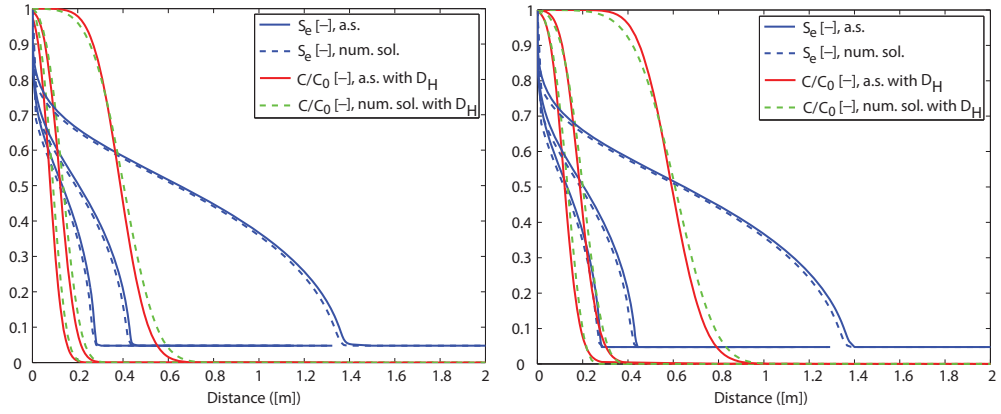

Figure 4.4: Dispersion approximation for cocurrent imbibition and transport for (a) a sorbing solute ($\mathcal{D}_s = 0.3\, m^3_{fluid}/m^3_{pv}$) and (b) an inert solute ($\mathcal{D}_s = 0$) at times $t = 0.7$ days, 1.7 days, 17 days. The corresponding ε is (a) $\varepsilon = 0.64, 0.25, 0.044$, and (b) $\varepsilon = 0.4, 0.3, 0.1$.

of counter-current imbibition for times $t = 0.7$ days, 1.7 days, 17 days and the parameter set given in Table 4.1. The perturbation expansion assumes $\varepsilon^{1/2} << 1, \varepsilon = \alpha_L/L_0$. The characteristic length of the system L_0 is the distance between the wetting front and the point where the concentrations start to break through. This is different from the perturbation expansions derived for the saturated and under-saturated single-phase case, where the characteristic length is the distance travelled by the solute front [Gelhar and Collins, 1971, Dagan, 1971, Eldor and Dagan, 1972, Nachabe et al., 1995, Wilson and Gelhar, 1981, 1974]. Figure 4.5 shows the comparison for spontaneous imbibition and the parameter set given in Table 4.1 for times $t = 2$ days, 17 days, 34 days. In this case, the connate wetting saturation is smaller than the ones in the previous

Table 4.1: Parameter sets for counter-current, spontaneous imbibition as shown in Figures 4.4, and 4.5.

Parameter	Unit	Set I (Figure 4.4)	Set II (Figure 4.5)
S_i	[–]	0.25	0.11
S_0	[–]	0.85	0.85
S_{wr}	[–]	0.22	0.1
S_{nr}	[–]	0.15	0.15
λ_{BC}	[–]	3.0	3.0
p_d	[Pa]	$1.5 \cdot 10^3$	$1.5 \cdot 10^3$
α_L	[m]	0.02	0.02
ϕ	[–]	0.25	0.25
μ_w	[Pa · s]	$1.0 \cdot 10^{-3}$	$1.0 \cdot 10^{-3}$
μ_n	[Pa · s]	$0.5 \cdot 10^{-3}$	$0.5 \cdot 10^{-3}$
$\mathcal{D}_s$	$[m_f^3/m_{PV}^3]$	0.3	0

Table 4.2: Parameter set for cocurrent case and viscous limit (Buckley-Leverett (BL) problem) as shown in Figures 4.3 and 4.7.

Parameter	Unit	Cocurrent case (Figure 4.3)	BL (Figure 4.7)
S_i	[–]	0.22	0.85
S_0	[–]	0.81	0.78
S_{wr}	[–]	0.22	0.22
S_{nr}	[–]	0.15	0.15
p_d	[Pa]	$1.5 \cdot 10^3$	-
λ_{BC}	[–]	3.0	3.0
α_L	[m]	0.01	0.00488
q_t	[m/s]	-	$2.1 \cdot 10^{-7}$
ϕ	[–]	0.25	0.25
μ_w	[Pa · s]	$1.0 \cdot 10^{-3}$	$1.0 \cdot 10^{-3}$
μ_n	[Pa · s]	$1.0 \cdot 10^{-3}$	$0.5 \cdot 10^{-3}$
$\mathcal{D}_s$	$[m_f^3/m_{PV}^3]$	0.5	0.3

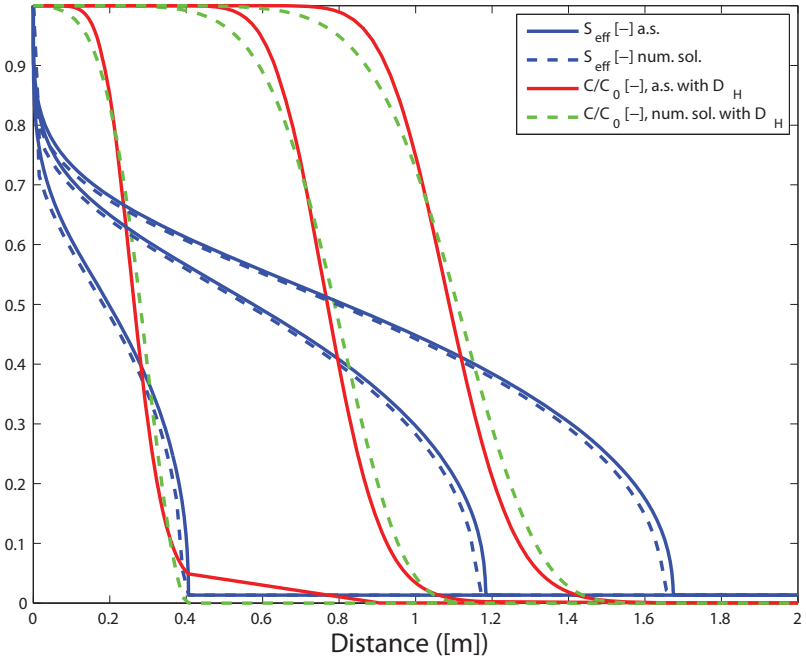

Figure 4.5: Dispersion approximation for spontaneous imbibition and parameter set II (Table 4.1) with $\alpha_L = 0.02m$ at times $t = 2d$, $17d$, $34d$. At time $t = 2d$, the distance between the solute and the wetting front is zero, which yields $\varepsilon_1 = \infty$ and thus the condition $\varepsilon << 1$ is violated. Consequently, the dispersion is overestimated and a dispersion of the components ahead of the solute front is wrongly predicted. For $t_2 = 17d$ and $t_3 = 34d$, $\varepsilon_2 = 0.43$ and $\varepsilon_3 = 0.2$, and the comparisons show good agreement.

two examples, and $\mathcal{D}_s = 0$, and consequently the retardation between the wetting front and the point where the solutes start to break through is smaller. At time $t = 2$ days, the distance travelled by the solute front is already longer than for $t = 0.7$ days for the case shown in Figure 4.4. However, the perturbation expansion for the case shown in Figure 4.5 overestimates the dispersion for this time, and predicts that the components disperse ahead of the solute front. This is physically impossible since there $q_w = 0$ and shows that the characteristic length for the two-phase system is not the distance traveled by the solute front but rather the distance between the wetting front and the point where the solutes start to break through. For later times, this distance increases, yielding declining values for ε and a good agreement between the numerical and the analytical solution is achieved.

Adsorbing components get retarded, and hence according to equation (4.10) 'see' a flow field different from the one for the inert solutes. Consequently, although the *order* over time for the growth of the dispersive zone stays the same, the *slope* will not. Adsorption results in a slightly higher S_w^* and thus a slightly higher flow rate. However, at the same time, $\delta(t)$ according to equation (4.40) is diminished by a factor

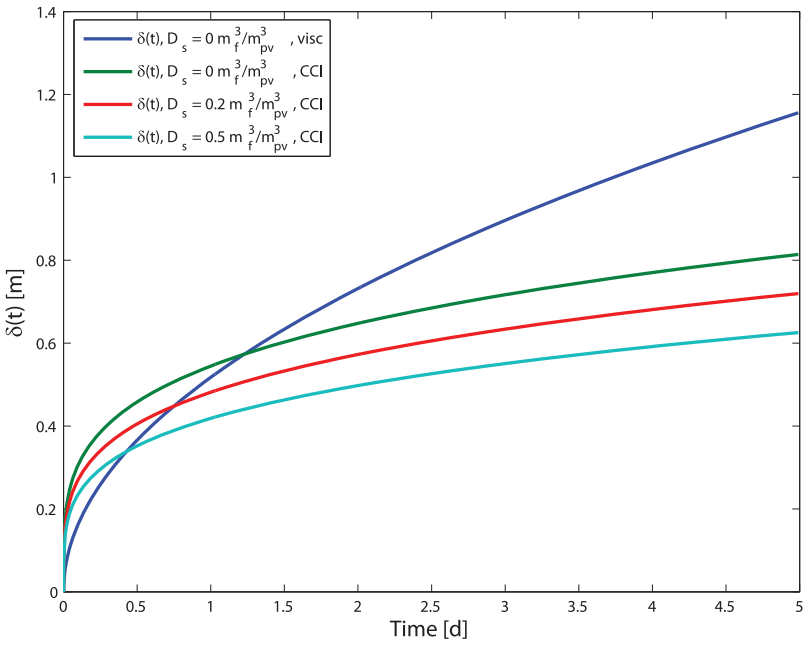

Figure 4.6: Comparison of growth of dispersive zones for spontaneous, counter-current imbibition, different adsorption rates $\mathcal{D}_s$, and the parameter set I given in Table 4.1 and for the viscous limit for the parameter set given in Table 4.2 with $\mathcal{D}_s = 0$.

$(S_w^*/(S_w^* + \mathcal{D}_s))$ which is a stronger effect than the increase in q_w, and altogether adsorption results in $\delta(t)$ growing more slowly compared to the inert case (Figure 4.6).

BUCKLEY-LEVERETT PROBLEM For the Buckley-Leverett problem with constant inflow rate q_t, and boundary conditions for S_w and C as specified in (2.17) and (4.5), respectively, equation (4.36) becomes

$$\begin{aligned} C(x,t) &= \frac{C_0}{2}\operatorname{erfc}\left(\frac{\int_0^x \phi(S_w+\mathcal{D}_s)\,d\xi - q_t\cdot t}{2(S_w^*(S_w^*+\mathcal{D}_s))^{1/2}\left[\phi\alpha_L q_t f_w(S_w^*)\cdot t\right]^{1/2}}\right), \\ \delta(t) &= 2\left[\left(\frac{\pi\alpha_l}{\phi}\right)\cdot\left(\frac{S_w^*}{S_w^*+\mathcal{D}_s}\right)\cdot q_t f_w(S_w^*)t\right]^{1/2}. \end{aligned} \tag{4.41}$$

For the Buckley-Leverett problem with constant inflow, the dispersive zone grows with order $\mathcal{O}(t^{1/2})$ compared to order $\mathcal{O}(t^{1/4})$ for spontaneous imbibition. Consequently, $\delta(t)$ for the situation of both laboratory setting of spontaneous imbibition and the situation in the field where spontaneous, (co-, or counter-current) imbibition is the dominant process (e.g. for the exchange between high- and low-permeability regions) and thus the rate of dispersive mixing, is smaller than that for the viscous case (Figure 4.6). Hence, for cases where the transport of components is considered whose *mixing* triggers reactions (e.g. wettability changes due to surface reactions), the amount or reactants available is

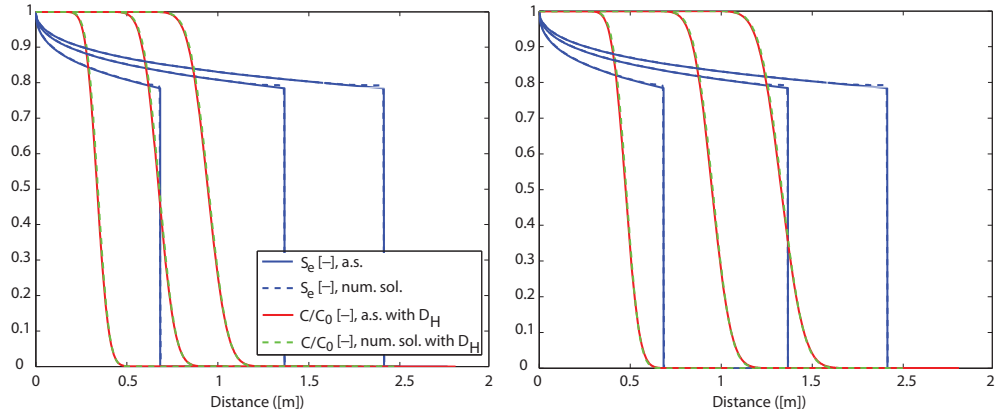

(a) (b)

Figure 4.7: Dispersion approximation for for viscous limit and transport for (a) a sorbing solute ($\mathcal{D}_s = 0.3\, m^3_{fluid}/m^3_{pv}$) and (b) an inert solute ($\mathcal{D}_s = 0$) at times $t = 5$ days, 8 days, 14 days. The corresponding ε is (a) $\varepsilon = 0.09, 0.02, 0.009$, and (b) $\varepsilon = 0.51, 0.06, 0.02$.

much smaller than for viscous dominated processes.
Figure 4.7 shows the comparison between numerical solutions and the analytical solution for times $t = 5$ days, 8 days, 14 days and the parameter set given in Table 4.2. The characteristic lengths are such that the condition $\varepsilon^{1/2} << 1$ is satisfied, and an excellent agreement between the numerical solution and the analytical one of this chapter is achieved.

4.7 SUMMARY AND CONCLUSIONS

We derived the first known set of semi-analytical solutions for solute transport in immiscible two-phase systems that describe the influence of adsorption, spontaneous co-, and counter-current imbibition, viscous forces and the time- and space dependent hydrodynamic dispersion. The solutions reveal for the first time a fundamental difference between the temporal order of spreading in viscous and capillary dominated flow.

- *Derivation via a singular perturbation expansion.* The closed-form analytical expressions for $C(x,t)$ (equation (4.36)) were obtained through a singular perturbation expansion. They are valid if the dispersion coefficient is small compared to the distance between the wetting front and the point where the solutes break through.

- *Representation as a Welge tangent.* For the dispersion-free limit, the solution with capillarity can be represented as a Welge-tangent to the capillary fractional flow function F (Fig. 4.1). This extends the

graphical representation for the extended Buckley–Leverett problem from the viscous case [Pope, 1980] to the case of spontaneous imbibition, and completes the analogue with the Buckley–Leverett solutions.

- $\delta(t)$ *depends on the flow regime (Fig. 4.6) and the chemical reaction (Fig. 4.6).* The growth rate $\delta(t)$ for the viscous dominated regime is proportional to $t^{1/2}$, and for imbibition it is is proportional to $t^{1/4}$ (equations (4.40) and (4.41)). The temporal order for the viscous limit confirms earlier numerical results [Arya et al., 1985]. The temporal order $t^{1/4}$ was previously unknown. As a consequence of the different temporal orders, the amount of mixing is far smaller for spontaneous imbibition than for the viscous case. Adsorption leaves the temporal order unchanged, but decreases the proportionality constant.

- *Application in numerical approximations.* The solutions for C (equation (4.36)) can be employed in connection with *any* solution for q_w and S_w. Thus, they also could act as building block for numerical schemes when numerical approximations for the flow and saturation field are used.

- *Dispersion and anomalous transport.* We used the classical parametrization of dispersion, equation (2.5). While there is an extensive debate concerning the modelling of dispersion in *single* phase flow, the effect of the added non-linearities due to the two phase flow field is unclear. Thus, the analytical solutions developed in this chapter may help in evaluating the reliability of a classical dispersion description for transport and two phase flow.

5

HIGHER ORDER FEFV METHODS ON UNSTRUCTURED GRIDS FOR TRANSPORT AND TWO-PHASE FLOW WITH VARIABLE VISCOSITY IN HETEROGENEOUS POROUS MEDIA

Analytical solutions for flow and transport are central for our understanding of flow and transport but they cannot resolve heterogeneous domains. In this chapter we therefore derive higher order methods for the numerical modelling of two-phase flow with simultaneous transport. The components we consider are adsorbing, viscosifying species within the individual phases. The algorithm we propose was implemented in the Complex System Modelling Platform (CSMP) which previously could resolve multiphase flow but not simultaneous transport and the associated challenging non-linearities.

The numerical scheme presented addresses three major challenges in simulating this process. Firstly, the component transport is strongly coupled with the viscous and capillary forces that act on the movement of the carrier phase. The discretization of the capillary parts is especially difficult since its effect on flow yields non-linear parabolic conservation equations. These are amenable to non-linear finite elements (FEs), while the capillary contribution on the component transport is first-order hyperbolic, where classical FEs are unsuitable. We solve this efficiently by a Strang splitting that uses finite volumes (FVs) with explicit time-stepping for the viscous parts and a combined finite element-finite volume (FEFV) scheme with implicit time-stepping for the capillary parts.

Secondly, the components undergo hydrodynamic dispersion and discerning between numerical and physical dispersion is essential. We develop higher-order formulations for the phase and component fluxes that keep numerical dispersion low and combine them with implicit FEs such that the non-linearities of the dispersion tensor are fully incorporated.

Thirdly, subsurface permeable media show strong spatial heterogeneity,

with coefficients varying over many orders of magnitude and geometric complexity that make the use of unstructured grids essential. In this work, we employ node-centered FVs that combine their ability to resolve flow with the flexibility of FEs. Numerical examples of increasing complexity are presented that demonstrate the convergence and robustness of our approach and prove its versatility for highly heterogeneous, and geometrically complex fractured porous media.

5.1 INTRODUCTION: NUMERICAL METHODS FOR FLOW AND TRANSPORT

The unsteady flow of two phases and the simultaneous transport of chemical components within each individual phase occurs in many environmental and engineering applications (Chapter 4). While analytical solutions play an important role in shedding light onto the underlying non-linearities (Chapters 3, 4) they often cannot resolve heterogeneity. Hence, efficient numerical schemes are necessary that can accurately capture the complex non-linearities of flow including changes in fluid properties and transport processes while allowing for highly flexible discretizations to represent the subsurface.
In recent years, combinations of Finite Element-Finite Volume (FEFV) methods [Huber and Helmig, 1999, Geiger et al., 2004, Matthäi et al., 2007, Durlofsky, 1993, Monteagudo and Firoozabadi, 2007, Reichenberger et al., 2006] have been developed to simulate laminar two-phase flow in heterogeneous porous media (e.g. oil and ground water reservoirs). FEFV methods unite the geometric flexibility of finite element (FE) discretizations necessary for the complex geological structures found in the subsurface (Fig. 1.1) with the capabilities of finite volume (FV) techniques to give a stable, locally mass-conservative approximation of the flow processes. Thus, these methods are ideally suited for multi phase flow simulation in realistic subsurface porous media (Fig. 1.1). In the FEFV approach, the FEs are used to solve the parabolic pressure equation from which the element-wise constant velocity field is obtained. This leads to flux continuity on the dual FV grid (Fig. 5.1). The velocities are then used in the FV scheme to transport the phases which guarantees mass conservation. Another advantage is that lower order elements can readily be applied to model high aspect ratio structures such as fractures and faults [Martin et al., 2005, Lee et al., 2001, Hoteit and Firoozabadi, 2008, Niessner and Helmig, 2007, Geiger et al., 2004, Matthäi et al., 2007] which are present in porous media but are

notoriously difficult to discretize with reasonable computational cost (Fig. 1.1). The FEFV methods proposed so far focus on either resolving multi-phase flow or single-phase transport but do not treat the simultaneous transport of chemical species and their impact on the flow field through component-induced viscosity changes. The latter effect is a key flow behavior in many environmental and engineering applications. In this chapter, we extend the FEFV method such that it can account for both flow and transport of adsorbing species dissolved in the water phase, where the transported solutes affect the viscosity of the carrying fluid, while reducing numerical dispersion.

First-order FV schemes introduce strong numerical dispersion which makes the distinction between the numerical and the actual physical dispersion difficult. We formulate two different second-order methods of the monotone upwind-centered scheme for conservation laws (MUSCL) type for the transport and flow equations. The conservation equation for the components is of advection-dispersion-reaction type, and we use a Strang splitting [Strang, 1968]. The hyperbolic advection-reaction part is solved using explicit in time, second order FV schemes. Together with the equation for the adsorption isotherm, this yields a system of non-linear equations that is solved via a Newton method combined with a line-search method to achieve better convergence [Nocedal and Wright, 1999]. The full space and time dependency of hydrodynamic dispersion on the flow field is modelled through a Fickian dispersion tensor and is solved via an implicit FE scheme. The situation we treat is different from that of two-phase multicomponent simulations. In our situation, the concentrations are reconstructed from the saturations, whereas for multicomponent simulations the phase components and pressure are used in flash calculations to reconstruct the saturations [Niessner and Helmig, 2007, Mallison et al., 2005, Mikyška and Firoozabadi, 2010, Karimi-Fard et al., 2006, Geiger et al., 2009, Moortgat et al., 2011, Moortgat and Firoozabadi, 2010].

Three other common methods developed during recent years for the simulation of multiphase flow include finite difference methods, combined FV-transmissibility tensor methods and the streamline method. As a starting point for the extension to a scheme for flow and transport, alternative to the FEFV method, flux-based finite difference methods or FV-transmissibility tensor methods may be used. For the finite difference methods, multipoint flux approximations are used to obtain correct discretizations of the flow equations for heterogeneous media and general non-orthogonal grids (e.g. [Aavatsmark, 2002, Lie et al., 2011]).

In the combined FV-transmissibility tensor methods, transmissibilities relate the pressure difference between adjacent FV cells to the flow between these cells (e.g. [Edwards and Zheng, 2010, Edwards, 2002]), an approach that can also be coupled with higher-order methods (e.g. [Lamine and Edwards, 2008]). The streamline method seems unsuitable for two-phase multicomponent flow. It transforms the flow equations onto a coordinate system that is aligned with the principal axis of flow which makes them one-dimensional, resulting in a fast solution method [Blunt et al., 1996, King and Datta-Gupta, 1998]. This approach makes accounting for dispersion of components orthogonal to the principal axis difficult.

The remainder of this chapter is structured as follows: First, we describe the numerical solution. The numerical discretization of two-phase flow without transport via FEFV-schemes has been described previously [Huber and Helmig, 1999, Geiger et al., 2004, Matthäi et al., 2007], and we show how the formulation is extended to the case where components affect the fluid properties. Then we first describe how the pressure and velocity field is obtained. Subsequently, we describe how the phase saturations and components are discretized. For the FV scheme, we initially describe the first order single-point upstream method, and then introduce two second order methods. The algorithm is summarized in section 4. We then give five numerical test cases that show the convergence of the different schemes and their versatility to resolve flow and transport in fractured, highly heterogeneous domains. In particular, we show the dependence of the resolution on the grid Peclet number. We finish the chapter with some a summary and conclusions.

5.2 NUMERICAL SOLUTIONS

The phase pressure equation for incompressible porous media, equation (2.8), and the equations for fluid flow, (2.11) and the ADRE equation (2.12) form a strongly coupled, non-linear system of PDEs. We compute the solutions of these PDEs numerically by solving implicitly in pressure and explicitly in saturation and in components (IMPEC approach, [Aziz and Settari, 1979, Gerritsen and Durlofsky, 2005]). This approach decouples the equations. Thus, the equations can be treated in a sequential manner which allows for the usage of different numerical solution techniques for the different equations. We use a combination of a higher order FV scheme for advection dominated problems and a FE approximation for diffusion-like problems.

We will first introduce the discretization method we use, then describe how the pressure field is calculated and how we obtain the velocity field from it. Subsequently, we describe, how the new component and saturation values are calculated.
For simplicity, we assume that the capillary pressure curves are functions that do not depend upon the spatial heterogeneity of the domain. Different capillary pressure curves lead to jumps in the saturation profiles along material interfaces [Nayagum et al., 2004, Hoteit and Firoozabadi, 2008]. For flow without the transport of a dissolved component, the influence of an inhomogeneous p_c can be incorporated by solving for two additional conditions across material interfaces that guarantee flux continuity and continuity of capillary pressure, but pose a major difficulty for the actual implementation [Reichenberger et al., 2006, Hoteit and Firoozabadi, 2008, Niessner et al., 2005]. Obviously, the case of homogeneous p_c curves is a special case of the general scenario, and thus any scheme that resolves the influences of heterogeneous p_c on both saturation and components necessarily has to build upon the simple, albeit often unrealistic homogeneous case discussed here. Also, since even the numerical resolution of the influence of homogeneous p_c and dispersion on unstructured grids on flow and transport so far has not been solved, the treatment of the situation of general p_c curves for both the saturations and the components is clearly beyond the scope of this chapter and will be discussed in forthcoming work.
We implemented the numerical schemes described here in the Complex System Modeling Platform (CSMP++) [Matthäi et al., 2007] library designed for modelling fluid flow in structurally complex geological geometries.

Discretization

The computational domain $\Omega \subset \mathbb{R}^d, d \in \{2, 3\}$ comprises two subdomains Ω_m and Ω_f. For simplicity, we will assume $\Omega \subset \mathbb{R}^2$ but our approach immediately carries over to three dimensions [Paluszny et al., 2007]. $\Omega_m \subset \mathbb{R}^2$ is the subdomain for the matrix, and $\Omega_f \subset \mathbb{R}^1$ is the set of fractures $\{f_1, \ldots, f_{n_f}\}$ of width δ so that [Reichenberger et al., 2006, Monteagudo and Firoozabadi, 2007]

$$\Omega = \Omega_m + \delta\Omega_f. \tag{5.1}$$

The pressure equation (2.8) and the mass-conservation equation for the saturation, equation (2.11) and the components, equation (2.12) apply to

both fractures and matrix. Hence, the integration over the domain can be written as [Reichenberger et al., 2006, Monteagudo and Firoozabadi, 2007]

$$\int_{\Omega} \mathcal{G} d\Omega = \int_{\Omega_m} \mathcal{G} d\Omega_m + \delta \int_{\Omega_f} \mathcal{G} d\Omega_f \tag{5.2}$$

where $\mathcal{G}$ stands for one of the unknowns p_w, S_w or the unknown product for the components $S_w \cdot C$.
We discretize the domain Ω_m with constrained conforming Delaunay triangles and/or quadrilaterals. Based on this FE mesh, a node centered FV subgrid is generated [Durlofsky, 1994, Huber and Helmig, 1999] through a barycentric tessellation [Paluszny et al., 2007] where the barycenter of each element is connected with the midpoints of the associated edge (Figure 5.1). High aspect ratio structures such as fractures are modelled as lower dimensional elements, i.e. 1D lines in $\mathbb{R}^2$, and 2D surfaces in $\mathbb{R}^3$. Material properties are defined on the elements (Figure 5.1) so that this approach makes their integration from element to element possible, and it yields FV cells that can be represented in parametric space [Paluszny et al., 2007] and thus is well-suited for the simulation of flow and transport in complex geometries.
In the following, the calculation of the left-hand side of equation (5.2) for the unknowns p_w, S_w, C by FEs and FVs is described. The influence of the fractures is then accounted for by extending the integral $\int_\Omega$ according to equation (5.2). Since $\Omega = \Omega_m + \delta\Omega_f$, the integral over Ω_m is identical to the integral over Ω whereas the integral over Ω_f must be multiplied by the width δ.

Pressure-, and velocity field

The calculation of the pressure field by the FE method is described first. We introduce the space of piecewise linear functions $\mathcal{V}$ which is spanned by the nodal basis $\{\Phi_i\}_{i=1}^m \subset \mathcal{V}$,

$$\Phi_i(\mathbf{x}_j) = \begin{cases} 1 & \text{for } i = j, \\ 0 & \text{otherwise,} \end{cases} \tag{5.3}$$

where $\mathbf{x}_j$ is the coordinate vector of node j. After transforming the pressure equation into weak form and applying the Galerkin projection onto $\mathcal{V}$, equation (2.8) becomes

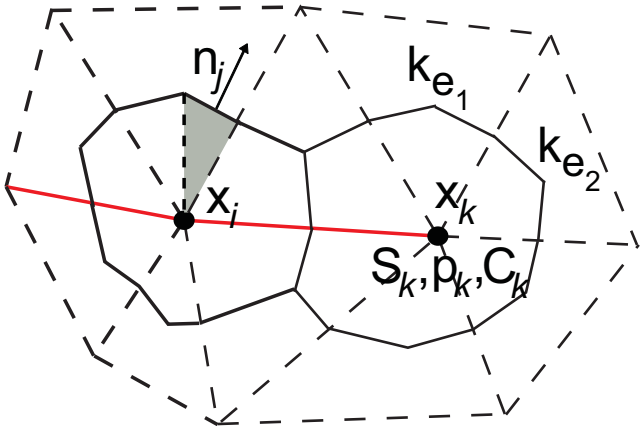

Figure 5.1: Discretization of the domain with conforming Delauny triangles and node-centered FV subgrid. The shaded region represents segment j of FV V_i and the respective normal vector $\mathbf{n}_j$. The pressure, saturation and components are defined on the nodes, and material properties, such as permeability $\mathbf{k}$ and porosity ϕ on the elements. $\mathbf{q}$ is computed as an element-wise constant property by interpolating S_w and C to the FE bary center. Note that the fluxes then are continuous across the FV interfaces. The red lines represent fractures which are modelled as lower dimensional elements.

$$\begin{aligned}\int_\Omega \lambda_t \nabla p_w \mathbf{k} \nabla \Phi_i dx = &- \int_\Omega \lambda_n \nabla p_c \mathbf{k} \nabla \Phi_i \, dx \\ &- \int_\Omega \nabla \cdot [(\rho_n \lambda_n + \rho_w \lambda_w)\, \mathbf{g}] \cdot \Phi_i \, dx, \qquad i = 1, \ldots, m\end{aligned} \tag{5.4}$$

with the basis representation of p_w,

$$p_w(x) = \sum_{j=1}^{m} p_{w,j} \Phi_j(x), \tag{5.5}$$

where $p_{w,i} = p_w(\mathbf{x}_i)$. Equation (5.4) together with (5.5) can be written as a system of linear equations $\mathbf{Ap} = \mathbf{b}$, where

$$\begin{aligned}&\mathbf{p}_{w,i} = p_w(\mathbf{x}_i), \quad \mathbf{p}_w \in \mathbb{R}^m, \\ &\mathbf{b}_i = -\int_\Omega \lambda_n \nabla p_c \mathbf{k} \nabla \Phi_i \, dx - \int_\Omega \nabla \cdot [(\rho_n \lambda_n + \rho_w \lambda_w)\, \mathbf{g}] \cdot \Phi_i \, dx, \quad \mathbf{b} \in \mathbb{R}^m, \\ &\mathbf{A}_{ij} = \int_\Omega \lambda_t \nabla \Phi_i \mathbf{k} \nabla \Phi_j \, dx, \quad \mathbf{A} \in \mathbb{R}^{m \times m}.\end{aligned} \tag{5.6}$$

$\mathbf{A}$ is the stiffness matrix, and is symmetric and positive definite [Ciarlet, 1979] and thus the linear system is uniquely solvable. Furthermore, the matrix $\mathbf{A}$ is sparse which allows for fast solving strategies. We use the

algebraic multigrid method implemented in CSMP++ for large problems that arise for geometrically complex domains [Stüben, 2001, Krechel and Stüben, 2001] and a classical Gauss solver for simple domains. The influence of the fractures is accounted for by simply expanding the integrals over Ω above according to equation (5.2). The oil pressure p_n is computed in the same manner. Once the pressure equations have been solved, the velocity field can be obtained which then is piecewise constant on the FEs. In CSMP++, the velocity is calculated by element-wise differentiation of the pressure-field

$$\mathbf{q}_{\alpha,j} = \sum_{i,j}^{n,d} -\mathbf{k}_{ij}\lambda_\alpha \left(p_{\alpha i}\nabla\Phi_{ij} - \rho_\alpha \mathbf{g}\right), \tag{5.7}$$

which leads to velocities that are element-wise constant and hence continuous between adjacent node-centered finite volumes (Fig. 5.1). Thus they can resolve discontinuities in material properties since material properties are defined on the FEs [Geiger et al., 2004]. Here, i and j are indices over the n nodes of element e, respectively, and d is its dimension. $\nabla\ \Phi$ is a matrix of size $d \times n$ holding the derivatives of Φ_i. λ_α is assumed to be constant for e. This method has been successfully employed in high-resolution fluid flow in complex reservoirs [Huber and Helmig, 1999, Geiger et al., 2004, Matthäi et al., 2007, Geiger et al., 2009, Paluszny et al., 2007, Matthäi et al., 2009]. Note that $\mathbf{k}$ and ϕ must be scaled by the fracture aperture to obtain the right volumetric flux and pore-volume for lower-dimensional elements.

Phase saturations

Equation 2.11 consists of a first-order hyperbolic advective part, and a second-order parabolic diffusion part [Huber and Helmig, 1999]. If an explicit time discretization is applied on 2.11, a necessary condition for stability is that the time-step Δt satisfies the Courant-Friedrich Levy (CFL) condition. If only the hyperbolic contribution in equation (2.11) is resolved, the CFL condition has the form [LeVeque, 2002]

$$\Delta t_{max} \leqslant \min_V \left(\frac{L_V}{q_{t,V_{max}}}\right), \tag{5.8}$$

where L_V is the length of the principal axis in finite volume V that is aligned with the direction of flow and $v_{t,V_{max}}$ is the maximal velocity in V.

It is well known [Aziz and Settari, 1979, LeVeque, 2002] that while the CFL condition for a pure advection problem, equation (5.8), leads to the requirement $\Delta t = \mathcal{O}(\Delta x)$, the presence of the diffusive term in equation (2.11) leads to a CFL condition of the form $\Delta t = \mathcal{O}(\Delta x^2)$, where Δx is the smallest cell diameter for the grid used. Thus for a fully explicit scheme, the diffusion leads to prohibitively small time-steps for fine grids. We avoid this problem by applying a Strang splitting [Strang, 1968, LeVeque, 2002]: We discretize the time-derivatives with the explicit Euler scheme and then alternately solve the problems

$$\begin{aligned} (A_S) \quad \phi \frac{\partial S_w}{\partial t} &= \nabla \cdot \Big(\mathbf{k} \frac{f(S_w, C) k_{rn}}{\mu_n} \frac{dp_c}{dS_w} \nabla S_w \Big) \qquad \text{and} \\ (B_S) \quad \phi \frac{\partial S_w}{\partial t} &= -\nabla \cdot \big(f(S_w, C) \mathbf{q}_t \big) - \nabla \cdot \big(\overline{\lambda}_t (\rho_w - \rho_n) \mathbf{k} \nabla \mathbf{g} \big) , \end{aligned} \tag{5.9}$$

where we write $\overline{\lambda}_t = \frac{\lambda_w \lambda_n}{\lambda_t}$. This splitting has been applied to two-phase flow in porous media before [Nayagum et al., 2004, Siegel et al., 1997]. It provides us with the advantage that we can solve problem (A_S) with an unconditionally stable implicit scheme and (B_S) with an explicit scheme where the time step only has to satisfy $\Delta t = \mathcal{O}(\Delta x)$. Alternatively, problem (B_S) also could be solved implicitly, but the use of an implicit method with higher order schemes is challenging, and therefore not employed here [Blunt and Rubin, 1992].

If (A_S) is solved with a full time step preceded by a full time step for (B_S), the resulting splitting error is of order $\mathcal{O}(\Delta t)$. For the sequence half-time step (A_S), full time-step (B_S), half time-step (A_S) the splitting error can be decreased to $\mathcal{O}(\Delta t^2)$ [LeVeque, 2002, Strang, 1968].

We first deal with the solution of problem (A_S). This is a parabolic problem, and can be solved in the same manner as the pressure equation.

We use an explicit Euler scheme for the time derivatives in (A_S) in equation (5.9), and then apply the Galerkin projection onto $\mathcal{V}$, which yields

$$\begin{aligned} &\Big(\int_\Omega S_w^* \cdot \Phi_i \, dx + \frac{\Delta t}{\phi} \int_\Omega \big(\mathbf{k} \frac{f k_{rn}}{\mu_n} \frac{dp_c}{dS_w} \nabla S_w^* \cdot \nabla \Phi_i \, dx \big) \Big) = \\ &\int_\Omega \Phi_i S_w^t \, dx \\ &i = 1, \ldots, m, \end{aligned} \tag{5.10}$$

where the saturation of the previous time step has been denoted by S_w^t, and we use the basis representation $S_w^* = \sum_j S_w^*(x_j)\Phi_j(x)$. We can write (5.10) as a system of linear equations

$$(\mathbf{A}_S + \mathbf{M}_S)\mathbf{S}_w^* = \mathbf{b}_S \tag{5.11}$$

with

$$\begin{aligned}
\mathbf{A}_{S,ij} &= \frac{\Delta t}{\phi}\int_\Omega \left(\lambda_t \mathbf{k}\frac{dp_c}{dS_w}\nabla\Phi_i \cdot \nabla\Phi_j\right) dx, && \mathbf{A} \in \mathbb{R}^{m\times m},\\
\mathbf{M}_{S,ij} &= \int_\Omega \Phi_i \cdot \Phi_j \, dx, && \mathbf{M} \in \mathbb{R}^{m\times m},\\
\mathbf{S}_{w,i}^* &= S_w^*(x_i), && \mathbf{S}_w^* \in \mathbb{R}^m,\\
\mathbf{b}_{S,i} &= \int_\Omega \Phi_i S_w^t \, dx, && \mathbf{b} \in \mathbb{R}^m.
\end{aligned} \tag{5.12}$$

$\mathbf{M}_S$ is the mass matrix, and it has been shown that mass lumping, i.e. diagonlization of $\mathbf{M}_S$, is essential to avoid spurious oscillations of unsaturated flow [Celia et al., 1990]. To evaluate the integrals over Ω, λ_t, $\mathbf{k}$ and $\frac{dp_c}{dS_w}$ need to be evaluated on the elements. To this end, one value for the saturation and the component per element is needed, which we obtain by interpolating S_w and C at the barycenter of one element with a linear interpolation. We solve the linear system of equations in the same manner as for the pressure equation. As for the pressure equation the influence of the fractures is accounted for by simply expanding the integrals over Ω above according to equation (5.2). If the initial S_w is close to the residual saturation S_{wr}, the change in capillary pressure can be steep, and evaluating p_c at the previous time-step can introduce large errors. An easy way of overcoming this, is to use a predictor-corrector scheme which after solving problem (A_S) re-evaluates the flow parameters with the updated S_w, and solves problem (A_S) again. We found that this procedure leads to good approximations after only few iteration steps.

The discretization of problem (B_S) in equation (5.9) is discussed next. The numerical approximation of advection dominated problems with classical FEs introduces spurious oscillations and is therefore unsuitable and a FV scheme or discontinuous FE methods should to be applied [Nayagum et al., 2004, Hoteit and Firoozabadi, 2008]. However, contrary to an FE-FV approach, discontinuous FE methods cannot readily be incorporated into an existing FE code and require several degrees of freedom per variable and node. We therefore employ an FE-FV approach. We use the element-wise constant velocities calculated from

equation (5.7) to compute the mass balance of the fluid phases. Discretizing equation (5.9) via an explicit Euler scheme in time and integration over a finite volume V_i yields

$$\begin{aligned}&\int_{V_i} \left(S_w^{t+1} - S_w^t\right) \, dV = \\ &-\frac{\Delta t}{\phi}\left(\int_{V_i} \nabla \cdot \left(f\mathbf{q}_t\right) dV\right) \\ &-\frac{\Delta t}{\phi}\left(\int_{V_i} \nabla \cdot \left[(\rho_w - \rho_n)\overline{\lambda}_t \mathbf{k}\nabla\mathbf{g}\right] \, dV\right)\end{aligned} \tag{5.13}$$

where for the evaluation of f, C and S_w from the previous time-step are used, and a summary of the algorithm is given in section 4. Applying the divergence theorem, equation (5.13) leads to the accumulation of all segment fluxes in and out of V_i

$$\begin{aligned}&\int_{V_i} \left(S_w^{t+1} - S_w^t\right) \, dV = \\ &-\frac{\Delta t}{A_i}\sum_j^{n_{si}} \left[f_j \mathbf{q}_{tj}\right] \cdot \mathbf{n}_j - \frac{\Delta t}{A_i}\sum_j^{n_{si}} \left[(\rho_w(S_w^*, C^*) - \rho_n)\overline{\lambda}_{t,j}\mathbf{k}\nabla\mathbf{g}\right] \cdot \mathbf{n}_j\end{aligned} \tag{5.14}$$

where $\sum_j^{n_{si}}$ is the summation of all fluxes $\left[f_j \mathbf{v}_{tj}\right] \cdot \mathbf{n}_j$ at segment j belonging to the group of segments n_{si} of finite volume V_i. A_i is the area of the control volume, and $\mathbf{n}_j$ is the outward normal vector to j-th segment, scaled by the area of the segment (Figure 5.1).

Components

Next, we discretize the conservation equation for the concentration with the ADR equation (2.12) describing the spatial-temporal evolution of a reacting component. It consists of three contributions: The first describes the movement of a concentration due to advection and adsorption; the second describes the transport due to capillary forces; the third describes the effects of dispersion. As for the saturation equation (2.11), the movement due to advection is a hyperbolic first order term. Since capillary pressure is only a function of the saturation and not the components, however, the contribution of the capillary part for the components, is also a first-order hyperbolic part, and thus must be discretized via a FV technique. The values of the component concentrations are calculated in the same time step as the saturation values. This poses a major difficulty, since the discretization of the capillary pressure contribution on the saturations only yield saturation values

at times t and $t + \Delta t$, where $t + \Delta t$ is a global time step that can be chosen freely, and as for the implicit scheme, no CFL criterion needs to be adhered to. On the contrary, the explicit discretization of the advective part needs to satisfy the CFL restriction (5.8) which leads to many more intermediate calculations with time steps $\Delta t^* \leqslant \Delta t$. One solution would be to solve problem (A_S) of the preceding paragraph at all the intermediate calculations which the time-steps condition (5.8) requires, and then use these saturation values to solve for the components with an explicit-in-time scheme. Obviously, this would be computationally inefficient. A second way would be to solve the system of equations (2.11) and (2.12) fully implicitly. Achieving convergence for implicit first or higher-order schemes for two-phase flow without transport is already challenging [Jenny et al., 2009, Blunt and Rubin, 1992]. If in addition several components need to be considered, the resulting non-linear system grows even larger and convergence becomes a major challenge. We therefore use a third way: We split the advective part of the component equations into the contribution of the viscous forces and that of capillary pressure. The dispersive part is again of parabolic nature, and to obtain a stable discretization, the same reasoning as for the saturation equation applies, and we again use an additional operator splitting for the dispersive part.
Altogether, we alternately solve the problems

$$\begin{aligned}
(A_c) \quad & \phi \frac{\partial (S_w C)}{\partial t} && = \quad -\nabla \cdot \left(\phi S_w \mathbf{D} \nabla C_i\right), \\
(B_{c,pc}) \quad & \phi \frac{\partial (S_w C)}{\partial t} && = \quad \nabla \cdot \left(C \bar{\lambda}_t \frac{dp_c}{dS_w} \nabla S_w\right), \\
(B_{c,\Gamma}) \quad & \phi \frac{\partial (S_w C)}{\partial t} + \frac{\partial \Gamma}{\partial t} && = \quad -\nabla \cdot \left(C f \mathbf{v}_t\right).
\end{aligned} \tag{5.15}$$

In the remainder of this section, we first describe how problem (A_c) is solved via an explicit FE method. Subsequently, we show how problem $(B_{c,pc})$ is solved using an implicit FV scheme to get a stable discretization of the capillary contribution on the same time levels as the capillary contribution of the saturations. Then, the discretization of problem $(B_{c,\Gamma})$ is solved via an explicit FV method.

Utilizing an implicit Euler scheme, and the Galerkin-projection onto $\mathcal{V}$, we obtain the discrete formulation and have to solve

$$\left(\mathbf{M}_c + \mathbf{A}_c\right) \mathbf{C} = \mathbf{b}_c, \tag{5.16}$$

where

$$\begin{aligned}
\mathbf{M}_{ck,j} &= \frac{1}{\Delta t}\int_\Omega \phi S^{t+\Delta t}\Phi_k\Phi_j \, dx, && \mathbf{M} \in \mathbb{R}^{m\times m} \\
\mathbf{A}_{ck,j} &= \frac{1}{\Delta t}\int_\Omega \phi S_w^{t+\Delta t}\nabla\Phi_k \mathbf{D}\nabla\Phi_j \, dx, && \mathbf{A} \in \mathbb{R}^{m\times m}
\end{aligned} \tag{5.17}$$

and

$$\mathbf{b}_{ck} = \frac{1}{\Delta t}\int_\Omega \phi S^{t+\Delta t}\Phi_k \, dx, \qquad \mathbf{b} \in \mathbb{R}^m.$$

For the mass matrix $\mathbf{M}_c$ we again apply mass lumping [Celia et al., 1990], and the linear system is solved in the same manner as the one resulting from the discretization of the pressure and the saturation equations. As for the pressure and saturation equation, the influence of the fractures is accounted for by simply expanding the integral over Ω above according to equation (5.2).

Integration of $(B_{c,pc})$ in equation (5.15), i.e. the hyperbolic part arising from capillary forces, and the divergence theorem lead to the accumulation of all segment fluxes, and we have to solve the system of linear equations

$$\mathbf{A}_{pc} \cdot \mathbf{C} = \mathbf{b}_{pc}, \tag{5.18}$$

where the off-diagonal entries of $\mathbf{A}_{pc}$ contain the capillary fluxes in and out of the finite volume, i.e.

$$\mathbf{A}_{pc,ik} = \begin{cases} \frac{\Delta t}{\phi}\sum_j^{n_{si}} \nabla S^*_{w,i} \cdot \mathbf{n}_i \mathbf{k}\bar{\lambda}_t(c_i^t, S_{w,i}^t)\frac{dp_c}{dS_w}|_{S^t_{w,i}} & \text{if } i \neq k \\ S^*_{w,i} & \text{if } i = k, \end{cases} \tag{5.19}$$

and

$$\mathbf{b}_i = (C \cdot S_w)_i^t. \tag{5.20}$$

The linear system is again sparse, and solved in the same manner as that for the pressure equation.

Integration of $(B_{c,\Gamma})$ in equation (5.15), i.e. the hyperbolic part arising from viscous forces, and the divergence theorem lead to the accumulation of all segment fluxes

$$\begin{aligned}\int_{V_i}\left(S_w^{t+\Delta t}C_k^{t+\Delta t}-C_k^t S_w^t\right)\,dV+\int_{V_i}\left(\Gamma^{t+\Delta t}-\Gamma^t\right)dV=\\ -\frac{\Delta t}{A_i}\sum_j^{n_{si}}\left[C_{kj}f_{wj}\mathbf{v}_{tj}\right]\cdot\mathbf{n}_j\\ +\frac{\Delta t}{A_i}\sum_j^{n_{si}}\left[C_{kj}(\rho_w-\rho_n)\overline{\lambda}_{t,j}\nabla\mathbf{g}\right]\cdot\mathbf{n}_j\end{aligned}\tag{5.21}$$

which has to be solved together with the equation for the reaction isotherm

$$\Gamma^{t+\Delta t}=\Gamma(C^{t+\Delta t}).\tag{5.22}$$

We reiterate that flux continuity is guaranteed because of how $\mathbf{v}_t$ is calculated, and how the FV stencils are chosen (Fig. 5.1). For general functional forms of the isotherm, equations (5.21) together with (5.22) build a system of two non-linear equations for the two unknowns $\Gamma^{t+\Delta t}$ and $C^{t+\Delta t}$ that we solve with a Newton method combined with a line-search algorithm to achieve global convergence [Nocedal and Wright, 1999].

The CFL criterion for the admissible time-steps in calculating the advective parts is obtained from equation (5.8) The maximal velocity depends on the gradient of $f(S_w, C)$. For viscosifying components, the fractional flow function shifts from the function $f(S_w, (C/C_0)) = 0)$ to $f(S_w, (C/C_0) = 1)$, see Figure 5.2, where the latter has the steeper change in S_w. We therefore use an estimate of the maximal velocity in V:

$$q_{t,max}=\max_{\text{node } j}\left(\frac{df}{dS_w}|_{S_w(\mathbf{x}_j),(C/C_0)=1}\mathbf{q}_t\right)\tag{5.23}$$

Higher order approximations

The flow parameters f, k_{rw}, μ_w and ρ_w in the discretizations given above are evaluated at each FV for some values C^* and S_w^* from the last time-step. In principle, two possibilities exist to obtain suitable values. First, C^* and S_w^* can be assumed as constant on a FV. This method gives a first order approximation. It is computationally inexpensive for that case

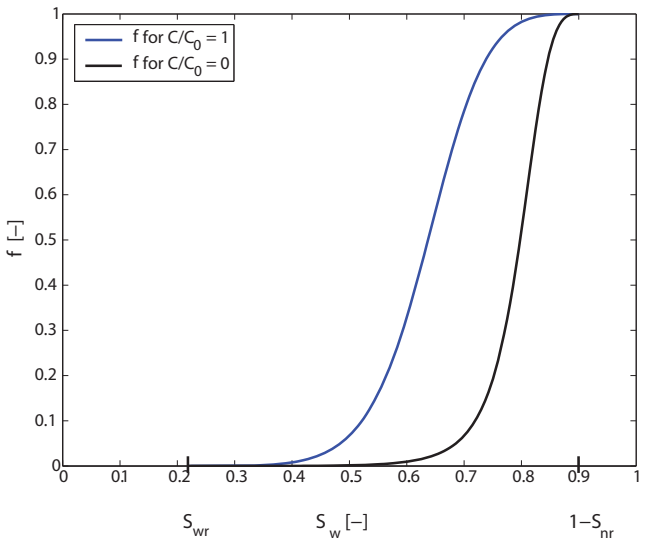

Figure 5.2: Two fractional flow functions for the Brooks-Corey model equation (4.39) with $\lambda_{BC} = 3$ and the viscosity-relationship given in equation (5.35) for the case where the concentration C/C_0 of the viscosifying component is zero and where it is one. Due to dispersion, C/C_0 varies continuously between 0 and 1, and consequently the water viscosity and the fractional flow function vary continuously between the bounding fractional flow functions shown.

because the values stored during the last time-step at the FE node can simply be used. However, for the resolution of sharp fronts that occur in viscous dominated problems, this is often insufficient. If the water viscosity depends on the component concentration, the water saturation forms two jumps. The first one appears due to the nonlinear dependence of q_w on S_w. It is a self-sharpening front that can be well resolved even with the upstream scheme [LeVeque, 1992]. The resolution of the second, non self-sharpening front with the upstream scheme leads to highly diffusive, non-physical fronts. For the component equation it introduces strong numerical diffusion. Since the effect of mixing on components due to dispersion and spatial heterogeneity is of major interest in many applications, an accurate computation is of central importance. In the following, we therefore describe two ways of obtaining a second-order approximation for S_w and C through a linear reconstruction. For the linear reconstruction, we can choose between two parameter sets: We can either determine a better approximation for the state parameters f, k_{rw}, μ_w and ρ_w; or we can approximate the primary variables S_w and C. We found the linear reconstruction of S_w and C already gives very good results and additionally it is computationally half as expensive as the first approach as only two rather than four variables have to be reconstructed. We therefore chose the second possibility. We use two different methods for calculating a local linear reconstruction of

C and S_w for a given FV. In both approaches, slopes for C and S_w are calculated first. These slopes are then limited in order to prevent the creation of new local maxima or minima of the reconstructed C and S_w. For constructing the slope, we compare two approaches: The first one uses a least-squares fit of a plane through the local values of C and S_w. The second one calculates an estimate of the slope given the minima and maxima of C and S_w in the respective FV and its neighbors. Other methods exist but are computationally more expensive without yielding a significantly better resolution, see [Buffard and Clain, 2010, Hubbard, 1999] for a recent overview and discussion. The least-square method is then combined with a MINMOD limiter [Hubbard, 1999], and the estimated gradient with a normalized variable diagram (NVD) limiter [Leonard, 1988]. Limiters were first introduced as total variation diminishing methods (TVD) for 1D advection problems [Van Leer, 1974], and further developed in [Roe, 1981, Harten, 1983, Sweby, 1984] and later generalized as Local Extrema Diminishing (LED) methods for higher dimensions and unstructured grids [Arminjon and Dervieux, 1993, Jameson, 1995, Batten et al., 1996]. The NVD limiter needs to be employed in connection with the estimated gradient [Leonard, 1988]. Obviously, even for the first order case different limiters may be chosen that result in different degrees of compression of a sharp front. Among these limiters the MINMOD limiter is the least compressive one, and it might be worthwhile to use the least square method in connection with a different limier in future work. Both the NVD and the MINMOD scheme belong to the family of Monotone Upstream Schemes for Conservation Laws (MUSCL) that have been used previously for the simulation of two-phase flow problems [Huber and Helmig, 1999, Geiger et al., 2004, Lamine and Edwards, 2008]. Note that while we directly apply the higher methods to reconstructions of S_w and C, an alternative possibility can be to write the conservation laws for S_w and C in vector notation and use higher–order reconstructions of the eigenvalues [Bell et al., 1989].

LEAST SQUARE GRADIENT AND MINMOD LIMITER We determine a linear reconstruction of a variable within a FV via

$$\widetilde{U}_i(\mathbf{x}) = U_i + [\mathbf{a} \cdot (\mathbf{x} - \mathbf{x}_i)] \,, \tag{5.24}$$

where U can stand for either S_w or C, and $x \in V_i$, and x_i is the center of mass of V_i. In order to avoid the creation of new, unphysical local

extrema, the gradient $\mathbf{a}$ needs to be limited with $0 \leqslant \psi \leqslant 1$, which yields the reconstruction

$$\overline{U}_i(\mathbf{x}) = U_i + \psi_i \cdot [\mathbf{a} \cdot (\mathbf{x} - \mathbf{x}_i)] \,. \tag{5.25}$$

We use the MINMOD limiter to calculate ψ_j as

$$\psi_j = \min [r_i, 1] \,, \tag{5.26}$$

and r_i is determined from

$$r_i = \begin{cases} (U_i^{max} - U_i) / \left(\widetilde{U}_{\alpha,j} - U_j \right) & \text{for } \widetilde{U}_{\alpha,j} > U_i, \\ (U_i^{min} - U_i) / \left(\widetilde{U}_{\alpha,j} - U_j \right) & \text{for } \widetilde{U}_{\alpha,j} < U_i, \\ 1 & \text{for } \widetilde{U}_{\alpha,j} = U_i, \end{cases} \tag{5.27}$$

and $U_{\alpha,i}^{min}, U_{\alpha,i}^{max}$ are the minimum and maximum value of U, respectively, at finite volume i. The flow parameters f, k_{rw}, μ_w and ρ_w are then evaluated for the resulting S_w and C.
The slopes are obtained from a hyperplane that minimizes the distance between the points $(\mathbf{x}_i, U_i)$ and $(\mathbf{x}_j, U_j), j = 1, ..., n_{si}$, by minimizing the functional [Geiger et al., 2004, Buffard and Clain, 2010]

$$E(\mathbf{a}) = \sum_{j=1}^{n_{si}} \left[U_j^n - (U_j^n + \mathbf{a} \cdot (\mathbf{x}_i - \mathbf{x}_j)) \right]^2 . \tag{5.28}$$

In two dimensions, this gives a linear system of equations for $\mathbf{a} = (a_1, a_2)$

$$\begin{aligned} \mathbf{M} \cdot \mathbf{a} &= b, \\ \mathbf{M}_{kl} &= \sum_{j=1}^{n_{si}} (x_{jk} - x_{ik})(x_{jl} - x_{il}), \quad \text{and} \\ \mathbf{b}_k &= \sum_{j=1}^{n_{si}} \left(U_j - U_i \right) \left(x_{jk} - x_{ik} \right) . \end{aligned} \tag{5.29}$$

ESTIMATED GRADIENT AND NVD-LIMITER The least-squares method combined with the MINMOD limiter requires the determination of the minimal and maximal values of S_w and C at a given finite volume, the calculations of r_i, and the solution of a $d \times d$ linear system, where d is the dimension, for every FV to solve the minimization problem. For two dimensions, the linear system (5.29) can be solved explicitly, and thus the total computational burden is that of determining the local extrema of S_w and C plus $\mathcal{O}(n)$ for the $d \times d$ linear system. A slightly

less expensive scheme is achieved by directly calculating an estimate of a one-dimensional gradient $\widetilde{a}$ for the variation of U, given only the local maxima and minima. First, the auxiliary variables γ_1 and γ_2 are calculated via [Leonard, 1988, Matthäi et al., 2009]

$$\gamma_1 = \frac{U_i - U_u}{U_d - U_u}, \tag{5.30}$$

$$\gamma_2 = \frac{U_k - U_u}{U_d - U_u}, \tag{5.31}$$

where the subscripts d and k stand for U taken at the downstream node and the facet integration point, respectively. U_u is an estimate of the upstream node value determined from

$$U_u = \begin{cases} U_i^{max} & \text{if } U_d \leqslant U_i \\ U_i^{min} & \text{if } U_d > U_i. \end{cases} \tag{5.32}$$

From γ_1 and γ_2, we obtain a gradient such that an overestimation of U_i is avoided. To this end, the gradient for the estimate of a linear variation of U is then obtained from a Normalized Variable Diagram (NVD) which gives

$$\widetilde{a} = \begin{cases} \min\left(\xi\gamma_1, 1, \max(0, \gamma_2)\right) & \text{if } \gamma_1 \in [0, 1] \\ \min\left(\xi\gamma_1, 1, \max(0, \gamma_2)\right) & \text{else} \end{cases} \tag{5.33}$$

for some parameter ξ, and and we choose $\xi = 2$. The approximation U_i is then obtained from

$$\overline{U}_i = a(U_d - U_u) + U_u. \tag{5.34}$$

Like the MINMOD-limiter approach, $\overline{U}_i$ is then used to evaluate f, k_{rw}, μ_w and ρ_w.

5.3 ALGORITHM

The computational steps are as follows:

1. Read the initial pressure, saturation and component values, and set the boundary conditions.

2. Solve equation (5.6) to obtain the initial pressure field; solve equation (5.7) for the initial velocity field.

3. Repeat the following steps until the specified end-time is reached:
4. Determine new CFL criterion from equation (5.23).
5. *Dispersion of components:* Solve problem A_c in equation (5.15) with time step $\Delta t/2$, obtain C^{disp}.
6. *Transport and flow due to viscous and capillary forces:*
   - *Capillary part:* Advance S_w^t and C^{disp} from t to $(t+\Delta t)_{pc_1}$ with time step $\Delta t/2$
     - Evaluate the flow parameters at time t and solve problem (A_S) in equation (5.9) for the effect of capillary pressure on the saturations; this yields $S_w^{(t+\Delta t)_{pc1}}$
     - Evaluate ∇S_w for $S_w^{(t+\Delta t)_{pc1}}$, and the other flow parameters for S_w^t, C^t; solve problem $(B_{c,pc})$ in equation (5.15) for the effect of capillary pressure on the components; this yields $C^{(t+\Delta t)_{pc1}}$
   - *Viscous part:* Advance $S_w^{(t+\Delta t)_{pc1}}$ and $C^{(t+\Delta t)_{pc1}}$ from $(t+\Delta t)^{pc1}$ to $(t+\Delta t)^{visc}$ with time step Δt
     - Calculate the second-order fluxes from equation (5.25) or (5.34)
     - Evaluate the flow parameters with $S_w^{(t+\Delta t)_{pc1}}$ and accumulate the fluxes for the saturations and solve the non-linear equations (5.14) and for the (5.22) components; obtain $S_w^{(t+\Delta t)_{visc}}, C^{(t+\Delta t)_{visc}}$.
   - *Capillary part:* Advance $S_w^{(t+\Delta t)_{visc}}$ and $C^{(t+\Delta t)_{visc}}$ to obtain $S_w^{t+\Delta t}$ and $C^{(t+\Delta t)_{visc\&pc}}$ with time step $\Delta t/2$
     - Evaluate the flow parameters at time $(t+\Delta t)_{visc}$ and solve problem (A_S) in equation (5.9) for the effect of capillary pressure on the saturations; this yields $S_w^{(t+\Delta t)}$
     - Evaluate ∇S_w for $S_w^{t+\Delta t}$, and the other flow parameters for $S_w^{(t+\Delta t)_{visc}}, C^{(t+\Delta t)_{visc}}$; solve problem $(B_{c,pc})$ in equation (5.15) for the effect of capillary pressure on the components; this yields $C^{(t+\Delta t)_{visc\&pc}}$
7. *Dispersion of components:* Solve problem (A_c) in equation (5.15) for time step $\Delta t/2$, obtain $C^{t+\Delta t}$.
8. Solve the pressure equation equation (5.6) to obtain the new pressure field; Solve equation (5.7) for the new velocity field.
9. Go back to step 4.

5.4 NUMERICAL TESTS

In this section, we show the accuracy and convergence of the numerical schemes presented above, and demonstrate their viability for resolving flow and transport in complex geometries. The numerical problems solved here are of increasing difficulty, starting with two 1D examples that show the convergence of our schemes for the cases with and without dispersive terms, and the dependence of the convergence on the grid Peclet number. Test cases III, IV and V present 2D results. Test case III presents the homogeneous quarter-of-five-spot problem that tests the schemes' insensitivity to grid orientation. Test case IV shows the versatility of our schemes to resolve flow and transport on a fractured geometry. Test case V shows the performance of the schemes for simulating flow and simultaneous transport in a realistic fracture network with a highly-heterogeneous rock matrix.

Test Case I: Extended Buckley-Leverett problem

If gravity and dispersion are neglected, the multiphase-multicomponent problem reduces to the extended Buckley-Leverett problem for which analytical solutions can be derived [Johansen and Winther, 1988] (Chapter 4). The relationships for $\mu_w(C)$ and $\Gamma(C)$ used in this test case, are

$$\begin{aligned} \mu_w(C) &= \mu_{w,0} + 5 \cdot 10^{-4} \frac{C}{C_0}, \\ \Gamma(C) &= \left(\frac{d\Gamma}{dC} \right) \cdot C =: D_s C, \end{aligned} \tag{5.35}$$

The relative permeabilities for this test case is the Brooks-Corey model (equation (4.39)).
The residual water and oil saturation, S_{wr} and S_{nr}, together with the other parameters used for this test case, can be found in Table 5.1. Figure 5.4 shows the comparison between the analytical solution and the three different numerical methods described in this chapter.
Although the component and the aqueous carrying phase are injected together, the component gets retarded due to adsorption and due to the presence of the initial water phase and does not travel together with the injected water [Pope, 1980]. As a consequence, the saturation forms two jumps. Going from downstream to upstream the water saturation jumps from its initial saturation to a value of constant saturation to form a water bank in which the component concentration stays at its initial value. Then the component breaks through, the viscosity of the

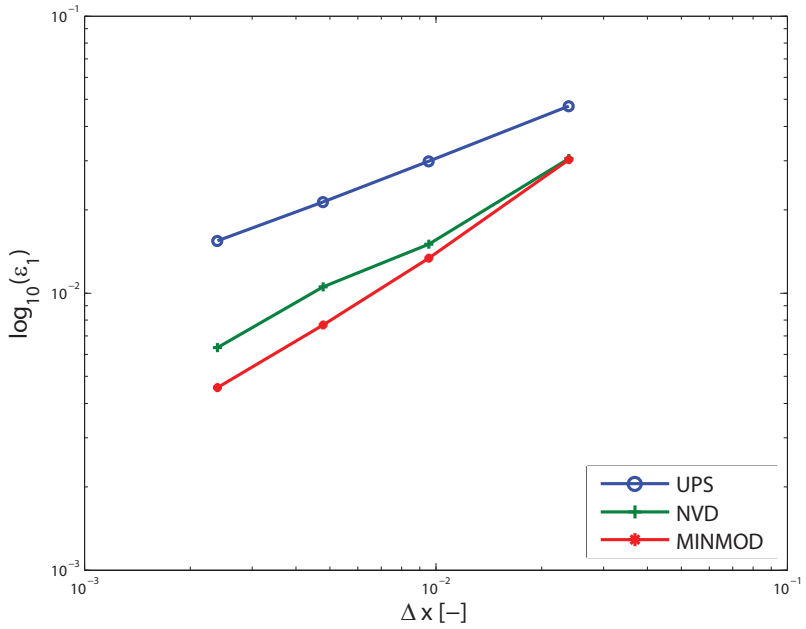

Figure 5.3: Convergence of the ℓ_1 norm as a function of the grid size Δx for Test Case I.

water increases according to equation (5.35), and the water saturation forms a second jump followed by a rarefaction wave. The first front is a self-sharpening shock front that forms as a consequence of the fact that the velocities of S_w depend on $f(S_w, C = 0)$ [LeVeque, 1992, Johansen and Winther, 1988], and the second jump forms as a consequence of the change from $f(S_w, C = 0)$ to $f(S_w, C = 1)$. Since the first front is self-sharpening, the upstream scheme resolves it well, but shows strong numerical diffusion effects for the second, non self-sharpening jump in water saturation and the jump in component concentration. Figure 5.3 shows the convergence of the error ε_1 in the discrete ℓ_1 norm

$$\varepsilon_1 := \Delta x \left[\sum_{i=1}^{m} \left| \frac{C_i - C_{a.s.}(x_i)}{C_0} \right| + \sum_{i=1}^{m} |S_{w,i} - S_{w,a.s.}(x_i)| \right].$$

Both the NVD and the MINMOD scheme show a far better resolution of the jumps in water saturation and the component, where the MINMOD scheme gives a slightly better compression than the NVD scheme.

Test Case II: Dispersion of tracers in two-phase flow

The accuracy of our scheme for dispersion is shown next. For the case, where gravity is neglected and the components are adsorbing but otherwise inert solutes, analytical solutions for the 1D case can be developed for the case with and without capillary pressure (Chapter 4). The implicit scheme for accounting for capillary pressure additionally

Parameter	Unit	Test Case I (Extended BL Problem)
S_{wr}	$[-]$	0.22
S_{nr}	$[-]$	0.15
λ_{BC}	$[-]$	3.0
ϕ	$[-]$	0.25
μ_w	$[Pa \cdot s]$	10^{-3}
μ_n	$[Pa \cdot s]$	$5 \cdot 10^{-4}$
$\mathcal{D}_s$	$[m_f^3/m_{PV}^3]$	0.2
q_t	$[m/s]$	$2 \cdot 10^{-8}$
$\mathbf{k}$	$[m^2]$	10^{-14}

Table 5.1: Parameter set for the extended Buckley-Leverett (BL) case.

introduces some numerical dispersion. Since we are interested in the accuracy of the upstream scheme, the MINMOD scheme and the NVD scheme, respectively, we consider one case where viscous forces dominate, capillarity can be ignored and the only errors are introduced by the explicit schemes (Test Case IIa); and a second one where capillarity is fully taken into account and the numerical error stems from both the implicit scheme and the explicit scheme (Test Case IIb). For case (a), we additionally study the maximum error in dependence of the grid Peclet number.

Note that in the previous chapter, we used the NVD scheme presented here to test the validity of the solutions while now we use the analytical solutions to test convergence of the numerical schemes. However, a 'circular argument' is avoided since in this chapter we test *three different* schemes. In particular we compare two higher-order schemes. Thus, it is reasonable to assume that the schemes are correct if the higher-order NVD scheme and the MINMOD scheme yield comparable results.

TEST CASE II (A) Here, we ignore capillary pressure, and use the Brooks-Corey model for the relative permeabilities and the parameter set given in Table 5.2. Figures 5.5a and 5.5b show the comparison between the analytical solution and the numerical methods. To study the interplay between numerical diffusion, controlled by grid size, and physical dispersion of the components, governed by the dispersivity constant α, we introduce the grid Peclet number as $Pe = \frac{\Delta x}{\alpha_{disp}}$. For the case of the small dispersivity constant $\alpha_{disp} = 0.001\,m$ and $Pe = 1.3$ (Figure 5.5a), the upstream scheme greatly overestimates the dispersion of the components, whereas both the NVD and the MINMOD scheme

Parameter	Unit	Test Case II (a)
S_0	$[-]$	0.85
S_{wr}	$[-]$	0.22
S_{nr}	$[-]$	0.15
λ_{BC}	$[-]$	3.0
ϕ	$[-]$	0.25
μ_w	$[Pa \cdot s]$	10^{-3}
μ_n	$[Pa \cdot s]$	10^{-3}
$\mathcal{D}_s$	$[m_f^3/m_{PV}^3]$	0.3
$\mathbf{k}$	$[m^2]$	10^{-12}
q_t	$[m/s]$	$2.1 \cdot 10^{-7}$

Table 5.2: Parameter set for adsorbing solutes in two-phase flow if dispersion is taken into account (Figures 5.5a and 5.5b). S_0 is the value for S_w at the left boundary.

show a very good agreement. Figure 5.5b shows the same test case as Figure 5.5a but with $\alpha_{disp} = 0.01$, and a grid Peclet number of $Pe = 10.3$. Compared to the NVD and the MINMOD scheme, the upstream scheme still overestimates the actual dispersion of the components but to a lesser degree than that for the smaller grid Peclet number. Figure 5.6 shows the behavior of the maximum error versus grid Peclet number. Since we are mainly interested in the dispersion of the components, we only consider the maximum error in the components, defined by

$$\varepsilon_{max} := \max_{i=1,\cdots,m} |(C_i - C_{a.s.}(x_i))/C_0| \,. \tag{5.36}$$

As in the pure advective test case, the MUSCL schemes clearly outperform the upstream scheme. The piecewise slopes of the NVD scheme and the MINMOD scheme are comparable, i.e. the order of the convergence with respect to the maximum norm is the same, but overall the NVD scheme performs slightly better than the MINMOD scheme. The smaller the grid Peclet numbers, the better the MUSCL schemes compared to the upstream scheme become with respect to ε_{max}. For a given α_{disp}, this can be used to roughly assess the grid size required to achieve a certain accuracy. If the dispersivity α_{disp} is small, the MUSCL schemes are clearly preferable since the upstream scheme would lead to a grid size that is prohibitively small. For example, to achieve the same accuracy with the upstream scheme that the NVD scheme shows for $Pe = 10$, a ten times finer grid size would be needed.

Parameter	Unit	Test Case II (b)
S_0	$[-]$	0.81
S_{wr}	$[-]$	0.22
S_{nr}	$[-]$	0.15
p_d	$[Pa]$	$1.5 \cdot 10^3$
λ_{BC}	$[-]$	3.0
α_L	$[m]$	0.01
ϕ	$[-]$	0.25
μ_w	$[Pa \cdot s]$	10^{-3}
μ_n	$[Pa \cdot s]$	10^{-3}
$\mathcal{D}_s$	$[m_f^3/m_{PV}^3]$	0.5
$\mathbf{k}$	$[m^2]$	10^{-12}

Table 5.3: Parameter set for cocurrent case as shown in Figure 5.7. S_0 is the value for S_w at the left boundary.

TEST CASE II (B) In this example, we take capillary pressure into account, where we use the Brooks-Corey model for the relative permeabilities, equation (4.39). The parameters are given in Table 5.3. Figure 5.7 shows the comparison between the analytical solution and the various numerical methods. For resolving the capillary front of the water saturation, the difference in accuracy between the three methods is minor, whereas the upstream scheme again overestimates the dispersion of the components. Both the NVD and the MINMOD scheme give comparably good results.

Test Case III: Homogeneous five spot problem

The next case tests the sensitivity of the numerical schemes to grid orientation because the flow direction is not necessarily aligned with the grid. We consider the homogeneous quarter of a five spot problem [Spivak et al., 1977]. In the original setting, gravity is ignored, and water is injected into the lower left corner of a square domain such that principal flow direction is diagonal to the grid, displacing the oil which is extracted from the upper right corner. In our case, the injected water additionally transports a dissolved component. If the numerical scheme is insensitive to grid orientation effects, the scheme should reproduce quarter circle shaped saturation and concentration patterns of the components. Since we are also interested in how well a sharp front is reproduced by the higher order methods on an unstructured grid, the dispersivity constants were set to zero, see Table 5.4.

Grid orientation effects arise from three different causes [Kozdon et al., 2008]: (a) rotationally dependent errors in the numerical scheme, (b) the flow in the immediate neighbourhood of a source, and (c) the physical instability of adverse mobility ratio flow. In the following we therefore first consider the case of stable displacement, i.e. the case where the grid orientation errors only stem from (a) and (b) (Test Case III a, $\mu_n/\mu_w = 1/2$, see Table 5.4). Then we investigate how well the schemes perform for unstable displacement (Test Case III b, $\mu_n/\mu_w = 20$, see Table 5.4). Figure 5.8 shows the grid used for this case.

Figure 5.10 shows the numerical results for the water saturation and the component for the three numerical schemes and stable displacement. All schemes show a good reproduction of the quarter circle shapes for both the saturation and the component. The front of the component concentration obtained from the upstream scheme is spread out over several cells, while both the NVD scheme and the MINMOD scheme significantly reduce this spread. Figure 5.12 shows the breakthrough curves at 25m, 50m and 75m for the flux-weighted oil saturation S_n, the water cut WTC, i.e. the ratio of the volumetric water flux over the total volume flux, and the flux-weighted normalized concentration C/C_0. The oil saturation stays at its initial level up to when the water breaks through at approximately 200d, 500d and 1300d at the points 25m, 50m and 75m, respectively, and then declines with increasing water cut. The increase in water cut sharply rises when the water reaches the upper boundary at approximately 2500d, 2700d and 2900d at the points 25m, 50m and 75m, respectively. Compared to the water breakthrough, the breakthrough of the components is retarded, and the retardation becomes more pronounced with increasing distance from the injector. Compared to the UPS scheme, the NVD and the MINMOD scheme result in a later breakthrough and less smeared out breakthrough curve of the component since the higher schemes result in a better resolution of the front. For the water cut, the differences between the UPS scheme, the NVD scheme and the MINMOD scheme are less pronounced since the water front is self-sharpening and thus can be well resolved with a first-order scheme [LeVeque, 1992].

Figure 5.11 shows the numerical results for the water saturation and the component for the three numerical schemes and unstable displacement. Here, the viscosity ratio is $\mu_n/\mu_w = 20$ which results in a frontal mobility ratio of $\lambda_t(S_{wf})/\lambda_t(S_{wi}) \approx 1.2 > 1$, and thus an unstable displacement [King and Dunayevsky, 1989]. As for the case

Parameter	Unit	Test Case III a	Test Case III b
p_{inj}	[Pa]	$1.37 \cdot 10^7$	$1.37 \cdot 10^7$
p_{prod}	[Pa]	$1.1032 \cdot 10^7$	$1.1032 \cdot 10^7$
S_{wr}	[–]	0.22	0.22
S_{nr}	[–]	0.1	0.1
λ_{BC}	[–]	3.0	3.0
α_L	[m]	0	0
α_T	[m]	0	0
ϕ	[–]	0.2	0.2
μ_w	[Pa · s]	10^{-3}	$5 \cdot 10^{-4}$
μ_n	[Pa · s]	$5 \cdot 10^{-4}$	10^{-2}
$\mathbf{k}$	[m^2]	10^{-13}	10^{-13}

Table 5.4: Parameter sets for quarter of five-spot problem for stable displacement (case a) and unstable displacement (case b) as shown in Figures 5.10, and 5.11. p_{inj} and p_{prod} are the fluid pressures at the lower left and upper right corner, respectively.

of stable displacement, the higher order schemes significantly reduce the numerical dispersion. However, the saturation front deviates from the quarter circle shape for all schemes. For the higher–order schemes, this effect becomes even stronger since they better resolve the front in S_w. The NVD scheme results in a slightly better reproduction of the quarter circle. In future work, this grid orientation effect could be further reduced by using a local treatment of flow around the fluid source [Kozdon et al., 2008].

Test Case IV: Fractured five spot problem

This test case shows the versatility of our schemes for resolving flow and transport in a fracture geometry. The setting is the same as for the five-spot problem, with the only difference being that some fractures of permeability $\mathbf{k} = 10^{-9}$ m^2 are embedded in the model (see Figure 5.9). The fractures are discretized as 1D line elements in the 2D geometry. This approach allows for reasonable grid size even close to the high-permeability regions [Geiger et al., 2004]. Figures 5.13-5.15 show the numerical results for both the saturation and the component. Since the permeability of the fractures is orders of magnitude higher than that of the unfractured matrix, where $\mathbf{k} = 10^{-13}$ m^2, the fractures build a network of preferential flow paths, and the fluid and the component first travel along the fractures and from there are slowly transported into the rock matrix. As in the previous test cases, the second order

Parameter	Unit	Test Case V
p_l	[Pa]	$1.01 \cdot 10^7$
p_r	[Pa]	$1.0 \cdot 10^7$
S_{wr}	[–]	0.2
S_{nr}	[–]	0.1
λ_{BC}	[–]	3.0
p_d	[Pa]	$1.3 \cdot 10^3$
ϕ	[–]	0.2
μ_w	[Pa · s]	10^{-3}
μ_n	[Pa · s]	$5 \cdot 10^{-4}$
α_L	[m]	10^{-2}
α_T	[m]	10^{-3}
$\mathcal{D}_{B,s}$	$[m_f^3/m_{PV}^3]$	0.5

Table 5.5: Parameter set for realistic fracture system, Test Case V (Figures 1.1 and 5.16). p_l and p_r are the fluid pressures at the left and the right boundary, respectively. The components A and B have the same dispersivity data α_L and α_T, and the adsorption of component B follows an isotherm with constant $\mathcal{D}_{B,s}$.

schemes result in a significantly better resolution of the saturation and component fronts, and the MINMOD and the NVD schemes yield similar resolutions. At $t = 500d$, the differences between the results obtained from the UPS scheme and the second order schemes are still negligible while at $t = 1600d$, the predictions for the saturation and especially the component distributions in the domain made by the UPS scheme compared to the second order schemes show major differences.

Test Case V: Flow and transport in a realistic fractured system

This test case shows the versatility of our schemes for resolving flow and transport of two components A and B in a complex realistic fracture system for the outcrop shown in Figure 1.1. The heterogeneous rock matrix consists of different geological layers (depicted by different colors in Figure 5.16) with permeabilities of $k = 10^{-16}\,m^2, k = 10^{-13}\,m^2, k = 0.5 \cdot 10^{-13}\,m^2, k = 10^{-13}\,m^2, k = 2 \cdot 10^{-13}\,m^2, k = 1.5 \cdot 10^{-14}\,m^2, k = 2 \cdot 10^{-14}\,m^2$, and $k = 1.5 \cdot 10^{-16}\,m^2$, respectively, going from the top to the bottom layer. The embedded low-permeability region (depicted in red in Figure 5.16) has a permeability of $k = 1.5 \cdot 10^{-14}\,m^2$, and the fractures have a permeability of $k = 8.3 \cdot 10^{-11}\,m^2$. Component A is inert, while component B adsorbs through a linear isotherm with $\mathcal{D}_{B,s} = 0.5$. The numerical results are shown in Figures 5.17-5.20, where the left

column shows the results at time $t = 150$ d when the water has started to flood the fracture network, and the right column shows the results at time $t = 420$ d when the flow has started to bypass the embedded low-permeability part to reach the connected higher-permeability layers and fractures. Figure 5.17 shows the reference solution obtained with the NVD scheme for the fine grid discretization shown in Figure 5.16 (b). Compared to the fine-grid solution, both the MINMOD scheme and the NVD scheme produce a saturation and component fields whose concentration and extent in great parts agree with the reference solution, but give a slightly inferior front resolution. On the coarse grid, both the NVD scheme and the MINMOD scheme yield comparable results as in the previous test examples. The vertical flow from layers of high permeability into those of low permeability due to advection is small because of the permeability contrast, and thus both flow and transport in vertical direction are governed by capillary and transversal hydrodynamic dispersion. While both higher order schemes resolve the fronts between these layers well, the UPS scheme results in smeared-out fronts that overestimate the flow and especially the transport into the low permeability layers. As already described in test case I, compared to the movement of the saturation front, component A is retarded because some water is already present in the reservoir which must be displaced. The retardation becomes stronger for the adsorbed component B, as expected.

5.5 SUMMARY AND CONCLUSIONS

In this chapter, we extended the FEFV scheme for the modelling of two-phase flow and the transport of viscosifying and reacting components in permeable porous media. We presented two higher order methods of the MUSCL type, a MINMOD scheme and an NVD scheme, and compared them to a classical single-point upstream method. We fully accounted for viscous forces, capillary pressure, hydrodynamic dispersion and adsorption. We used a mass-conservative and flux-continuous node-centered FEFV scheme and gave numerical examples that show that this scheme is capable of resolving flow and transport even in fractured, highly heterogeneous geometries. The scheme presented can easily be parallelized [Geiger et al., 2009, Coumou et al., 2008]. We assumed a homogeneous p_c. Working with inhomogeneous p_c fields is challenging, but can be resolved if the state variables are incorporated as discontinuous at interfaces between media with different properties

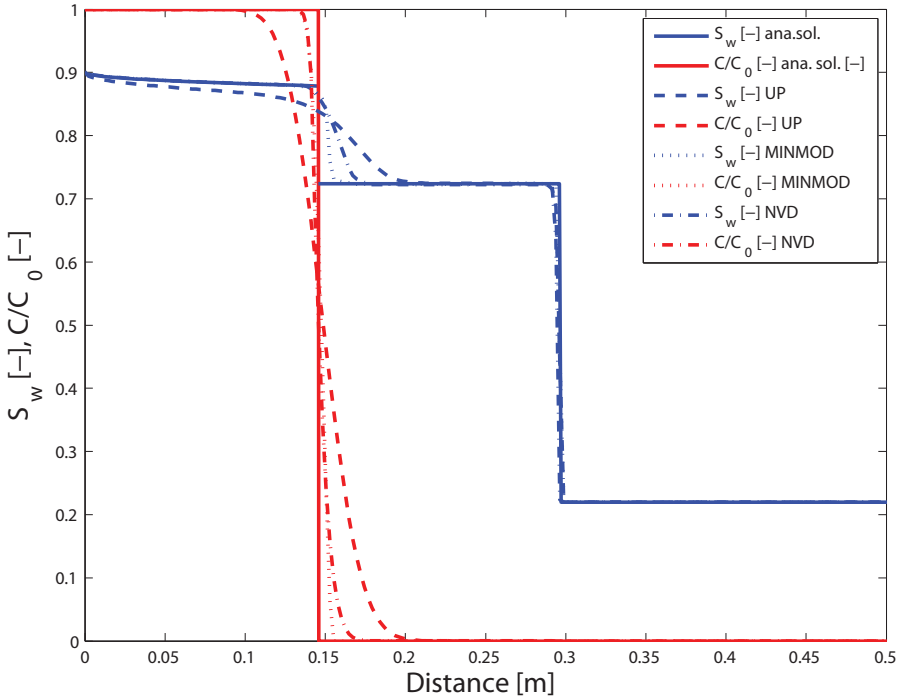

Figure 5.4: Comparison of the 1D analytical solution for the extended Buckley-Leverett problem to the three different numerical methods of this chapter at time t = 25d. Water together with a viscosifying component is injected at the left and displaces oil in a homogeneous porous medium.

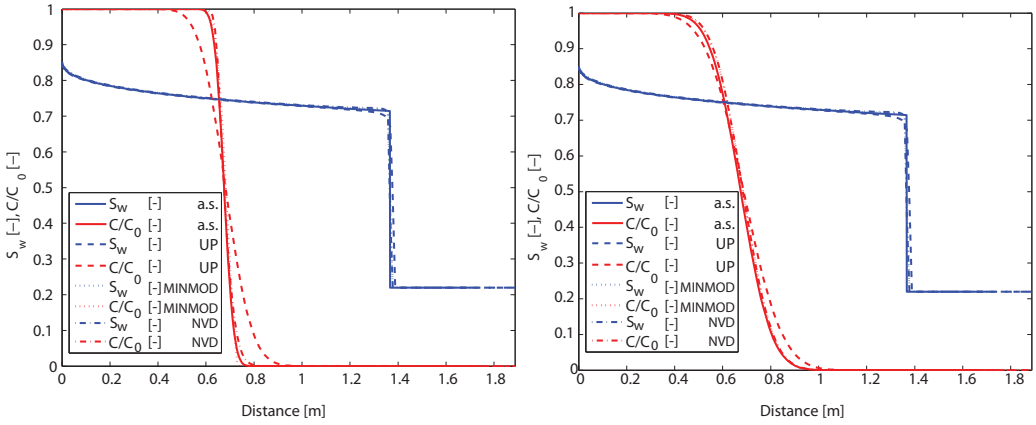

(a) (b)

Figure 5.5: Comparison of 1D analytical solutions for the case where the solutes adsorb but otherwise do not change the flow field (Test Case II). (a) shows the case for Pe = 1.3, and (b) the case Pe = 10.3.

[Reichenberger et al., 2006, Hoteit and Firoozabadi, 2008, Niessner et al., 2005, Nick and Matthäi, 2011]. The 2D test examples show the methods' ability to resolve flow and transport on unstructured grids both for the case without fractures and for the case where fractures are embedded as lower-dimensional elements.

- *Hydrodynamic dispersion and Strang splitting.* The tensor of hydrodynamic dispersion strongly depends upon the two-phase flow

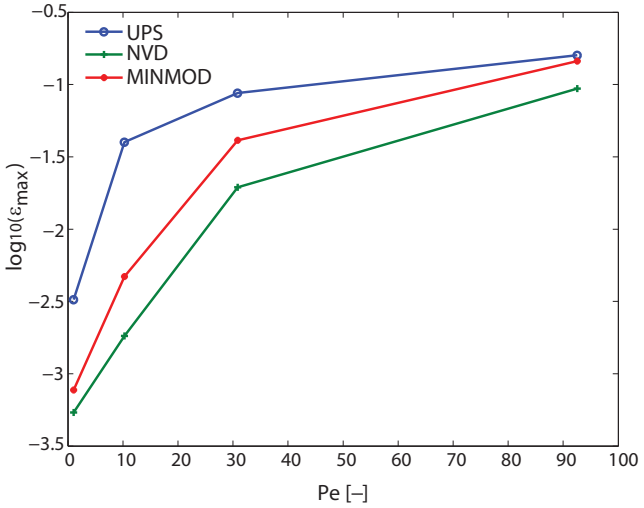

Figure 5.6: Dependence of $\varepsilon_{max} := \max_{i=1,\cdots,m} |(C_i - C_{a.s.}(x_i))/C_0|$. on the grid Peclet number.

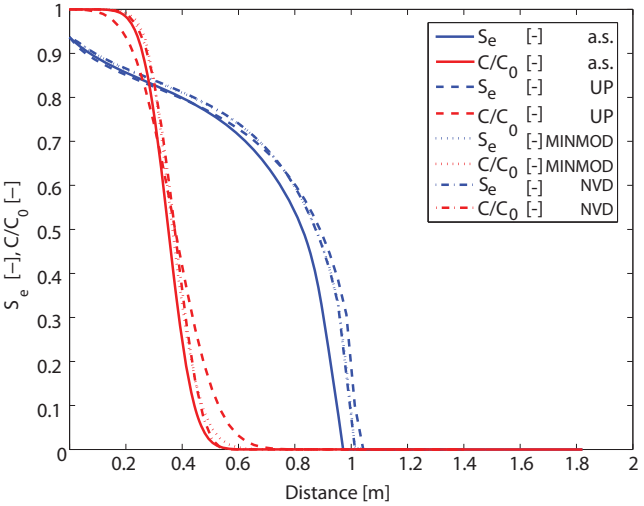

Figure 5.7: Comparison of the 1D analytical solution for the extended Buckley-Leverett problem to the three different numerical methods of this chapter at time $t = 2.5$d. Water together with an adsorbing solute is injected at the left and the water displaces the oil in a homogeneous porous medium.

field and thus is highly non-linear. We incorporated its effect using a Strang splitting where we use first or second order explicit FVs for the viscous part and implicit FEs for the effects of dispersion. Numerical tests show the strong dependence of the accuracy on the grid Peclet number. The NVD scheme slightly outperforms the MINMOD scheme while both clearly outperform the upstream scheme. For purely advective problems, the MINMOD scheme gives a slightly better compression than the NVD scheme, and the upstream scheme introduces very strong numerical dispersion.

- *Influence of* p_c. Incorporating the effect of capillary pressure on both the fluid flow and the components is challenging. p_c in the

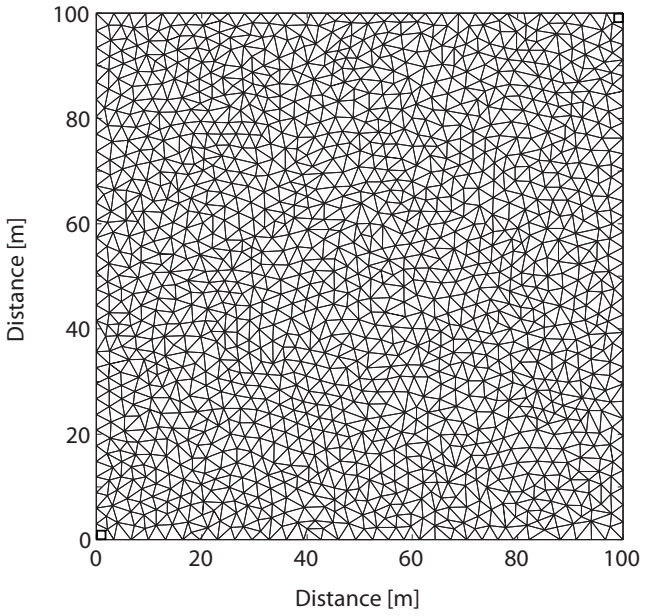

Figure 5.8: Grid used for the quarter of five-spot problem (Test Case III). The injector is in the lower left corner, and the producer in the upper right corner, both indicated by a square.

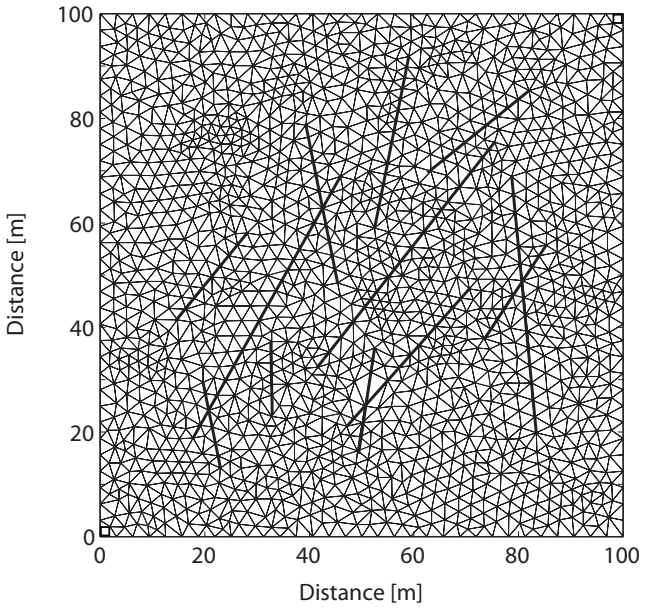

Figure 5.9: Grid used for Test Case IV. The long solid lines represent the high-permeability fractures discretized as 1D FEs and FVs. The injector is in the lower left corner, and the producer in the upper right corner, both indicated by a square.

fluid conservation equations leads to a second-order parabolic term with a CFL number of order $\mathcal{O}(\Delta x^2)$. This which would lead to prohibitively small time-steps for an explicit scheme, and we used implicit FEs to solve for this part of the problem. The capillary influence on the component transport, however, is a first-order hyperbolic term and FEs cannot be used. Since the component conservation equation is strongly coupled with that for the fluid

phase, both need to be resolved at the same time-levels. To that end, we introduced an implicit FEFV scheme that splits between the viscous and the capillary parts, bypassing the restrictive CFL condition while obtaining a stable, mass-conserving scheme for both the saturations and the components. Comparisons with analytical solutions showed the robustness and convergence of our approach.

- *Other numerical methods for flow and transport.*While we chose an FEFV method here as a starting point for the extension to a scheme for flow and simultaneous transport, overall the combination of different techniques, like the splitting approach to tackle capillary and hydrodynamic dispersion or the setup for higher order methods, can also be used to develop numerical schemes for flow and transport based on other methods such as MPFA schemes.

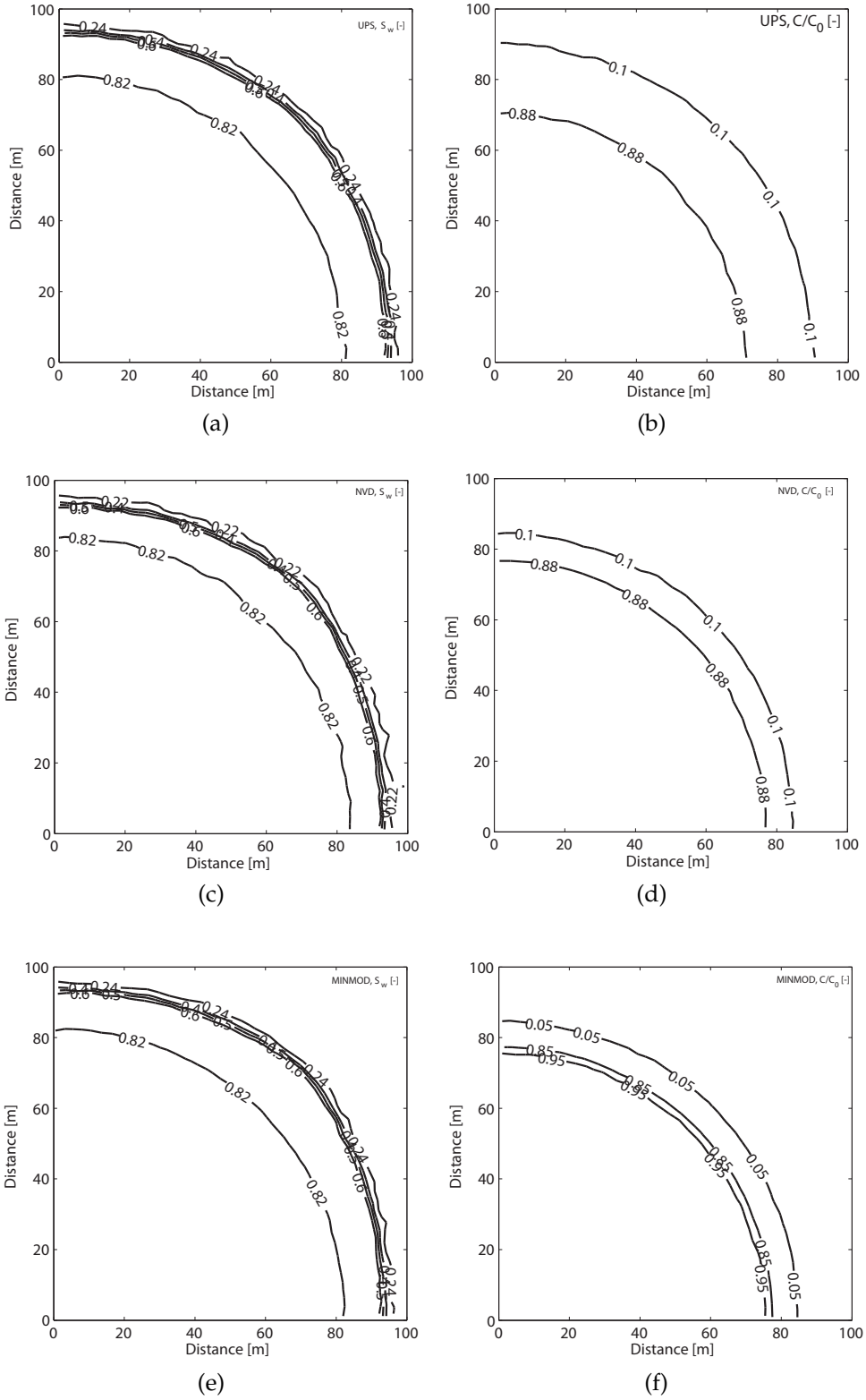

Figure 5.10: Numerical results for the homogeneous five-spot problem for stable displacement (Test Case III a). Contour plots for the water saturation at time t = 2200d for the three different numerical schemes are shown on the left, and contour plots of the concentration are shown on the right.

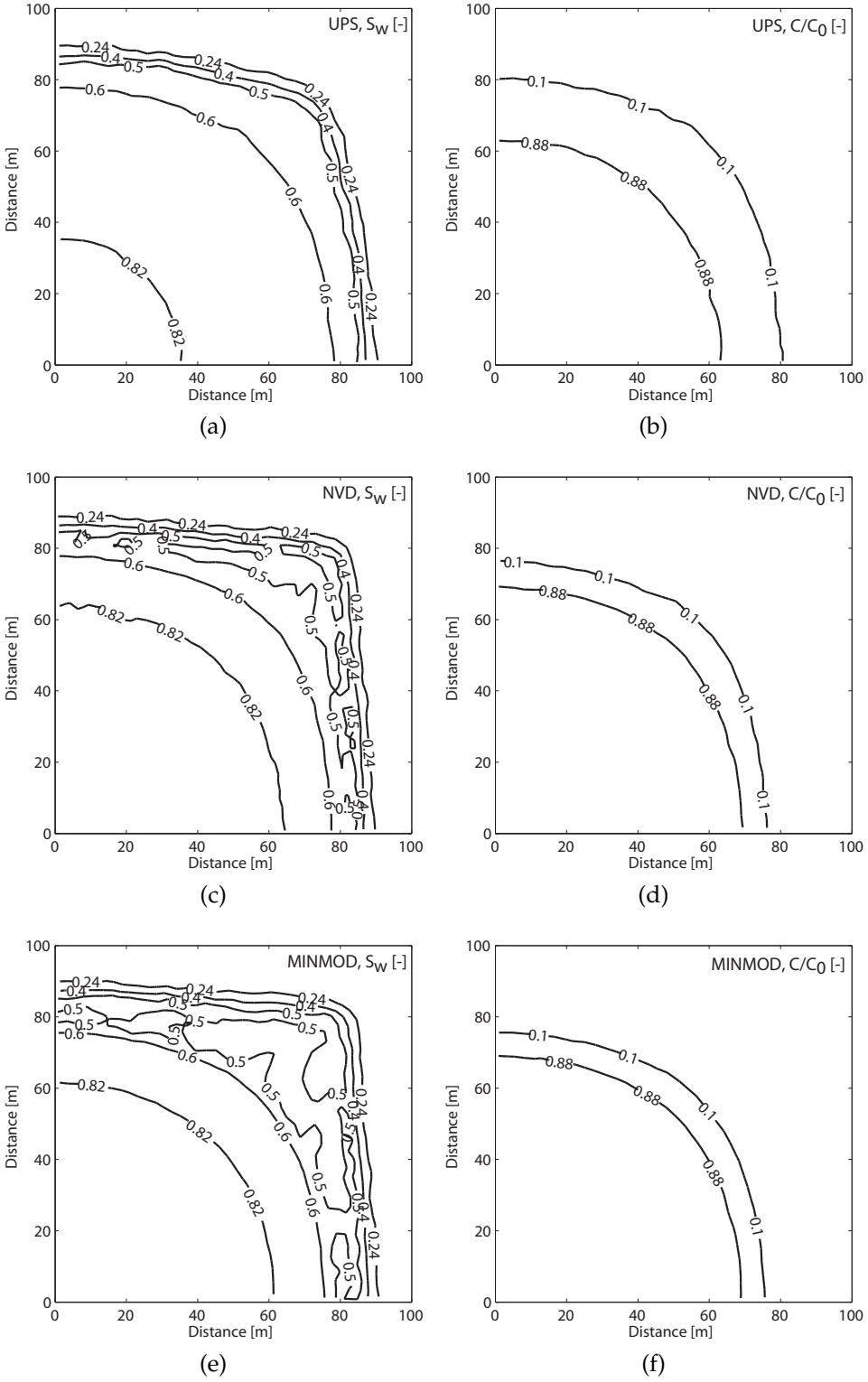

Figure 5.11: Numerical results for the homogeneous five-spot problem for unstable displacement (Test Case III b). Contour plots for the water saturation at time t = 3000d for the three different numerical schemes are shown on the left, and contour plots of the concentration are shown on the right.

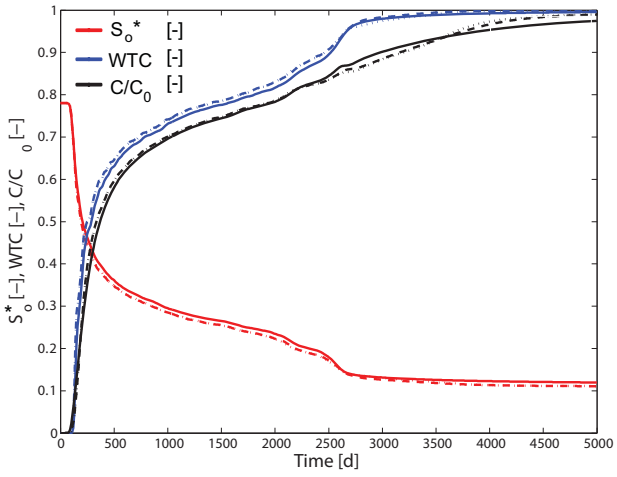

(a)

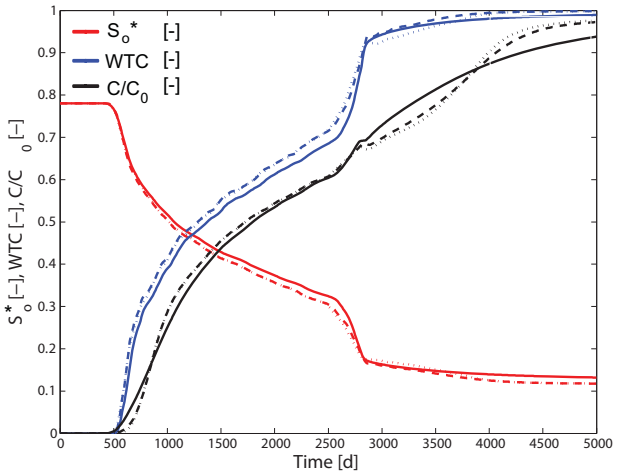

(b)

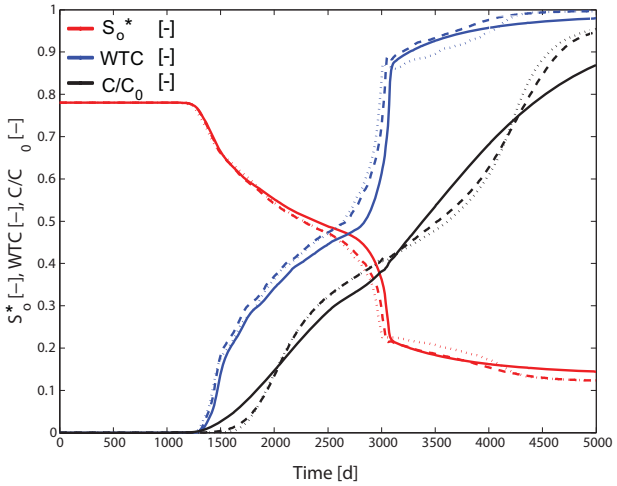

(c)

Figure 5.12: Breakthrough curves for the the homogeneous Five-Spot Problem (Test Case III) at (a) 25m, (b) 50m and (c) 75m. The breakthrough curves show the flux-weighted oil saturation S_n^*, the water cut WTC and the normalized component C/C_0 for the UPS scheme $(-)$, the NVD scheme $(--)$ and the MINMOD scheme $(\cdot\cdot)$.

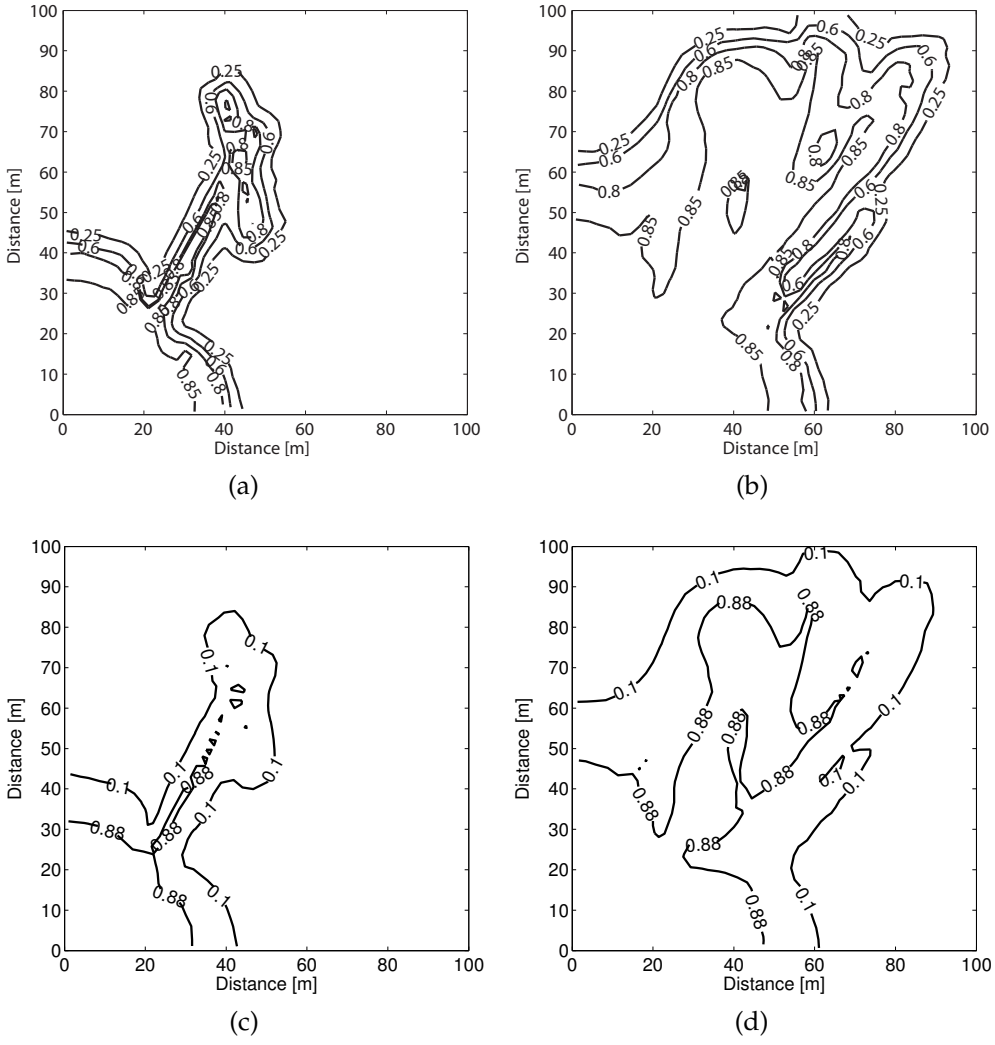

Figure 5.13: Numerical results for the fractured quarter of a five-spot problem (test case IV) obtained with the UPS scheme for times $t = 500$ d (left column) and $t = 1600$ d (right column) just before the water breaks through at the producer. The injector is in the lower left corner, and the producer in the upper right corner, both indicated by a square. Figures (a) and (b) show the result for the water saturation and (c) and (d) the concentration.

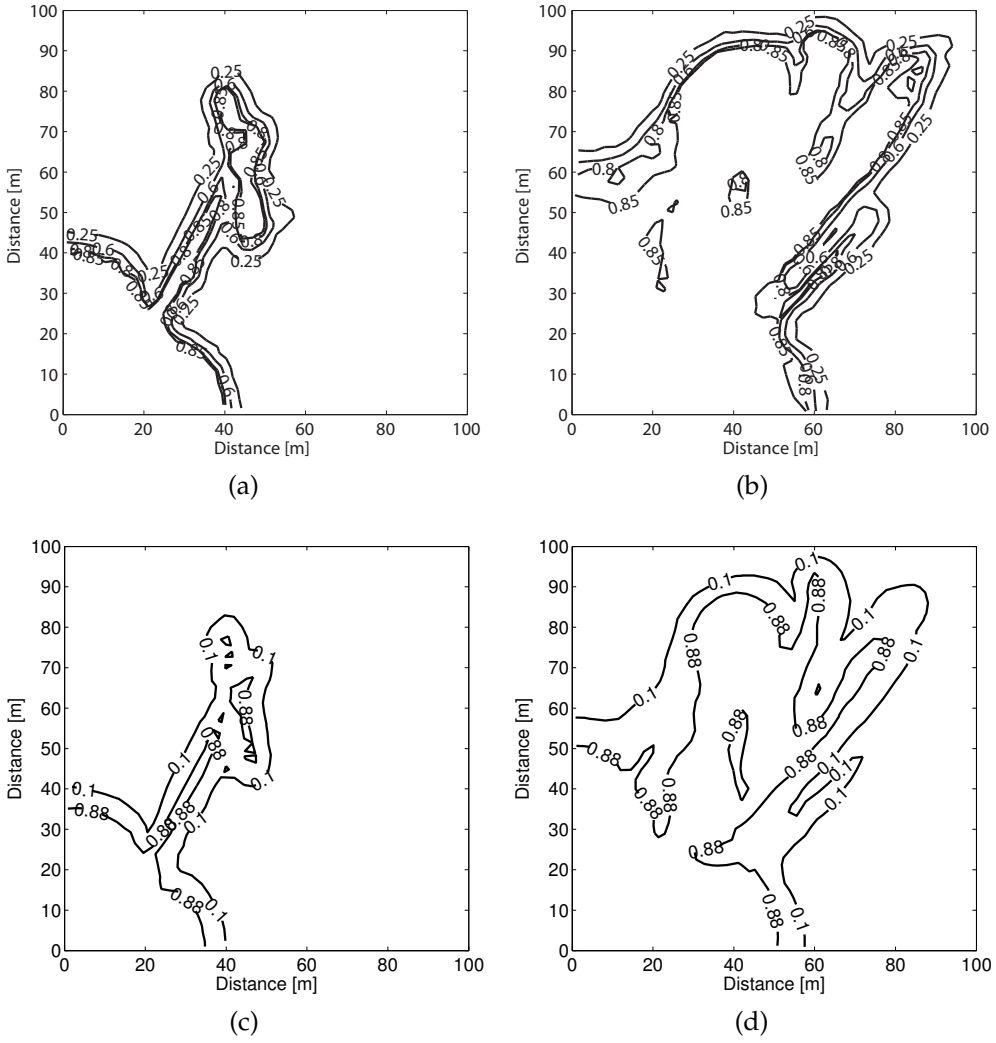

Figure 5.14: Numerical results for the fractured quarter of a five-spot problem (test case IV) obtained with the NVD scheme for times $t = 500$ d (left column) and $t = 1600$ d (right column) just before the water breaks through at the producer. The injector is in the lower left corner, and the producer in the upper right corner, both indicated by a square. Figures (a) and (b) show the result for the water saturation and (c) and (d) the concentration.

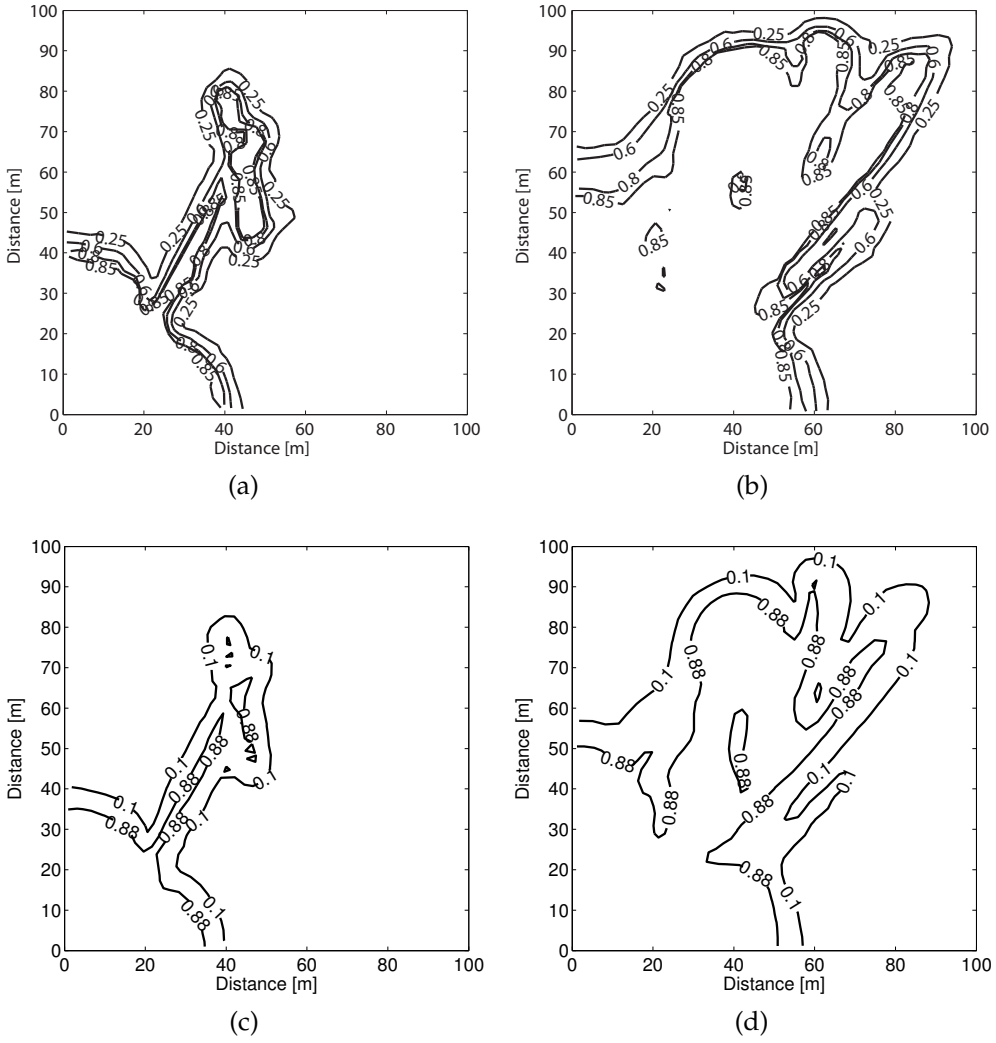

Figure 5.15: Numerical results for the fractured quarter of a five-spot problem (test case IV) obtained with the MINMOD scheme for times $t = 500$ d (left column) and $t = 1600$ d (right column) just before the water breaks through at the producer. The injector is in the lower left corner, and the producer in the upper right corner, both indicated by a square. Figures (a) and (b) show the result for the water saturation and (c) and (d) the concentration.

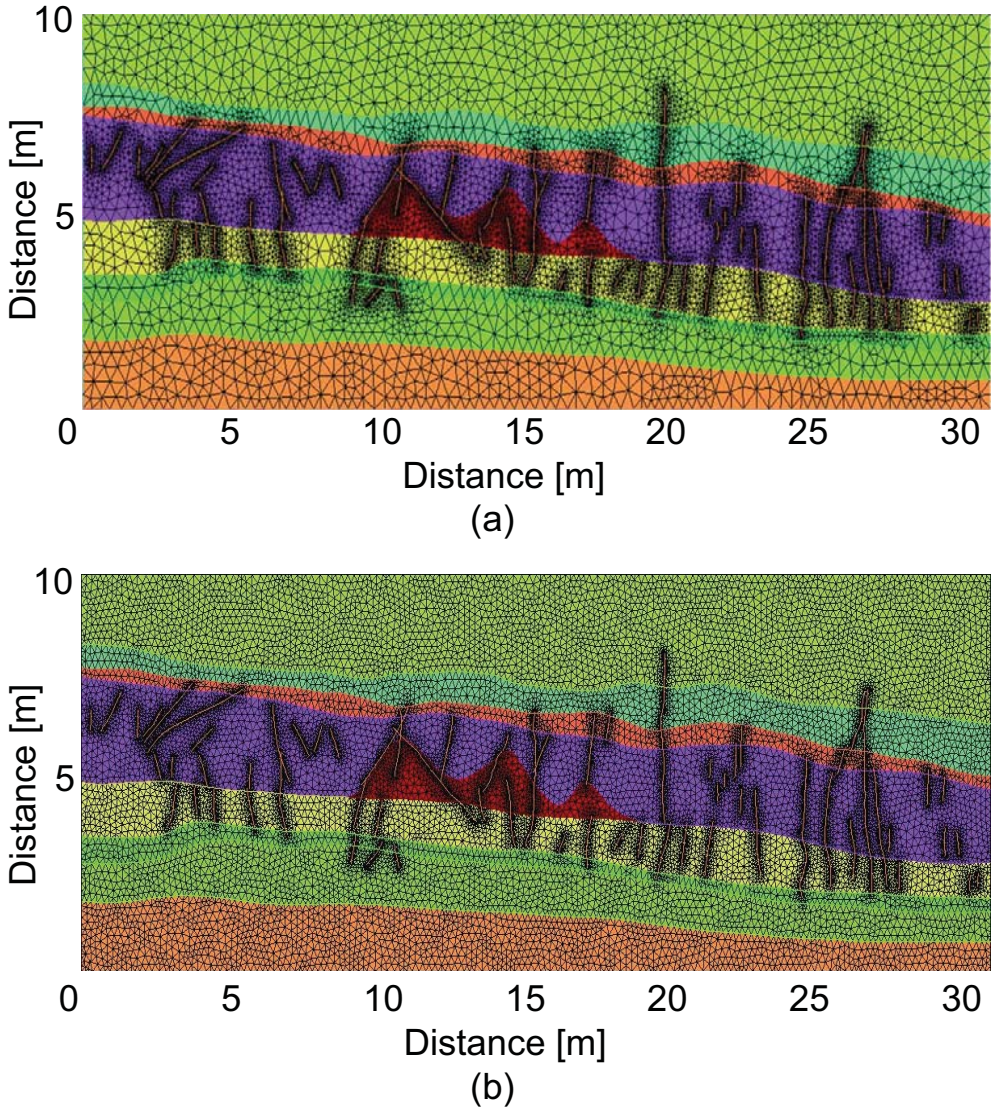

Figure 5.16: a) Discretization of the outcrop shown in Figure 1.1, and used for Test Case V. The FE grid has been refined around the fractures. The heterogeneous rock matrix consists of different geological layers (depicted by different colors) with different permeabilities. The permeabilities vary over four orders of magnitude. (b) The fine grid discretization used for generating a reference solution.

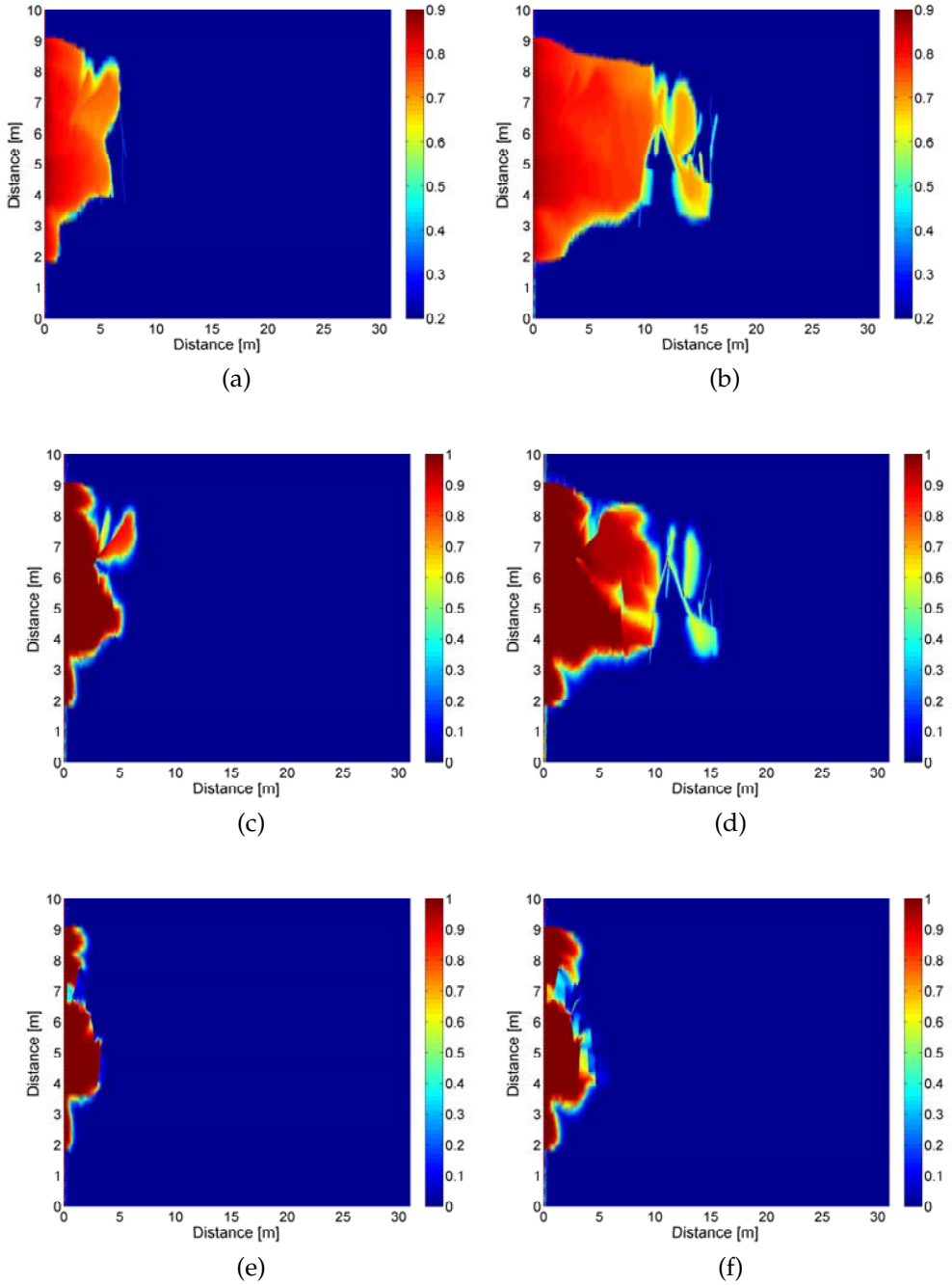

Figure 5.17: Numerical reference solution for flow and transport through the outcrop shown in Figure 1.1 obtained with the NVD scheme for the fine-gid discretization shown in Figure 5.16 (b) at times $t = 150d$ (left column) and $t = 420d$. Figures (a) and (b) show the water saturation S_w, (c) and (d) the inert component A, and (e) and (f) an adsorbing component B.

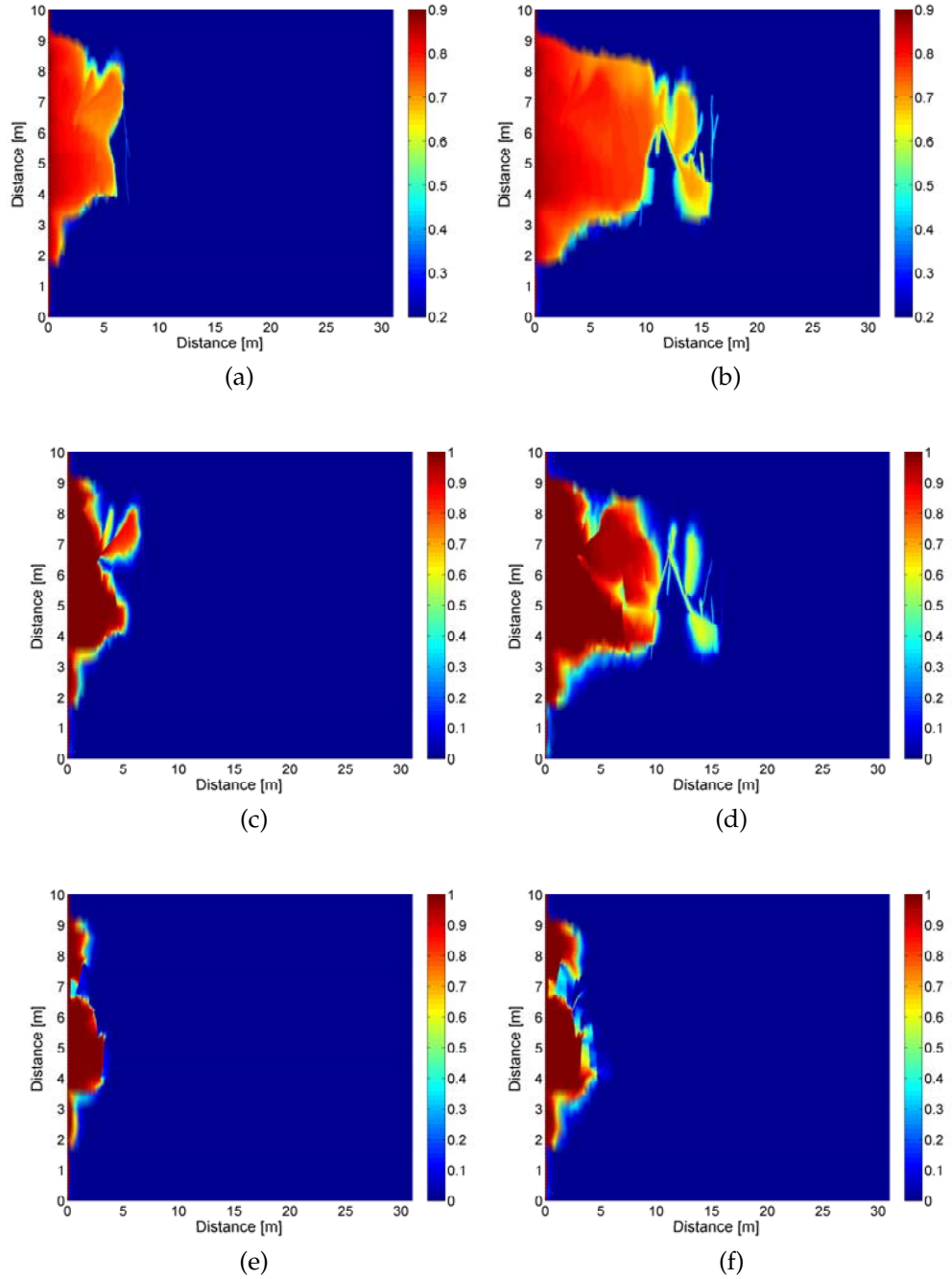

Figure 5.18: Numerical results for flow and transport through the outcrop shown in Fig. 1.1 obtained with the NVD scheme for the discretization shown in Figure 5.16 (a) at times $t = 150d$ (left column) and $t = 420d$. Figures (a) and (b) show the water saturation S_w, (c) and (d) the inert component A, and (e) and (f) an adsorbing component B.

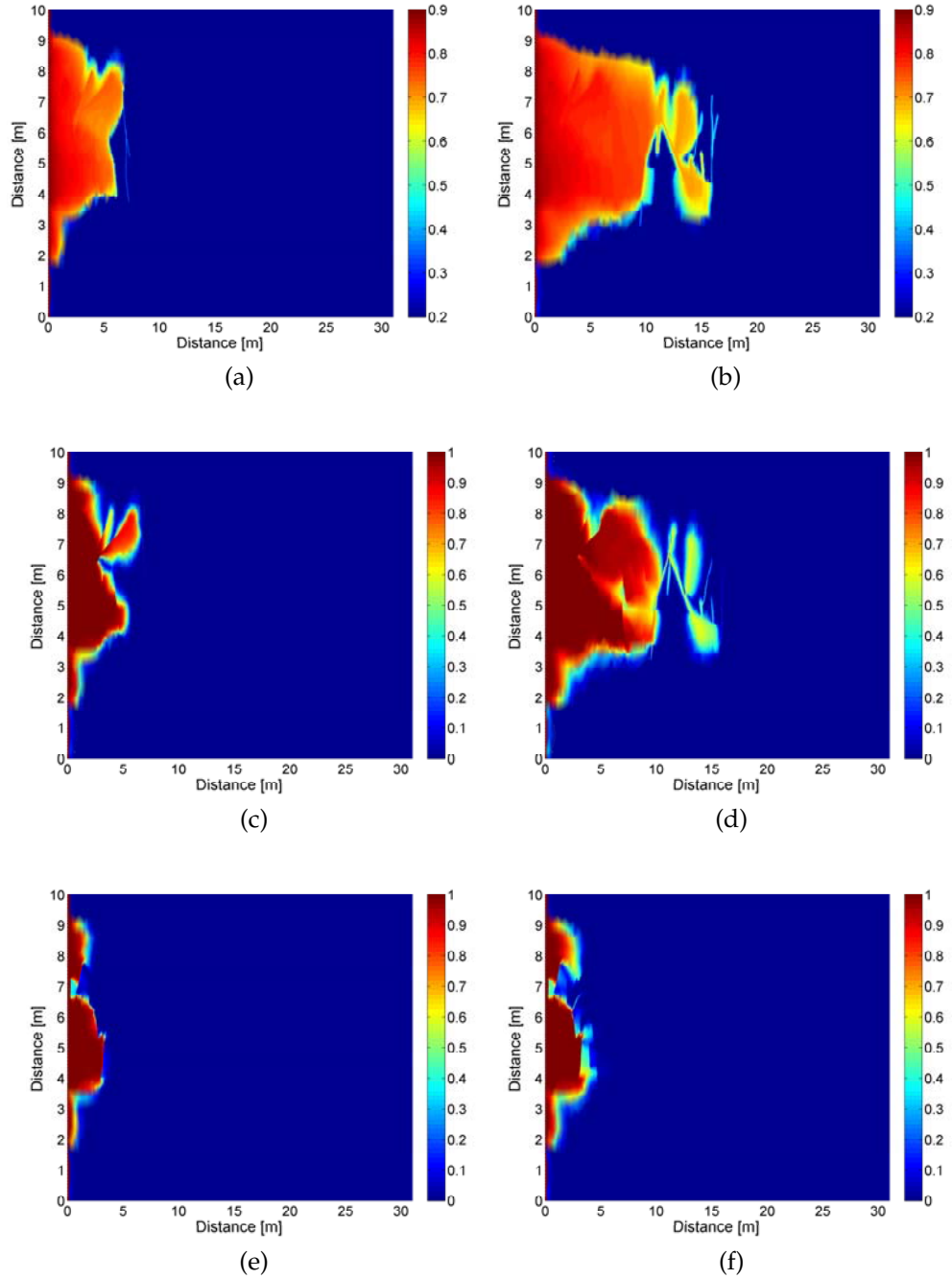

Figure 5.19: Numerical results for flow and transport through the outcrop shown in Fig. 1.1 obtained with the MINMOD scheme for the discretization shown in Figure 5.16 (a) at times $t = 150$d (left column) and $t = 420$d. Figures (a) and (b) show the water saturation S_w, (c) and (d) the inert component A, and (e) and (f) an adsorbing component B.

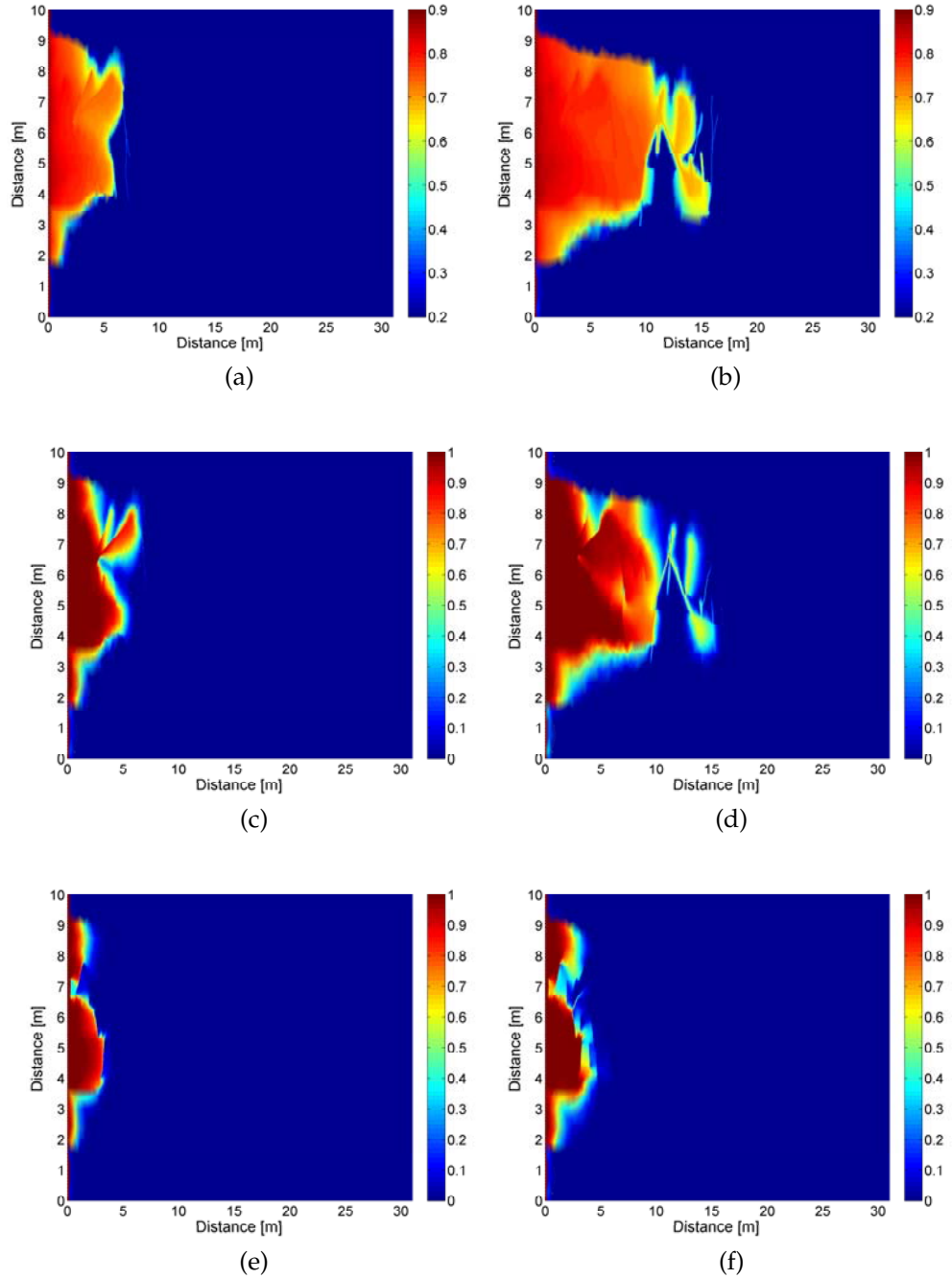

Figure 5.20: Numerical results for flow and transport through the outcrop shown in Figure 1.1 obtained with the UPS scheme for the discretization shown in Figure 5.16 (a) at times $t = 150$d (left column) and $t = 420$d. Figures (a) and (b) show the water saturation S_w, (c) and (d) the inert component A, and (e) and (f) an adsorbing component B.

6

SUMMARY, CONCLUSIONS AND FUTURE WORK

6.1 SUMMARY AND CONCLUSIONS

Two mechanisms are of fundamental importance for flow and transport in fractured media. *Spontaneous imbibition* (SI) is often the only way by which an aqueous phase can enter the oil-rich rock, and thus is often the only recovery mechanism for the oil or contaminant. *Hydrodynamic dispersion* limits mixing and reaction of different components and thus controls the efficiency of any chemical flood. This thesis therefore investigates the influence of capillary forces and dispersion on flow and transport during immiscible two-phase flow:

- *Buckley-Leverett analogue for SI.* The long-missing exact analytical solutions for spontaneous co-, and counter-current imbibition were derived. They are valid in homogeneous, horizontal media for arbitrary capillary-hydraulic properties. The solutions may be viewed as the capillary analogue to the Buckley–Leverett solutions for viscous dominated flow (see the overview in Table 2.2 and Figure 4.1). This should finalize the decades-long search for analytical solutions for spontaneous imbibition. The analogue carries over to the extended Buckley–Leverett theory of flow and transport.

- *Universal scaling group for SI.* We derived the first scaling group t_d for SI that rigorously incorporates the influence of all parameters present in the two-phase Darcy formulation - a problem that was open for more than 90 years. No fitting parameters were introduced. t_d is based on an analytic expression for the total volume imbibed as given by the Buckle-Leverett analogue. We presented two key applications of t_d: First, the group can serve as the long sought-after general transfer rate for imbibition used in dual-porosity models. Second, it is the so far missing proportionality constant in imbibition-germination models for plant seeds.

- *The standard Darcy model can describe SI.* t_d was validated against 45 published water-oil and water-air SI studies for water-wet systems, different degrees of mixed-wettability, a wide range of viscosity ratios, initial water content, different porous media and different boundary conditions. The ability of t_d to correlate such a wide range of data sets strongly indicates that accounting for non-equilibrium effects in capillary pressure is unnecessary, contrary to what has been hypothesized.

- *Influence of adsorption and flow regime on mixing.* To resolve how the flow regime and a simple chemical reaction affects $\delta(t)$ in a homogeneous medium we derive the first known set of analytical solutions for transport that fully accounts for the effects of capillarity, viscous forces and the effects of hydrodynamic dispersion. If dispersion is ignored the solute front can be located graphically by a modified Welge tangent on the fractional flow functions F and f. For transport with dispersion the solutions reveal that for the viscous dominated regime the growth of $\delta(t)$ is proportional to $t^{1/2}$. This confirms earlier numerical results [Arya et al., 1985]. On contrary, for spontaneous imbibition the analytical solutions for the first time show that the temporal order is proportional to $t^{1/4}$, and that adsorption leaves the temporal order unchanged, but decreases the proportionality constant.

- *Higher order FEFV methods on unstructured grids for transport and two-phase flow.* To investigate for heterogeneity (see Chapter 1), we extended the FEFV scheme for the modelling of two-phase flow implemented in CSMP such that it can describe both flow and the transport of viscosifying and reacting components in permeable porous media. We presented two higher order methods of the MUSCL type, a MINMOD scheme and an NVD scheme, and compared them to a classical single-point upstream method. We fully accounted for viscous forces, capillary pressure, hydrodynamic dispersion and adsorption. We used a mass-conservative and flux-continuous node-centered FEFV scheme and gave numerical examples that show that this scheme is capable of resolving flow and transport even in fractured, highly heterogeneous geometries. Dispersion and capillary pressure were resolved via a Strang splitting.

6.2 FUTURE WORK

Obviously, the subject of capillary forces and dispersion on flow and transport allows for many fascinating and important directions for future work. We only pick a few:

- *Gravity, time-dependent imbibition areas, and late time effects.* Besides SI, gravity is the other most important recovery mechanism in fractured reservoirs t_d has been derived making the standard assumptions used for analytical modes, and in particular, viscous and gravity forces were ignored. Whether the presence of these forces can be accounted for through e.g. equation (3.9) remains open. Also, t_d is based on laboratory results where the core used was surrounded by a constant saturation. If and how t_d should be changed for e.g. fractured systems, where the saturation changes depending on the speed of the fracture flow, is open. Finally, the analytical solutions are valid for early times only and currently no exact analytical model for late times exists.

- *Inhomogeneous* p_c *and the controlled-salinity effect.* For the numerical algorithm we worked with homogeneous p_c. However, in heterogeneous media p_c often also is inhomogeneous. Similarly, if the components change the wetting behaviour, this also will change p_c. How to account for that efficiently in numerical simulations is open.

- *Anomalous dispersion.* It is well established that tracer transport in single phase flow through heterogeneous porous media shows anomalous behaviour that cannot be modelled through a simple up scaling of Fickian dispersion. Two phase flow, however, adds complex non-linearities that have been shown to fundamentally change the influence of heterogeneity. It is not clear how that affects transport. Since our analytical and numerical solutions have been derived assuming that dispersion is Fickian, these tools might be used to evaluate the validity of a Fickian model and the $t^{1/2}$ and $t^{1/4}$ scaling for transport during two phase flow.

- *3D simulations and field-scale analysis.* The numerical scheme has been implemented for 2D and should be extended to 3D. This then could be used to perform field-scale analyses of the interplay between heterogeneity, viscous, capillary and chemical effects and dispersion.

- *Multirate dual-porosity models*[1] The classical dual-porosity models miss some key physics of fracture-matrix fluid exchange due to spontaneous imbibition, and it should be investigated how t_d can be incorporated efficiently in a multi-rate mass-transfer model.

1 C. Maier, K. S. Schmid, and S. Geiger: *Multi-rate mass-transfer dual-porosity modelling using the exact analytical solution for spontaneous imbibition*, ECMOR XIII

Part III

APPENDIX

The appendix has no known function [...] Evidence suggests that our evolutionary ancestors used their appendixes to digest tough food like tree bark [...] [It] can cause acute pain, fever, nausea [...] and loss of appetite [which] can be cured easily by removing the appendix.

- from the BBC online fact files on the human body and mind

A

PREVIOUSLY DEFINED GROUPS ARE SPECIAL CASES OF T_D

In this chapter, we show how the different specialized groups can be obtained from t_d if the respective assumptions used for the specialized groups are evoked (Table 3.1).

A.1 THE GROUP OF LUCAS [1918] AND WASHBURN [1921]

The Lucas-Washburn equation follows if the original assumption Lucas [1918], Washburn [1921] of an inviscid non-wetting phase is invoked, i.e. $\mu_o \ll \mu_w$. Then

$$\frac{\lambda_w \lambda_{nw}}{\lambda_t} = \frac{1}{\sqrt{\mu_w \mu_{nw}}} \frac{\sqrt{k_{rw} k_{ro}}}{\sqrt{M} + 1/\sqrt{M}} \approx \frac{k_{rw}}{\mu_w},$$

since $\sqrt{M} \ll 1/\sqrt{M}$, where $M = \frac{\mu_n k_{rw}}{\mu_w k_{ro}}$, and the capillary radius is substituted by the Leverett-radius Bear [1972], $r = \sqrt{\frac{K}{\phi}}$. This then gives

$$F(S_w) \approx 1 - \Big(\int_{S_w}^{S_i} \frac{(\beta - S_w) k_{rw} p_c'}{F(S_w)} d\beta \Big) \cdot \Big(\int_{S_i}^{S_0} \frac{(S_w - S_i) k_{rw} p_c'}{F(S_w)} dS_w \Big)^{-1} \tag{A.1}$$

and thus

$$\begin{aligned} \Big(\frac{A}{\phi L_c} \Big)^2 &\approx \sigma \sqrt{\frac{K}{\phi}} \frac{1}{\mu_w L_c^2} \int_{S_i}^{S_0} \frac{(S_w - S_i) k_{rw} J'}{F(S_w)} dS_w \int_{S_i}^{S_0} \frac{(S_w - S_i) k_{rw} J'}{F(S_w)} dS_w \\ &= \sigma \sqrt{\frac{K}{\phi}} \frac{1}{\mu_w L_c^2} \cdot c. \end{aligned} \tag{A.2}$$

A.2 THE GROUP OF RAPOPORT [1955], MATTAX AND KYTE [1962]

Mattax and Kyte [1962] used the scaling laws developed by Rapoport [1955] to derive a scaling group for the case where $\mu_o = \mu_w$. This yields

$$\frac{\lambda_w \lambda_o}{\lambda_t} = \frac{1}{2\mu_w}\sqrt{k_{rw}k_{ro}}$$

which gives

$$F(S_w) = 1 - \Big(\int_{S_w}^{S_i} \frac{(\beta - S_w)\sqrt{k_{rw}k_{ro}}p_c'}{F(S_w)}\,d\beta\Big)\cdot\Big(\int_{S_i}^{S_0} \frac{(S_w - S_i)\sqrt{k_{rw}k_{ro}}p_c'}{F(S_w)}\,dS_w\Big)^{-1}$$

and thus

$$\begin{aligned}\Big(\frac{2A}{\phi L_c}\Big)^2 &= \sigma\sqrt{\frac{K}{\phi}}\frac{1}{L_c^2\mu_w}\int_{S_i}^{S_0}\frac{(S_w - S_i)\sqrt{k_{rw}k_{ro}}J'}{F}\,dS_w \\ &= \sigma\sqrt{\frac{K}{\phi}}\frac{1}{L_c^2\mu_w}\cdot c\end{aligned} \tag{A.3}$$

A.3 THE GROUP OF MA ET. AL, [1997]

Ma et al. [1997] use the assumption that $\mu_w \approx \mu_o$ which together with

$$\frac{\lambda_w \lambda_o}{\lambda_t} \approx \frac{1}{2\sqrt{\mu_w\mu_o}}\sqrt{k_{rw}k_{ro}} \tag{A.4}$$

leads to

$$F(S_w) \approx 1 - \Big(\int_{S_w}^{S_i} \frac{(\beta - S_w)\sqrt{k_{rw}k_{ro}}p_c'}{F(S_w)}\,d\beta\Big)\cdot\Big(\int_{S_i}^{S_0} \frac{(S_w - S_i)\sqrt{k_{rw}k_{ro}}p_c'}{F(S_w)}\,dS_w\Big)^{-1}.$$

Therefore,

$$\begin{aligned}\Big(\frac{2A}{\phi L_c}\Big)^2 &\approx \sigma\sqrt{\frac{K}{\phi}}\frac{1}{L_c^2\sqrt{\mu_w\mu_o}}\int_{S_i}^{S_0}\frac{(S_w - S_i)\sqrt{k_{rw}k_{ro}}J'}{F}\,dS_w \\ &= \sigma\sqrt{\frac{K}{\phi}}\frac{1}{L_c^2\mu_w}\cdot c.\end{aligned} \tag{A.5}$$

Note that the influence of viscosities in equation (A.4) could only be eliminated because matched viscosities were assumed. If that assumption does not hold for all the data sets that are correlated, then F does not have the form given above, and c is different for the different data sets.

A.4 THE GROUP OF ZHOU ET AL. [2002]

Zhou et al. [2002] used the assumption $\left(\frac{\lambda_w\lambda_o}{\lambda_t}\right)(S_w) \approx \left(\frac{\lambda_w\lambda_o}{\lambda_t}\right)^*$ which immediately yields

$$\begin{aligned}\left(\frac{2A}{\phi L_c}\right)^2 &\approx 2\sigma\sqrt{\frac{K}{\phi}}\frac{1}{L_c^2}\left(\frac{\lambda_w\lambda_o}{\lambda_t}\right)^*\int_{S_i}^{S_0}\frac{(S_w-S_i)J'}{F}dS_w \\ &= 2\sigma\sqrt{\frac{K}{\phi}}\frac{1}{L_c^2}\left(\frac{\lambda_w\lambda_o}{\lambda_t}\right)^*\cdot c.\end{aligned} \tag{A.6}$$

A.5 THE GROUP OF BEHBAHANI AND BLUNT [2005]

Behbahani and Blunt [2005] considered MW systems, where they found from pore-scale studies that $\lambda_w \ll \lambda_o$ and consequently

$$\frac{\lambda_w\lambda_o}{\lambda_t} \approx \lambda_w.$$

If furthermore is assumed that (although this assumption was not stated explicitly) $\lambda_w(S_w) \approx \lambda(S_w^*)$, then

$$\begin{aligned}\left(\frac{2A}{\phi L_c}\right)^2 &\approx 2\sigma\sqrt{\frac{K}{\phi}}\frac{1}{L_c^2}\int_{S_i}^{S_0}\frac{(S_w-S_i)\lambda_w(S_w)J'}{F}dS_w \\ &\approx 2\sigma\sqrt{\frac{K}{\phi}}\frac{1}{L_c^2}\lambda_w^*\int_{S_i}^{S_0}\frac{(S_w-S_i)J'}{F}dS_w \\ &= 2\sigma\sqrt{\frac{K}{\phi}}\frac{1}{L_c^2}\lambda_w^*\cdot c.\end{aligned} \tag{A.7}$$

A.6 THE GROUP OF LI AND HORNE [2006]

Li and Horne [2006] considered piston-like flow, i.e. they assumed that $F(S_w) = \frac{q_w(x^*,t)}{q_w(0,t)}$ and $p_c(S_w)' = \frac{p_c}{S_w}$. $F(x,t)$ can be re-written in terms of saturation as $F(S_w) = \frac{q_w(S_w^*)}{q_w(S_i)} = const. = 1/c$. Consequently

$$\begin{aligned}\left(\frac{2A}{\phi L_c}\right)^2 &\approx 2\sigma\sqrt{\frac{K}{\phi}}\frac{1}{L_c^2}\int_{S_i}^{S_0}\frac{(S_w - S_i)\frac{\lambda_w\lambda_o}{\lambda_t}J'}{F}dS_w \\ &= 2\sigma\sqrt{\frac{K}{\phi}}\frac{1}{L_c^2}c\int_{S_i}^{S_0}(S_w - S_i)\frac{J}{(S_w - S_i)}dS_w \\ &= 2\sigma\sqrt{\frac{K}{\phi}}\frac{1}{L_c^2}c\int_{S_i}^{S_0}JdS_w \\ &\approx 2\sigma\sqrt{\frac{K}{\phi}}\frac{1}{L_c^2}J^*(S_0 - S_i)\cdot c.\end{aligned} \tag{A.8}$$

B

TRANSFORMATIONS EMPLOYED IN CHAPTER 4

B.1 THE CONSERVATION EQUATION FOR C CAN BE WRITTEN AS AN ODE

For transformation (2.24) and with the notion that the components are transported with the respective fluid phase, i.e. $C = C(S_w)$, the equation for C can be transformed into an ordinary differential equation:

$$\frac{dC}{dS_w}\Big(-\lambda + \frac{2A\,(F(1-F_iR)+f_iR}{\phi\,(S_w+D_s)}\Big) = 0. \tag{B.1}$$

subject to

$$C = C_0 \qquad S_w = S_0 \tag{B.2a}$$

$$C = C_i \qquad S_w = S_i. \tag{B.2b}$$

This follows from

$$\begin{aligned} \frac{dC}{dS_w}\frac{\partial S_w}{\partial t} &= -\frac{q_w}{\phi S_w}\frac{dC}{dS_w}\frac{\partial S_w}{\partial x} \\ \frac{dC}{dS_w}\frac{dS_w}{d\lambda}\Big(-\frac{1}{2}xt^{-3/2}\Big) &= -\frac{q_0\,[F(1-f_iR)+f_iR]}{\phi S_w}\frac{dC}{dS_w}\frac{dS_w}{d\lambda}t^{-1/2}, \end{aligned} \tag{B.3}$$

and further we can assume, that $\frac{dS_w}{d\lambda}$ cancels out, i.e. that $\frac{dS_w}{d\lambda} \neq 0$, and with $q_0 = At^{-1/2}$ we then arrive at:

$$\begin{aligned} \frac{dC}{dS_w}\Big(-\frac{1}{2}xt^{-3/2}\Big) &= -At^{-1}\frac{[F(1-f_iR)+f_iR]}{(\phi S_w+\phi D_s)}\frac{dC}{dS_w} \\ \frac{dC}{dS_w}\big(xt^{-3/2}\cdot t\big) &= 2A\frac{[F(1-f_iR)+f_iR]}{(\phi S_w+\phi D_s)}\frac{dC}{dS_w} \\ \frac{dC}{dS_w}\big(xt^{-1/2}\big) &= 2A\frac{[F(1-f_iR)+f_iR]}{(\phi S_w+\phi D_s)}\frac{dC}{dS_w} \\ \frac{dC}{dS_w}\left[-\lambda + \frac{2A\,(F(1-f_iR)+f_iR)}{(\phi S_w+\phi D_s)}\right] &= 0. \end{aligned} \tag{B.4}$$

B.2 AGREEMENT BETWEEN PHYSICAL AND MATHEMATICAL APPROACH

The value for the saturation S_w^* at which the advective front travels as determined by our physically motivated approach and by the method of characteristics, agree. For determining S_w^* from the method of characteristics, we have:

$$\eta \stackrel{!}{=} 0 \Leftrightarrow \int_{S_0}^{S_w} \phi\xi \frac{\partial x}{\partial \xi} d\xi \stackrel{!}{=} \int_0^t q_w(0,\tau)d\tau \tag{B.5}$$

where for $q_w(0,t) = At^{-1/2}$ the right hand side becomes $\tau(t) = 2At^{1/2}$. The left hand side becomes

$$\begin{aligned}
&\int_{S_0}^{S_w} \phi\xi \frac{\partial x}{\partial \xi} d\xi \\
&= t^{1/2} \int_{S_0}^{S_w} \phi\xi \frac{2A(1-f_iR)}{\phi} F''(\xi) d\xi \\
&= t^{1/2} \int_{S_0}^{S_w} \phi\xi \frac{2A(1-f_iR)}{\phi} \left[-\frac{\phi}{2A^2(1-f_iR)^2} \frac{D}{F-f_n} \right] d\xi \\
&= \int_{S_0}^{S_w} \phi\xi \frac{-D(\xi)}{A(1-f_iR)(F(\xi)-f_n)} d\xi.
\end{aligned} \tag{B.6}$$

Taking the expression for the right hand side τ and the left hand side θ we thus obtain that S_w needs to be such that

$$\frac{2A^2(1-f_iR)}{\phi} \stackrel{!}{=} \int_{S_w}^{S_0} \beta \frac{D(\beta)}{(F(\beta)-f_n)} d\beta. \tag{B.7}$$

The left hand side of (B.7) contains the constant A as determined by the analytical solution derived by McWhorter & Sunada (Chapter 2.3).

Successively inserting explicit expressions for A, F and F' shows that equation (B.7) is satisfied. In detail, these steps are as follows:

$$\begin{aligned}
&\frac{2A^2(1-f_iR)}{\phi} = \frac{1}{(1-f_iR)}\int_{S_i}^{S_0}\frac{(\xi-S_i)D(\xi)}{(F-f_n)}d\xi \\
&= \frac{1}{(1-f_iR)}\left[F(S_w)\cdot\int_{S_i}^{S_0}\frac{(\gamma-S_i)D(\gamma)}{F(\gamma)-f_n}d\gamma + \int_{S_w}^{S_0}\frac{(\beta-S_w)D(\beta)}{(F(\beta)-f_n)}d\beta\right] \\
&= \frac{1}{(1-f_iR)}\left[\left(S_wF'(S_w)\int_{S_i}^{S_0}\frac{(\gamma-S_i)D(\gamma)}{(F(\gamma)-f_n)}d\gamma\right)+\right. \\
&\left.\int_{S_w}^{S_0}\frac{(\beta-S_w)D(\beta)}{(F(\beta)-f_n)}d\beta - \frac{1}{(1-f_iR)}f_iR\int_{S_i}^{S_0}\frac{(\gamma-S_i)D(\gamma)}{(F(\gamma)-f_n)}d\gamma\right] \\
&= \frac{1}{(1-f_iR)}\left[\int_{S_w}^{S_0}\frac{S_wD}{F-f_n}d\gamma + \int_{S_w}^{S_0}\frac{(\beta-S_w)D}{(F-f_n)}d\beta\right. \\
&\quad\left. - \frac{1}{(1-f_iR)}f_iR\int_{S_i}^{S_0}\frac{(\gamma-S_i)D(\gamma)}{(F(\gamma)-f_n)}d\gamma\right] \\
&= \frac{1}{(1-f_iR)}\left[\int_{S_w}^{S_0}\frac{\beta D}{(F-f_n)d\gamma} - \frac{f_iR}{(1-f_iR)}\int_{S_i}^{S_0}\frac{(\gamma-S_i)D}{(F-f_n)}d\gamma\right].
\end{aligned} \tag{B.8}$$

Thus, for the case $S_{wi} = S_{wr}, f_i = 0$ equation (B.7) is satisfied if S_w satisfies (4.10) which yields the mathematical rigorous justification for the assumption $C = C(S_w)$ for the advective case made initially. Since the assumption $C = C(S_w)$ stays valid for $f_i \neq 0$, we obtain (4.9).

B.3 TRANSFORMATION OF EQUATION (4.29) ONTO THE $(\bar{\theta}, \bar{\tau})$ COORDINATE SYSTEM

In this section, we transform equation (4.29) onto the $(\bar{\theta}, \bar{\tau})$ coordinate system. To that end, it is helpful, to first transform equation (4.29) onto the $(S_w, \bar{\tau})$ coordinate system. Subsequently, the transformation onto the $(\bar{\theta}, \bar{\tau})$ coordinate system is performed. Only basic calculus is used (triple product rule and the Leibnitz rule). All the tranformations are exact. Thus, the result is a normalized conservation equation for c in the $(\bar{\theta}, \bar{\tau})$ that is equivalent to the PDE written in the $(\bar{t}, \bar{x})$ system.

Transforming the PDE (4.29) from the $(\bar{x}, \bar{t})$-coordinate system onto the $(S_w, \bar{t})$ coordinate system we obtain

$$\begin{aligned}
(\phi S_w + \phi D_s)\frac{\partial c}{\partial \bar{t}} + \left((\phi S_w + \phi D_s)\frac{\partial S_w}{\partial \bar{t}} + \bar{q_w}\nu\frac{\partial S_w}{\partial \bar{x}}\right)\frac{\partial c}{\partial S_w} = \\
\frac{\partial S_w}{\partial \bar{x}}\varepsilon\nu\frac{\partial}{\partial S_w}\left(S_w\bar{q_w}\frac{\partial S_w}{\partial \bar{x}}\frac{\partial c}{\partial S_w}\right)
\end{aligned} \tag{B.9}$$

where we used the product rule

$$\begin{aligned} \frac{\partial}{\partial \bar{x}} &= \frac{\partial}{\partial S_w}\frac{\partial S_w}{\partial \bar{x}} \\ \frac{\partial}{\partial \bar{t}} &= \frac{\partial}{\partial S_w}\frac{\partial S_w}{\partial \bar{t}} + \frac{\partial}{\partial \bar{t}} \end{aligned} \tag{B.10}$$

which in an intermediate step gives

$$\begin{aligned} (\phi S_w + \phi D_s)\left(\frac{\partial c}{\partial S_w}\frac{\partial S_w}{\partial \bar{t}} + \frac{\partial c}{\partial \bar{t}}\right) = \\ -\bar{q}_w \nu \frac{\partial c}{\partial S_w}\frac{\partial S_w}{\partial \bar{x}} + \varepsilon\nu\frac{\partial S_w}{\partial \bar{x}}\frac{\partial}{\partial S_w}\left(S_w \bar{q}_w \frac{\partial S_w}{\partial \bar{x}}\frac{\partial c}{\partial S_w}\right). \end{aligned} \tag{B.11}$$

The system (B.9) together with the continuity equation for water is completely described by two of the three variables $(S_w, \bar{x}, \bar{t})$ and one variable can be expressed as implicit function of the other two, e.g. $\bar{x} = \bar{x}(S_w, \bar{t})$, and thus, the triple product rule holds

$$\left(\frac{\partial S_w}{\partial \bar{x}}\right)_{\bar{t}} \cdot \left(\frac{\partial \bar{t}}{\partial S_w}\right)_{\bar{x}} \cdot \left(\frac{\partial \bar{x}}{\partial \bar{t}}\right)_{S_w} = -1 \tag{B.12}$$

where subscripts here denote that this variable is kept constant. Using this in (B.9) yields

$$\begin{aligned} \left((\phi S_w + \phi D_s)\frac{\partial \bar{x}}{\partial S_w}\right)\frac{\partial c}{\partial \bar{t}} + \left(\nu \bar{q}_w - (\phi S_w + \phi D_s)\frac{\partial \bar{x}}{\partial \bar{t}}\right)\frac{\partial c}{\partial S_w} = \\ \varepsilon\nu\frac{\partial}{\partial S_w}\left(S_w \bar{q}_w \frac{\partial S_w}{\partial \bar{x}}\frac{\partial c}{\partial S_w}\right). \end{aligned} \tag{B.13}$$

In the next step, we transform equation (B.13) from the $(S_w, \bar{t})$ coordinate system onto the $(\bar{\theta}, \bar{\tau})$-coordinate system. The product rule yields

$$\begin{aligned} \frac{\partial}{\partial S_w} &= \frac{\partial}{\partial \bar{\theta}}\frac{\partial \bar{\theta}}{\partial S_w} + \frac{\partial}{\partial \bar{\theta}}\frac{\partial \bar{\theta}}{\partial S_w} = \frac{\partial}{\partial \bar{\theta}}\frac{\partial \bar{\theta}}{\partial S_w} \\ \frac{\partial}{\partial \bar{t}} &= \frac{\partial}{\partial \bar{\theta}}\frac{\partial \bar{\theta}}{\partial \bar{t}} + \frac{\partial}{\partial \bar{\tau}}\frac{\partial \bar{\tau}}{\partial \bar{t}} \\ \frac{\partial}{\partial S_w}\left(\frac{\partial}{\partial \bar{\theta}}\right) &= \left(\frac{\partial}{\partial \bar{\theta}}\frac{\partial \bar{\theta}}{\partial S_w}\right)\frac{\partial}{\partial \theta} = \frac{\partial \theta}{\partial S_w}\frac{\partial}{\partial \bar{\theta}}\left(\frac{\partial}{\partial \bar{\theta}}\right) = \frac{\partial \bar{\theta}}{\partial S_w}\frac{\partial^2}{\partial \bar{\theta}^2}. \end{aligned} \tag{B.14}$$

We have

$$\frac{\partial \bar{\theta}}{\partial S_w} = \frac{\partial}{\partial S_w}\left(\int_{S_0}^{S_w} (\phi\xi + \phi D_s)\frac{\partial \bar{x}}{\partial \xi} d\xi\right) \overset{\text{Leibnitz}}{=} \phi S_w \frac{\partial \bar{x}}{\partial S_w} \tag{B.15}$$

and

$$\frac{\partial \bar{\tau}}{\partial \bar{t}} = \frac{\partial}{\partial \bar{t}} \int_0^{\bar{t}} \nu \bar{q}_w(x = 0, \xi) d\xi = \nu \bar{q}_w(x = 0, \bar{t}) = \nu \bar{q}_w(S_0, \bar{t}). \quad \text{(B.16)}$$

For the calculation of $\partial\bar{\theta}/\partial\bar{t}$ we need the relationships

$$\frac{\partial}{\partial \bar{t}} \left((\phi S_w + \phi D_s) \frac{\partial \bar{x}}{\partial S_w} \right) = (\phi S_w + \phi D_s) \frac{\partial \bar{x}}{\partial S_w \partial \bar{t}} = \quad \text{(B.17a)}$$

$$\frac{\partial}{\partial S_w} \left((\phi S_w + \phi D_s) \frac{\partial \bar{x}}{\partial \bar{t}} \right) - \phi \frac{\partial \bar{x}}{\partial \bar{t}}, \quad \text{(B.17b)}$$

$$\nu \frac{\partial \bar{q}_w}{\partial \bar{x}} = \nu \frac{\partial \bar{q}_w}{\partial S_w} \frac{\partial S_w}{\partial \bar{x}} = -\phi \frac{\partial S_w}{\partial \bar{t}} \overset{\text{(B.12)}}{=} \phi \frac{\left(\frac{\partial \bar{x}}{\partial \bar{t}}\right)}{\left(\frac{\partial \bar{x}}{\partial S_w}\right)}, \quad \text{(B.17c)}$$

$$\frac{dS_w}{d\bar{t}} = \frac{\partial S_w}{\partial \bar{x}} \frac{dx}{d\bar{t}} + \frac{\partial S_w}{\partial \bar{t}} = \frac{\partial S_w}{\partial \bar{x}} \bar{q}_w + \frac{\partial S_w}{\partial \bar{t}} \overset{(2.1)}{=} 0, \quad \text{(B.17d)}$$

and

$$\frac{dS_0}{d\bar{t}} = 0 + \frac{\partial S_0}{\partial \bar{t}} \overset{\text{(B.12)}}{=} -\left(\frac{\left(\frac{\partial \bar{x}}{\partial \bar{t}}\right)}{\left(\frac{\partial \bar{x}}{\partial S_w}\right)} \right)_{S_0}. \quad \text{(B.17e)}$$

Then $\partial\bar{\theta}/\partial\bar{t}$ becomes

$$\begin{aligned}
\frac{\partial \bar{\theta}}{\partial \bar{t}} &= \frac{\partial}{\partial \bar{t}} \left(\int_{S_0}^{S_w} (\phi \xi + \phi D_s) \frac{\partial \bar{x}}{\partial \xi} d\xi \right) \\
&\overset{\text{Leibnitz}}{=} \int_{S_0}^{S_w} \frac{\partial}{\partial \bar{t}} \left((\phi \xi + \phi D_s) \frac{\partial \bar{x}}{\partial \xi} \right) d\xi + \left((\phi S_w + \phi D_s) \frac{\partial \bar{x}}{\partial S_w} \right)_{S_w} \frac{dS_w}{d\bar{t}} \\
&\quad - \left((\phi S_0 - \phi D_s) \frac{\partial \bar{x}}{\partial S_w} \right)_{S_0} \frac{dS_0}{d\bar{t}} \\
&\overset{\substack{\text{(B.17b)} \\ \text{(B.17d)}}}{=} \int_{S_0}^{S_w} \left(\frac{\partial}{\partial \xi} \left((\phi \xi + \phi D_s) \frac{\partial \bar{x}}{\partial \bar{t}} \right) - \phi \frac{\partial \bar{x}}{\partial \bar{t}} \right) d\xi - \left((\phi S_0 + \phi D_s) \frac{\partial \bar{x}}{\partial S_w} \right)_{S_0} \frac{dS_0}{d\bar{t}} \\
&\overset{\text{(B.17c)}}{=} \int_{S_0}^{S_w} \frac{\partial}{\partial \xi} \left[(\phi \xi + \phi D_s) \frac{\partial \bar{x}}{\partial \bar{t}} - \nu \bar{q}_w \right] d\xi - \left((\phi S_0 + \phi D_s) \frac{\partial \bar{x}}{\partial S_w} \right)_{S_0} \frac{dS_0}{d\bar{t}} \quad \text{(B.18)} \\
&= \left((\phi S_w + \phi D_s) \frac{\partial \bar{x}}{\partial \bar{t}} - \nu \bar{q}_w \right) |_{S_0}^{S_w} - \left((\phi S_0 + \phi D_s) \frac{\partial \bar{x}}{\partial S_w} \right) |_{S_0} \frac{dS_0}{d\bar{t}} \\
&\overset{\text{(B.17e)}}{=} (\phi S_w + \phi D_s) \frac{\partial \bar{x}}{\partial \bar{t}} |_{S_w} - (\phi S_0 + \phi D_s) \frac{\partial \bar{x}}{\partial \bar{t}} |_{S_0} \\
&\quad + \nu \bar{q}_w(S_0, \bar{t}) - \nu \bar{q}_w(S_w, \bar{t}) + \left((\phi S_w + \phi D_s) \frac{\partial \bar{x}}{\partial S_w} \cdot \frac{\left(\frac{\partial \bar{x}}{\partial \bar{t}}\right)}{\left(\frac{\partial \bar{x}}{\partial S_w}\right)} \right) |_{S_0} \\
&= (\phi S_w + \phi D_s) \frac{\partial \bar{x}}{\partial \bar{t}} |_{S_w} + \nu \bar{q}_w(S_0, \bar{t}) - \nu \bar{q}_w(S_w, \bar{t}).
\end{aligned}$$

With the above relations, the PDE (B.13) can be transformed onto the $(\bar{\theta}, \bar{\tau})$-coordinate system:

$$\begin{aligned}
&\left((\phi S_w + \phi D_s)\frac{\partial \bar{x}}{\partial S_w}\right)\left[\frac{\partial c}{\partial \bar{\theta}}\cdot\frac{\partial \bar{\theta}}{\partial \bar{t}} + \frac{\partial c}{\partial \bar{\tau}}\frac{\partial \bar{\tau}}{\partial \bar{t}}\right] + \left(v\bar{q}_w - (\phi S_w + \phi D_s)\frac{\partial \bar{x}}{\partial \bar{t}}\right)\frac{\partial c}{\partial \bar{\theta}}\frac{\partial \bar{\theta}}{\partial S_w} = \\
&v\varepsilon\left[\frac{\partial}{\partial S_w}\left(S_w\bar{q}_w\frac{\partial S_w}{\partial \bar{x}}\right)\frac{\partial \bar{\theta}}{\partial S_w}\cdot\frac{\partial c}{\partial \bar{\theta}}\right] + v\varepsilon\left[S_w\bar{q}_w\frac{\partial S_w}{\partial \bar{x}}\left[\frac{\partial^2 c}{\partial^2 \bar{\theta}}\cdot\left(\frac{\partial \bar{\theta}}{\partial S_w}\right)^2 + \frac{\partial c}{\partial \bar{\theta}}\frac{\partial^2 \bar{\theta}}{\partial S_w^2}\right]\right] \\
&\overset{\text{(B.14),(B.15)}}{\underset{\text{(B.16),(B.18)}}{\Leftrightarrow}} \\
&\left((\phi S_w + \phi D_s)\frac{\partial \bar{x}}{\partial S_w}\right)\left[\left((\phi S_w + \phi D_s)\frac{\partial \bar{x}}{\partial \bar{t}}|_{S_w} + v\bar{q}_{w0} - v\bar{q}_w\right)\frac{\partial c}{\partial \bar{\theta}} + v\bar{q}_{w0}\frac{\partial c}{\partial \bar{\tau}}\right] \\
&+ \left((\phi S_w + \phi D_s)\frac{\partial \bar{x}}{\partial S_w}\right)\left[\bar{q}_w - (\phi S_w + \phi D_s)\frac{\partial \bar{x}}{\partial \bar{t}}\right]\frac{\partial c}{\partial \bar{\theta}} = \\
&\left[v\varepsilon\frac{\partial}{\partial S_w}\left((\phi S_w + \phi D_s)S_w\bar{q}_w\frac{\partial S_w}{\partial \bar{x}}\frac{\partial \bar{x}}{\partial S_w}\right)\right]\frac{\partial c}{\partial \bar{\theta}} + \left[v\varepsilon\left((\phi S_w + \phi D_s)\frac{\partial \bar{x}}{\partial S_w}\right)^2\right. \\
&\left.\left(S_w\bar{q}_w\frac{\partial S_w}{\partial \bar{x}}\right)\right]\frac{\partial^2 c}{\partial \bar{\theta}^2}
\end{aligned} \tag{B.19}$$

$$\begin{aligned}
&\Leftrightarrow \\
&\left((\phi S_w + \phi D_s)\frac{\partial \bar{x}}{\partial S_w}\right)\bar{q}_{w0}v\frac{\partial c}{\partial \bar{\tau}} + \left(\phi S_w\frac{\partial \bar{x}}{\partial S_w}\right)\bar{q}_{w0}v\frac{\partial c}{\partial \bar{\tau}} = \\
&\left[v\varepsilon\frac{\partial}{\partial S_w}\Big((\phi S_w + \phi D_s)\bar{q}_{w0}\Big)\right]\frac{\partial c}{\partial \bar{\theta}} + \left[v\varepsilon\left((\phi S_w + \phi D_s)\frac{\partial \bar{x}}{\partial S_w}\right)^2\cdot(S_w\bar{q}_w)\right]\frac{\partial^2 c}{\partial \bar{\theta}^2}
\end{aligned}$$

and thus

$$\begin{aligned}
&\frac{\partial c}{\partial \bar{\tau}} + \frac{\partial c}{\partial \bar{\theta}} = \frac{\varepsilon}{\bar{q}_{w0}}\left[\frac{1}{(S_w + D_s)(\partial \bar{x}/\partial S_w)}\frac{\partial}{\partial S_w}\Big((S_w + D_s)S_w\bar{q}_w\Big)\frac{\partial c}{\partial \bar{\theta}}\right. \\
&\left.+ \Big(\phi(S_w + D_s)S_w\bar{q}_w\Big)\frac{\partial^2 c}{\partial \bar{\theta}^2}\right].
\end{aligned}$$

Note that if $\varepsilon = 0$ in equation (4.30), we obtain the normalized version of the hyperbolic advection equation(4.26).

B.4 TRANSFORMATION ONTO THE $(\bar{\theta}, \xi)$ COORDINATE SYSTEM

We next transform equation (B.20) onto the $(\bar{\theta}, \xi)$ coordinate system. The product rule yields

$$\begin{aligned}
\frac{\partial}{\partial \bar{\theta}} &= \frac{\partial}{\partial \xi}\frac{\partial \xi}{\partial \bar{\theta}} + \frac{\partial}{\partial \bar{\tau}}\frac{\partial \bar{\tau}}{\partial \bar{\theta}} = \frac{1}{\varepsilon^m}\frac{\partial}{\partial \xi} \\
\frac{\partial}{\partial \bar{\tau}} &= \frac{\partial}{\partial \bar{\tau}} + \frac{\partial}{\partial \xi}\frac{\partial \xi}{\partial \bar{\tau}} = \frac{\partial}{\partial \bar{\tau}} - \frac{1}{\varepsilon^m}\frac{\partial}{\partial \bar{\eta}}.
\end{aligned} \tag{B.20}$$

Inserting this into equation (B.20) yields

$$\frac{\partial c}{\partial \bar{\tau}} = \frac{1}{\bar{q}_{w0}\varepsilon^{2m-1}} \left[\frac{\varepsilon^m}{(S_w + D_s)(\frac{\partial \bar{x}}{\partial S_w})} \frac{\partial}{\partial S_w} \Big((S_w + D_s) S_w \bar{q}_w \Big) \frac{\partial c}{\partial \xi} + \Big(\phi (S_w + D_s) S_w \bar{q}_w \Big) \frac{\partial^2 c}{\partial \xi^2} \right]. \tag{B.21}$$

NOMENCLATURE

Greek symbols

α	dispersivity constant, p.8	$[m]$
δ	fracture width, p.84	$[m]$
$\delta(t)$	dispersive zone, p.3	$[m]$
$\delta_{i,j}$	Kronecker delta, p.7	$[-]$
ε	dimensionless parameter, p.68	$[-]$
ε_1	error in l_1 norm, p.100	$[-]$
ε_{max}	error in maximum norm, p.102	$[-]$
$\theta(S_w, t)$	characteristic coordinate, p.66	$[m]$
λ	similarity variable, p.16	$[mt^{-1/2}]$
λ_α	mobility of phase α, p.7	$[s/Pa]$
λ_{BC}	Brooks-Corey parameters, p.74	$[-]$
λ_t	total mobility, p.9	$[s/Pa]$
$\overline{\lambda}_t$	shorthand for $\frac{\lambda_w \lambda_n}{\lambda_t}$, p.88	$[Pa/s]$
μ_α	viscosity of phase α, p.7	$[Pa/s]$
ν	dimensionless parameter, p.68	$[-]$
ξ	coordinate transformation, p.70	inflow dep.
ρ_α	density of phase α, p.7	$[kg/m^3]$
ρ_r	rock density, p.8	$[kg/m^3]$
σ	surface tension, p.40	$[N/m]$
$\tau(t)$	characteristic coordinate, p.66	inflow dep.
$\tau(S_w)$	coefficient for dynamic p_c,p.39	$[Pa \cdot s]$
τ_c	characteristic time,p.31	$[1/s]$
ϕ	porosity, p.7	$[-]$
ψ	MINMOD limier, p.96	$[-]$
Γ	isotherm, p.8	$[-]$
$\{\Phi_i\}_{i=1}$	nodal basis	$[-]$
Ω	computational domain, p.84	$[-]$

Roman symbols

$\mathbf{a}$	gradient of linear reconstruction, p.95	
$\mathbf{A}$	stiffness matrix, p.88	
$\mathbf{b}$	right-hand side vector, p.86	
A	measurement of a porous medium's ability to imbibe, pp.12,18	$[ms^{-1/2}]$
$A_{s,i}$	adsorption of C_i per unit of mass rock	$[m^3/kg]$
A_i	area open to imbibition	$[m^2]$
B_s	adsorption of χ per unit of mass rock, p.65	$[m^3/kg]$
Bo	Bond number, p.50	$[-]$
$\mathbf{C}$	vector of component concentration in phase w, p.8	$[mol/L]$
χ	vector of component concentration in phase n, p.64	$[mol/L]$
c	proportionality constant	$[-]$
c_t	total compressibility of the fluid-rock system, p.8	$[1/Pa]$
$\mathbf{D}, D_H$	tensor and 1D hydrodynamic dispersion, pp.8,59	$[m^2/s]$
$\mathcal{D}_s$	slope of isotherm, p.59	$[-]$
$D(S_w)$	capillary dispersion, p.11	$[m^2/s]$
f	fractional flow function without p_c, p.9	$[-]$
f_i	$f(S_{wi})$, p.16	$[-]$
f_n	normalized fractional flow function, p.16	$[-]$
F	fractional flow function with p_c, pp.16,18	$[-]$
$\mathbf{g}$	gravitational acceleration vector, p.7	$[m/s^2]$
g	gravitational constant, p.7	$[m/s^2]$
J	Leverett J−function, p.40	$[-]$
$\mathbf{K}, K$	tensor of and 1D permeability, p.7	$[m^2]$
L_c	characteristic length, p.30	$[m]$
L_0	characteristic length, p.70	$[m]$
L_V	length of the principal axis in a FV, p.88	$[m]$
l_{A_i}	distance between A_i and now-flow boundary, p.30	$[m]$
$\mathbf{M}$	mass matrix, p.88	$[m]$
$\mathbf{n}_j$	normal vector on segment j, p.85	$[-]$
p	fluid pressure, p.7	$[Pa]$
$\mathbf{p}$	vector of nodal points for p, p.86	$[Pa]$
Pe	grid Peclet number, p.101	$[-]$
p_d	entry pressure, p.74	$[Pa]$
$V_w(t)$	cumulative 1D volume of wetting phase injected/imbibed	$[m]$

Roman symbols

$\mathbf{q}_\alpha$	vector of fluid velocity of phase α, p.7	[m/s]
$\mathbf{q}_t$	vector of total velocity, p.7	[m/s]
R	ratio between total flow and inflow, p.16	[–]
Rec	recovery, p.51	%
R_∞	ultimate recovery, p.51	%
S	saturation, p.7	[–]
S_e	effective saturation, p.41	[–]
S_{wi}	initial water saturation, p.12	[–]
S_0	water saturation at left boundary, p.12	[–]
$S_{\alpha r}$	residual saturation of the phase α	[–]
t	time	[s]
t_a	ageing time, p.27	[s]
t^*	time when the analytical solutions stop to be valid, p.21	[s]
$t_{d,inflow}$	dimensionless time, p.31	[s]
$t_{d,front}$	dimensionless time, p.31	[s]
$t_{d,Ma}$	dimensionless time, p.31	[s]
$\mathcal{V}$	space of piecewise linear functions, p.86	[–]
$\widetilde{U}_i$	linear reconstruction of a variable at node i, p.96	
$\overline{U}_i$	linear reconstruction of a variable at node i, p.96	
V_b	the bulk volume of the matrix, p.30	[m^3]
$\mathbf{x}_j$	coordinate vector of node j	[m]

Subscripts

α	$\alpha \in \{w, n\}$, p.7
c	capillary
C	concentration
L	longitudinal
m	matrix
f	fractures
S	saturation
SI	spontaneous imbibition, p.41
T	transversal
w	non-wetting, p.7
w	wetting, p.7
WF	water flood, p.41

Superscripts

comp	composite
equiv.	equivalent
in	inner
match	matched
max	maximal
min	minimal
out	outer
$*$	characteristic value

BIBLIOGRAPHY

I. Aavatsmark. An introduction to multipoint flux approximations for quadrilateral grids. *Computational Geosciences*, 6(3):405–432, 2002.

A. Abushaikha and O. Gosselin. Matrix-fracture transfer function in dual-media flow simulation: Review, comparison and validation. In *Europec/EAGE Conference and Exhibition*, 2008.

G. Acs, S. Doreschall, and E. Farkas. General purpose compositional model. *SPE Journal*, 25(4):543–553, 1985.

Chinedu C. Agbalaka, Abhijit Y. Dandekar, Shirish L. Patil, Santanu Khataniar, and James R. Hemsath. Coreflooding studies to evaluate the impact of salinity and wettability on oil recovery efficiency. *Transport in Porous Media*, 76(1):77–94, 2009. doi: 10.1007/s11242-008-9235-7.

M. Alava, M. Dubé, and M. Rost. Imbibition in disordered media. *Advances in Physics*, 53(2):83–175, 2004.

R. Anderson, B. Tohidi, and J. B. W. Webber. Gas hydrate growth and dissociation in narrow pore networks: capillary inhibition and hysteresis phenomena. *Geol. Soc., London, Special Publications*, 319(1): 145, 2009.

W. G. Anderson. Wettability literature survey-part 4: Effects of wettability on capillary pressure. *Journal of Petroleum Technology*, 39(10): 1283–1300, 1987a.

W. G. Anderson. Wettability literature survey part 5: The effects of wettability on relative permeability. *Journal of Petroleum Technology*, 39(11):1453–1468, 1987b.

L. Anton and R. Hilfer. Trapping and mobilization of residual fluid during capillary desaturation in porous media. *Physical Review E*, 59 (6):6819, 1999.

P. Arminjon and A. Dervieux. Construction of TVD-like artificial viscosities on two-dimensional arbitrary FEM grids. *Journal of Computational Physics*, 106:176–198, 1993.

J. S. Aronofsky, L. Masse, and S. G. Natanson. A model for the mechanism of oil recovery from the porous matrix due to water invasion in fractured reservoirs. In *Trans. AIME*, pages 17–19, 1958.

A. Arya, T. A. Hewitt, R. Larson, and L. W. Lake. Dispersion and reservoir heterogeneity. In *SPE14364*, 1985.

T.; Austad and D. C. Standnes. Spontaneous imbibition of water into oil-wet carbonates. *Journal of Petroleum Science and Engineering*, 39 (3-4):363 – 376, 2003. doi: 10.1016/S0920-4105(03)00075-5.

T. Austad, S. Strand, M.V. Madland, T. Puntevold, and R. Korsnes. Seawater in chalk: An eor and compaction of fluid. *SPE Reservoir Evaluation&Engineering*, –:648–654, 2008.

T. Austad, A. Rezaeidoust, and T. Puntervold. Chemical Mechanism of Low Salinity Water Flooding in Sandstone Reservoirs. In *SPE Improved Oil Recovery Symposium*, 2010.

K. Aziz and A. Settari. *Petroleum Reservoir Simulation*. Applied Science Publishers, London, UK., 1979.

T. Babadagli and C. U. Hatiboglu. Analysis of counter-current gas-water capillary imbibition transfer at different temperatures. *Journal of Pet. Sc. and Eng.*, 55(3-4):277–293, 2007.

T. Babadagli and K. Zeidani. Evaluation of matrix-fracture imbibition transfer functions for different types of oil, rock and aqueous phase. In *SPE/DOE Symposium on Improved Oil Recovery*, 2004.

G. I. Barenblatt, I. P. Zheltov, and I. N. Kochina. Basic concepts in the theory of seepage of homogeneous liquids in fissured rocks. *J. Appl. Math. Mech.*, 24(5):1286–1303, 1960.

G. I. Barenblatt, T. W. Patzek, and D. B. Silin. The mathematical model of nonequilibrium effects in water-oil displacement. *SPE Journal*, 8(4): 409–416, 2003.

G.I. Barenblatt, V.M. Entov, and V.M. Ryzhik. *Theory of fluid flows through natural rocks*. Springer, 1990.

P. Batten, C. Lambert, and D.M. Causon. Positively conservative high-resolution convection schemes for unstructured elements. *International Journal for Numerical Methods in Engineering*, 39(11):1821–1838, 1996.

J. Bear. *Dynamics of Fluids in Porous Media*. Dover, New York, NY., 1972.

P. Bedrikovetsky. *Mathematical theory of oil and gas recovery: with applications to ex-USSR oil and gas fields*, volume 4. Kluwer Academic Publishers, 1993.

H. Behbahani and M. Blunt. Analysis of imbibition in mixed-wet rocks using pore-scale modeling. *SPE Journal*, 10(4):466–474, 2005.

H. S. Behbahani, G. Di Donato, and M. J. Blunt. Simulation of countercurrent imbibition in water-wet fractured reservoirs. *Journal of Petroleum Science and Engineering*, 50(1):21–39, 2006.

J.B. Bell, P. Colella, and J.A. Trangenstein. Higher order godunov methods for general systems of hyperbolic conservation laws. *Journal of Computational Physics*, 82(2):362–397, 1989.

B. Berkowitz. Characterizing flow and transport in fractured geological media: A review. *Advances in Water Resources*, 25(8-12):861–884, 2002.

Z. R. Beydoun. Arabian plate oil and gas: why so rich and so prolific? *Episodes-Newsmagazine of the International Union of Geological Sciences*, 21(2):74–81, 1998.

M. J. Bickle. Geological carbon storage. *Nature Geoscience*, 2(12):815–818, 2009.

M. Blunt and B. Rubin. Implicit flux limiting schemes for petroleum reservoir simulation. *Journal of Computational Physics*, 102(1):194–210, 1992.

M. J. Blunt, K. Liu, and M. R. Thiele. A generalized streamline method to predict reservoir flow. *Petroleum Geoscience*, 2(3):259, 1996.

D. Bolster, M. Dentz, and J. Carrera. Effective two-phase flow in heterogeneous media under temporal pressure fluctuations. *Water Resour. Res*, 45, 2009. doi: 10.1029/2008WR007460.

D. Bolster, F. V. Valdés-Parada, T. LeBorgne, M. Dentz, and J. Carrera. Mixing in confined stratified aquifers. *Journal of Contaminant Hydrology*, 120-121:198 – 212, 2011. doi: 10.1016/j.jconhyd.2010.02.003.

S. Bottero, S.M. Hassanizadeh, P.J. Kleingeld, and T.J. Heimovaara. Nonequilibrium capillarity effects in two-phase flow through porous media at different scales. *Wat. Resour. Res.*, 47(10):W10505, 2011.

B. Bourbiaux and F. Kalaydjian. Experimental study of cocurrent and countercurrent flows in natural porous media. *SPE Res. Eng.*, 5(3): 361–368, 1990.

R. H. Brooks and A. T. Corey. Hydraulic properties of porous media. *Hydrological Paper 3, Colorado State University, CO, USA*, 1964.

S. E. Buckley and M. C. Leverett. Mechanisms of fluid displacement in sands. *Trans. AIME*, 146:107–116, 1942.

T. Buffard and S. Clain. Monoslope and multislope muscl methods for unstructured meshes. *Journal of Computational Physics*, 229(10): 3745–3776, 2010. doi: 10.1016/j.jcp.2010.01.026.

J. Cai and B. Yu. A discussion of the effect of tortuosity on the capillary imbibition in porous media. *Transp. in Por. Med.*, 89:1–13, 2011. doi: 10.1007/s11242-011-9767-0.

H. S. Carslaw and J. C. Jaeger. *Conduction of heat in solids*. Oxford University Press, 1959.

M. A. Celia, E. T. Bouloutas, and L. R. Zarba. A general mass-conservative numerical solution for the unsaturated flow equation. *Water Resources Research*, 26:1483–1496, 1990.

T. Chaturvedi, JM Schembre, and AR Kovscek. Spontaneous imbibition and wettability characteristics of powder river basin coal. *Int. J. of Coal Geol.*, 77(1-2):34–42, 2009.

J. Chen, M. A. Miller, and K. Sepehrnoori. Theoretical investigation of countercurrent imbibition in fractured reservoir matrix blocks. In *SPE Reservoir Simulation Symposium*, 1995.

Z. X. Chen. Some invariant solutions to two-phase fluid displacement problems including capillary effect. *SPE Reservoir Engineering*, 3(2): 691–700, 1988.

Z.X. Chen, GS Bodvarsson, PA Witherspoon, DB MCWHORTER, and DK SUNADA. COmment on 'Exact Integral solutions for two-phase flow' by D. B. McWhorter and D. K. Sunada. Author's Reply. *Water resources research*, 28(5):1477–1479, 1992.

P. G. Ciarlet. *The Finite Element Method for Elliptic Problems*. North Holland Publishing Company, 2nd edition, 1979.

M. Cil and J. C. Reis. A multi-dimensional, analytical model for counter-current water imbibition into gas-saturated matrix blocks. *Journal of Petroleum Science and Engineering*, 16(1-3):61–69, 1996.

M. Cil, J. Reis, M. Miller, and D. Misra. An examination of counter-current capillary imbibition recovery from single matrix blocks and recovery predictions by analytical matrix/fracture transfer functions. In *SPE Annual Technical Conference and Exhibition*, 1998.

O. A. Cirpka. Choice of dispersion coefficients in reactive transport calculations on smoothed fields. *Journal of Contaminant Hydrology*, 58 (3-4):261–282, 2002.

F. Civan and M. Rasmussen. Asymptotic analytical solutions for imbibition waterfloods in fractured reservoirs. *SPE Journal*, 6(2):171–181, 2001.

M.B. Clennell, M. Hovland, J.S. Booth, P. Henry, and W.J. Winters. Formation of natural gas hydrates in marine sediments 1. conceptual model of gas hydrate growth conditioned by host sediment properties. *J. of Geophys. Res.*, 104(B10):22985–23, 1999.

D. Coumou, S. Matthäi, S. Geiger, and T. Driesner. A parallel FE-FV scheme to solve fluid flow in complex geologic media. *Computers & Geosciences*, 34(12):1697–1707, 2008.

J. Crank. *The mathematics of diffusion*. Oxford University Press, USA, 1979.

L. Cueto-Felgueroso and R. Juanes. Nonlocal interface dynamics and pattern formation in gravity-driven unsaturated flow through porous media. *Phys. Rev. Lett.*, 101(24):244504, Dec 2008. doi: 10.1103/PhysRevLett.101.244504.

V. Cvetkovic and G. Dagan. Reactive transport and immiscible flow in geological media. ii. applications. *Proceedings: Mathematical, Physical and Engineering Sciences*, 452(1945):303–328, 1996.

G. Dagan. Perturbation solutions of the dispersion equation in porous mediums. *Water Resources Research*, 7:135–142, 1971.

A. Datta-Gupta and M. J. King. A semianalytic approach to tracer flow modeling in heterogeneous permeable media. *Advances in Water Resources*, 18(1):9–24, 1995.

A. Datta-Gupta, S. Yoon, D. W. Vasco, and G. A. Pope. Inverse modeling of partitioning interwell tracer tests: A streamline approach. *Water Resources Research*, 38(6):10–1029, 2002.

M. De Simoni, J. Carrera, X. Sanchez-Vila, and A. Guadagnini. A procedure for the solution of multicomponent reactive transport problems. *Water Resources Research*, 41(11), 2005. doi: 10.1029/2005WR004056.

M. De Simoni, X. Sanchez-Vila, J. Carrera, and M. W. Saaltink. A mixing ratios-based formulation for multicomponent reactive transport. *Water Resources Research*, 43(7), 2007. doi: 10.1029/2006WR005256.

E.B. Delijani and M.R. Pishvaie. Green element solution of one-dimensional counter-current spontaneous imbibition in water wet porous media. *Journal of Petroleum Science and Engineering*, 70(3-4): 302–307, 2010.

T. Delker, D.B. Pengra, and P. Wong. Interface pinning and the dynamics of capillary rise in porous media. *Phys. Rev. Let.*, 76(16):2902–2905, 1996.

M. Dentz, T. Le Borgne, A. Englert, and B. Bijeljic. Mixing, spreading and reaction in heterogeneous media: A brief review. *Journal of Contaminant Hydrology*, 120-121:1 – 17, 2011. doi: 10.1016/j.jconhyd.2010.05.002.

G. Di Donato, H. Lu, Z. Tavassoli, and M. Blunt. Multirate-transfer dual-porosity modeling of gravity drainage and imbibition. *SPE Journal*, 12(1):77–88, 2007.

M. Dubé, S. Majaniemi, M. Rost, M. J. Alava, K. R. Elder, and T. Ala-Nissila. Interface pinning in spontaneous imbibition. *Physical Review E*, 64(5):051605, 2001.

L.J. Durlofsky. A Triangle Based Mixed Finite Element-Finite Volume Technique for Modeling Two Phase Flow through Porous Media. *Journal of Computational Physics*, 105:252–252, 1993.

L.J. Durlofsky. Accuracy of mixed and control volume finite element approximations to Darcy velocity and related quantities. *Water Resources Research*, 30(4):965–973, 1994.

M.G. Edwards. Unstructured, control-volume distributed, full-tensor finite-volume schemes with flow based grids. *Computational Geosciences*, 6(3):433–452, 2002.

M.G. Edwards and H. Zheng. Double-families of quasi-positive darcy-flux approximations with highly anisotropic tensors on structured and unstructured grids. *Journal of Computational Physics*, 229(3):594–625, 2010.

M. Eldor and G. Dagan. Solutions of hydrodynamic dispersion in porous media. *Water Resources Research*, 8:1316–1331, 1972.

S. Emmanuel and B. Berkowitz. Mixing-induced precipitation and porosity evolution in porous media. *Advances in Water Resources*, 28 (4):337–344, 2005.

M. A. Fernø, Å. Haugen, and A. Graue. Wettability effects on the matrix-fracture fluid transfer in fractured carbonate rocks. *Journal of Petroleum Science and Engineering*, 2011.

W. E. Finch-Savage and G. Leubner-Metzger. Seed dormancy and the control of germination. *New Phytologist*, 171(3):501–523, 2006.

W. E. Finch-Savage, H. R. Rowse, and K. C. Dent. Development of combined imbibition and hydrothermal threshold models to simulate maize (Zea mays) and chickpea (Cicer arietinum) seed germination in variable environments. *New Phytologist*, 165(3):825–838, 2005.

H. Fischer and N. R. Morrow. Scaling of oil recovery by spontaneous imbibition for wide variation in aqueous phase viscosity with glycerol as the viscosifying agent. *Journal of Pet. Sc. and Eng.*, 52(1-4):35–53, 2006.

H. Fischer, S. Wo, and N. R. Morrow. Modeling the effect of viscosity ratio on spontaneous imbibition. *SPE Reservoir Eval. and Eng.*, 102641: 577–589, 2006.

A. S. Fokas and Y. C. Yortsos. On the exactly solvable equation$s_t = [(\beta s+\gamma)^{-2}s_x]_x + \alpha(\beta s+\gamma)^{-2}s_x$ occurring in two-phase flow in porous media. *SIAM Journal on Applied Mathematics*, 42(2):318–332, 1982. doi: 10.1137/0142025.

U. Frank and N. Barkley. Remediation of low permeability subsurface formations by fracturing enhancement of soil vapor extraction. *Journal of hazardous materials*, 40(2):191–201, 1995.

S. Geiger, S. Roberts, SK Matthäi, C. Zoppou, and A. Burri. Combining finite element and finite volume methods for efficient multiphase flow simulations in highly heterogeneous and structurally complex geologic media. *Geofluids*, 4(4):284–299, 2004.

S. Geiger, S. K. Matthäi, J. Niessner, and R. Helmig. Black-oil simulations for three-component - three-phase flow in fractured porous media. *SPE Journal*, 14:338–354, 2009.

L. W. Gelhar and M. A. Collins. General analysis of longitudinal dispersion in nonuniform flow. *Water Resources Research*, 7:1511–1521, 1971.

M.G. Gerritsen and L.J. Durlofsky. Modelling fluid flow in oil reservoirs. *Annual Review of Fluid Mechanics*, 37(1):211–238, 2005.

G. Goel and D.M. O'Carroll. Experimental investigation of nonequilibrium capillarity effects: Fluid viscosity effects. *Water Resour. Res.*, 47 (9):W09507, 2011.

A. Graue, B. G. Viksund, and B. A. Baldwin. Reproducible wettability alteration of low-permeable outcrop chalk. *SPE Reservoir Evaluation & Engineering*, 2(2):134–140, 1999.

R. J. Gummerson, C. Hall, W. D. Hoff, R. Hawkes, G. N. Holland, and W. S. Moore. Unsaturated water flow within porous materials observed by NMR imaging. *Nature*, 281:56–57, 1979.

A. Gupta and F. Civan. An improved model for laboratory measurement of matrix to fracture transfer function parameters in immiscible displacement. *SPE*, 28929:25–28, 1994.

R. Haggerty and S.M. Gorelick. Multiple-rate mass transfer for modeling diffusion and surface reactions in media with pore-scale heterogeneity. *Water Resources Research*, 31(10):2383–2400, 1995.

C. Hall. Anomalous diffusion in unsaturated flow: Fact or fiction? *Cement and Concrete Research*, 37(3):378–385, 2007.

G. Hamon and J. Vidal. Scaling-up the capillary imbibition process from laboratory experiments on homogeneous and heterogeneous samples. In *SPE 15852, Proc. of the Europ. Pet. Conf., London, October*, number 15852, pages 37–49, 1986.

L. L. Handy. Determination of effective capillary pressures for porous media from imbibition data. *Trans. AI*, 219:75–80, 1960.

A. Harten. High resolution schemes for hyperbolic conservation laws. *Journal of Computational Physics*, 49:357–393, 1983.

M. Hassanizadeh. Derivation of basic equations of mass transport in porous media, part 2. generalized darcy's and fick's laws. *Advances in Water Resources*, 9(4):207–222, 1986.

S. M. Hassanizadeh and W. G. Gray. Toward an improved description of the physics of two-phase flow. *Advances in Water Resources*, 16(1): 53–67, 1993.

S.M. Hassanizadeh and W.G. Gray. Mechanics and thermodynamics of multiphase flow in porous media including interphase boundaries. *Adv. in Wat. Res.*, 13(4):169–186, 1990.

R. D. Hazlett. Simulation of capillary-dominated displacements in microtomographic images of reservoir rocks. *Transport in Porous Media*, 20(1):21–35, 1995.

R. Helmig. *Multiphase Flow and Transport Processes in the Subsurface*. Springer, 1997.

A. W. Herbert, C. P. Jackson, and D. A. Lever. Coupled groundwater flow and solute transport with fluid density strongly dependent upon concentration. *Water Resources Research*, 24(10):1781–1795, 1988.

A. Hiorth, L. M. Cathles, and M. V. Madland. The Impact of Pore Water Chemistry on Carbonate Surface Charge and Oil Wettability. *Transport in Porous Media*, 2010. doi: 10.1007/s11242-010-9543-6.

E. J. Høgnesen, D. C. Standnes, and T. Austad. Scaling spontaneous imbibition of aqueous surfactant solution into preferential oil-wet carbonates. *Energy & Fuels*, 18(6):1665–1675, 2004.

H. Hoteit and A. Firoozabadi. Numerical modeling of two-phase flow in heterogeneous permeable media with different capillary pressures. *Advances in Water Resources*, 31(1):56–73, 2008.

R. W. Howarth, A. Ingraffea, and T. Engelder. Should fracking stop? extracting gas from shale increases the availability of this resource, but the health and environmental effects may be too high. counterpoint: No, it is too valuable. *Nature*, 2011. doi: 10.1038/477271a.

M. E. Hubbard. Multidimensional slope limiters for muscl-type finite volume schemes on unstructured grids. *Journal of Computational Physics*, 155(1):54 – 74, 1999. doi: 10.1006/jcph.1999.6329.

R. Huber and R. Helmig. Multiphase flow in heterogeneous porous media: A classical finite element method versus an implicit pressure-explicit saturation-based mixed finite element-finite volume approach. *International Journal for Numerical Methods in Fluids*, 29(8):899–920, 1999.

J. Hulshof and J.R. King. Analysis of a darcy flow model with a dynamic pressure saturation relation. *SIAM J. on Appl. Math.*, 59:318–346, 1998.

M. D. Jackson, P. H. Valvatne, and M. J. Blunt. Prediction of wettability variation and its impact on flow using pore-to reservoir-scale simulations. *Journal of Petroleum Science and Engineering*, 39(3-4):231–246, 2003.

P. P. Jadhunandan and N. R. Morrow. Spontaneous imbibition of water by crude oil/brine/rock systems. *In Situ*, 15(4):319–345, 1991.

A. Jameson. Analysis and design of numerical schemes for gas dynamics, 1: artificial diffusion, upwind biasing, limiters and their effect on accuracy and multigrid convergence. *International Journal of Computational Fluid Dynamics*, 4(3):171–218, 1995.

F. Javadpour. CO_2 Injection in Geological Formations: Determining Macroscale Coefficients from Pore Scale Processes. *Transport in Porous Media*, 79(1):87–105, 2009.

P. Jenny, H.A. Tchelepi, and S.H. Lee. Unconditionally convergent nonlinear solver for hyperbolic conservation laws with S-shaped flux functions. *Journal of Computational Physics*, 228(20):7497–7512, 2009.

T. Johansen and R. Winther. The solution of the Riemann problem for a hyperbolic system of conservation laws modeling polymer flooding. *SIAM journal on mathematical analysis*, 19(3):541–566, 1988.

R. Juanes and M. J. Blunt. Analytical solutions to multiphase first-contact miscible models with viscous fingering. *Transport in Porous Media*, 64(3):339–373, 2006.

F.J.M. Kalaydjian. Dynamic capillary pressure curve for water/oil displacement in porous media: Theory vs. experiment. In *SPE Annual Technical Conference and Exhibition*, pages 491–506, 1992.

M. Karimi-Fard, B. Gong, and LJ Durlofsky. Generation of coarse-scale continuum flow models from detailed fracture characterizations. *Water resources research*, 42(10):10423, 2006.

D. Kashchiev and A. Firoozabadi. Analytical Solutions for 1-D Countercurrent Imbibition in Water-Wet Media. *SPE Journal*, 8(4):401 – 408, 2002.

H. Kazemi, L. S Merrill, K. L. Porterfield, and P. R. Zeman. Numerical simulation of water-oil flow in naturally fractured reservoirs. *SPE Journal*, 16:317–326, 1976.

H. Kazemi, J. R. Gilman, and A. M. Eisharkawy. Analytical and numerical solution of oil recovery from fractured reservoirs with empirical transfer functions. *SPE Reservoir Engineering*, 7(2):219–227, 1992.

J. Kevorkian and J. D. Cole. *Perturbation methods in applied mathematics*. Springer-Verlag, New York, 1981.

S. A. Khan, G. A. Pope, and J. A. Trangenstein. Micellar/polymer physical-property models for contaminant cleanup problems and enhanced oil recovery. *Transport in Porous Media*, 24(1):35–79, 1996.

M. J. King and A. Datta-Gupta. Streamline simulation: A current perspective. *In Situ*, 22(1):91, 1998.

M. J. King and V. A. Dunayevsky. Why waterflood works: a linearized stability analysis. 1989.

J. Kozdon, M. Gerritsen, and M. Christie. Grid orientation revisited: Near-well, early-time effects and solution coupling methods. *Transport in porous media*, 73(3):255–277, 2008.

A. Krechel and K. Stüben. Parallel algebraic multigrid based on subdomain blocking. *Parallel Computing*, 27(8):1009–1031, 2001.

T. LaForce and R.T. Johns. Analytical solutions for surfactant-enhanced remediation of nonaqueous phase liquids. *Water Resources Research*, 41(10):W10420, 2005. doi: 10.1029/2004WR003862.

L. W. Lake and F. Helfferich. Cation Exchange in Chemical Flooding: Part 2 – The Effect of Dispersion, Cation Exchange, and Polymer/-Surfactant Adsorption on Chemical Flood Environment. *SPE Journal*, 6769:435–444, 1977.

L.W. Lake. *Enhanced oil recovery*. Old Tappan, NJ; Prentice Hall Inc., 1989.

S. Lamine and M.G. Edwards. Higher-resolution convection schemes for flow in porous media on highly distorted unstructured grids.

International Journal for Numerical Methods in Engineering, 76(8):1139–1158, 2008.

P. Langlo and M. S. Espedal. Macrodispersion for two-phase, immiscible flow in porous media. *Advances in Water Resources*, 17(5):297–316, 1994.

B. Lavi, A. Marmur, and J. Bachmann. Porous media characterization by the two-liquid method: effect of dynamic contact angle and inertia. *Langmuir*, 24(5):1918–1923, 2008.

S. S. Le Guen and A. R. Kovscek. Nonequilibrium effects during spontaneous imbibition. *Transport in porous media*, 63(1):127–146, 2006.

S. H. Lee, M. F. Lough, and C. L. Jensen. Hierarchical modeling of flow in naturally fractured formations with multiple length scales. *Water Resources Research*, 37(3):443–455, 2001.

B. P. Leonard. Simple high-accuracy resolution program for convective modelling of discontinuities. *International Journal for Numerical Methods in Fluids*, 8(10):1291–1318, 1988.

R. J. LeVeque. *Finite Volume Methods for Hyperbolic Problems*. Cambridge Tests in Applied Mathematics, 2002.

R.J. LeVeque. *Numerical methods for conservation laws*. Birkhäuser, 1992. ISBN 3764327235.

K. Li and R. Horne. Generalized scaling approach for spontaneous imbibition: an analytical model. *SPE Reservoir Eval. & Eng.*, 9(3): 251–258, 2006.

K. Li and R. N. Horne. Method to evaluate the potential of water injection in naturally fractured reservoirs. *Transp. in Por. Med.*, 83: 699–709, 2009.

K. Li, K. Chow, and R. Horne. Effect of initial water saturation on spontaneous water imbibition. In *SPE Western Regional/AAPG Pacific Section Joint Meeting*, 2002.

Y. Li, N. R. Morrow, and D. Ruth. Similarity solution for linear countercurrent spontaneous imbibition. *Journal of Petroleum Science and Engineering*, 39(3-4):309–326, 2003.

K.A. Lie, S. Krogstad, I.S. Ligaarden, J.R. Natvig, H.M. Nilsen, and B. Skaflestad. Open source matlab implementation of consistent

discretisations on complex grids. *Comput. Geosci*, pages 1–26, 2011. doi: 10.1007/s10596-011-9244-4.

R. Lucas. Über das Zeitgesetz des kapillaren Aufstiegs von Flüssigkeiten. *Colloid & Polymer Science*, 23(1):15–22, 1918.

S. Ma, N. R. Morrow, and X. Zhang. Generalized scaling of spontaneous imbibition data for strongly water-wet systems. *Journal of Pet. Sc. and Eng.*, 18(3-4):165–178, 1997.

E. Mackay. Predicting in situ sulphate scale deposition and the impact on produced ion concentrations. *Chemical Engineering Research and Design*, 81(3):326–332, 2003.

B.T. Mallison, M.G. Gerritsen, K Jessen, and F.M. Orr Jr. High-order upwind schemes for two-phase, multicomponent flow. *SPE Journal*, 79691:297–311, 2005.

S. Manthey, S.M. Hassanizadeh, R. Helmig, and R. Hilfer. Dimensional analysis of two-phase flow including a rate-dependent capillary pressure-saturation relationship. *Adv. in Wat. Res.*, 31(9):1137–1150, 2008.

A. Marmur. Kinetics of penetration into uniform porous media: testing the equivalent-capillary concept. *Langmuir*, 19(14):5956–5959, 2003.

G. Martic, F. Gentner, D. Seveno, D. Coulon, J. De Coninck, and T. D. Blake. A molecular dynamics simulation of capillary imbibition. *Langmuir*, 18(21):7971–7976, 2002.

V. Martin, J. Jaffré, and J.E. Roberts. Modeling fractures and barriers as interfaces for flow in porous media. *SIAM Journal on Scientific Computing*, 26(5):1667–1691, 2005.

G. Mason, H. Fischer, N. R. Morrow, and D. W. Ruth. Correlation for the effect of fluid viscosities on counter-current spontaneous imbibition. *Journal of Pet. Sc. and Eng.*, 72(1-2):195–205, 2010.

C. C. Mattax and J. R. Kyte. Imbibition oil recovery from fractured, water-drive reservoir. *SPE Journal*, 2(2):177–184, 1962.

S. K. Matthäi, S. Geiger, S. G. Roberts, A. Paluszny, M. Belayneh, A. Burri, A. Mezentsev, H. Lu, D. Coumou, T. Driesner, and C. A. Heinrich. Numerical simulation of multi-phase fluid flow in structurally complex reservoirs. *Geological Society London Special Publications*, 292(1): 405, 2007.

S.K. Matthäi, H.M. Nick, C. Pain, and I. Neuweiler. Simulation of solute transport through fractured rock: A higher-order accurate finite-element finite-volume method permitting large time steps. *Transport in Porous Media*, 83(2):1–30, 2009.

Chatman F.K. McGuire, P.L., D.M. Sommer, and F.H. Carini. Low salinity oil recovery: An exciting new eor opportunity for alaska's northe slope. *SPE*, 93903:1–15, 2005.

D. B. McWhorter. Infiltration affected by flow of air. *Hydrological Paper 49, Colorado State University, CO, USA*, 1971.

D. B. McWhorter and D. K. Sunada. Exact integral solutions for two-phase flow. *Water Resour. Res.*, 26(3):399–413, 1990.

J. Mikyška and A. Firoozabadi. Implementation of higher-order methods for robust and efficient compositional simulation. *Journal of Computational Physics*, 229(8):2898–2913, 2010.

M. Mirzaei and D.B. Das. Dynamic effects in capillary pressure-saturations relationships for two-phase flow in 3d porous media: Implications of micro-heterogeneities. *Chemical Engineering Science*, 62(7):1927–1947, 2007.

A. Mirzaei-Paiaman, M. Masihi, and D. C. Standnes. An analytic solution for the frontal flow period in 1d counter-current spontaneous imbibition into fractured porous media including gravity and wettability effects. *Transport in Porous Media*, 89:1–14, 2011. doi: 10.1007/s11242-011-9751-8.

J. Monteagudo and A. Firoozabadi. Control-volume model for simulation of water injection in fractured media: incorporating matrix heterogeneity and reservoir wettability effects. *SPE Journal*, 12(3): 355–366, 2007.

J. Moortgat and A. Firoozabadi. Higher-order compositional modeling with fickian diffusion in unstructured and anisotropic media. *Advances in Water Resources*, 33(9):951–968, 2010.

J. Moortgat, S. Sun, and A. Firoozabadi. Compositional modeling of three-phase flow with gravity using higher-order finite element methods. *Water Resources Research*, 47(5):W05511, 2011.

N. Morrow, S. Ma, X. Zhou, and X. Zhang. Characterization of wettability from spontaneous imbibition measurements. In *Annual Technical Meeting, Calgary, Alberta, Canada*, 1994.

N. M.; Morrow, G.; Tang, M.; Valat, and X. Xie. Prospects of improved oil recovery related to wettability and brine composition. *Journal of Petroleum Science and Engineering*, 20(3-4):267 – 276, 1998. doi: 10.1016/S0920-4105(98)00030-8.

N. R. Morrow and G. Mason. Recovery of oil by spontaneous imbibition. *Current Opinion in Colloid & Interface Science*, 6(4):321 – 337, 2001. doi: 10.1016/S1359-0294(01)00100-5.

C.N. Mulligan, R.N. Yong, and B.F. Gibbs. Surfactant-enhanced remediation of contaminated soil: a review. *Engineering Geology*, 60(1-4): 371–380, 2001. doi: 10.1016/S0013-7952(00)00117-4.

M. Muskat. *Physical principles of oil production*. McGrawhill, New York, 1949.

M. H. Nachabe, A. L. Islas, and T. H. Illangasekare. Analytical solutions for water flow and solute transport in the unsaturated zone. *Ground Water*, 33:304–310, 1995.

G. M. Narahara, A. L. Pozzi Jr, and T. H. Blackshear Jr. Effect of connate water on gas/oil relative permeabilities for water-wet and mixed-wet berea rock. *SPE Advanced Technology Series*, 1(2):114–122, 1993.

D. Nayagum, G. Schäfer, and R. Mosé. Modelling two-phase incompressible flow in porous media using mixed hybrid and discontinuous finite elements. *Computational Geosciences*, 8:49–73, 2004.

I. Neuweiler, S. Attinger, W. Kinzelbach, and P. King. Large scale mixing for immiscible displacement in heterogeneous porous media. *Transport in Porous Media*, 51(3):287–314, 2003.

H. M. Nick and S. K. Matthäi. A Hybrid Finite-Element Finite-Volume Method with Embedded Discontinuities for Solute Transport in Heterogeneous Media. *Vadose Zone Journal*, 10(1):299, 2011.

D.A. Nield and A. Bejan. *Convection in porous media*. Springer Verlag, 2006.

J. Niessner and R. Helmig. Multi-scale modeling of three-phase-three-component processes in heterogeneous porous media. *Advances in Water Resources*, 30(11):2309–2325, 2007.

J. Niessner, R. Helmig, H. Jakobs, and J. E. Roberts. Interface condition and linearization schemes in the newton iterations for two-phase flow

in heterogeneous porous media. *Advances in Water Resources*, 28(7): 671–687, 2005.

J. Nocedal and S.J. Wright. *Numerical optimization*. Springer Verlag, 1999.

D. M. O'Carroll, K. G. Mumford, L. M. Abriola, and J. I. Gerhard. Influence of wettability variations on dynamic effects in capillary pressure. *Water Resour. Res*, 46, 2010. doi: 10.1029/2009WR008712.

A. Paluszny, SK Matthäi, and M. Hohmeyer. Hybrid finite element–finite volume discretization of complex geologic structures and a new simulation workflow demonstrated on fractured rocks. *Geofluids*, 7 (2):186–208, 2007.

M. Panfilow and S. Floriat. Nonlinear two-phase mixing in heterogeneous porous media. *Transport in Porous Media*, 57(3):347–375, 2004.

A. Paster and G. Dagan. Mixing at the interface between two fluids in aquifer well upconing steady flow. *Water Resources Research*, 44(5): 107–117, 2008.

D.W. Peaceman. *Fundamentals of numerical reservoir simulation*. Elsevier, 1977.

J. R. Philip. A very general class of exact solutions in concentration-dependent diffusion. *Nature*, 4708:233, 1960.

JR Philip. On solving the unsaturated flow equation: 1. The flux-concentration relation. *Soil Science*, 116(5):328, 1973.

M. Pooladi-Darvish and A. Firoozabadi. Cocurrent and countercurrent imbibition in a water-wet matrix block. *SPE Journal*, 5(1):3–11, 2000.

G. A. Pope. Cation exchange in chemical flooding: Part 1 - basic theory without dispersion. *SPE*, 6771:418–434, 1978.

G. A. Pope. The application of fractional flow theory to enhanced oil recovery. *SPE Journal*, 20(3):191–205, 1980.

M. Rahman, S. C. Jose, W. Nowak, and O. A. Cirpka. Experiments on vertical transverse mixing in a large-scale heterogeneous model aquifer. *Journal of Contaminant Hydrology*, 80(3-4):130–148, 2005.

E. R. Rangel-German and A. R. Kovscek. Time-dependent matrix-fracture shape factors for partially and completely immersed fractures. *Journal of Petroleum Science and Engineering*, 54(3-4):149–163, 2006.

E. R. Rangel-German and A.R. Kovscek. Experimental and analytical study of multidimensional imbibition in fractured porous media. *Journal of Petroleum Science and Engineering*, 36(1-2):45–60, 2002.

L. A. Rapoport. Scaling laws for use in design and operation of water-oil flow models. *Trans. AIME*, 204(1955):143–150, 1955.

M. L. Rasmussen and F. Civan. Analytical solutions for waterfloods in fractured reservoirs obtained by an asymptotic approximation. *SPE Journal*, 3(3):249–252, 1998.

V. Reichenberger, H. Jakobs, P. Bastian, and R. Helmig. A mixed-dimensional finite volume method for two-phase flow in fractured porous media. *Advances in Water Resources*, 29(7):1020–1036, 2006.

J. C. Reis and M. Cil. A model for oil expulsion by counter-current water imbibition in rocks: one-dimensional geometry. *Journal of Petroleum Science and Engineering*, 10(2):97–107, 1993.

P. L. Roe. Numerical algorithms for the linear wave equation. *Royal Aircraft Establishment Technical Report*, 81047, 1981.

D. Ruth, N. R. Morrow, L. Yu, and J. Buckley. Simulation study of spontaneous imbibition. In *International Society of Core Analysts Annual Meeting, Abu Dhabi, UAE, October*, 2000.

D. W. Ruth and J. K. Arthur. A revised analytic solution to the linear displacement problem including capillary pressure effects. *Transport in Porous Media*, 86:881–894, 2011.

D. W. Ruth, G. Mason, N. R. Morrow, and Y. Li. The effect of fluid viscosities on counter-current spontaneous imbibition. In *Proceedings of the Society of Core Analysts Symposium, Abu Dhabi, SCA2004-11*, pages 1–13, 2004.

D. W. Ruth, Y. Li, G. Mason, and N. R. Morrow. An approximate analytical solution for counter-current spontaneous imbibition. *Transport in porous media*, 66(3):373–390, 2007.

R. A. Salathiel. Oil recovery by surface film drainage in mixed-wettability rocks. *Journal of Petroleum Technology*, 25(10):1216–1224, 1973.

J. L. Sanchez Bujanos, M. A. Miller, and K. Sephernoori. Scaling parameters for characterizing waterflood recovery from anisotropic matrix

blocks in naturally fractured reservoirs. In *SPE international petroleum conference*, pages 61–69, 1998.

J. M. Schembre and A. R. Kovscek. Estimation of dynamic relative permeability and capillary pressure from countercurrent imbibition experiments. *Transp. in Por. Media*, 65(1):31–51, 2006.

J. M. Schembre, S. Akin, L. M. Castanier, and A. R. Kovscek. Spontaneous water imbibition into diatomite. In *SPE Western Regional Meeting*, 1998.

Schlumberger. Carbonate reservoirs - meeting unique challenges to maximize recovery, 2007.

K. S. Schmid, S. Geiger, and K.S. Sorbie. Semi-analytical solutions for co- and countercurrent imbibition and dispersion of solutes in immiscible two-phase flow. *Water Resources Research*, 47(2):1–16, 2011. doi: 10.1029/2010WR009686.

C. J. Seto and F. M. Orr. Analytical Solutions for Multicomponent, Two-Phase Flow in Porous Media with Double Contact Discontinuities. *Transport in Porous Media*, 78(2):161–183, 2009.

P. Siegel, R. Mosé, Ph. Ackerer, and J. Jaffre. Solution of the advection-diffusion equation using a combination of discontinuous and mixed finite elements. *Internat. J. Numer. Methods Fluids*, 24:595–613, 1997.

K. S. Sorbie. *Polymer-Improved Oil Recovery*. Blackie Ed., 1991.

K. S. Sorbie and E. J. Mackay. Mixing of injected, connate and aquifer brines in waterflooding and its relevance to oilfield scaling. *Journal of Petroleum Science and Engineering*, 27(1-2):85 – 106, 2000. doi: 10.1016/S0920-4105(00)00050-4.

K. Spayd and M. Shearer. The buckley-leverett equation with dynamic capillary pressure. *SIAM J. on Appl. Math.*, 71:1088–1108, 2011.

A. Spivak, HS Price, and A. Settari. Solution of the equations for multidimensional, two-phase, immiscible flow by variational methods. *SPE Journal*, 17(1):27–41, 1977.

D. C. Standnes. Spontaneous imbibition of water into cylindrical cores with high aspect ratio: Numerical and experimental results. *Journal of Petroleum Science and Engineering*, 50(2):151–160, 2006.

D. C. Standnes. Scaling group for spontaneous imbibition including gravity. *Energy & Fuels*, 24(5):2980–2984, 2010a.

D. C. Standnes. Scaling spontaneous imbibition of water data accounting for fluid viscosities. *Journal of Petroleum Science and Engineering*, 73:214–219, 2010b.

K. D. Stephen, G. E. Pickup, and K. S. Sorbie. The local analysis of changing force balances in immiscible incompressible two-phase flow. *Transport in Porous Media*, 45:63–88, 2001.

M. Stoll, J. Hofman, D. Ligthelm, M. Faber, and P. van den Hoek. Toward Field-Scale Wettability Modification - The Limitations of Diffusive Transport. *SPE Reservoir Evaluation & Engineering*, 11(3):633–640, 2008.

G. Strang. On the construction and comparison of difference schemes. *SIAM Journal on Numerical Analysis*, 5:506–517, 1968.

K. Stüben. A review of algebraic multigrid. *Journal of Computational and Applied Mathematics*, 128:281–309, 2001.

P. K. Sweby. High resolution schemes using flux limiters for hyperbolic conservation laws. *SIAM Journal on Numerical Analysis*, 21:995–1011, 1984.

Guo-Qing Tang and Norman R. Morrow. Influence of brine composition and fines migration on crude oil/brine/rock interactions and oil recovery. *Journal of Petroleum Science and Engineering*, 24(2-4):99 – 111, 1999. doi: 10.1016/S0920-4105(99)00034-0.

Z. Tavassoli, R. W. Zimmerman, and M. J. Blunt. Analytic analysis for oil recovery during counter-current imbibition in strongly water-wet systems. *Transp. in Por. Media*, 58(1):173–189, 2005a.

Z. Tavassoli, R.W. Zimmerman, and M.J. Blunt. Analysis of counter-current imbibition with gravity in weakly water-wet systems. *Journal of Petroleum Science and Engineering*, 48(1-2):94–104, 2005b.

Z. Tong, X. Xie, and N. R. Morrow. Scaling of viscosity ratio for oil recovery by imbibition from mixed-wet rocks. In *Petrophysics*, volume 43, pages 338–346, 2002.

Y. Tsang, J. T. Birkholzer, and S. Mukhopadhyay. Modeling of thermally driven hydrological processes in partially saturated fractured rock. *Reviews of Geophysics*, 47:RG3004, 2009. doi: doi:10.1029/2008RG000265.

E. Unsal, S. K. Matthäi, and M. J. Blunt. Simulation of multiphase flow in fractured reservoirs using a fracture-only model with transfer functions. *Computational Geosciences*, 14:1–12, 2010.

P. H. Valvatne and M. J. Blunt. Predictive pore-scale modeling of two-phase flow in mixed wet media. *Water Resour. Res.*, 40(7):doi: 10.1029/2003WR002627, 2004.

M. I. J. Van Dijke and K. S. Sorbie. Pore-scale network model for three-phase flow in mixed-wet porous media. *Physical Review E*, 66 (4):046302, 2002.

M. I. J. Van Dijke and K. S. Sorbie. Pore-scale modelling of three-phase flow in mixed-wet porous media: multiple displacement chains. *Journal of Petroleum Science and Engineering*, 39(3-4):201–216, 2003.

M. Van Dyke. *Perturbation methods in fluid mechanics/Annotated edition*, volume 75. The Parabolic Press, 1975.

B. Van Leer. Towards the ultimate conservative difference scheme. II. Monotonicity and conservation combined in a second-order scheme. *Journal of Computational Physics*, 14(4):361–370, 1974.

J. E. Warren and P. J. Root. The behavior of naturally fractured reservoirs. *SPE Journal*, 3(3):245–255, 1963.

E. W. Washburn. The dynamics of capillary flow. *Phys. Rev.*, 17(3): 273–283, 1921.

K.J. Webb, C.J.J. Black, and I.J. Edmonds. Low salinity oil recovery - log inject log. *SPE*, 89379, 2004.

K.J. Webb, C.J.J. Black, and H. Al-Jeel. Low salinity oil recovery - the role of reservoir condition corefloods. In *EAGE*, 2005.

H. J. Welge. A simplified method for computing oil recovery by gas or water drive. *Trans. AIME*, 195:91–98, 1952.

C. J. Werth, O. A. Cirpka, and P. Grathwohl. Enhanced mixing and reaction through flow focusing in heterogeneous porous media. *Water Resources Research*, 42(12):W12414, 2006.

C. C. West and J. H. Harwell. Surfactants and subsurface remediation. *Environmental Science & Technology*, 26(12):2324–2330, 1992.

T. W. Willingham, C. J. Werth, and A. J. Valocchi. Evaluation of the effects of porous media structure on mixing-controlled reactions using pore-scale modeling and micromodel experiments. *Environmental Science & Technology*, 42:3185–3193, 2008.

J. L. Wilson and L. W. Gelhar. Dispersive mixing in a partially saturated porous medium. Technical report, Ralp M. Parsons Lab. for Water Resour. and Hydrodyn., Mass. Inst. of Technol., Cambridge, 1974.

J. L. Wilson and L. W. Gelhar. Analysis of longitudinal dispersion in unsaturated flow 1. the analytical method. *Water Resources Research*, 17(1):122–130, 1981.

Y.S. Wu and L. Pan. Special relative permeability functions with analytical solutions for transient flow into unsaturated rock matrix. *Water resources research*, 39(4):3–1, 2003.

X. Xie and N. R. Morrow. Oil recovery by spontaneous imbibition from weakly water-wet rocks. volume 42, pages 313–322, 2001.

T. Xu, E. Sonnenthal, N. Spycher, and K. Pruess. TOUGHREACT–A simulation program for non-isothermal multiphase reactive geochemical transport in variably saturated geologic media: Applications to geothermal injectivity and CO_2 geological sequestration. *Computers & Geosciences*, 32(2):145–165, 2006.

H. O. Yildiz and N. R Morrow. Effect of brine composition on recovery of moutray crude oil by waterflooding. *Journal of Petroleum Science and Engineering*, 14(3-4):159 – 168, 1996. doi: 10.1016/0920-4105(95)00041-0.

Y. C. Yortsos and A. S. Fokas. An analytical solution for linear waterflood including the effects of capillary pressure. *SPE Journal*, 23(1): 115–124, 1983.

A. A. Yousef, S. Al-Saleh, A. Al-Kaabi, and M. Al-Jawfi. Laboratory investiation of novel ouil recovery method for carbonate resevoirs. In *Canadian Unconventional Resources & International Petroleum Conference, Alberta, Canada*, 2010.

A. F. Zazovskii. Structure of discontinuities in problems of oil displacement by reactants that influence the phase equilibrium. *Fluid Dynamics*, 20(5):765–774, 1985.

X. Zhang, N. Morrow, and S. Ma. Experimental verification of a modified scaling group for spontaneous imbibition. *SPE Res. Eng.*, 11(4): 280–285, 1996.

Y Zhang and N R Morrow. Waterflood performance by injection of brine with different salinity for reservoir cores. *SPE Journal*, 109849: 1–12, 2007.

D. Zhou, L. Jia, J. Kamath, and A. R. Kovscek. Scaling of counter-current imbibition processes in low-permeability porous media. *Journal of Pet. Sc. and Eng.*, 33(1-3):61–74, 2002.

X. Zhou, N. R. Morrow, and S. Ma. Interrelationship of wettability, initial water saturation, aging time, and oil recovery by spontaneous imbibition and waterflooding. *SPE Journal*, 5(2):199–207, 2000.

R. W. Zimmerman and G. S. Bodvarsson. An approximate solution for one-dimensional absorption in unsaturated porous media. *Water Resources Research*, 25(6):1422–1428, 1989.

R.W. Zimmerman and G.S. Bodvarsson. A simple approximate solution for horizontal infiltration in a brooks-corey medium. *Transport in Porous Media*, 6(2):195–205, 1991.

'Stay hungry, stay foolish.'

- Stewart Brand, *The Whole Earth Catalog*